Title of thesis: Some Studies on the Electrochemical Behavior of Actinides and Fission Products in Room Temperature Ionic Liquids for Nuclear Fuel Cycle Applications

Homi Bhabha National Institute

Recommendations of the Viva Voce Committee

As members of the Viva Voce Committee, we certify that we have read the dissertation prepared by G. Murali Krishna entitled **Some Studies on the Electrochemical Behavior of Actinides and Fission Products in Room Temperature Ionic Liquids for Nuclear Fuel Cycle Applications** and recommend that it may be accepted as fulfilling the thesis requirement for the award of Degree of Doctor of Philosophy.

N. Sivaraman Date: 16/9/2020
Chairman – Dr. N. Sivaraman

Date: Sep 16, 2020
Guide / Convener – Dr. K. Ananthasivan

Siddharth Pandey Date: Sep. 16, 2020
Examiner - Prof. Siddharth Pandey

Date: 16/09/2020
Member 1- Dr. B. Prabhakara Reddy

N.V. Chandra Shekar Date: 16/9/2020
Member 2- Dr. N.V. Chandra Shekar

Date: 16/9/2020
Member 3- Dr. R.V. Subba Rao

K.A. Venkatesan Date: 16/9/20
Technology Adviser – Dr. K.A. Venkatesan

Final approval and acceptance of this thesis is contingent upon the candidate's submission of the final copies of the thesis to HBNI.

I/We hereby certify that I/we have read this thesis prepared under my/our direction and recommend that it may be accepted as fulfilling the thesis requirement.

Date: 16/9/20
Place: Kalpakkam

Dr. K. Ananthasivan
Guide

STATEMENT BY AUTHOR

This dissertation has been submitted in partial fulfillment of requirements for an advanced degree at Homi Bhabha National Institute (HBNI) and is deposited in the Library to be made available to borrowers under rules of the HBNI.

Brief quotations from this dissertation are allowable without special permission, provided that accurate acknowledgement of source is made. Requests for permission for extended quotation from or reproduction of this manuscript in whole or in part may be granted by the Competent Authority of HBNI when in his or her judgment the proposed use of the material is in the interests of scholarship. In all other instances, however, permission must be obtained from the author.

G. Murali Krishna

G. Murali Krishna

DECLARATION

I, hereby declare that the investigation presented in the thesis has been carried out by me. The work is original and has not been submitted earlier as a whole or in part for a degree / diploma at this or any other Institution / University.

G. Murali Krishna

G. Murali Krishna

List of Publications arising from the thesis

(a) Publications in Refereed Journal:

1. “Electrochemical behaviour of zirconium(IV) in 1-butyl-3-methylimidazolium bis(trifluoromethyl sulfonyl) imide ionic liquid”, G. Murali Krishna, A.S. Suneesh, K.A. Venkatesan, M.P. Antony, Journal of Electroanalytical Chemistry, 2016, 776, 120-126.
2. “Electrochemical interference of some fission products during the electrodeposition of uranium oxide from 1-butyl-3-methylimidazolium chloride ionic liquid”, G. Murali Krishna, A.S. Suneesh, K.A. Venkatesan, M.P. Antony, Journal of Electroanalytical Chemistry, 2016, 780, 225-232.
3. “Dissolution of U_3O_8 in 1-butyl-3-methylimidazolium chloride and spectroscopic and electrochemical behavior of U(VI) in the resultant solution”, G. Murali Krishna, A.S. Suneesh, R. Kumaresan, K.A. Venkatesan, M.P. Antony, Journal of Electroanalytical Chemistry, 2017, 795, 51-58.
4. “Electrochemical behavior of U(VI) in imidazolium ionic liquid medium containing tri-n-butyl phosphate and chloride ion and spectroscopic characterization of uranyl species”, G. Murali Krishna, A.S. Suneesh, R. Kumaresan, K.A. Venkatesan, M.P. Antony, Chemistry select, 2017, 2, 8706-8715.
5. “Anodic dissolution of uranium and zirconium metals and electrochemical behavior of U(IV) and Zr(IV) in ionic liquid medium for metallic fuel reprocessing”, G. Murali Krishna, A.S. Suneesh, K.A. Venkatesan, M.P. Antony, Journal of Electrochemical society, 2018, 165, C206-C212.

6. “Electrochemical, thermodynamics, and spectroscopic investigation of Eu(III) in T2EHDGA–[C_4mim][NTf_2] mixture”, Alok Rout, G. Murali Krishna, K.A. Venkatesan, Separation Science and Technology, 2018, 54, 1669-1680.
7. “Coordination and electrochemical behavior of U(VI) in dicyanamide ionic liquid”, G. Murali Krishna, K.A. Venkatesan, Journal of Vibrational Spectroscopy,103, 2019, 102927.
8. “Voltammetric investigation of some lanthanides in neutral ligand-ionic liquid”, G. Murali Krishna, Alok Rout, K.A. Venkatesan, Journal of Electroanalytical Chemistry, 856, 2019, 113671.

(b) Conference/Symposium:

1. Dissolution of U_3O_8 and electrochemical behavior of U(VI) in 1-butyl-3-metylimidazolium chloride, G. Murali Krishna, A.S. Suneesh, K.A. Venkatesan, M.P. Antony, (2016). In: Emerging Trends in Separation Science and Technology (SESTEC -2016), IIT, Guwahati. A.C. Deb, S. Sodaye, M.S. Murali, T. Banarjee, P.K. Moharatra, K.L. Ramkumar (eds) (2016) p-106.
2. Interference of some fission products during electrodeposition of UO_2 in ionic liquid medium, G. Murali Krishna, A.S. Suneesh, K.A. Venkatesan, M.P. Antony, In: Nuclear and radiochemistry, KIIT University, Bhubaneswar, Odisha. M. Mohapatra, S. Dash, P.K. Pujari, S.K. Raskhit, B.S. Tomar (eds) (2017) p-308.
3. Dissolution of zirconium and electrochemical behavior of Zr(IV) in composite ionic liquid medium, G. Murali Krishna, A.S. Suneesh, K.A. Venkatesan, M.P. Antony, In: Nuclear and radiochemistry, KIIT University, Bhubaneswar, Odisha. M. Mohapatra, S. Dash, P.K. Pujari, S.K. Raskhit, B.S. Tomar (eds) (2017) p-310.

4. Underpotential deposition of uranium oxide from tri-n-butyl phosphate/ionic liquid solution in the presence of chloride ions, G. Murali Krishna, A.S. Suneesh, R. Kumaresan, K.A. Venkatesan, M.P. Antony, In Proceedings of the second international conference on electrochemical science and technology (ICONEST-2017), Indian Institute of Science, Bengaluru, (2017) p-1.

ACKNOWLEDGEMENT

I express my sincere thanks to my Ph.D supervisor **Dr. K. Ananthasivan**, Director, Reprocessing Group, IGCAR, for his constant encouragement, support and valuable suggestions to improve the quality of work throughout my tenure.

I am extremely grateful to **Dr. B.K. Panigrahi**, Director, MC&MFCG, IGCAR for his constant support and encouragement. I extend of my sincere thanks to **Dr. N. Sivaraman**, Dean, Chemical Sciences, Associate Director, MFCG, MC&MFCG and **Dr. M. Joseph**, former Director, MC&MFCG for their constant support.

I express my sincere thanks to **Dr. A.K. Bhaduri**, Director, IGCAR, **Dr. S.A.V. Satya Murty**, former Director, IGCAR and **Dr. P.R. Vasudeva Rao**, former Director, IGCAR for providing me the opportunity to continue the research work at IGCAR.

I am also extremely indebted to my technology advisor **Dr. K.A. Venkatesan**, for providing necessary infrastructure and resources to accomplish my research work. I am very much thankful to him for his valuable guidance, advice, extensive discussions and his timely help through out my research work.

My special thanks to **Dr. M.P. Antony** for his kind support and helping me in various ways during the course of this work.

I am pleased to express my deep sense of gratitude to my doctoral committee chairman, **Dr. N. Sivaraman**, members, **Dr. B. Prabhakara reddy**, **Dr. N.V. Chandra Shekar** and **Dr. R.V. Subba Rao** for their fruitful discussions, valuable suggestions, constant support and encouragement.

I am thankful to **Dr. T. S. Lakshmi Nararasimhan** and **Dr. M. Sai Baba** for their kind advice, support and encouragement. I express my hearty thanks to **Dr. R. Kumaresan** for his help in learning the experimental procedures during my initial stage of PhD work and also his constant support and encouragement.

I am very much thankful to **Dr. A.S. Suneesh**, **Dr. Alok Rout**, **Shri. Robert selvan** for their technical support, guidance and timely help through out my research work.

I wish to record my sincere thanks to all my lab members, **Dr. T. Prathibha**, **Mrs. Amutha suba**, **Dr. P.K. Nayak**, **Mrs. K.V. Syamala**, my senior **Dr. R. Rama**, my juniors, **Mr. K. Rama swamy**, **Mr. Ch Venkateswara Rao** and **Mr. P. Amesh** for their kind support and timely help through out my research work.

I express my special thanks to **Mr. G.G.S. Subramanian**, **Mr. T. Bapuji** and **Shri. M. Karunanidhi**, MHCS, ACSD, for their support and help during my experiments.

The strong co-operation and kind support of all the members of Solution Chemistry and Separation Science section, **Dr. A. Suresh**, **Dr. C.V.S. Brahmananda Rao**, **Dr. B. Srinivasulu**, **Dr. Benadict Rakesh**, **Mrs. N. Navamani**, **Mrs. Jayalakshmi**, **Mrs. Ganga**, **Dr. Adithi** and **Mr. Amarendran** are deeply acknowledged.

I would like to extend my sincere thanks to **Dr. R Sudha**, Materials Chemistry Division, for recording the SEM-EDX spectra of the samples, and I also acknowledge **Dr. H.N. Jena,** Head, Materials Processing Chemistry Section, MCD & **Dr. Raja Madhavan** for the XRD analysis of samples.

I am very much thankful to **Homi Bhabha National Institue**, Mumbai, for providing me the opportunity to carry out my PhD work.

I express my hearty thanks to all the project students worked in my lab, **Amrutha Mohan**, **Akshaya Udhayam** and **K. Dasthaiah** (PhD Scholar, IITM) for their sincere help in doing some experiments.

I would like to express my special thanks to my batchmates **Amit Mishra**, **Chiranjith Poddar**, **Rajesh Sharma** and all my research scholar friends for their support.

I would like to express my heartiest gratitude to, my **family members**, for their love, affection, encouragement and support throughout my life. I thank the supreme soul for helping me to reach this level.

Finally, I thank one and all who helped me during the research work.

Table of Contents

Homi Bhabha National Institute

1. **Name of the Student** : G. Murali Krishna
2. **Name of the Constituent Institution** : IGCAR, Kalpakkam
3. **Enrolment No.** : **CHEM02201404004**
4. **Title of the Thesis** : Some Studies on the Electrochemical Behavior of Actinides and Fission Products in Room Temperature Ionic Liquids for Nuclear Fuel Cycle Applications
5. **Board of Studies** : Chemical Sciences

ABSTRACT

Room temperature ionic liquids (RTILs) are organic salts, melt at temperatures $\leq$ 100°C. They have several fascinating properties suitable for industrial exploitation. The properties such as negligible vapor pressure, ability to dissolve organic and inorganic compounds, good thermal and radiation stability, possibility of separating target metals from aqueous phase followed by electrodeposition directly from the ionic liquid phase etc, makes them suitable for nuclear fuel cycle applications.

The work reported in this thesis involved evaluation of some room temperature ionic liquids, synthesized in the laboratory, for studying the electrochemical behaviour of lanthanides and actinides (uranium), and studies on the recovery of these metal ions by electrodeposition from the ionic liquid medium containing organic ligands coordinated to these metal ions. For this purpose, the oxidative dissolution behaviour of U_3O_8 in ionic liquid medium was studied and electrochemical behaviour of UO_2^{2+} was investigated in presence and absence of fission products such as Pd^{2+}, Eu^{3+} and Ru^{3+}. The electrochemical behaviour of UO_2^{2+} in ionic liquid medium containing tri-*n*-butylphosphate and chloride ion, and UO_2^{2+} in dicyanamide ionic liquid was investigated to achieve improved solubility of UO_2^{2+} in ionic liquid and to tame the uranium-TBP complex during electrodeposition. In addition, the electrochemical behaviour of Zr(IV) and U(IV) in RTIL medium was studied to understand the technical feasibility of using ionic liquid for metallic fuel reprocessing applications of U-Pu-Zr ternary alloy fuels. The results obtained from these studies are reported in the thesis.

LIST OF FIGURES

LIST OF TABLES

Name of the Student: G. Murali Krishna

Name of the CI/OCC: HBNI-IGCAR Kalpakkam **Enrolment No.:** CHEM02201404004

Thesis Title: Some Studies on the Electrochemical Behavior of Actinides and Fission Products in Room Temperature Ionic Liquids for Nuclear Fuel Cycle Applications

Discipline: Chemical Sciences **Sub-Area of Discipline:** Electrochemical studies

Date of viva voce: 16-09-2020

Highlights

RTILs are compounds composed only of ions and melt at temperatures lower than 373 K. RTILs have been explored for possible electrochemical applications in nuclear fuel cycle owing to the favourable properties such as good solubility of actinides, excellent conductivity and wide electrochemical window. In the present work, the RTILs were explored as electrolytic medium for applications related to non-aqueous reprocessing of spent nuclear fuels. RTILs were also employed as organic phase for the extraction of metal ions from acidic/aqueous medium and studied for the feasibility of direct electrodeposition of the metal from loaded organic phase.

The present work involves the electrochemical behaviour of uranium and fission products in RTIL medium, and the recovery of these metal ions by electrodeposition from the RTIL medium containing organic ligands coordinated to these metal ions. For this purpose, the oxidative dissolution behaviour of U_3O_8 in the presence of small amount of nitric acid in ionic liquid medium was studied and electrochemical behaviour of UO_2^{2+} was investigated in presence and absence of fission products such as Pd^{2+}, Eu^{3+} and Ru^{3+}. The electrochemical behaviour of UO_2^{2+} in $C_4mimNTf_2$ ionic liquid containing tri-*n*-butylphosphate was investigated in the presence of chloride ions to facilitate the electrodeposition of uranium oxide. The solubility of UO_2^{2+} in ionic liquid was improved by employing dicyanamide based RTILs and electrochemical behaviour of UO_2^{2+} was also investigated in dicyanamide ionic liquids. The co-ordination environment of uranium in ionic liquid was investigated by FTIR, Raman and UV-Visible spectroscopy.

To understand the technical feasibility of using ionic liquid for metallic fuel reprocessing applications of U-Pu-Zr ternary alloy fuels, the anodic dissolution of U and Zr metals was performed and the electrochemical behaviour of Zr(IV) and U(IV) was investigated in $C_4mpyNTf_2$ ionic liquid medium. In addition, the neutral ligand ionic liquid (NLIL) containing rare earth ions was prepared by the dissolving of $Ln(NTf_2)_3$ (Ln = Eu, Nd, Dy) in DHOA to improve the solubility of trivalents in ionic liquid. The added $Ln(NTf_2)_3$ undergoes facile dissolution in DHOA, resulting in the formation of NLIL, $[Ln(DHOA)_3]^{3+}[(NTf_2)_3]^{-}$, and the electrochemical behavior of Ln^{3+} present in NLIL was investigated by cyclic voltammetry. The coordination and speciation behavior of uranium and lanthanides in ionic liquid medium was probed by the spectroscopic studies such as UV-Visible, Raman and FTIR spectroscopy.

Chapter 1: Introduction

1.1. Nuclear fuel cycle and Indian nuclear programme

Uranium is one of the major fissile elements found in the earth crust. The nuclear fuel cycle is a series of industrial processes, that involves mining of uranium, production of electricity from nuclear fission reaction of U in a nuclear power reactor, reprocessing of spent nuclear fuel and the disposal of nuclear waste (shown in figure 1.1) [1, 2]. The process that includes the steps of mining and milling, conversion, enrichment and preparation of the U bearing fuel in a suitable form of its fabrication as a fuel element are collectively called as 'front end' of the nuclear fuel cycle. After uranium gets burnt in a reactor to produce electricity, the used fuel is subjected to a series of processes including its temporary storage, reprocessing, recycling of U & Pu and the disposal of radioactive waste. Collectively these steps are called as the 'back end' of the fuel cycle.

In 1950s, Dr. Homi Jahangir Bhabha proposed a three-stage nuclear programme for India, based on a closed nuclear fuel cycle, in order to ensure the effective utilization of the limited uranium resources and abundant reserves of thorium in India [3]. In the first stage pressurised heavy water reactors (PHWR), that use natural uranium as the fuel would be operated to produce power. The spent fuel obtained from PHWRs containing a small amount of the fissile isotope ^{239}Pu [4], is reprocessed for recovering the residual uranium and plutonium from the fission products. Currently, there are 18 PHWRs, two BWRs, and one PWR operating in India with a total installed capacity of 6780 MWe. The second stage involves utilization of plutonium recovered from PHWRs, to fuel Fast breeder reactors (FBRs) [5]. In the FBRs, the fertile thorium is used as a blanket in order to breed more fuel than that is consumed by converting the fertile ^{232}Th into fissile ^{233}U. A Fast Breeder Test Reactor (FBTR) with the capacity of 40 MWt in operation at

Kalpakkam since 1985 is part of the second stage. India's first commercial fast breeder reactor, the Prototype Fast Breeder Reactor (PFBR) (500 MWe) is in an advanced stage of completion. The third stage aims to utilize ^{233}U, generated in the second stage to fuel thermal breeders (PHWRs), partly this could also be accomplished through the AHWRs. The viability of the third stage has been demonstrated by using a (30 kWt) research reactor named KAlpakkam MINI (KAMINI) Reactor fuelled with ^{233}U that is currently at Kalpakkam [6].

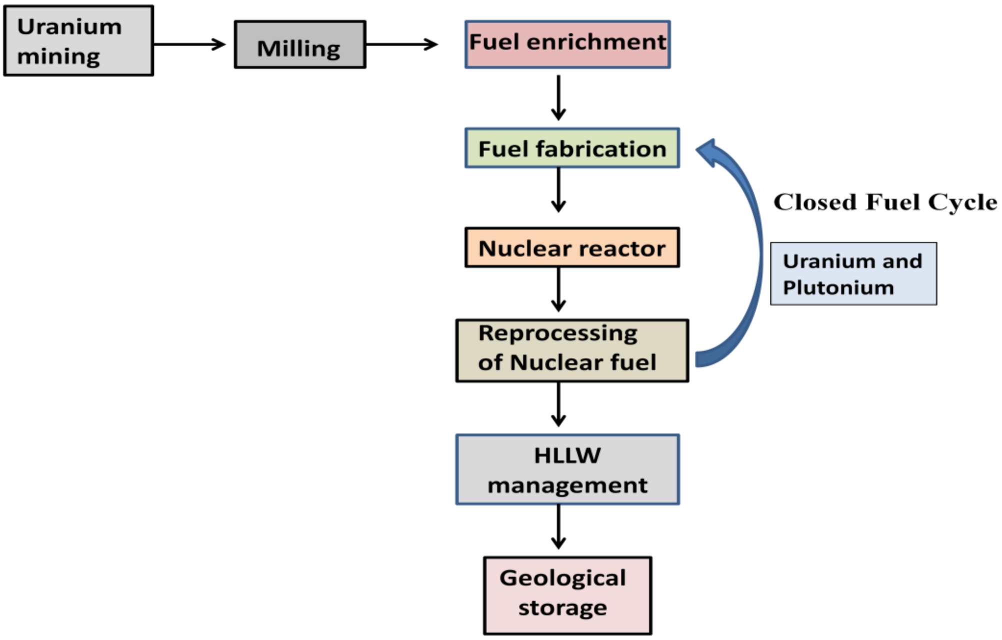

Figure 1.1. Schematic representation of Nuclear fuel cycle.

1.2. Reprocessing

The spent nuclear fuel discharged from the nuclear reactor is composed of fissile elements such as plutonium and depleted uranium and several other elements formed by the nuclear fission reaction, known as fission products. The spent nuclear fuel is therefore reprocessed for the recovery of these fissile elements, for the refabrication of nuclear fuel from the recovered U & Pu. Two different technologically viable methods that are available for reprocessing the spent nuclear fuel [7, 8]. These methods are based on (1)

Aqueous reprocessing and (2) Non-Aqueous reprocessing, partitioning of the chemical elements in the solution made by dissolution of the spent fuel

1.2.1. Aqueous Process

PUREX (Plutonium and Uranium Recovery by Extraction) process is an industrially well established, aqueous solvent extraction process. The PUREX process involves the dissolution of spent nuclear fuel in nitric acid followed by the selective extraction of uranium and plutonium into an organic solution composed of 1.1 M tri-n-butylphosphate (TBP) in n-dodecane (DD). The first step of PUREX process involves chopping of the fuel pins and dissolution of spent fuel in nitric acid followed by adjustment of the pH and valence of Pu suitable for co-extraction of uranium and plutonium. The second step involves the co-extraction of uranium and plutonium from the spent fuel solution by using 1.1 M TBP/*n*-DD, and subsequently the partitioning and recovery of uranium and plutonium from the loaded organic phase. The final step involves the purification and conversion of the recovered uranium and plutonium into their respective oxides. The ligand TBP can selectively extract uranium and plutonium from a nitric acid feed solution. The raffinate rejected after the extraction of uranium and plutonium constitutes as the High Level Liquid Waste (HLLW).

During partitioning, the organic phase containing U & Pu is equilibrated with an aqueous solution containing ferrous sulfamate or uranous nitrate stabilized with hydrazine, in order to selectively reduce Pu(IV) present in the organic phase into inextractable Pu(III). The resultant Pu(III) now contained in the organic is then stripped (or back extracted) into the aqueous phase. The uranium present in the organic phase is then recovered with dilute nitric acid, followed by concentration and precipitation of uranium as ammonium diuranate. The precipitate is then calcined to obtain uranium oxide. The recovered plutonium(III) product in the aqueous phase is once again purified by ion exchange method or by solvent extraction and then finally precipitated as plutonium oxalate. The precipitate is filtered and calcined to obtain plutonium oxide [9]. However, the undesirable limitation of the PUREX process is the chemical and radiolytic degradation of the solvent system and the generation of large volume of secondary waste [9]. The flammability of hydrocarbons employed in the PUREX process is also another disadvantage [9].

1.2.2. Non-aqueous Process

Non-aqueous reprocessing is a high temperature (pyrochemical) method. In non-aqueous reprocessing, an inorganic molten salt ($\simeq$ at 773 K) medium composed of chlorides of alkali or alkaline earth metals is used as the electrolyte for reprocessing the spent nuclear fuel. This method exploits the differences in the thermodynamic stabilities of the chlorides of various actinides and fission products for the dissolution of spent nuclear fuel in the inorganic molten salt medium. The different electrochemical methods viz., electrowinning, electrorefining, fluoride volatility and direct oxide reduction have been used in the non-aqueous reprocessing [10-13].

Non-aqueous reprocessing of spent oxide fuels by oxide-electrowinning is one of the promising methods for the recovery of actinides viz., uranium and plutonium as oxides [12]. In this oxide-electrowinning method, the oxides of uranium and plutonium are dissolved as chlorides or oxychlorides in the molten salt (LiCl-KCl) through the chlorination reaction. Subsequently UO_2 is electrodeposited by the electrolysis of uranium oxychloride present in the molten salt and plutonium is precipitated as PuO_2 by purging Cl_2 and O_2 mixture. Before performing uranium oxide deposition, pre-electrolysis of the molten salt is carried out in order to separate the noble metal fission products viz., ruthenium, rhodium and palladium etc. This is due to the close proximity of the reduction potential of UO_2^{2+} to UO_2 to those of the noble metal ions.

Electrorefining is another type of pyrochemical method, especially used for reprocessing of spent metallic fuels [14-16]. In the electrorefining process, chopped pieces of spent metal fuel are taken in the anode basket of the electrorefining cell containing LiCl-KCl eutectic salt ($\underset{\sim}{}$ 773 K) as electrolyte and liquid cadmium or stainless steel as the cathode. This process is depends on the differences in the thermodynamic stabilities of the chlorides of U, Pu and those of fission products. The electrorefining process involves different steps such as anodic dissolution of spent nuclear fuel containing fissile elements and fission products (FPs) in the molten salt electrolyte, selective deposition of uranium on a solid metal cathode and recovery of other actinide elements (Pu, Am, Np and Cm) in a molten cadmium cathode pool.

Pyrochemical methods have several advantages over the conventional PUREX process that include higher margin for criticality, less number of process steps, lower volumes of waste, lesser radiolytic degradation and relatively easier waste management. These methods also have some disadvantages viz., tedious purification of the feed salts need for sophisticated equipments, need for carrying out the process under inert atmosphere, high temperature of operation, much lower separation factors for actinides from fission products and the use of corrosive halides.

1.3. Room temperature ionic liquids

In the recent past, the idea of clean and green technology is being pursued in many an industry with an objective to develop of environmentally benign processes, that aims st minimizing the waste generation at source to a minimum acceptable level [17]. The idea of green technology includes the design of the environmentally safe chemical processes to minimize or to eliminate the use and generation of hazardous materials (eg. volatile organic compounds). The green chemistry protocols [18] for the chemical processes include the use of aqueous solvents, dense phase or supercritical fluids, immobilized solvents, ionic liquids (ILs), and solvent less processes [19]. Among these alternatives, room temperature ionic liquids are regarded as the most promising candidates for adapting to green chemistry/technology protocol due to their fascinating properties, viz., negligible vapour pressure, wide liquid range, high thermal stability and high solubility for organic species [20-24].

Room temperature ionic liquids (ILs) are organic compounds, composed entirely of dissociated ions. They exhibit a melting point ≤ 373 K [20-24]. ILs comprise of asymmetric and bulky organic cations such as tetra-alkylammonium, 1-alkyl-3-methylimidazolium, N-alkyl-N-methylpyrrolidinium, 1-alkylpyridinium and 4-alkylmorpholinium ions, along with an inorganic or poly nuclear organic anion that could be halides, dicyanamides, PF_6^-, BF_4^-, tosylates, triflates, bis(trifluoromethanesulfonyl)imide etc. Earle and Seddon [17, 25] estimated that there is a possibility of making 10^{12} ILs from the cations and anions cited in the literature. By knowing the properties of the reactants and products, it is possible to design these ILs for a specific application and in this context, the ILs are regarded as designer solvents and are often called as tailor-made ionic liquids [17, 25].

The history of ILs has been reviewed by Seddon and Wilkes [23, 24] and several reports are available in literature for the application of ILs. Gabriel synthesized the protic IL, ethanol ammonium nitrate having a melting point of 55^0C [26]. In 1914, Walden synthesized the first stable IL, namely ethyl ammonium nitrate with the melting of 12.5^0C [27]. ILs can be classified into three generations based on their properties [28, 29]. The first generation ILs are those that are made up of of bulky organic chlorides and $AlCl_3$. This type of ILs are again classified into three different sub-divisions based on the amount of $AlCl_3$ present in them, viz., acidic, basic and neutral chloroaluminates [30]. The important properties of the $AlCl_3$ based RTILs are that they exhibit low melting points, tunable viscosity and variable melt acidity [30]. However, the $AlCl_3$ based ILs have the disadvantage that, they require inert atmosphere for handling because they are hygroscopic.

The second generation of ILs are compounds that are stable towards moisture and these ILs contain anions like BF_4^-, PF_6^- etc. [31]. Among these, the BF_4^- containing ILs are miscible with water and those having PF_6^-, perfluoroalkylphosphate (FAP) and bis(trifluoromethanesulfonyl)imide (NTf_2^-) anions are hydrophobic. The third generation ILs are known as 'task specific ionic liquids (TSILs)' [32-37]. In this type of ILs, the cationic or anionic part of the IL is covalently tethered with an organic functional moiety. This type of ILs are also known as functionalized ionic liquid [32-37]. These TSILs exhibit the properties of both organic functionality and an IL. Another sub class of TSILs is known as ILs with strongly coordinating anion, wherein the anion of the IL itself acts as a functional moiety [38-41].

1.3.1. Synthesis of ILs

Several reports are available for the synthesis of ILs [42, 43]. Most of the ILs are synthesized by alkylation followed by an anion exchange reaction (metathesis) [42, 43]. The alkylation of organic compounds such as N-methylimidazole, pyridine, N-methylpyrrolidine or N-methylpiperidine using alkyl halides results in the formation of organic halides. The anion exchange of these organic halides with some metal salts results in the formation of ILs. The ILs, after the synthesis is usually purified by solvent extraction followed by charcoal treatment [44]. An illustration of the synthesis of IL is described in figure 1.2.

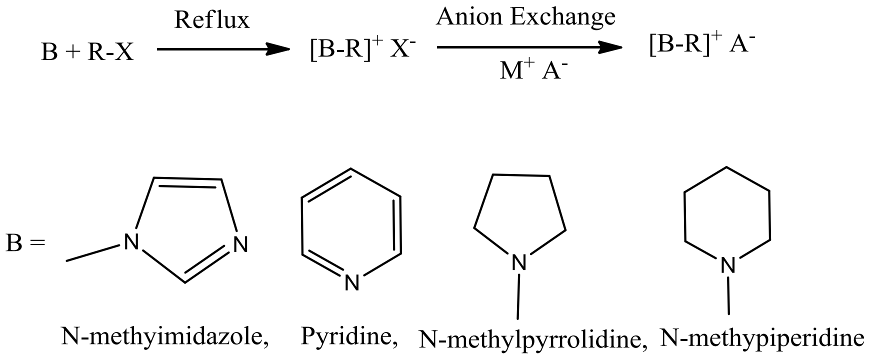

R = C_nH_{2n+1}, n = 2, 3 and so on.
X = Cl, Br, I etc.
M = H or Li or Na tec.
A = BF_4, PF_6, SCN, $N(CF_3SO_2)_2$

Figure 1.2. Synthetic procedure for the preparation of ILs

1.3.2. Properties of ILs

ILs have several fascinating properties, unique to the combination of a particular cation and anion. These include negligible vapor pressure at ambient temperatures, wide liquid range, high thermal stability, solubility of organic species, appreciable electrical conductivity and a wide electrochemical window (thermodynamic stability) [20-24]. Some properties of the ILs relevant to the present study are described below.

1.3.2.1. Melting Point

The melting points of ILs depend on the size and asymmetry of the ions, crystal structure, charge density of the ions, efficiency of hydrogen bonding and vander waal's interaction etc. [45-47]. The reduction in the melting points of ILs compared to that of inorganic salts is due to replacement of small inorganic cations with bulky asymmetric organic cations. For instance, melting point of NaCl is 803 ^oC and that of C_4mimCl is 67 ^oC. Most of the ILs containing halides (Cl, Br etc.) as anions exhibits melting temperature slightly higher than room temperature but ILs containing NTf_2^-, dicyanamides (ex. m.p. of $[C_3mPip][NTf_2]$ is 9 ^oC) as anions exists in liquid form at room temperature.

1.3.2.2. Density

The densities of most of the ILs are more than that of water and these values are in the range of 1.12 to 2.4 g cm^{-3} [45]. The densities of many ILs have been reported in the book 'Ionic liquid in synthesis' edited by Wasserscheid and Welton [45]. In the case of imidazolium based ILs, the density of an IL decreases with an increase in the chain length of the alkyl group attached to the imidazolium cation [48]. For quaternary ammonium based ILs with different anions such as $[NO_3]^-$, Cl^- and $[CH_3COO]^-$, the density is in the range of 0.8-0.9 [49]. The presence of impurities and water has an influence on their densities [49] to a large extent. However, their density is less influenced by temperature [45].

1.3.2.3. Viscosity

The viscosity of ILs is two to ten times greater than the viscosity of the conventional organic solvents due to the strong electrostatic and other interaction forces between the oppositely charged ions. For example, the viscosity of C_4mimPF_6 is ~430 cP, C_4mimBF_4 is ~154 cP, and $C_4mimNTf_2$ is ~52 cP at 25^{o}C [48, 50]. Since, viscosity of the IL is directly affected by electrostatic interaction, it is assumed that ILs composed of an ion with delocalization of charge shows lower viscosity [50-53]. Mcfarlane *et al.* [54] reported that ILs based on dicyanamide anions show very low viscosities, for instance, the viscosity of $C_4mimN(CN)_2$ is 21 cP at 25^{o}C. Seddon *et al.* [48] reported that the viscosity of 1-alkyl-3-methylimidazolium based ILs increases with increasing the alkyl chain length attached to imidazolium cation. Moreover, it was reported that quaternary ammonium based ILs are more viscous than imidazolium based ILs containing the same anion [55].

1.3.2.4. Vapour pressure

The pressure exerted by a vapour in equilibrium with its liquid phase is known as vapour pressure. Generally, ILs exhibit very low vapour pressure due to their ionic nature [56, 57]. Therefore, ILs have been recognized as non-volatile liquids at normal pressures and even at high temperatures. ILs have been suggested as electrolytic media for electrochemical applications due to their negligible vapour pressure. However, Zaitsau et al. reported that the vapor pressures of some alkyl-methylimidazolium bistriflamide ILs around 0.01 to 0.1 Pa at temperature above 457 K using Knudsen effusion method [56]. Seddon *et al.* [58] reported that many known ILs could be evaporated at 573 K under high vacuum.

1.3.2.5. Thermal stability

Most of the ILs have high thermal stability due to their ionic nature. [59]. For instance, Bonhote *et al.* [51] reported that $C_4mimNTf_2$ was stable up to 400°C and decomposes rapidly above 440°C. Ngo *et al.* [60] reported that the thermal stabilities of imidazolium based ILs increase with alkyl chain length attached to the imidazolium cation. Jagadeeswara Rao *et al.* [61] have investigated and reported the thermochemical properties of ILs such as $HbetNTf_2$, $C_3mPipNTf_2$ and $C_4mPyNTf_2$.

1.3.2.6. Electrical conductivity

The specific conductivities of ILs are in the range of 0.1-18 $mS.cm^{-1}$ due to the presence of cations and anions [62]. The conductivities of ILs are less than that of strong aqueous electrolytes. For example, the specific conductivity of 30 wt.% H_2SO_4 is about 730 $mS.cm^{-1}$ [63] which is more than one order of magnitude higher than that of ILs. However, the specific conductivities of ILs are adequate for using them as electrolyte for electrochemical applications (electrical conductivity of electrolytic medium either ionic liquid or organic/aqueous solvent containing supporting electrolyte could be recommended in the order of 1 mS.cm^{-1}). The conductivities of ILs can be influenced by viscosity, temperature and presence of impurities (mostly moisture). Galinski *et al.* [63] discussed the influence of viscosity and temperature on specific conductivities of ILs and Widegren *et al.* [64] reported that the conductivities of some 1-alkyl-3-methylimidazomium ILs in the presence of residual moisture. Oliver Zech *et al.* [65] reported that the electrical conductivities of some imidazolium based ILs with different anions at different temperatures.

1.3.2.7. Electrochemical window

The range of potential over which the IL/electrolyte is stable is called as its electrochemical window**.** The large electrochemical stability of ILs enables them to be used as electrolytes in electrochemical applications. ILs have wide electrochemical window, of the order of 5 to 6 V which is higher than that of aqueous electrolytes [66]. Some of the ILs have cathodic stability range upto -3.5 V and anodic stability upto 2.5 V. Basically, phosphonium and pyrrolidinium based ILs exhibit a larger electrochemical window than the immidazolium based ILs, especially ILs containing bis(trifluoromethanesulfonyl)imide as anion exhibit large electrochemical window as compared to others [69]. Maan Hayyan *et al.* [69] reported the electrochemical stabilities of some ILs with the combination of different cations and anions, they found that those ILs exhibit large electrochemical window and the nature of both cation and anion of these ILs affect the electrochemical window of them. Recently, Banerjee *et al.* [68] reported that electrochemical stabilities of some imdazolium based ILs are greatly affected by the structure of the anion. Reports are also available in the literature on electrochemical stabilities of ILs with different combinations of cations and anions [66-70].

1.3.3. Applications of RTILs

The ILs have potential applications in many areas of science and technology due to their fascinating properties. The applications of ILs are on the increase in various fields such as organic synthesis, electrochemistry, catalysis, analytical chemistry, separation technology, cellulose processing and biochemistry etc. [71].

Initially, the ILs were proposed as solvents to be used in organic synthesis by Fry and Pienta [72]. The applications of RTILs in the organic synthesis have also been discussed by Sethi *et al.* [73] as well as in the book 'Ionic Liquids in Organic Synthesis' edited by Malhotra [74]. Reviews on various applications of RTILs by Koel [75], applications of task specific ILs as catalysts authored by Geirnoth [34], electrodeposition of metals using ILs by Simka *et al.* [76] and applications of ILs in electrochemical sensors by Wei *et al.* [77] have been reported. Similarly, Davis *et al.* [32] and D. Han *et al*. [78] reported the applications of ILs in different areas of separation technology. In addition to academic research, ILs have also been used in several industrial applications. For instance, some reviews on the applications of ILs in the chemical industry have been reported by Plechkova and Seddon [67]. The industrial application of ILs as performance additives was reported by Weyershausen *et al.* [79]. The first attempt made of using ILs in industrial process was in BASIL (Biphasic Acid Scavening utilizing ILs) process by BASF. Moreover, Eastman operated an IL based plant for the synthesis of 2,5-dihdrofuran from 1996 to 2004 [67]. Several other applications of RTILs in various fields also have been reported in the literature [80-83].

1.3.4. The role of ILs in nuclear fuel industry

ILs are receiving an upsurge for their possible applications in the different stages of the nuclear fuel cycle. ILs are being studied for various applications in both aqueous and non-aqueous reprocessing.

In aqueous reprocessing, ILs have been used as diluent and extractant for solvent extraction. The replacement of molecular diluent (n-dodecane) with IL in solvent extraction process was introduced by Huddenston *et al.* [83] and Dietz and Dzielawa [84]. Dai *et al.* [85] reported that the extraction of strontium from aqueous medium by crown ether in an imidazolium based IL, Visser *et al.* [86] extensively studied the extraction of cesium and strontium from nitric acid medium in a solution containing various crown ethers in $[C_n mim][PF_6]$ (n = 4, 6, 8). Xie *et al.* [87] studied the extraction behaviour of uranium(VI) in malonamide using IL as diluent. Rama *et al.* [88] investigated the extraction of U(VI) in trialkylphosphates in IL. Alok *et al.* [89] reported the mutual separation of europium(III) and americium(III) using IL as diluent with acidic extractents.

Exploration on the "metal ion" specific extractions from aqueous solutions has urged the researchers to look at ILs as a potential and viable option. The organic functionalities that can perform specific applications are covalently tethered to the cationic or anionic parts of the ILs are known as functionalized ionic liquids (FILs) or task specific ionic liquids (TSILs). The presence of the functional group and ionic moieties in the resultant FIL is expected to show the properties of both organic functionality and IL. In this context, various studies have been reported in the recent past for the separation of actinides and fission products from a wide variety of acid feed solutions using FILs [36-38, 90-97].

1.3.5. ILs for non-aqueous reprocessing

In the past two decades, ILs have been extensively investigated as electrolytic medium for applications related to non-aqueous reprocessing of spent nuclear fuels [98-111]. The electrochemical studies of actinides and some other metal ions in chloroaluminate based ILs were reported few decades ago. Initially, the studies on electrochemistry of uranium in acidic and basic ($AlCl_3$ + N-(*n*-butyl)pyridinium chloride) chloroaluminate melt was reported by D’Oliieslanger *et al.* [98]. But these cholroaluminates showed less electrochemical window with poor cathodic stability [98, 99].

The second generation ILs especially bis(trifluoromethanesulfonyl)imide based ILs exhibited wide electrochemical window and large cathodic stability [100-108]. The spectroscopic and electrochemical behaviour of U(IV)-hexachloro complexes in $C_4mimNTf_2$ and $Bu_3MeNNTf_2$ (Bu_3MeN = tri-n-butylmethyl ammonium) was investigated by Nikitenko *et al.* [100] and reported that redox behaviour of U(IV) to uranium metallic form. Electrochemical behaviour of U(IV) dissolved as $U(NTf_2)_4$ in $MPPiNTf_2$ was studied by Rao *et al.* [105]. Some reports are available on the redox behavior U(VI) to U(IV) in various ILs [107, 110-113]. In the recent past, electrochemical studies on the behaviour of different metal ions in ILs containing molecular extractants has been reported [101-104, 116, 117]. In this context, Rama *et al.* [102, 103] extensively investigated the electrochemical behavior of U(VI) and Eu(III) in the presence of different extractants in IL.

The conventional liquid-liquid extraction procedures involve the extraction of a desired metal ion from the aqueous phase at a particular feed condition followed by stripping by using aqueous reagents. However, the extracted metal ion could also be electrodeposited as the metal oxide directly from the organic phase, provided the organic phase has a suitable electrochemical window and good conductivity. This method is known as extraction-electrodeposition (EX-EL) [112-117]. The EX-EL method has been employed for the recovery of valuable metals from aqueous solutions in two steps (i) the extraction of metal ions from acid feed solutions by using ILs containing an extractant in the organic phase (ii) the electrochemical recovery of extracted metal ions present in IL phase as metal or metal oxide by electrodeposition from the IL. Giridhar *et al.* [112]

reported that extraction of U(VI) and electrodeposition of uranium oxide from an imidazolium based IL. Recently, Matsumiya *et al.* [116] investigated the extraction and electrochemical behaviour of rare earth elements in IL using tributylphosphate. Murakami *et al.* [117] also studied the extraction and electrochemical behavior of rare earth elements in tetraoctylglycolamide (TODGA) present in IL.

Some of the key features of ILs that make them the potential candidates for nuclear fuel applications are; (i) selective extraction of a target metal by choosing an appropriate IL with a desirable combination of cation-anion, (ii) possible recovery of metals by electrodeposition in an IL, (iii) functionalization of ILs with a moiety to the given application , (iv) designing ILs with incinerable constituents, rendering them suitable for easy management of spent organic waste, (v) insignificant vapour pressure of ILs.

1.4. Objectives of the present study

The objective of the present study is to explore the possibility of using ILs for the separation and recovery of actinides and fission products from both aqueous and non-aqueous media. They are

(i) The oxide-electrowinning method involves the dissolution of spent oxide fuel in IL. During this process, the oxides of uranium, plutonium and fission products present in the spent nuclear fuel are converted to the corresponding oxychloride and chloride salts. Practical considerations of electrolysis demand the operation of cathodic reduction to be performed at high current density for quantitative recovery of uranium. Under such conditions, it is quite likely that the fission products present in the molten salt medium, albeit in low concentration, also undergo reduction or interfere in the electrochemical behaviour of UO_2^{2+}. In view of this, the electrochemical behaviour of UO_2^{2+} in 1-butyl-3-

methylimidazolium chloride (C_4mimCl) IL in the presence of fission products such as palladium(II), ruthenium(III) and europium(III) was investigated by using cyclic voltammetry. These fission products were chosen for electrochemical interference studies since they are formed in significant concentration during fission reaction and their reduction potentials are very close to the reduction potential of UO_2^{2+} to UO_2. Since the dissolution of uranium oxide such as U_3O_8 was quite slow during chlorination, an attempt has been made to dissolve U_3O_8 in the IL, C_4mimCl, in the presence of a small quantity of nitric acid and the uranyl species present in the resultant solution was characterized by UV-Visible, ATR-FTIR and Raman spectroscopy. The electrochemical behaviour of UO_2^{2+} present in the resultant solution was studied at glassy carbon electrode by cyclic voltammetry and chronopotentiometry to understand the feasibility of using the resultant solution for the recovery of uranium oxide.

(ii) The EXtraction-ELectrodeposition (EX-EL) approach has been proposed for the separation of the uranyl ion from nitric acid medium by a solvent phase containing tri-*n*-butyl phosphate (TBP) in IL, followed by electrodeposition of uranium oxide directly from the uranium(VI) extracted IL phase. However, the efficiency of electrodeposition was significantly low. To enhance the recovery or uranium oxide by electrodeposition, the electrochemical behaviour of $UO_2(NO_3)_2$ in a solution of TBP present in 1-butyl-3-methylimidazolium bis(trifluoromethylsulfonyl)imide (C_4mimNTf$_2$) IL was studied in the presence of chloride ion by adding C_4mimCl. It was expected that the presence of chloride ion in organic phase can decomplex uranyl ion (UO_2^{2+}) ion from TBP coordination, and favour underpotential reduction of UO_2^{2+}. The complexes formed in IL phase were characterized by UV-Visible, ATR-FTIR and Raman spectroscopy.

(iii) The solubility of uranyl nitrate in many ILs was invariably very low. For electrowinning applications, it was necessary to dissolve significant amount of uranium salt in IL that exhibits low viscosity also. In view of this, the dissolution of uranyl nitrate in IL containing dicyanamide anion was studied and the coordination and electrochemical behaviour of uranyl ion in IL was investigated by advanced spectroscopic and electrochemical techniques. Similarly to enhance the solubility of rare earth metals, the IL containing lanthanide specific ligands and neutral ligand-ionic liquid were prepared and electrochemical and coordination behaviour of lanthanide salts present in those ILs was investigated by voltammetry and FTIR spectroscopy.

(iv) The metallic fuel in a nuclear reactor is composed of an alloy of uranium and zirconium (5-10 wt.%). Non-aqueous electrorefining method was employed for the reprocessing of spent nuclear fuel in molten salt medium. In electrorefining process, U-Zr alloy was anodically dissolved into electrolytic medium and the uranium was recovered as metal on the cathode material from zirconium and fission products. To understand the feasibility of using ILs for reprocessing of spent metallic fuels, the anodic dissolution of U and Zr metals and electrochemical behaviour of U(IV) and Zr(IV) was studied in the room temperature ILs such as $C_4mPyNTf_2$ and $C_4mimNTf_2$.

The results obtained from these studies are reported in this thesis.

References

1. R.G. Cochran, E.E. Lewis, N. Tsoulfanidis, W.F. Miller, The nuclear fuel cycle: analysis and management, American Nuclear Society (1990).
2. S.A. Bhardwaj, Indian nuclear power programmed–Past, present and future, Sadhana 38 (2013) 775-794.
3. H.J. Bhabha, The role of atomic power in India and its immediate possibilities, Proc. of the international conference on the peaceful uses of atomic energy held in Geneva, 1 (1955) 103.
4. http://www.npcil.nic.in/main/AllProjectOperationDisplay.aspx
5. IGC news letter, volume 86, October 2010, page 3.
6. http://www.dae.gov.in/ni/nisep02/xx/kamini.htm
7. J.L. Swanson, “PUREX Process Flow sheets”, In: Science and Technology of Tributyl phosphate, Eds. W.W. Schulz, L.L. Burger, J.D. Navratil, K.P. Bender, CRC Press Inc. Boca Raton, (1984) p. 55.
8. A. Ramanujam, An introduction to the PUREX process, IANCAS 14 (1998) 11-20.
9. P.K. Dey, N.K. Bansal, Spent fuel reprocessing: A vital link in Indian nuclear power program, Nucl. Eng. Des. 236 (2006) 723-729.
10. A.V. Bychkov, O.V. Skiba, Review of non-aqueous nuclear fuel reprocessing and separation methods, Chemical Separation Technologies and Related Methods of Nuclear Waste Management (1999) 71-98.
11. C.C. Mcpheeters, R.D. Pierce, T.P. Mulcahey, Application of the pyrochemical process to recycle of actinides from LWR spent fuel, Prog. Nucl. Energ. 31 (1997) 175-186.
12. S. Vavilov, T. Kobayashi, M. Myochin, Principle and test experience of the RIAR's oxide pyro-process, J. Nucl. Sci. Technol. 41 (2004) 1018-1025.

13. J.J. Laidler, J.E. Battles, W.E. Miller, A.P. Ackerman, E.L. Carls, Development of pyroprocessing technology, Prog. Nucl. Energ. 31 (1997) 131-140.
14. V.B. Ivanov, O.V. Skiba, A.A. Mayershin, A.V. Bychkov, L.S. Demidova, P.T. Porodnov, Experimental, economical and ecological substantiation of fuel cycle based on pyroelectrochemical reprocessing and vibropac technology, In International conference on future nuclear systems, Challenge towards second nuclear era with advanced fuel cycles, Proceedings (1997).
15. T. Koyama, K. Kinosmta, T. Inoue, M. Ougier, R. Malmbeck, J. P. Glatz, L. Koch, Study of molten salt electrorefining of U-Pu-Zr alloy fuel, J. Nucl. Sci. Technol. 39 (2002) 765-768.
16. S.X. Li, T. Sofu, T.A. Johnson, D.V. Laug, Experimental observations on electrorefining spent nuclear fuel in molten LiCl-KCl/liquid cadmium system, J. New Mat. Electr. Sys. 3 (2000) 259-268.
17. J.D. Holbrey, K.R. Seddon, Ionic Liquids, Clean Products and Processes 1 (1999) 223- 236.
18. United Nations Environment Programme. Ozone Secretariat, Handbook for the Montreal protocol on substances that deplete the ozone layer, UNEP/Earthprint (2006).
19. J. Sherman, B. Chin, P.D. Huibers, R. Garcia-Valls, T.A. Hatton, Solvent replacement for green processing, Environmen. Health Perspect. 10 (1998) 253-236.
20. T. Welton, Room-temperature ionic liquids, Solvents for synthesis and catalysis, Chem. Rev. 99 (1999) 2071–2084.
21. P.V. Natalia, K.R. Seddon, Applications of ionic liquids in the chemical industry, Chem. Soc. Rev. 37 (2008) 123–150.

22. M. Freemantle, An introduction to ionic liquids, RSC Publishing (2010).

23. K.R. Seddon, Ionic liquids: A taste of the future, Nat. Mater. 2 (2003) 363–365.

24. J.S. Wilkes, A short history of ionic liquids-from molten salts to neoteric solvents, Green Chem. 4 (2002) 73–80.

25. M.J. Earle, K.R. Seddon, Ionic liquids. Green solvents for the future, Pure Appl. Chem. 72 (2000) 1391-1398.

26. S. Gabriel, J. Weiner, Ueber einige abkommlinge des propulamins, Eur. J. Inorg. Chem. 21 (1888) 2669-2679.

27. P. Walden, Bull. Acad. Imper. Sci. (St. Petersberg), (1914) 1800.

28. M. Smiglak, A. Metlen, R. D. Rogers, The second evolution of ionic liquids: From solvents and separations to advanced materials-energetic examples from the ionic liquid cookbook, Acc. Chem. Res. 40 (2007) 1182–1192.

29. W.L. Hough, M. Smiglak, H. Rodríguez, R.P. Swatloski, S.K. Spear, D.T. Daly, J. Pernak, J.E. Grisel, R.D. Carliss, M.D. Soutullo, J.H. Davis, The third evolution of ionic liquids: active pharmaceutical ingredients, New J. Chem. 31 (2007) 1429-1436.

30. J.S. Wilkes, J.A. Levisky, R.A. Wilkes, C.L. Hussey, Dialkylimidazolium chloroaluminate melts: a new class of room temperature ionic liquids for electrochemistry, spectroscopy and synthesis, Inorg. Chem. 21 (1982) 1263-1264.

31. J.S. Wilkes, M.J. Zaworotko, Air and water stable 1-ethyl-3-methylimidazolium based ionic liquids, J. Chem. Soc., Chem. Commun. 13 (1992) 965 - 967.

32. J.H. Davis Jr, Task-specific ionic liquids, Chem. Lett. 33 (2004) 1072.

33. C.C. Brasse, U. Englert, A. Salzer, H. Waffenschmidt, P. Wasserscheid, Ionic phosphine ligands with cobaltocenium backbone: Novel ligands for the highly

selective, biphasic, rhodium-catalyzed hydroformylation of 1-octene in ionic liquids, Organometallics 19 (2000) 3818 - 3823.

34. R. Giernoth, Task-Specific Ionic Liquids, Angew. Chem. Int. Ed. 49 (2010) 2834–2839.

35. I.L. Odinets, E.V. Sharova, O.I. Artyshin, K.A. Lyssenko, Y. Nelyubina, V. Myasoedova, V. Galina, N.P. Molochnikova, E.A. Zakharchenro, Novel class of functionalized ionic liquids with grafted CMPO-moieties for actinides and rare earth elements recovery, Dalton Trans. 39 (2010) 4170-4178.

36. H. Luo, S. Dai, P. V. Bonnesen, A.C. Buchanan, Separation of fission products based on ionic liquids: Task-specific ionic liquids containing an aza-crown ether fragment, J. alloys Compd. 418 (2006) 195–199.

37. P. Nockemann, B. Thijs, S. Pittois, J. Thoen, C. Glorieux, K.V. Hecke, L. Van Meervelt, B. Kirchner, K. Binemanns, Task specific ionic liquid for solubilising metal oxides, J. Phys. Chem. B 110 (2006) 20978-20992.

38. X. Sun, Y. Ji, L. Zhang, J. Chen, D. Li, Separation of cobalt and nickel using inner synergic extraction from bifunctional ionic liquid extractant (Bif-ILE), J. Hazard. Matter. 182 (2010) 447-452.

39. H. Mehdi, K. Binnemans, V. Hecke, L.V. Meervelt, P. Nockemann, Hydrophobic ionic liquids with strongly corodinating anions, Chem. Commun. (2010) 234-236.

40. Y. Hua-Ling, W. Wei, C. Hong-Min, C. Ji, Extraction mechanism of rare earths with bifuncional ionic liquids (Bif-ILs) [A336][CA-12]/[A336][CA-100] in nitrate medium, Chin. J. Anal. Chem. 39 (2011) 1561–1566.

41. X. Sun, Y. Ji, F. Hu, Bo. He, Ji. Chen, D. Li, The inner synergic effect of bifunctional ionic liquid extractant for solvent extraction, Talanta 81 (2010) 1877–1883.

42. A. Stark, K.R. Seddon, Ionic liquids, In: Kirk-Othmer Encyclopedia of Chemical Technology, John Wiley, New York, 26 (2007).
43. J.G. Huddleston, A.E. Visser, W.M. Reichert, H.D. Willauer, G.A. Broker, R.D. Rogers, Characterization and comparison of hydrophilic and hydrophobic room temperature ionic liquids incorporating the imidazolium cation, Green Chem. 3 (2001) 156–164.
44. T. Welton, Electrodeposition from Ionic Liquids, Edited by F. Endres, A.P. Abbott, D.R. MacFarlane (2008) 4468-4468.
45. P. Wasserscheid, E.T. Welton, Ionic Liquids in Synthesis. Wiley-VCH verlag GmbH & Co. KGaA, (2008).
46. H.L. Ngo, K. LeCompte, L. Hargens, A.B. McEwen, Thermal properties of imidazolium ionic liquids, Thermochim. Acta 357 (2000) 97 – 102.
47. Y. Song, L. Liu, X. Zhu, X. Wang, H. Jia, X. Xiao, H. Yu, X. Yang, Physicochemical properties of ionic liquids based on imidazolium/pyrrolidinium cations and maleate/phthalate anions, Solid State Ionics 179 (2008) 516-521.
48. K.R. Seddon, A. Stark, M.J. Torres, Viscosity and density of 1-alkyl-3-ethylimidazolium ionic liquids, Clean Solvents 819 (2002) 34-49.
49. J. Jacquemin, P. Husson, A. Padua, V. Majer, Density and viscosity of several pure and water-saturated ionic liquids, Green Chem. 8 (2006) 172-180.
50. H. okuda, K. Hayamizu, K. Ishii, M.A.B.H. Susan, M. Watanabe, Physicochemical properties and structures of room temperature ionic liquids. 2. Variation of alkyl chain length in imidazolium cation, J. Phys. Chem. B, 109 (2005) 6103-6110.
51. P. Bonhote, A.P. Duasm, B. Papageorgiou, K. Kalyanasundaram, M. Graetzel, Hydrophobic, highly conductive ambient-temperature molten salts, Inorg. Chem. 35 (1996) 1168-1178.

52. K.N. Marsh, J.A. Boxall, R. Lichtenthaler, Room temperature ionic liquids and their mixtures-a review, Fluid Phase Equilibr. 219 (2004) 93-98.

53. K.R. Seddon, A. Stark, M.J. Torres, Influence of chloride, water, and organic solvents on the physical properties of ionic liquids, Pure Appl. Chem. 72 (2001) 2275-2287.

54. D.R. MacFarlane, J. Golding, S. Forsyth, M. Forsyth, G.B. Deacon, Low viscosity ionic liquids based on organic salts of the dicyanamide anion, Chem. Commun. 16 (2001) 1430-1431.

55. J.P. Mikkola, P. Virtanen, R. Sjöholm, Aliquat 336 - A versatile and affordable cation source for an entirely new family of hydrophobic ionic liquids, Green Chem. 8 (2006) 250-255.

56. M. J. Earle, J.M.S.S. Esperança, M.A. Gilea, J.N.C. Lopes, L.P.N. Rebelo, J.W. Magee, K.R. Seddon, J.A. Widegren, The distillation and volatility of ionic liquids, Nature 439 (2006) 831.

57. D.H. Zaitsau, G.J. Kabo, A.A. Strechan, Y.U. Paulechka, A. Tschersich, S.P. Verevkin, A. Heintz, Experimental vapor pressures of 1-alkyl-3-methylimidazolium bis (trifluoromethylsulfonyl) imides and a correlation scheme for estimation of vaporization enthalpies of ionic liquids, J. Phys. Chem. A 110 (2006) 7303-7306.

58. J.D. Holbrey, K.R. Seddon, The phase behaviour of 1-alkyl-3-methylimidazolium tetrafluoroborates: Ionic liquids and ionic liquid crystals, J. Chem. Soc. Dalton Trans. 13 (1999) 2133 - 2139.

59. M.J. Earle, J.M. Esperança, M.A. Gilea, J.N.C. Lopes, L.P. Rebelo, J.W. Magee, K.R. seddon, J.A. Widegren, The distillation and volatility of ionic liquids, Nature 439 (2006) 831.

60. H.L. Ngo, K. LeCompte, L. Hargens, A. B. McEwen, Thermal properties of imidazolium ionic liquids, Thermochim. Acta 357 (2000) 97 – 102.

61. Ch. Jagadeeswara Rao, K.A. Venkatesan, B. V. R. Tata, K. Nagarajan, T. G. Srinivasan, P.R Vasudeva Rao, Radiation stability of some room temperature ionic liquids, Radiat. Phys. Chem. 80 (2011) 643-649.

62. M.G. Freire, P.J. Carvalho, A.M. Fernandes, I.M. Marrucho, A.J. Queimada, J.A. Coutinho, Surface tensions of imidazolium based ionic liquids: anion, cation, temperature and water effect, J. Colloid Interf. Sci. 314 (2007) 621-630.

63. M. Galinski, A. Lewandowski, I. Stepniak, Ionic liquids as electrolytes, Electrochim. Acta 51 (2006) 5567-5580.

64. J.A. Widegren, E.M. Saurer, K.N. Marsh, J.W. Magee, Electrolytic conductivity of four imidazolium-based room-temperature ionic liquids and the effect of a water impurity, J. Chem. Thermodyn. 37 (2005) 569-575.

65. O. Zech, A. Stoppa, R. Buchner, W. Kunz, The conductivity of imidazolium-based ionic liquids from (248 to 468) KB Variation of the anion, J. Chem. Eng. Data 55 (2010) 1774-1778.

66. S.P. Ong, O. Andreussi, Y. Wu, N. Marzari, G. Ceder, Electrochemical windows of room-temperature ionic liquids from molecular dynamics and density functional theory calculations, Chem. Mater. 23 (2011) 2979-2986.

67. N.V. Plechkova, K.R. Seddon, Applications of ionic liquids in the chemical industry, Chem. Soc. Rev. 37 (208) 123-150.

68. S. Kazemiabnavi, Z. Zhang, K. Thornton, S. Banerjee, Electrochemical stability window of imidazolium-based ionic liquids as electrolytes for lithium batteries, J. Phys. Chem. B 120 (2016) 5691-5702.

69. M. Hayyan, F.S. Mjalli, M.A. Hashim, I.M. AlNashef, T.X. Mei, Investigating the electrochemical windows of ionic liquids, Ind. Eng. Chem. Res. 19 (2013) 106-112.
70. P.A. Suarez, V.M. Selbach, J.E. Dullius, S, Einloft, C.M. Piatnicki, D.S. Azambuja, J. Dupont, Enlarged electrochemical window in dialkyl-imidazolium cation based room-temperature air and water-stable molten salts, Electrochim. Acta 42 (1997) 2533-2535.
71. M. Shukla, S. Saha, A comparative study of piperidinium and imidazolium based ionic liquids: thermal, spectroscopic and theoretical studies, INTECH Open Access Publisher (2013).
72. S.E. Fry, N.J. Pienta, Effects of molten salts on reactions. Nucleophilic aromatic substitution by halide ions in molten dodecyltributylphosphonium salts, J. Am. Chem. Soc. 107 (1985) 6399-6400.
73. A.R. Sethi, P. Smith, N. Srinivasan, T. Welton, Ionic liquids as solvents for organic synthesis, In: Green industrial applications of ionic liquids, Eds. R.D. Rogers, K.R. Seddon, S. Volkov, NATO science series, Kluwer Academic publishers, Netherlands, (2002).
74. S.V. Malhotra, ed., Ionic liquids in organic synthesis, American Chemical Society (2007).
75. M. Koel, Ionic liquids in chemical analysis, Crit. Rev. Anal. Chem. 35 (2005) 177-192.
76. W. Simka, D. Puszczyk, G. Nawrat, Electrodeposition of metals from non-aqueous solutions, Electrochim. Acta 54 (2009) 5307-5319.
77. D. Wei, A. Ivaska, Applications of ionic liquids in electrochemical sensors, Anal. Chim. Acta, 607 (2008) 126-135.

78. D. Han, K.H. Row, Recent applications of ionic liquids in separation technology, Molecules 15 (2010) 2405-2426.

79. B. Weyershausen, K. Lehmann, Industrial application of ionic liquids as performance additives, Green Chem. 7(2005)15-19.

80. T. Tsuda, C. L. Hussey, Electrochemical applications of room-temperature ionic liquids, Interface-Electrochemical Society 16 (2007) 42-49.

81. M. P. Marszałł, R. Kaliszan, Application of ionic liquids in liquid chromatography, Crit. Rev. Anal. Chem. 37 (2007) 127-140.

82. P. Kubisa, Application of ionic liquids as solvents for polymerization processes, Prog. Polym. Sci. 29 (2004) 3-12.

83. J.G. Huddleston, H.D. Willauer, R.P. Swatloski, A.E. Visser, R.D. Rogers, Room temperature ionic liquids as novel media for ‘clean’ liquid–liquid extraction, Chem. Commun. 16 (1998) 1765-1766.

84. M.L. Dietz, J.A. Dzielawa, Ion-exchange as a mode of cation transfer into room-temperature ionic liquids containing crown ethers: implications for the ‘greenness’ of ionic liquids as diluents in liquid–liquid extraction, Chem. Commun. 20 (2001) 2124-2125.

85. S. Dai, Y.H. Ju, C.E. Barnes, Solvent extraction of strontium nitrate by a crown ether using room-temperature ionic liquids, J. Chem. Soc. Dalton Trans. 1 (1999) 1201-1202.

86. A.E. Visser, R.P. Swatloski, W.M. Reichert, S.T. Griffin, R.D. Rogers, Traditional extractants in non-traditional solvents: Group 1 and 2 extractions by crown ethers in room temperature ionic liquids, Ind. Eng. Chem. Res. 39 (2000) 3596 - 3604.

87. Z.B. Xie, H.T. Kang, Z.S. Chen, S.H. Zhang, Z.G. Le, Liquid–liquid extraction of U (VI) using malonamide in room temperature ionic liquid, J. Radioanal. Nucl. Chem. 308 (2016) 573-578.

88. R. Rama, Alok Rout, K.A. Venkatesan, M.P. Antony, A. Suresh, Comparison in the solvent extraction behavior of uranium (VI) in some trialkyl phosphates in ionic liquid, Radiochim. Acta. 104 (2016) 865-872.

89. A. Rout, S. Karmakar, K.A. Venkatesan, T.G. Srinivasan, P.R. Vasudeva Rao, Room temperature ionic liquid diluent for the mutual separation of europium (III) from americium (III), Sep. Purif. Technol. 81 (2011) 109-115.

90. Alok Rout, K.A. Venkatesan, T.G. Srinivasan, P.R. Vasudeva Rao, Extraction behavior of actinides and fission products in amide functionalized ionic liquid, Sep. Purif. Technol. 97 (2012) 164-171.

91. Alok Rout, K.A. Venkatesan, T.G. Srinivasan, P.R. Vasudeva Rao, Unusual extraction of plutonium (IV) from uranium (VI) and americium (III) using phosphonate based task specific ionic liquid, Radiochim. Acta. 98 (2010) 459-466.

92. R. Rama, Alok Rout, K.A. Venkatesan, M.P. Antony, A novel phosphoramide task specific ionic liquid for the selective separation of plutonium (IV) from other actinides, Sep. Purif. Technol. 172 (2017) 7-15.

93. A. Sengupta, P.K. Mohapatra. M. Iqbal, J. Huskens, W.A. Verboom, Diglycolamide-functionalized task specific ionic liquid (TSIL) for actinide extraction: solvent extraction, thermodynamics and radiolytic stability studies, Sep. Purif. Technol. 118 (2013) 264-270.

94. P.K. Mohapatra, P. Kandwal, M. Iqbal, J. Huskens, M.S. Murali, W.A. Verboom, novel CMPO-functionalized task specific ionic liquid: synthesis, extraction and

spectroscopic investigations of actinide and lanthanide complexes, Dalton Trans. 42 (2013) 4343-4347.

95. M. Paramanik, D.R. Raut, A. Sengupta, S.K. Ghosh, P.K. Mohapatra, A trialkyl phosphine oxide functionalized task specific ionic liquid for actinide ion complexation: extraction and spectroscopic studies, RSC Adv.6 (2016) 19763-19767.

96. A. Ouadi, B. Gadenne, P. Hesemann, J.E. Moreau, I. Billard, C. Gaillard, S. Mekki, G. Moutiers, Task-Specific Ionic Liquids Bearing 2-Hydroxybenzylamine Units: Synthesis and Americium-Extraction Studies, Chem. Eur. J. 12 (2006) 3074– 3081.

97. A. Ouadi, O. Klimchuk, C. Gaillard, I. Billard, Solvent extraction of U(VI) by task specific ionic liquids bearing phosphoryl groups, Green Chem. 9 (2007) 1160–1162.

98. De Waele, L. Heerman, W.D.’ Olieslager, Potentiometric and spectroscopic study of uranium (IV)-uranium (III) in acidic $AlCl_3$-N-(*n*-BUTYL) pyridinium chloride melts, J. Less-Common Metals 122 (1983) 319-327.

99. J.P. Schoebrechts, B. Gilbert, Electrochemical and spectroscopic studies of neptunium in the aluminum chloride-1-n-butylpyridinium chloride melt at 40. degree. C, Inorg Chem. 24 (1985) 2105-2110.

100. S.I. Nikitenko, C. Cannes, C. Le Naour, P. Moisy, D. Trubert, Spectroscopic and electrochemical studies of U(IV)− hexachloro complexes in hydrophobic room-temperature ionic liquids [BuMeIm][Tf_2N] and [$MeBu_3N$][Tf_2N], Inorg. Chem. 44 (2005) 9497-9505.

101. Y. Pan, C. L. Hussey, Electrochemical and Spectroscopic Investigation of Ln^{3+} (Ln= Sm, Eu, and Yb) solvation in bis(trifluoromethylsulfonyl) imide-based ionic

liquids and coordination by N, N, N′, N′-tetraoctyl-3-oxa-pentane diamide (TODGA) and chloride, Inorg. Chem. 52 (2013) 3241-3252.

102. R. Rama, Alok Rout, K.A. Venkatesan, M.P. Antony, P.R. Vasudeva Rao, Electrochemical behavior of Eu(III) in imidazolium ionic liquid containing tri-*n*-butyl phosphate and N, N-dihexyloctanamide ligands, J. Electroanal. Chem. 757 (2015) 36-43.
103. R. Rama, A. Rout, K.A. Venkatesan, M.P. Antony, Effect of alkyl chain length of tri-n-alkyl phosphate extractants on the electrochemical behaviour of U(VI) in ionic liquid medium, J. Electroanal. Chem. 771 (2016) 87-93.
104. A. Sengupta, M.S. Murali, P.K. Mohapatra, M. Iqbal, J. Huskens, W. Verboom, Extracted species of Np (IV) complex with diglycolamide functionalized task specific ionic liquid: diffusion, kinetics and thermodynamics by cyclic voltammetry, J. Radioanal. Nucl. Chem. 304 (2015) 563-570.
105. C.J. Rao, K.A. Venkatesan, K. Nagarajan, T.G. Srinivasan, P.V. Rao, Electrodeposition of metallic uranium at near ambient conditions from room temperature ionic liquid, J. Nucl. Mat. 408 (2011) 25-29.
106. Ch. Jagadeeswara Rao, K. A. Venkatesan, K. Nagarajan, T.G. Srinivasan, P. R. Vasudeva Rao, Electrochemical behavior of europium(III) in N-butyl-N-methylpyrrolidinium bis(trifluoromethylsulfonyl)imide, Electrochem. Acta 54 (2009) 4718 – 4725.
107. J.W. Freiderich, E. Wanigasekara, X.G. Sun, R.A. Meisner, H.M. Meyer, H. Luo, L.H. Delmau, S. Dai, B.A. Moyer, Direct Electrodeposition of UO_2 from Uranyl bis(trifluoromethanesulfonyl) imide dissolved in 1-ethyl-3-methylimidazolium bis(trifluoromethanesulfonyl) imide room temperature ionic liquid system, Electrochim. Acta 115 (2014) 630-638.

108. R. Gupta, S.K. Gupta, J.S. Gamre, K.V. Lohithakshan, V. Natarajan, S.K. Aggarwal, Understanding the dynamics of Eu^{3+} ions in room temperature ionic liquids–electrochemical and time resolved fluorescence spectroscopy studies, J. Inorg. Chem. 1 (2015) 104-111.

109. M. Jayakumar, K.A. Venkatesan, T.G. Srinivasan, Electrochemical behavior of fission palladium in 1-butyl-3-methylimidazolium chloride, Electrochim. Acta 52 (2007) 7121-7127.

110. B. Joseph, K.A.Venkatesan, K. Nagarajan, P.R. Vasudeva Rao, Electrowinning of UO_2 from Ionic Liquid Medium, Sep. Sci. Technol. 48 (2013) 2506–2511.

111. P. Giridhar, K.A. Venkatesan, T.G. Srinivasan, P.R. Vasudeva Rao, Electrochemical behavior of uranium(VI) in 1-butyl-3-methylimidazolium chloride and thermal characterization of uranium oxide deposit, Electrochim. Acta 52 (2007) 3006-3012.

112. P. Giridhar, K.A. Venkatesan, S. Subramaniam, T.G. Srinivasan, P.V. Rao, Extraction of uranium (VI) by 1.1 M tri-*n*-butylphosphate/ionic liquid and the feasibility of recovery by direct electrodeposition from organic phase, J. Alloys Comp. 448 (2008) 104-108.

113. N. Asanuma, M. Harada, Y. Yasuike, M. Nogami, K. Suzuki, Y. Ikeda, Electrochemical properties of uranyl ion in ionic liquids as media for pyrochemical reprocessing, J. Nucl. Sci. Technol. 44 (2007) 368-372.

114. P. Giridhar, K.A. Venkatesan, T.G. Srinivasan, P.R. Vasudeva Rao, Extraction of fission palladium by Aliquat 336 and electrochemical studies on direct recovery from ionic liquid phase, Hydrometallurgy 81 (2006) 30-39.

115. R. Kumaresan, Rakesh Jain, K.A. Venkatesan, M.P. Antony, B.M. Bhanage, Extraction and electrochemical behavior of fission palladium in room-temperature ionic liquid, J. Radioanal. Nucl. Chem. 303 (2015) 1047-1052.
116. M. Matsumiya, Y. Kikuchi, T. Yamada, S. Kawakami, Extraction of rare earth ions by tri-n-butylphosphate/phosphonium ionic liquids and the feasibility of recovery by direct electrodeposition, Sep. Purif. Technol.130 (2014) 91-101.
117. S. Murakami, M. Matsumiya, T. Yamada, K. Tsunashima, Extraction of Pr(III), Nd(III), and Dy(III) from HTFSA aqueous solution by TODGA/phosphonium-based ionic liquids, Solvent Extr. Ion Exc. 34 (2016) 172-187.

Chapter 2

Chapter 2: Experimental techniques, equipment, facilities and instrumentation

This chapter describes experimental procedures involved in the electrochemical studies and spectroscopic investigation of some actinides and fission products. The synthesis of room temperature ionic liquids (ILs) used in the present study have been described in this chapter. Methods and materials employed for the electrochemical and spectroscopic studies as well as the details of the instruments used have been described here. Basic principles behind the voltammetric techniques viz., cyclic voltammetry, chronoamperometry and chronopotentiometry have also been explained.

2.1. Chemicals and reagents

All the chemicals and reagents used in this study were of analytical grade and were used "as received" unless otherwise mentioned.

1-Methylimidazole (Purity: 99%) was procured from M/s. Fluka, United Kingdom and it was used after distillation.

N-Methylpyrrolidine (Purity: > 97%) was procured from M/s. Fluka, United Kingdom and it was used after distillation.

TBP (Purity: > 99%) was obtained from M/s. Sigma Aldrich, USA / M/s. Merck, Germany. It was washed with dilute sodium carbonate solution (~0.2 M) followed by distilled water and then dried under vacuum before use.

DHOA was obtained from Heavy Water Board, Tuticorin, India.

1-Chlorobutane (Purity: > 99%) was procured from M/s. Sigma Aldrich, USA and it was purified by distillation.

1-Bromobutane (Purity: 99%) was procured from M/s. Merck, Germany / M/s SD Fine Chemical, India Limited.

$LiNTf_2$ (Bis(trifluoromethanesulfonyl)imide lithium salt) was procured from M/s Sigma Aldrich (> 99%), USA / M/s. Iolitec (>98%), Germany.

Bis(trifuoromethanesulfonyl)imide (80% aqueous solution) was procured from M/s. Iolitec, Germany.

Sodium nitrate (Purity: 99%) was obtained from M/s. Alfa Aesar, USA.

Acetonitrile (Purity: > 99%) was procured from M/s. Merck, Germany.

Anhydrous Zirconium (IV) chloride (99.9 %) was procured from M/s. Sigma Aldrich, USA.

Anhydrous palladium (II) chloride (99.9 %) was procured from M/s. Sigma Aldrich, USA.

Ruthenium chloride hydrate and Europium (III) chloride hexahydrate (99.99 %) were procured from M/s. Sigma Aldrich, USA.

Uranium oxychloride, uranyl nitrate and U_3O_8 were obtained from Nuclear Fuel Complex, India, and the uranium content was estimated by Davies and Grey method.

Sodium tetrafluoroborate ($NaBF_4(H_2O)_6$) (98%) and sodium dicyanamide ($Na(N(CN)_2(H_2O)_6)$ (> 98.0%) were procured from TCI chemicals, Japan.

Eu_2O_3, Nd_2O_3 and Dy_2O_3 were obtained from M/s. SD Fine Chemicals, India.

Glassy Carbon and Palladium wires were obtained from M/s. Johnson Matthey, UK.

Metallic uranium and zirconium were obtained from Nuclear Fuel Complex, Hyderabad, India.

$CaCl_2$ (Purity: ≥ 99.9%) was procured from M/s. Sigma Aldrich, USA.

Ethylacetate, Dichloromethane and Chloroform were obtained from M/s. Fischer Inorganics and Aromatics Limited, Chennai, India and they were used as such.

Concetrated acids HNO_3, HCl, $HClO_4$ (GR grade) were procured from M/s. Merck Specialities Private Limited, Mumbai, India

Sodium hydroxide (AR grade) was obtained from M/s. SD Fine Chemicals, India / M/s Sigma Aldrich, USA.

Phenolpthalein (Merck Specialities Private Limited, India) solution was prepared by dissolving ~ 500 mg of solid in 100 mL of 1:1 mixture of distilled water and methanol.

Sodium nitrite was obtained from M/s. SD Fine Chemicals, Mumbai, India.

2.2. Equipment

All the electrochemical experiments in the present work were carried out using an Autolab electrochemical system (model: PGSTAT-302N by Eco Chemie B.V, Netherlands) equipped with an IF 030 interface. It uses computer based software, namely, General Purpose Electrochemical System (GPES) version 4.9. This electrochemical cell had a single leak-tight glass container and all electrodes were placed in the same container. The glass assembly was kept in an oil bath maintained at a constant temperature ($\pm 0.1^{o}C$). The cell was purged with argon gas for one hour to drive away the moisture, if any, and kept under with argon atmosphere during electrochemical measurements.

A rotary evaporator (model: R-3000 from M/s. Buchi Laboratories Technique AG, Switzerland) was used for drying ILs samples at 353 K and to distill off volatile solvents under vacuum.

A glove box with argon atmosphere maintained at a positive pressure with respect to the ambient was used to preserve and handle air sensitive ILs. The argon gas in the glove box was purified by passing through a column containing molecular sieves and deoxo copper catalyst respectively in order to maintain the amount of oxygen and moisture below 10 ppm.

A vacuum oven (Model-VT-AP-11 from M/s. Technico) with digital temperature controler was used for drying the ILs prior to use. This oven was connected to a vacuum pump with a pirani guage and a pressure regulator. All the samples were dried initially by using this oven at the desired temperatures.

A Karl- Fischer Titrator (AT 36 from Spectralab) was used for the determination of the residual moisture. This titrator was initially calibrated by using a known quantity of water. Samples with known weight (typically about 1-100 mg) were taken for the determination of water content.

The UV-Visible-NIR spectra of all the samples were recorded by using Shimadzu UV-VIS-NIR spectrophotometer (UV-3600). Quartz cuvettes with 1 cm path length were used in all these spectroscopic measurements.

The Fourier transform infrared (FTIR) spectrum of the sample was recorded by using BRUKER TENSOR II FT-IR spectrometer equipped with an ATR (attenuated total reflectance) diamond crystal and deuterated-triglycine sulfate (DTGS) detector.

Raman spectra were recorded on an inVia Raman microscope system (Renishaw plc, Gloucestershire, UK) equipped with a Leica microscope using 785 nm excitation laser with a power of 300 mW and a charge couple devise (CCD) as the detector. A 20X objective lens was used and the laser exposure time was 10 s.

The X-ray diffraction patterns of the deposits were obtained by using Philips 1011 X-ray diffractometer (operating with 40 KV and 45 mA) with Cu Kα (1.5406 Å) radiation.

Field emission gun-scanning electron microscopy (FEG-SEM) images were obtained using TESCAN MIRA 3 model, Tescan, Czech Repuclic at 15 kV.

Energy dispersive X-ray spectral analysis (EDX) was carried out in order to examine elemental composition of the deposit.

Size of aggregates in the IL phase were measured using Zetasizer-3000 (nano ZS) DLS spectrometer (Malvern Instrument Company, UK) with a 5 mW He-Ne laser beam at a wavelength of 632.8 nm. The scattering angle for measurement was set at 90° in a cell of 4 mm path length. All these experiments were carried out at 298 + 10 K. Standard colloidal suspension (polystyrene latex) was used for the verification of the particle size measured by this DLS instrument.

All the luminescence spectra were recorded by using Edinburgh spectrofluorimeter FLS920 (Edinburgh instruments, UK) with a 450 W xenon lamp as the excitation source. Fused silica cuvette with a path length of 2 mm was used as the sample cell for recording these luminescence spectra. The band pass of 3 nm was set for both the excitation and emission monochromators. A long-wavelength pass filter (UV–39, Shimadzu) with a maximum and uniform transmittance (>85%) >400 nm was placed in front of the emission monochromator, to reduce the scatter of the incident beam into the emission monochromator. Spectra were recorded at room temperature with a 90° collection geometry.

2.3. Analytical procedures

2.3.1. Preparation of lanthanide tris[bis(trifluoromethanesulfonyl)imide ($Ln(NTf_2)_3$)

$Ln(NTf_2)_3$ (Ln = Eu, Nd and Dy) was prepared as per the procedure reported in reference [1]. 0.5 mol of Ln_2O_3 was added to an aqueous solution of 3 mol of $HNTf_2$ and the mixture was stirred at 343 K for six hours. $Ln(NTf_2)_3$ (1 mol) formed was dried in a rotary evaporator at 353 K.

2.4. Experimental procedures

The experimental procedures adapted for obtaining the results discussed in each chapter are presented here.

2.4.1. Electrochemical interference of some fission products during the electrodeposition of uranium oxide from 1-butyl-3-methylimidazolium chloride ionic liquid

2.4.1.1. Sample preparation for voltammetric studies

50 mM solutions each of Pd^{2+}, UO_2^{2+}, Ru^{3+} and Eu^{3+} in C_4mimCl were prepared by dissolving independently the anhydrous $PdCl_2$, UO_2Cl_2, $RuCl_3$ and $EuCl_3$, respectively in C_4mimCl at 353 K. The solution required for studying the combination of two different metal ions was prepared by mixing equal fractions (by weight basis) of the above the prepared solutions. Cyclic voltammograms pertaining to the redox reactions of UO_2^{2+}, Pd^{2+}, Eu^{3+} and Ru^{3+} in IL medium were recorded at glassy carbon working electrode (cylindrical SA=0.16 cm^2). A glassy carbon rod (cylindrical SA=0.25 cm^2) and Pd wire (cylindrical SA=0.10 cm^2) acted as counter and quasi-reference electrodes respectively.

2.4.2. Dissolution of U_3O_8 in 1-butyl-3-methylimidazolium chloride and spectroscopic and electrochemical behavior of U(VI) in the resultant solution

2.4.2.1. Dissolution studies of U_3O_8

All the dissolution studies were carried out under ambient conditions. The dissolution of U_3O_8 in C_4mimCl was performed by adding a desired quantity of U_3O_8 (of particle size 50 µm) in 10 g of C_4mimCl taken in a beaker. This beaker was kept in an oil bath and heated to 353 K. A required volume of 5 M nitric acid was added dropwise to the solution such that the HNO_3 : U ratio was either 4 : 1 or 6 : 1 or 8 : 1. The solution was stirred by magnetic stirrer until U_3O_8 was completely dissolved (based on uranium analysis in the solution) to give a clear solution. For all the spectroscopic measurements the C_4mimCl samples were dried under vacuum at 373 K.

2.4.2.2. Sample preparation for spectroscopic measurements

The ILs C_4mimNTf$_2$ and C_4mimCl were dried at 373 K under vacuum for 24 h before use. Uranyl nitrate in C_4mimNTf$_2$ was prepared by dissolving the required quantity of $UO_2(NO_3)_2(H_2O)_{6\text{–}7}$ in C_4mimNTf$_2$ containing C_4mimCl, such that the mole ratio of Cl : U was varied from 0 : 1 to 6 : 1. The solution obtained after dissolution was heated to 353 K under vacuum for about six hours and kept in an inert argon box few hours. The UV–Visible spectra of the sample were recorded at 298 K from 200 nm to 700 nm, using a quartz cell containing C_4mimNTf$_2$ + C_4mimCl in some cases as reference.

Since C_4mimCl was solid at room temperature, this could not be taken in a reference cell for recording UV–Visible absorption spectrum. Therefore, C_4mimCl was dissolved in acetonitrile and taken in the reference cell for recording the UV–Visible absorption spectrum. Similarly, an aliquot was taken from the dissolver solution i.e. U_3O_8 dissolved in C_4mimCl in the presence of nitric acid, and diluted with acetonitrile before recording the UV–Visible absorption spectrum of uranium.

After the UV–Visible measurements of all samples indicated above, few microlitres of each sample was placed on a diamond disk for ATR-FTIR analysis. The ATR-FTIR spectrum was recorded from 600 cm^{-1} to 4000 cm^{-1}. For each sample the data were acquired in about 16 scans with a resolution of 4 cm^{-1}. The acquired data was corrected from the background spectrum (without sample) and presented as ATR-FTIR spectrum of the sample. In each case, all the spectroscopic measurements were checked their reproducibility.

After dissolution of U_3O_8 (Section 2.5.2.1), an aliquot was taken from the solution for recording the Raman spectrum, using a macrosampling unit. In these cases ~2 mL of sample was taken in a vial (1 cm diameter) and spectra were recorded for 50 accumulations in order to achieve good signal to noise ratio. After the measurement, the spectrum was refined by correcting it for the background. The results obtained after these measurement were compared with that of C_4mimCl.

2.4.2.3. Voltammetric studies

The electrochemical behaviour of C_4mimCl, UO_2^{2+} (UO_2Cl_2 dissolved) and UO_2^{2+} (U_3O_8 dissolved in the presence of nitric acid) in C_4mimCl was investigated by cyclic voltammetric studies at glassy carbon working electrode (cylindrical SA = 0.16 cm^2). A glassy carbon rod (cylindrical SA =0.25 cm^2) and Pd wire (cylindrical SA =0.10 cm^2) acted as counter and quasi-reference electrodes respectively. The Cl^-/Cl_2 was aslo considered as internal reference for CV measurements.

2.4.3. Electrochemical Behavior of U(VI) in Imidazolium Ionic Liquid Medium Containing Tri-n-butyl Phosphate and Chloride Ion and Spectroscopic Characterization of Uranyl Species

2.4.3.1. Sample Preparation

The ILs, $C_4mimNTf_2$ and C_4mimCl were dried under vacuum in a rotary evaporator, at 373 K about 24 hours before use. The required quantity of $UO_2(NO_3)_2(H_2O)_{6-7}$ and TBP were added to $C_4mimNTf_2$ to prepare a solution of 80 mM uranyl nitrate + 160 mM TBP/ $C_4mimNTf_2$. The uranium concentration in IL was then estimated by ICP-AES measurements after destroying the organics by perchloric acid. Ultima C spectroanalyser (John Yvon, France) equipped with ICP excitation source was used in the present study. The required amount of C_4mimCl added to the IL solution to vary the mole ratio of U : NO_3 : TBP : Cl from 1 : 2 : 2 : 0 to 1 : 2 : 2 : 6. The solution thus prepared was dried in a rotary evaporator, at 373 K under vacuum for 24 hours and kept in an inert argon box.

2.4.3.2. Voltammetric studies

The U(VI) samples prepared at diffrent mole ratio of U : Cl, as mentioned in the previous section were investigated by cyclic voltammetric studies. A glassy carbon rod (cylindrical SA =0.16 cm^2) was used as working electrode. A glassy carbon rod (cylindrical SA= 0.25 cm^2) and palladium wire (cylindrical SA=0.10 cm^2) acted as counter and quasi-reference electrodes respectively during voltammetric measurements.

2.4.3.3. Spectroscopic Measurements

The UV-Visible spectra of the sample were recorded at 298 K from 350 nm to 550 nm, a quartz cell containing $C_4mimNTf_2$ used as reference. After the UV-Visible measurements, few microlitres of the sample was placed on a diamond disk of ATR for ATR-FTIR analysis. The ATR-FTIR spectrum was recorded from 600 cm^{-1} to 4000 cm^{-1} with the resolution of 4 cm^{-1}. For each sample the data were acquired in about 16 scans and the acquired data was corrected with the background spectrum ($C_4mimNTf_2$) and presented as differential ATR-FTIR spectrum of the sample. In all these cases, the spectrum was recorded at least three times in order to check the consistency and reproducibility of these results. The Raman spectrum of sample was recorded using a liquid macro-sampling unit. The IL samples (about 2 mL) were taken in a 1 cm diameter sealed vial and spectra were recorded for about 50 accumulations in order to obtain a good signal to noise ratio. After the measurement, the collected spectrum was refined by background correction and presented.

2.4.4. Coordination and electrochemical behavior of U(VI) in dicyanamide IL

2.4.4.1. Sample preparation for spectroscopic measurements

The samples for spectroscopic studies was prepared by adding the required quantity (in gram) of $UO_2(NO_3)_2(H_2O)_6$ and C_4mimDCA in C_4mimBF$_4$ such that the mole ratio of U : NO_3 : DCA was varied from 1 : 2 : 2 to 1 : 2 : 5 and the uncertainty in the composition was less than 5%. The uranium content in $UO_2(NO_3)_2(H_2O)_6$ was estimated by a standard procedure [2]. Based on this value the required quantity of $UO_2(NO_3)_2(H_2O)_6$ was added in order to obtain the requisite mole ratio of U : DCA. The solution was dried in a rotary evaporator for about ten hours at 343 K under vacuum to remove the traces of moisture. The water content present in the IL was estimated (Karl Fischer method) to be < 0.5 wt%. The structures of the ILs are shown in Fig. 4.9.

2.4.4.2. Voltammteric and spectroscopic studies of U(VI) in dicyanamide ILs

Uranyl nitrate added to C_4mImDCA and C_4mPyDCA under inert atmosphere at room temperature and kept the solution under ultrasonication for about 30 min. The solution obtained after complete dissolution was used for spectroscopic and electrochemical measurements in this study. A glassy carbon rod (cylindrical SA=0.3 cm^2) was used as working electrode. A glassy carbon rod (cylindrical SA=0.5 cm^2) and Pd wire (cylindrical SA=0.10 cm^2) acted as counter and quasi-reference electrodes respectively during voltammetric studies.

2.4.5. Electrochemical behavior of zirconium(IV) in 1-butyl-3-methylimidazolium bis(trifluoromethylsulfonyl) imide IL

2.4.5.1. Voltammetric and electrodeposition studies

A solution of Zr(IV) (30 mM) in $C_4mimNTf_2$ was prepared by dissolving anhydrous $ZrCl_4$ in $C_4mimNTf_2$, under constant stirring at room temperature. Voltammetric studies were carried out in a temperature range 353–383 K. A glassy carbon rod (cylindrical SA = 0.16 cm^2) was used as working electrode. A glassy carbon rod (cylindrical SA = 0.25 cm^2) and Pd wire (cylindrical SA=0.10 cm^2) acted as counter and quasi-reference electrodes, respectively. For open circuit potential measurements, zirconium metal rod (cylindrical SA = 0.32 cm^2) was used as working electrode. Electrodeposition was conducted on glassy carbon working electrode under inert atmosphere, with glassy carbon acted as counter electrode and palladium wire acted as quasi-reference electrode. After deposition, the electrode was washed extensively with acetone and deionized water before subjecting it for thermal analysis and surface morphology.

2.4.5.2. Sample preparation for SEM-EDX and XRD measurement

Sample for SEM-EDX and XRD measurement was prepared by electrodepositing zirconium metal on a glassy carbon substrate (cylindrical SA=0.25 cm^2) and Pd wire (cylindrical SA=0.10 cm^2) acted as counter and quasi-reference electrodes, respectively. A solution of Zr(IV) (30 mM) in $C_4mimNTf_2$ was prepared by dissolving anhydrous $ZrCl_4$ in $C_4mimNTf_2$, under constant stirring at room temperature. To obtain this deposit, electrolysis of Zr(IV) in $C_4mimNTf_2$ was carried out for about 1 hour at glassy carbon working electrode at -1.7 V (Vs Pd). The deposit was washed with moisture-free acetone and dried in air. The zirconium deposit present on the glassy carbon substrate was subjected to SEM-EDX analysis. For XRD measurements, the electrodeposited sample was removed and smeared on an aluminium sample holder before recording.

2.4.6. Anodic Dissolution of Uranium and Zirconium Metals and Electrochemical Behavior of U(IV) and Zr(IV) in IL

2.4.6.1. Linear sweep voltammetry of uranium and zirconium

The metallic uranium or zirconium was used as the working electrode for recording linear sweep voltammograms as well as for the anodic dissolution of uranium or zirconium in IL $C_4MPyNTf_2$ in presence and absence of $HNTf_2$. A glassy carbon rod (cylindrical SA = 0.55 cm^2) and palladium wire (cylindrical SA = 0.10 cm^2) were used as counter and quasi-reference electrodes, respectively.

2.4.6.2. Anodic dissolution of metallic uranium and zirconium

The anodic dissolution of uranium and zirconium in $C_4MPyNTf_2$ in the presence and absence of $HNTf_2$ was carried out by applying the required anodic potential, to the uranium or zirconium working electrode (0.4 cm^2), which was immersed in IL medium for about 2 hours. For dissolving uranium, an anodic potential of 1.5 V was applied to the working electrode, and for dissolving zirconium an anodic potential of 0.5 V was applied. After dissolution, the solution was dried at 353 K for 24 hours under vacuum in a rotary evaporator, and then it was subjected to voltammetric measurements. An aliquot was taken from this solution in order to determine the concentration of uranium and zirconium in the aliquot. The aliquot was added to an excess of perchloric acid and evaporated to dryness. The dried product thus obtained was redissolved in dilute nitric acid and the amount of uranium and zirconium present in the solution was determined by inductively coupled plasma - optical emission spectroscopy (ICP-OES).

2.4.6.3. Sample preparation for spectroscopic measurements of U(IV) samples

The solution obtained after the anodic dissolution of metallic uranium was dried at 353 K for about 24 hours under vacuum and kept in an inert argon box for few hours before recording the visible absorption spectrum. The solution containing uranium was placed in a quartz cell and the visible absorption spectrum was recorded from 400 nm to 700 nm against $C_4MPyNTf_2$ as a reference. In another sample, the required quantity of C_4MPyCl was added to the solution of $C_4MPyNTf_2$ containing U(IV). The solution was dried at 353 K under vacuum in a rotary evaporator for about 24 hours and kept in an inert argon glove box. The visible spectrum of the solution was then recorded from 400 to 700 nm, against the solution of $C_4MPyNTf_2$ + C_4MPyCl as reference.

2.4.6.4. Voltammetric measurements

The solution obtained after anodic dissolution of uranium or zirconium was dried at 353 K under vacuum in a rotary evaporator for 24 hours. The water content present in the IL was determined to be < 0.5 wt%. The electrochemical cell consisted of a three electrode assembly in which a glassy carbon rod (cylindrical SA = 0.20 cm^2) acted as working electrode for recording cyclic voltammograms. A glassy carbon rod (cylindrical SA = 0.55 cm^2) and palladium wire (cylindrical SA = 0.10 cm^2) were used as counter and quasi-reference electrodes, respectively.

2.4.7. Electrochemical and spectroscopic investigation of Eu(III) in T2EHDGA–[C_4mim][NTf_2] mixture

2.4.7.1. Preparation of Eu (III) solutions in [C_4mim][NTf_2]

A solution of Eu(III) in [C_4mim][NTf_2] was prepared by dissolving the required quantity of $Eu(NTf_2)_3$ in [C_4mim][NTf_2] and heating the resulting mixture at 373 K for few hours under argon atmosphere [1]. The solution was dried in a rotary evaporator under vacuum at 353 K for ~24 h prior to electrochemical studies. For T2EHDGA containing IL solution, the required quantity of T2EHDGA and $Eu(NTf_2)_3$ were added to $[C_4mim][NTf_2]$. The resulting mixture was heated at 373 K for 3 h under argon atmosphere. The solution was then dried by rotary evaporation as discussed above.

2.4.7.2. Voltammetric studies

The solution of Eu(III) in the IL ($[C_4mim][NTf_2]$) phase containing various concentration of T2EHDGA was prepared. The concentration of Eu(III) in $[C_4mim][NTf_2]$ was 0.1 M and the concentration of T2EHDGA was fixed at 0.02 M in $[C_4mim][NTf_2]$ medium. Voltammetric studies were carried out in a temperature range 343 K to 373 K. A glassy carbon rod (cylindrical SA = 0.3 cm^2) was used as working electrode. A glassy carbon rod and Pd wire acted as counter and quasi-reference electrodes, respectively. All the redox potentials were referred against Fc/Fc^+ [7-9].

2.4.8. Voltammetric investigation of some lanthanides in neutral ligand-ionic liquid

2.4.8.1. Preparation of Neutral Ligand-Ionic Liquid (NLIL)

The NLIL was prepared by dissolving the required quantity of lanthanide tris[bis(trifluoromethylsulfonyl)imide] ($Ln(NTf_2)_3$) (Ln = Eu, Nd and Dy) in dihexyloctanamide (DHOA), which is kept under inert atmosphere. The beaker containg solution was kept in a sonicator for about one hour. The solution obtained after dissolution was heated to 353 K about six hours to drive away the moisture and kept in an inert argon box.

2.4.8.2. Dissolution of lanthanide oxides in DHOA…$HNTf_2$ adduct

For the dissolution of lanthanide oxides in ligand phase, the DHOA was equilibrated with $HNTf_2$ to obtain DHOA…$HNTf_2$ adduct in organic phase. The Ln_2O_3 were added to DHOA…$HNTf_2$ adduct with the mole ratio of Ln : $HNTf_2$ as 1 : 3. The solution was heated to 353 K and stirred the solution for about 2 hours. After the dissolution of Ln_2O_3 in DHOA, this solution was dried in a rotary evaporator at 343 K and the NLIL was stored in an inert argon atmosphere glove box. The structures of the chemicals used in present work are shown in figure 6.9.

2.4.8.3.Voltammetric studies

A solution of 100 mM Ln(III) in DHOA (NLIL) was prepared by the procedure mentioned in section (2.5.8.1). For voltammetric experiments a glassy carbon rod was used as working (cylindrical SA=0.20 cm^2) and counter (cylindrical SA=0.30 cm^2) electrode. A palladium wire (cylindrical SA=0.10 cm^2) acted as quasi-reference electrode.

2.5. Synthesis of Ionic liquids

2.5.1. 1-Butyl-3-methylimidazolium chloride (C_4mImCl)

1-Butyl-3-methylimidazolium chloride was prepared as described elsewhere [3] and the synthesis scheme is shown in figure 2.1. The preparation of 1-butyl-3-methylimidazolium chloride (C_4mImCl) involves refluxing a mixture of 1-methylimidazole with 1-chlorobutane in the mole ratio of 1:1.2 at 343 K for 72 hours. The resulting product (C_4mImCl) was washed a few times with ethyl acetate and acetonitrile. Then the solvent was removed by rotary evaporation and product was dried under vacuum at 353 K for more than 24 hours. A quantitative yield was obtained.

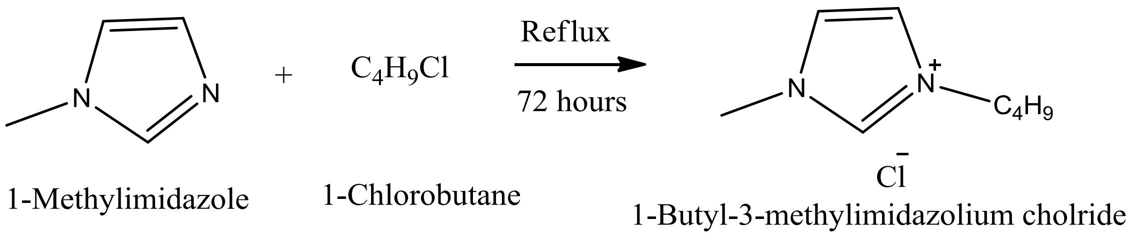

Fig. 2.1. Synthesis of 1-Butyl-3-methylimidazolium chloride

2.5.2. 1-Butyl-3-methylimidazolium bis(trifluoromethanesulfonyl)imide (C_4mImNTf$_2$)

The preparation involves a metathesis reaction between C_4mImCl and Lithium bis(trifluoromethanesulfonyl)imide ($Li^+\ ^-N(CF_3SO_2)_2$) in the mole ratio of 1:1 [3]. This reaction mixture was stirred for overnight at 298 K in water medium. After stirring, the bottom layer of IL was removed and washed several times with distilled water in order to remove unreacted precursors and LiCl salt. The final product was treated with charcoal and dried at 343 K under vacuum in order to remove the moisture [4]. Around 85% yield was obtained for each IL.

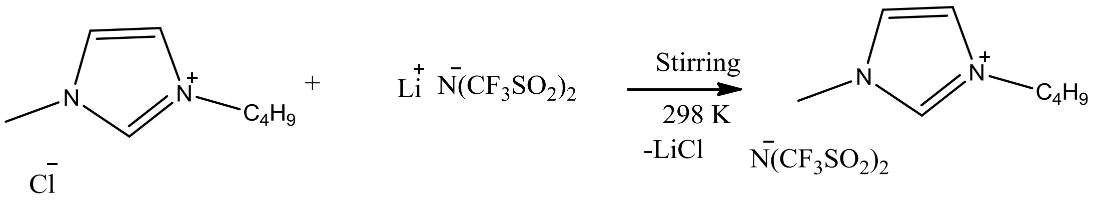

1-Butyl-3-methylimidazolium cholride

Lithium bis(trifluoromethanesulfonyl)imde

1-Butyl-3-methylimidazolium bis(trifluoromethanesulfonyl)imide

Fig. 2.2. Synthesis of 1-Butyl-3-methylimidazolium bis(trifluoromethanesulfonyl)imide

2.5.3. N-butyl N-methylpyrrolidinium chloride (C_4MPyCl)

N-Butyl-N-methylpyrrolidinium chloride was prepared as described elsewhere [5] and the synthetic procedure is depicted in figure 2.3. The preparation of N-butyl-N-methylpyrrolidinium chloride (C_4MPyCl) involves refluxing a mixture of N-methylpyrrolidine with 1-chlorobutane in the mole ratio of 1:1.2 at 343 K for 72 hours. The resulting product (C_4MPyCl) was washed a few times with ethyl acetate. The excess ethyl acetate was removed under vacuum at 353 K and the product was purified by recrystallization in acetonitrile medium. Yield of C_4MPyCl is 85%.

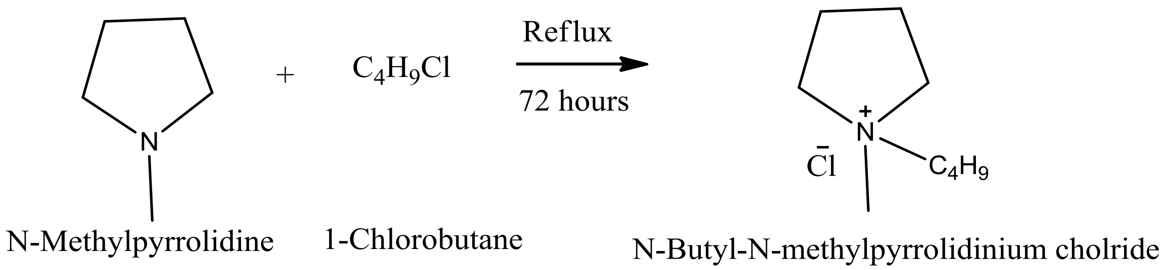

Fig. 2.3. Synthesis of N-butyl-N-methylpyrrolidinium chloride

2.5.4. N-butyl-N-methylpyrrolidinium bis(trifluoromethanesulfonyl)imide (C_4MPyNTf$_2$)

The synthesis involves a metathesis reaction between C_4MPyCl and Lithium bis(trifluoromethanesulfonyl)imide (Li^+ $^-N(CF_3SO_2)_2$) in the mole ratio of 1:1 [5]. This reaction mixture was stirred for 4 hours at 298 K in water medium. After stirring, the bottom layer of IL was washed several times with distilled water and the product was treated with charcoal. Then it was dried at 353 K under vacuum in order to remove the moisture. Around 90% yield was obtained for C_4MPyNTf$_2$.

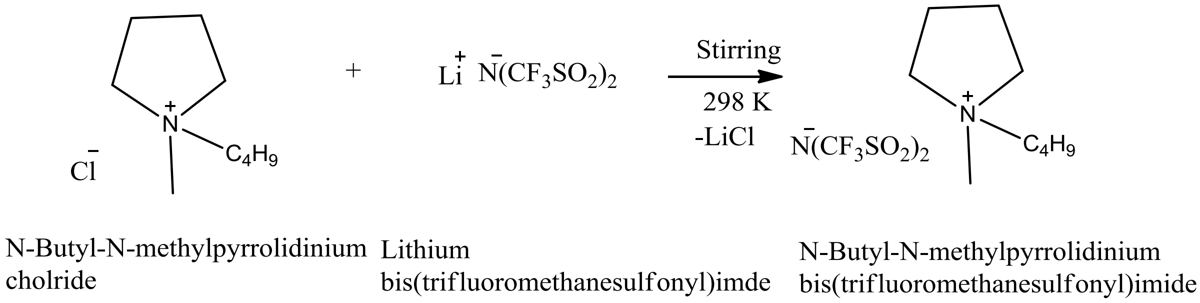

Fig. 2.4. Synthesis of N-butyl-N-methylpyrrolidinium bis(trifluoromethanesulfonyl)imide

2.5.5. 1-Butyl-3-methylimidazolium dicyanamide (C_4mImDCA)

The synthesis involves in the reaction between C_4mImCl and Sodium dicyanamide (Na^+ $^-N(CN)_2$) in the mole ratio of 1:1 [6]. This reaction mixture was stirred for 6 hours at 298 K in water medium. After stirring, the solution was dried at 353 K and the product was dissolved dry acetonitrile/acetone for removing NaCl by filtration. Then it was dried at 353 K in order to remove acetonitrile and the absence of Cl^- in the final product was ascertained by testing it with $AgNO_3$ solution.

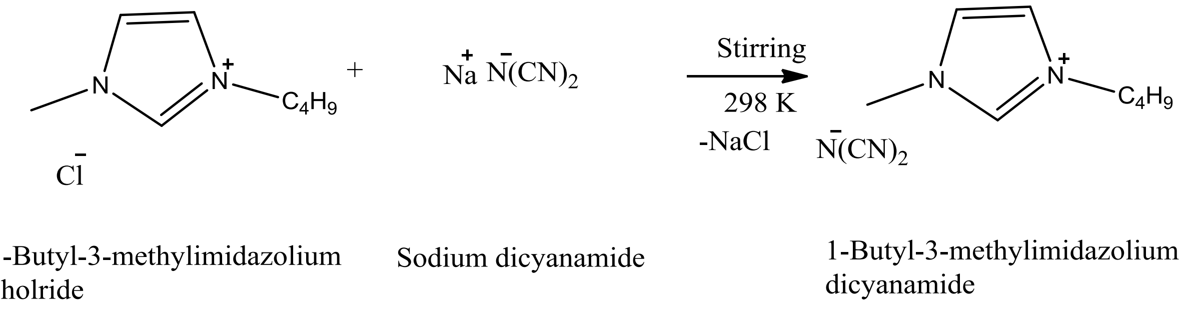

Fig. 2.5. Synthesis of 1-Butyl-3-methylimidazolium dicyanamide

2.5.6. 1-Butyl-3-methylpyrrolidinium dicyanamide (C_4mPyDCA)

The synthesis involves in the reaction between C_4mPyCl and Sodium dicyanamide (Na^+ $^-N(CN)_2$) in the mole ratio of 1:1. This reaction mixture was stirred for 6 hours at 298 K in water medium [6]. After stirring, the solution was dried at 353 K under vaccum and the product was dissolved dry acetonitrile/acetone for removing NaCl by filtration. Then it was dried at 353 K in order to remove acetonitrile and the absence of Cl^- in the final product was ascertained by testing it with $AgNO_3$ solution.

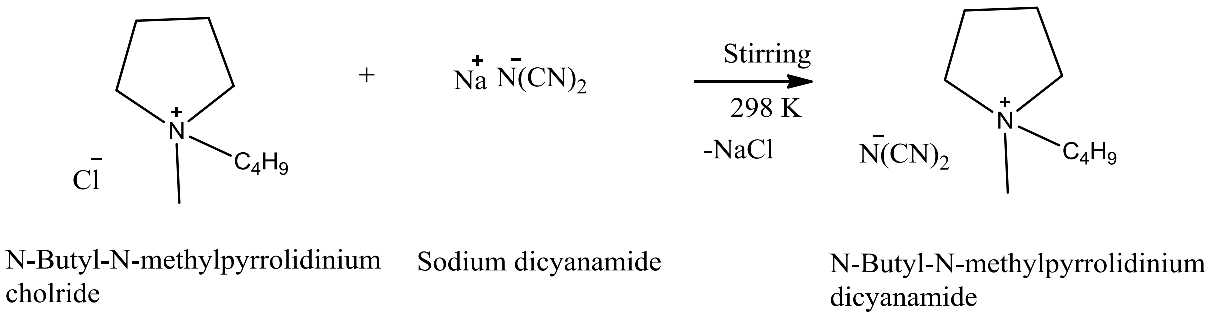

Fig. 2.6. Synthesis of N-butyl-N-methylpyrrolidinium dicyanamide

The basis behind the electrochemical techniques used in the present study was described in the Annexure.

References

1. A.I. Bhatt, I. May, V.A. Volkovich, D. Collison, M. Helliwell, I.B. Polovov, R.G. Lewin, Structural Characterization of a Lanthanum Bistriflimide Complex, La(N $(SO_2CF_3)_2)_3(H_2O)_3$, and an Investigation of La, Sm, and Eu Electrochemistry in a Room-Temperature Ionic Liquid, $[Me3N^nBu][N(SO_2CF_3)_2]$, Inorg. Chem. 44 (2005) 4934-4940.
2. W. Davies, W. Gray, A rapid and specific titrimetric method for the precise determination of uranium using iron (II) sulphate as reductant, Talanta 11 (1964) 1203–1211.
3. J.G. Huddleston, A.E. Visser, W.M. Reichert, H.D. Willauer, G.A. Broker, R.D. Rogers, Characterization and comparison of hydrophilic and hydrophobic room temperature ionic liquids incorporating the imidazolium cation, Green Chem. 3 (2001) 156–164.

4. P. Bonhote, A.P. Duasm, B. Papageorgiou, K. Kalyanasundaram, M. Graetzel, Hydrophobic, highly conductive ambient-temperature molten salts, Inorg. Chem. 35 (1996) 1168-1178.
5. D.R. MacFarlane, P. Meakin, J. Sun, N. Amini, M. Forsyth, Pyrrolidinium imides: a new family of molten salts and conductive plastic crystal phases, J. Phys. Chem. B 103 (1999) 4164-4170.
6. D.R. MacFarlane, S.A. Forsyth, J. Golding, G.B. Deacon, Ionic liquids based on imidazolium, ammonium and pyrrolidinium salts of the dicyanamide anion, Green Chem. 4 (2002) 444–448.
7. A. Lewandowski, L. Waligora, M. Galinski, Ferrocene as a reference redox couple for aprotic ionic liquids, Electroanalysis: An International Journal Devoted to Fundamental and Practical Aspects of Electroanalysis 21 (2009) 2221-2227.
8. N. G. Tsierkezos, Cyclic voltammetric studies of ferrocene in nonaqueous solvents in the temperature range from 248.15 to 298.15 K, Journal of Solution Chemistry 36 (2007) 289-302.
9. C.J. Rao, K.A. Venkatesan, K. Nagarajan, T.G. Srinivasan, Dissolution of uranium oxides and electrochemical behavior of U(VI) in task specific ionic liquid, Radiochimica acta 96 (2008) 403-409.

Chapter 3: Interference of some fission products and nitric acid during the electrochemical reduction of UO_2^{2+} in ionic liquid medium

Introduction

The high-temperature electrochemical methods, viz., oxide-electrowinning and electrorefining are popular for reprocessing of spent nuclear fuels [1-2]. The traditional oxide-electrowinning method involves the oxidative dissolution of spent oxide fuel in a high-temperature molten salt mixture composed of alkali and alkaline-earth metal chlorides, by chlorination reaction. In this process, the oxides of uranium, plutonium and fission products present in the spent nuclear fuel are converted to the corresponding oxychloride and chloride salts [3]. The uranium oxychloride present in the molten salt is then recovered as UO_2 by electrolysis and the plutonium remaining in the melt is precipitated as PuO_2 by passing a mixture of chlorine, oxygen and nitrogen gases. It is important to note that the operating temperature required for this process is usually above 873 K, depending upon the composition of the chosen alkali metal chloride eutectic.

In contrast to the high-temperature molten salts, the demployment of ILs in place of molten inorganic chlorides could facilitate a near ambient condition. In this context, Asanuma and co-workers [4] proposed a new approach for reprocessing the spent nuclear fuel by using IL. The proposed method involved oxidative dissolution of spent nuclear fuel in an IL by passing Cl_2 gas. The solution was then subjected electrolysis to reduce UO_2^{2+} to UO_2. However, these authors studied only the electrochemical behaviour of UO_2^{2+} in three different ILs viz., 1-butyl-3-methylimidazolium chloride (C_4mimCl), 1-butyl-3-methylimidazolium tetrafluoroborate (C_4mimBF_4) and 1-butyl-3-methylimidazolium nonafluorobutanesulfonate (C_4mimNfO) [5]. The electrochemical reduction of UO_2^{2+} in C_4mimNfO at -1.0 V (Vs Ag/AgCl) was reported to produce a uranium oxide deposit on a carbon electrode. In the recent past, Biju joseph *et al.* [6] reported the dissolution behaviour of uranium oxides, UO_3 and UO_2, in C_4mimCl medium by chlorination reaction at 353 K and the electrochemical behaviour of UO_2^{2+} in the resultant solution.

The dissolution behaviour of UO_2CO_3 in the neat and “wet” IL namely trimethyl-n-butylammonium bis(trifluoromethanesulfonyl)imide and its electrochemical behaviour of the resultant solution was examined by Pemberton *et al.* [7]. These authors reported that UO_2CO_3 can be dissolved to some extent in this IL. However, the rate of dissolution and quantity of uranium in this IL could be enhanced by the addition of a mixture of water and bis(trifluoromethanesulfonyl)imide (HTFSI). The dissolution of UO_2CO_3 increased from 5 mM to 50 mM with the addition of HTFSI and water. The UO_2^{2+} present in IL medium after dissolution underwent a two electron transfer reduction to uranium oxide at the working electrode. Similarly, Freiderich *et al.* [8] studied the direct electrodeposition of uranium oxide from a solution of uranyl bis(trifluoromethanesulfonyl)imide present in 1-ethyl-3-methylimidazolium bis(trifluoromethanesulfonyl)imide IL. These authors reported a two-step one-electron transfer reduction of UO_2^{2+} to uranium oxide in this IL.

Chapter 3

3.1. Electrochemical interference of some fission products during the electrodeposition of uranium oxide from ionic liquid medium

Uranium in molten choride salt medium exists in the form of $[UO_2Cl_4]^{2-}$ while the fission products exists as their chlorides or oxychlorides [9]. During electrolysis, $[UO_2Cl_4]^{2-}$ undergoes a two electron transfer reduction to uranium oxide (UO_2) at a particular reduction potential and is deposited at the cathode. Practical considerations of electrolysis demand that the cathodic reduction be performed at a high current density in order to ensure quantitative recovery of uranium. In this context, the potential of the cathode is usually kept at a higher negative potential, beyond the potential pertaining to the reduction of UO_2^{2+} to UO_2. Under such conditions, it is quite likely that the fission products present in the molten salt medium, albeit in low concentration, also would undergo reduction or would interfere with the electrochemical reactions of UO_2^{2+} [10]. This interference could be more severe when the reduction potential of a given fission product overlaps with that of the UO_2^{2+}. Knowledge of electrochemical series [10] indicates that the noble metals viz., Pd^{2+}, Rh^{3+} and Ru^{3+} that have a very similar reduction potential to that of UO_2^{2+} could interfere considerably in the electrochemical reactions of UO_2^{2+}. Since these noble metals are formed in significant quantities during nuclear their interference in the electrolytic process for the recovery of uranium would be rather significant. In addition, the one electron reduction potential of some trivalent lanthanide ions into their respective divalent ions (for e.g. Eu^{3+} to Eu^{2+}) [10] is very close to the reduction potential of UO_2^{2+} to UO_2 [10]. Therefore, these lanthanides also pose interfere in the recovery of uranium. However, there is no report available in literature on the studies related to the interference of fission products during electrodeposition of uranium oxide, neither in room temperature ILs nor in high temperature molten salts.

Therefore, in the present work is to the electrochemical behaviour of UO_2^{2+} in 1-butyl-3-methylimidazolium chloride (C_4mimCl) IL medium in the presence of fission products such as palladium(II), ruthenium(III) and europium(III), has been studied. The electrochemical behaviour of UO_2^{2+} both in the presence and absence of these elements has been studied by cyclic voltammetry.

The experimental procedure pertaining to the sample preparation has been discussed in the section 2.4.1 and synthesis of IL (C_4mimCl) has been detailed in the section 2.5.1.

3.1.1. Results and Discussions

3.1.1.1. Cyclic voltammetry of UO_2^{2+} in C_4mimCl

Figure 3.1 shows the cyclic voltammogram of C_4mimCl recorded at a glassy carbon working electrode at a scan rate of 100 mV.s^{-1} at 353 K. This IL, C_4mimCl, exhibits an electrochemical window of 2.5 V which is depicted in figure 3.1. This figure also shows the cyclic voltammogram pertaining to UO_2^{2+} recorded at glassy carbon working electrode at a scan rate of 100 mV.s^{-1} at 353 K. This voltammogram shows that the onset of reduction at -0.5 V (Vs Pd) resulting in a cathodic peak at the potential (E_p^{c1}) of -0.7 V (Vs Pd). A couple of oxidation waves (E_p^{a1} & E_p^{a2}) are also observed at -0.54 V (Vs Pd) and 0.30 V (Vs Pd) respectively during the scan reversal at -1.0 V. The reduction of UO_2^{2+} into UO_2 is responsible for the cathodic wave observed at -0.55 V (Vs Pd), as reported in our previous work [11]. A similar behaviour was also reported by others [4, 5]. However, the reason for the occurrence of a couple of oxidation waves is not clear. Perhaps there could be attributed to the adsorption of the reduced product UO_2 on to the glassy carbon working electrode. The first anodic wave (E_p^{a1}) could be due to the oxidation of UO_2 to UO_2^{2+} and E_p^{a2} could be due to the oxidation of adsorbed UO_2 to UO_2^{2+}. Such adsorption behaviour has been reported by some authors in other systems [12]. The difference in the value of $|E_p^{c1} – E_{p/2}^{c1}|$ is marginally higher (68 mV at 353 K) as compared to the value needed for a reversible (33.5 mV at 353 K) two-electron process [13, 14]. This shows that the reduction of UO_2^{2+} to UO_2 could be quasi-reversible.

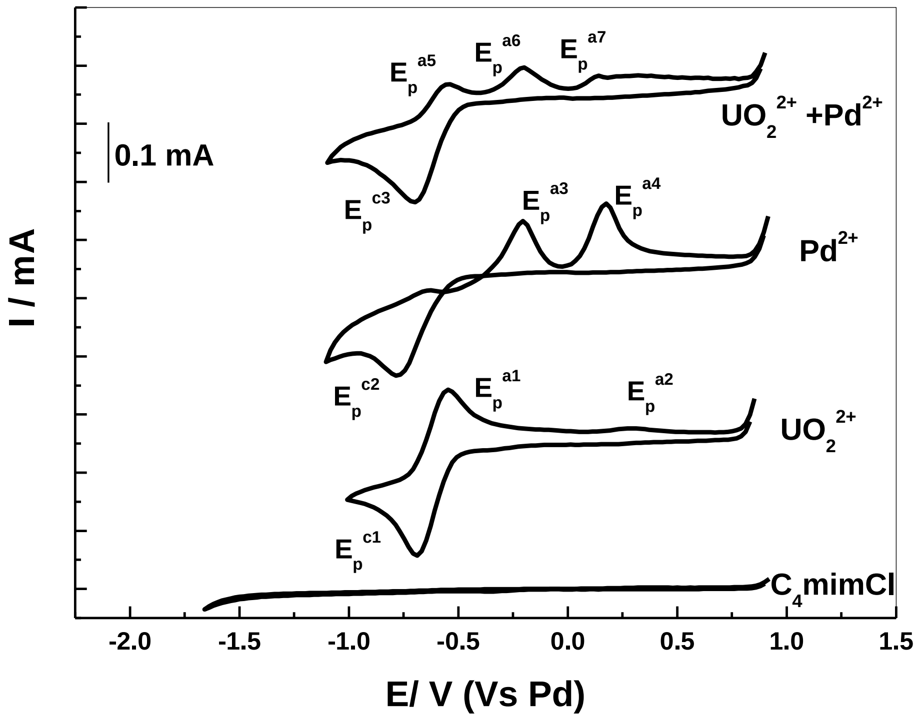

Figure 3.1. Cyclic voltammogram (CV) of neat C_4mimCl and its solutions containing 50 mM UO_2^{2+} or 50 mM Pd^{2+} or (25 mM UO_2^{2+} + 25 mM Pd^{2+}) recorded at a glassy carbon working electrode at a scan rate of 100 mV.s^{-1} at 353 K.

3.1.1.2. Cyclic voltammetry of Pd^{2+} in C_4mimCl

The cyclic voltammogram of Pd^{2+} recorded at a glassy carbon working electrode at a scan rate of 100 mV.s^{-1} at 353 K, is shown in figure 3.1. A prominent reduction wave (E_p^{c2}) observed at -0.78 V (Vs Pd) is due to the reduction of Pd^{2+} to Pd, and two oxidation waves are observed at -0.20 V (E_p^{a3}) and 0.17 V (E_p^{a4}), when the scan is reversed at -1.1 V. A nucleation loop is observed at -0.57 V. The difference between the values of E_p^{c1} and $E_{p/2}^{c1}$ is higher (42 mV at 353 K) than the value needed for a reversible (33.5 mV at 353 K) two-electron reduction [13, 14]. This shows that the reduction of Pd^{2+} to Pd could be quasi-reversible. These observations are similar to those reported in our previous work [15]. However, the cyclic voltammogram clearly indicates that the presence of Pd^{2+} in the IL could pose a strong interference during the electrochemical recovery of UO_2, due to the close proximity in the onset of reduction of both UO_2^{2+} to UO_2 and Pd^{2+} to Pd. Therefore, it would be interesting to study the electrochemical behaviour of a mixture containing both UO_2^{2+} and Pd^{2+} in C_4mimCl IL.

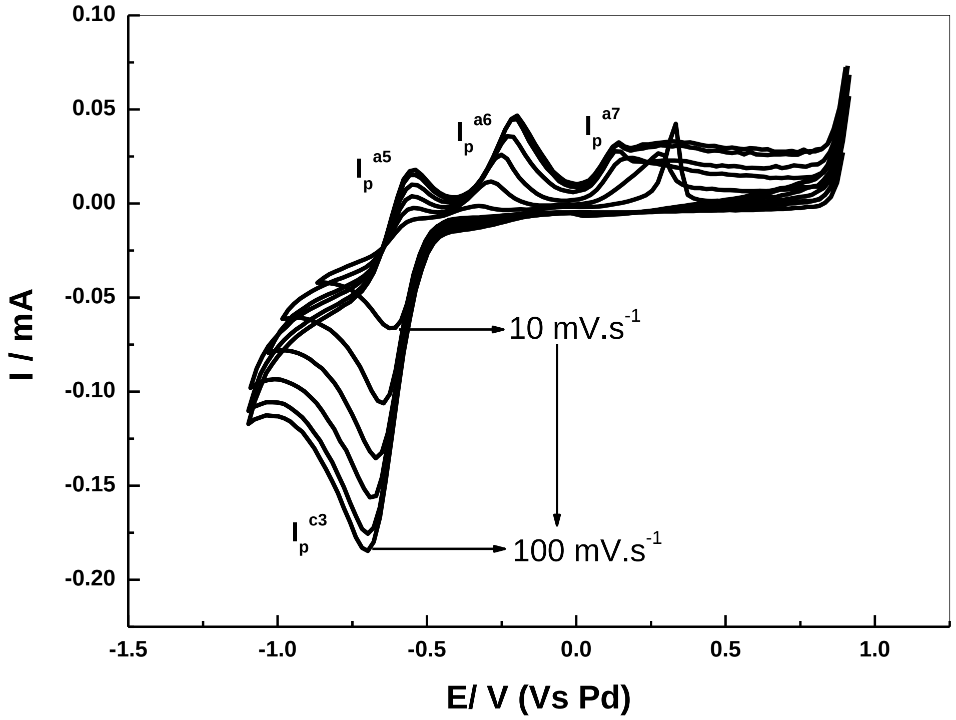

Figure 3.2. CV of a mixture (UO_2^{2+} + Pd^{2+}) in C_4mimCl recorded at a glassy carbon electrode at various scan rates. [UO_2^{2+}] = 25 mM, [Pd^{2+}] = 25 mM, T at 353 K.

The voltammogram of a solution containing 25 mM UO_2^{2+} + 25 mM Pd^{2+} in C_4mimCl recorded at a scan rate of 100 mV.s^{-1} at 353 K is shown in figure 3.1. The total concentration of metal ions (UO_2^{2+} and Pd^{2+}) in the mixture is 50 mM, which is equivalent to the individual concentration of either Pd^{2+} or UO_2^{2+} alone in C_4mimCl used in the other solution. The voltammogram perataining to the mixture shows the onset of cathodic wave at -0.5 V leading to a cathodic wave (E_p^{c3}) at -0.7 V. Three prominent anodic waves, E_p^{a5}, E_p^{a6} and E_p^{a7} are observed during the scan reversal. The magnitude of the cathodic peak current observed in the mixture (50 mM total) is similar to that of the cathodic current observed independently in Pd^{2+} (50 mM) and UO_2^{2+} (50 mM) solutions. However, the anodic current observed with the mixture is much lower than that observed in the individual solutions. A comparison of the relative position of anodic waves observed in the mixture with that of the individual solutions indicates that E_p^{a5} could be attributed to the oxidation of UO_2, while E_p^{a6} and E_p^{a7} could be due to the oxidation of the palladium deposit. Therefore, this study indicates that the presence of palladium in the IL is likely to interfere in the electrodeposition of uranium oxide.

3.1.1.3. Diffusion coefficients

Figure 3.2 shows the cyclic voltammogram of a mixture containing 25 mM UO_2^{2+} and 25 mM Pd^{2+} in C_4mimCl, recorded at different scan rates at 373 K. It could be seen that the cathodic peak current (I_p^{c3}) increases, while the peak potential (E_p^{c3}) is shifted cathodically with an increase in scan rate. This result shows that the reduction of UO_2^{2+} to UO_2 and Pd^{2+} to Pd in the mixture is not reversible. It also indicates that the reduction is not only controlled by the diffusion of the metal ions towards the working electrode but also by the transfer of electron across the electrode electrolyte interface suggesting a heterogeneous charge transfer kinetics. The charge transfer coefficient (α, $0.1 \leq \alpha \leq 0.9$) which is a measure of the symmetryof the barrier in a non-reversible electrode reaction can be determined from the magnitude of $\left| E_p^{c3} - E_{p/2}^{c3} \right|$ by using equation (3.1) [14].

$$|E_p^{c3} - E_{p/2}^{c3}| = 1.857RT/\alpha n_\alpha F \qquad (3.1)$$

Where n_α pertains to the number of electrns involved and F is the Faraday’s constant.

Using equation (3.1) the magnitude of αn_α was found to vary from 0.8 to 0.9 with the increase in scan rate from 10 $mV.s^{-1}$ to 100 $mV.s^{-1}$ at 353 K.

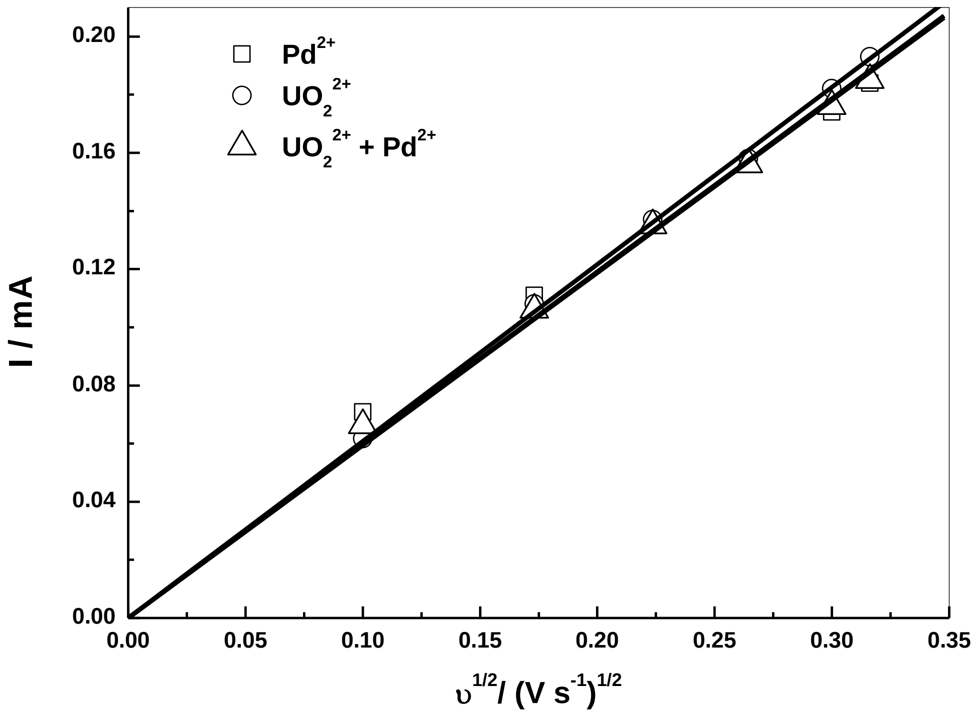

Figure 3.3. Plot of cathodic peak current against the square root of scan rate ($\upsilon^{1/2}$) pertaining to the reduction of UO_2^{2+}, Pd^{2+} and their mixture in C_4mimCl at 353 K.

The cathodic peak current (I_p^{c3}) observed in the combined system is related to scan rate, is given by equation (3.2).

$$I_p^{c3} = 0.496\ nFCAD^{1/2}\ ((\alpha n_\alpha)\ F\upsilon/RT)^{1/2} \tag{3.2}$$

where the electrode area (A) is 0.16 cm^2, the concentration (C) of metal ion is 0.05 mol.cm^{-3} (50 mM) and the number of electrons exchanged is 2. The concentration of the metal ion in equation (3.2) is taken as 50 mM, since both the reduction of Pd^{2+} and UO_2^{2+} are responsible for the observed cathodic peak current, (I_p^{c3}). Figure 3.3 shows the cathodic peak current (I_p^{c3}) plotted as a function of the square root of the scan rate ($\upsilon^{1/2}$). It can be seen that the cathodic peak current increases with $\upsilon^{1/2}$. Linear dependence of cathodic peak current with zero intercept indicates the validity of equation 3.2 and allows the determination of the diffusion coefficient. The diffusion coefficient of (UO_2^{2+} + Pd^{2+}) in the mixture was determined from the slope of the straight line shown in figure 3.3. The diffusion coefficient of the mixture (UO_2^{2+} + Pd^{2+}) is of the order 10^{-8} cm^2/s.

To compare the diffusion coefficient obtained in a mixture of cations with that obtained for the individual cations, the cyclic voltammogram of 50 mM UO_2^{2+} in C_4mimCl and 50 mM Pd^{2+} in C_4mimCl were recorded at different scan rate at 353 K. These results are shown in figure 3.4. The cathodic peak current obtained in these individual voltammograms was plotted as a function of scan rate in figure 3.3 for comparison. Linear dependence of cathodic peak current with zero-intercept in these cases also indicates the validity of equation (3.2). From the slope of this straight line, the individual diffusion coefficients of Pd^{2+} and UO_2^{2+} in C_4mimCl were determined and compared with the diffusion coefficient of the mixture UO_2^{2+} and Pd^{2+} in C_4mimCl. These values are presented in table 3.1. It can be seen that the values of all the diffusion coefficients are comparable and are of the order 10^{-8} cm^2/s. This shows that the presence of Pd^{2+} in the melt strongly interferes in the electrodeposition of UO_2. Tan *et al.* [23] reported a diffusion coefficient of 4.74 x 10^{-8} cm^2 s^{-1} for U(VI) in C_4mimCl at 367 K, which is in very close agreement with the value of 6.2 x 10^{-8} cm^2 s^{-1} obtained in the present study for the same IL at 353 K. Moreover, these authors [23] also determined the diffusion coefficients of U(VI) in C_4mimCl in the presence of a small amount of water that varied from 0.1 wt% to 5 wt%. It was reported that the diffusion coefficient increases from 4.74 x 10^{-8} cm^2 s^{-1} to 2.1 x 10^{-7} cm^2 s^{-1} with an increase in the water residue. The value of diffusion coefficient of 6.2 x 10^{-8} cm^2 s^{-1} obtained in the present study shows that the amount of water in the IL is insignificantly low (~0.1 wt.%).

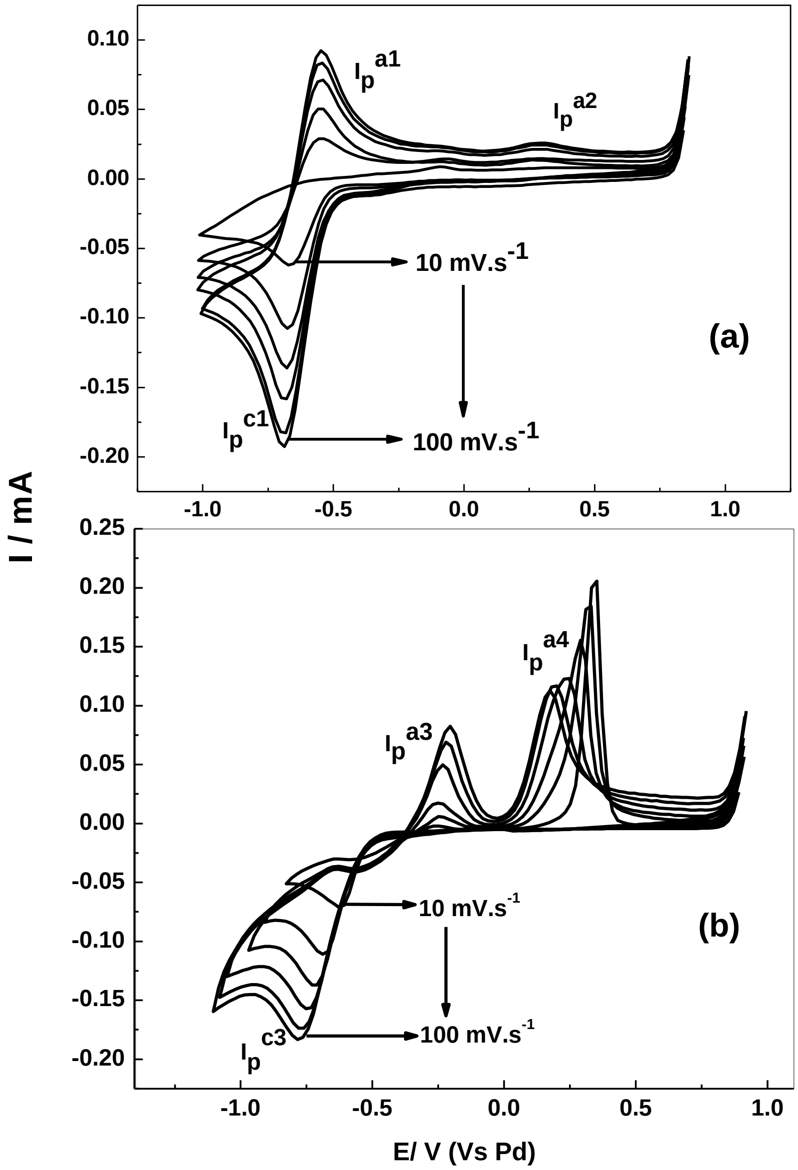

Figure 3.4. CV of (a) UO_2^{2+} and (b) Pd^{2+} in C_4mimCl recorded at a glassy carbon electrode at various scan rates. [UO_2^{2+}] = 50 mM, [Pd^{2+}] = 50 mM, T at 353 K.

3.1.1.4. Cyclic voltammetry of Eu^{3+} in C_4mimCl

The cyclic voltammogram of Eu^{3+} recorded at a glassy carbon working electrode at a scan rate of 100 mV.s^{-1} at 353 K, is shown in figure 3.5. This voltammogram is compared with that pertaining to UO_2^{2+} in C_4mimCl and a mixture containing UO_2^{2+} and Eu^{3+} in C_4mimCl under similar conditions. A prominent reduction wave (E_p^{c4}) observed in the cyclic voltammogram of Eu^{3+} at -0.85 V (Vs Pd) is due to the reduction of Eu^{3+} to Eu^{2+} and the corresponding oxidation wave, while the peak potential (E_p^{a8}) is observed at -0.53 V could be attributed to the oxidation of Eu^{2+} [16]. The difference between the values of E_p^{c4} and $E_{p/2}^{c4}$ is marginally higher (75 mV at 353 K) than the value needed for a reversible (33.5 mV at 353 K) one-electron transfer process [13, 14]. This shows that the reduction of Eu^{3+} to Eu^{2+} is probably quasi-reversible. A comparison of the reduction of Eu^{3+} with that of UO_2^{2+} and the proximity of their reduction potentials indicates that the presence of Eu^{3+} in the IL could interfere in the electrochemical recovery of uranium.

Figure 3.5 also shows the voltammogram obtained for the solution containing 25 mM UO_2^{2+} and 25 mM Eu^{3+}, in C_4mimCl recorded at a scan rate of 100 mV.s^{-1} at 353 K. The total concentration of metal ions (UO_2^{2+} and Eu^{3+}) in this mixed solution was maintained at 50 mM. The voltammogram of the mixed solution shows a couple of cathodic waves, E_p^{c5} and E_p^{c6} occurring at -0.67 V and -0.9 V (Vs Pd) respectively. The cathodic wave E_p^{c5} could be due to the reduction of UO_2^{2+} to UO_2 and E_p^{c6} is due to the reduction of Eu^{3+} to Eu^{2+}. It is noted that the presence of europium shifts marginally the reduction potential of U(VI) to the anodic half (20 to 30 mV), indicating the underpotential deposition of uranium oxide in the presence of europium(III). The oxidation wave E_p^{a9} corresponds to the combined oxidation of UO_2^{2+} and Eu^{3+} and E_p^{a10} is similar to E_p^{a2}.

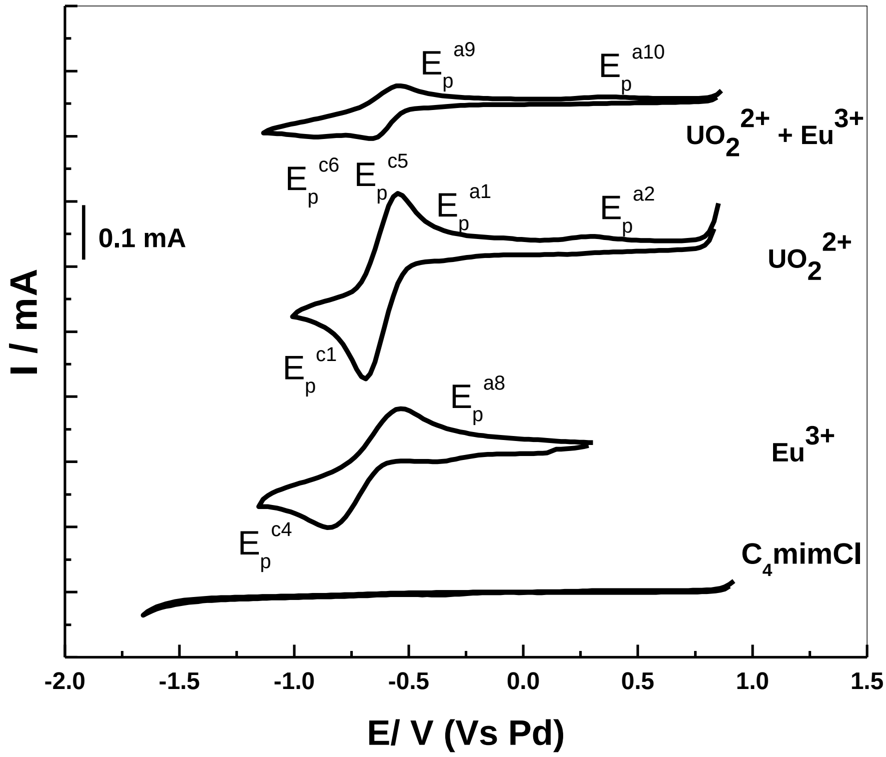

Figure 3.5. CV of C_4mimCl and its solutions containing 50 mM UO_2^{2+} or 50 mM Eu^{3+} or (25 mM UO_2^{2+} + 25 mM Eu^{3+}) recorded at a glassy carbon working electrode at a scan rate of 100 mV.s^{-1} at 353 K.

The diffusion coefficient of UO_2^{2+} in the combined system could be determined from E_p^{c5}. The cyclic voltammogram of the solution containing 25 mM UO_2^{2+} and 25 mM Eu^{3+} in C_4mimCl was recorded as a function of scan rate at 353 K. These results are shown in figure 3.6. This figure also shows the cyclic voltammogram of 50 mM Eu^{3+} in C_4mimCl recorded at various scan rates at 353 K. The cathodic peak currents (I_p^{c4} and I_p^{c5}) obtained in these voltammograms has been plotted as a function of the square root of scan rate, in figure 3.7. Linear dependence of the cathodic peak current with a zero-intercept in these cases also indicates the validity of Delahey equation (3.2). Using equation (3.1) and (3.2), the diffusion coefficients of Eu^{3+} in C_4mimCl and UO_2^{2+} in the mixed solution were determined and the same have been compared with the diffusion coefficients of other metal ions in table 3.1. It is seen that the values of all these diffusion coefficients both individual and mixed solutions are comparable and they are of the order 10^{-8} cm^2/s. The diffusion coefficients increased in the following order, UO_2^{2+} in (UO_2^{2+} + Eu^{3+}) < Eu^{3+} < UO_2^{2+}.

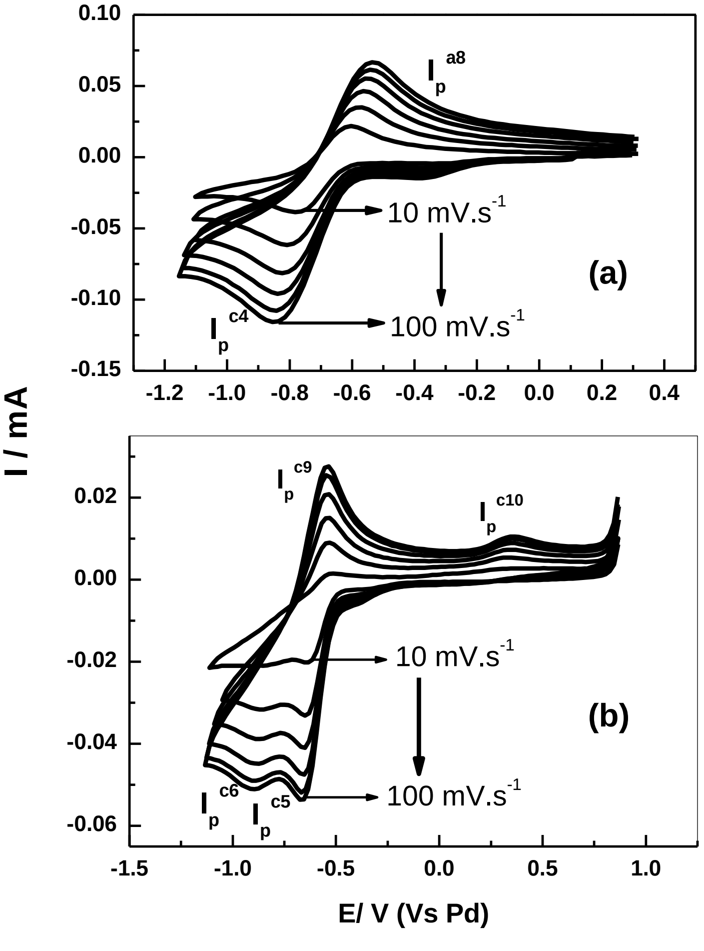

Figure 3.6. CV of (a) Eu^{3+} (50 mM) and (b) mixure (25 mM UO_2^{2+} and 25 mM Eu^{3+}) in C_4mimCl recorded at a glassy carbon electrode at different scan rates, T at 353 K.

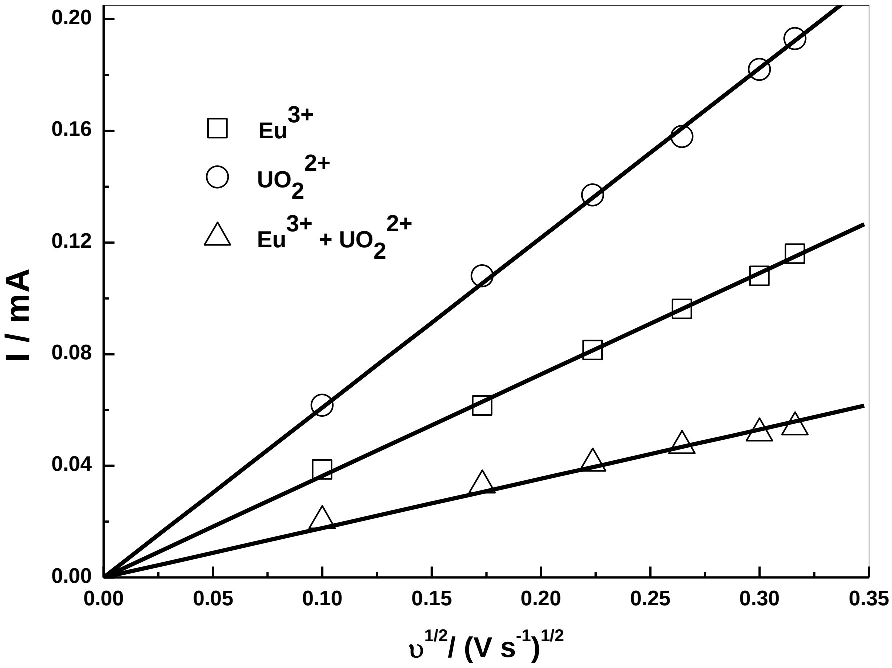

Figure 3.7. Plot of cathodic peak current against square root of scan rate ($\upsilon^{1/2}$) pertaining to the reduction of UO_2^{2+}, Eu^{3+} and that of their mixture in C_4mimCl at 353 K.

3.1.1.5. Cyclic voltammetry of Ru^{3+} in C_4mimCl

Figure 3.8 shows the cyclic voltammogram of Ru^{3+} recorded at a glassy carbon working electrode at a scan rate of 100 mV.s^{-1} at 353 K. This voltammogram is compared with that of UO_2^{2+} in C_4mimCl and a mixture containing UO_2^{2+} and Ru^{3+} in C_4mimCl under similar conditions. Three prominent reduction waves (E_p^{c7}, E_p^{c8}, E_p^{c9}) are observed in the cyclic voltammogram pertaining to Ru^{3+} at -0.15V, -0.6 V and -0.83 V (Vs Pd). A couple of prominent oxidation waves are observed at -0.26 V and 0.6 V. Since the redox chemistry of ruthenium is very complex, it is difficult to characterize these redox reactions happening at various potentials and the nature of reductions. A comparison of the reduction waves observed for Ru^{3+} and UO_2^{2+} reveals that the proximity in the reduction potential (especially E_p^{c7} and E_p^{c8}) shows that the presence of Ru^{3+} in IL could interfere in the electrochemical recovery of uranium.

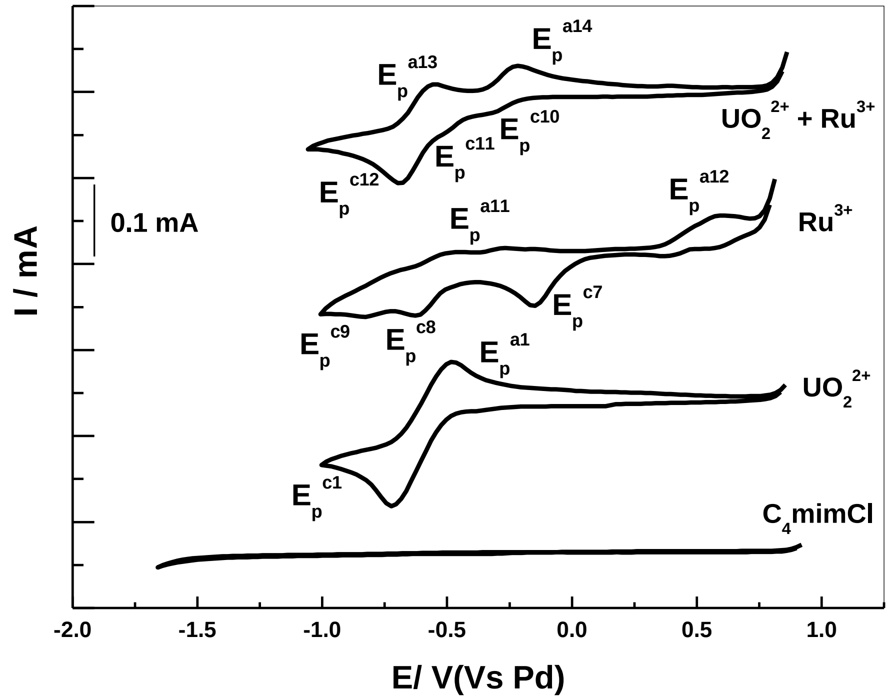

Figure 3.8. CV of C_4mimCl and its solutions containing 50 mM UO_2^{2+}, 50 mM Ru^{3+}, (25 mM UO_2^{2+} and 25 mM Ru^{3+}) recorded at a glassy carbon working electrode at a scan rate of 100 mV.s^{-1} at 353 K.

Figure 3.8 also shows the voltammogram obtained from the solution containing 25 mM UO_2^{2+} + 25 mM Ru^{3+} in C_4mimCl recorded at a scan rate of 100 mV.s^{-1} at 353 K. The voltammogram of the mixed solution shows a three cathodic waves, E_p^{c10}, E_p^{c11} and E_p^{c12} occurring at -0.3 V, -0.5 V and -0.7 V (Vs Pd) respectively. The cathodic wave E_p^{c7} occuring in Ru^{3+} seems to have shifted cathodically to E_p^{c10} when Ru^{3+} was mixed with UO_2^{2+}. The E_p^{c12} could be due to the reduction of both to UO_2^{2+} and ruthenium. The presence of Ru^{3+} shifts marginally the reduction potential of U(VI) to anodic side (20 to 30 mV) indicating the underpotential deposition of uranium oxide in the presence of ruthenium(III). The wave E_p^{a13} corresponds to the oxidation of UO_2 and E_p^{a14} corresponds to the oxidation of the reduced form of ruthenium.

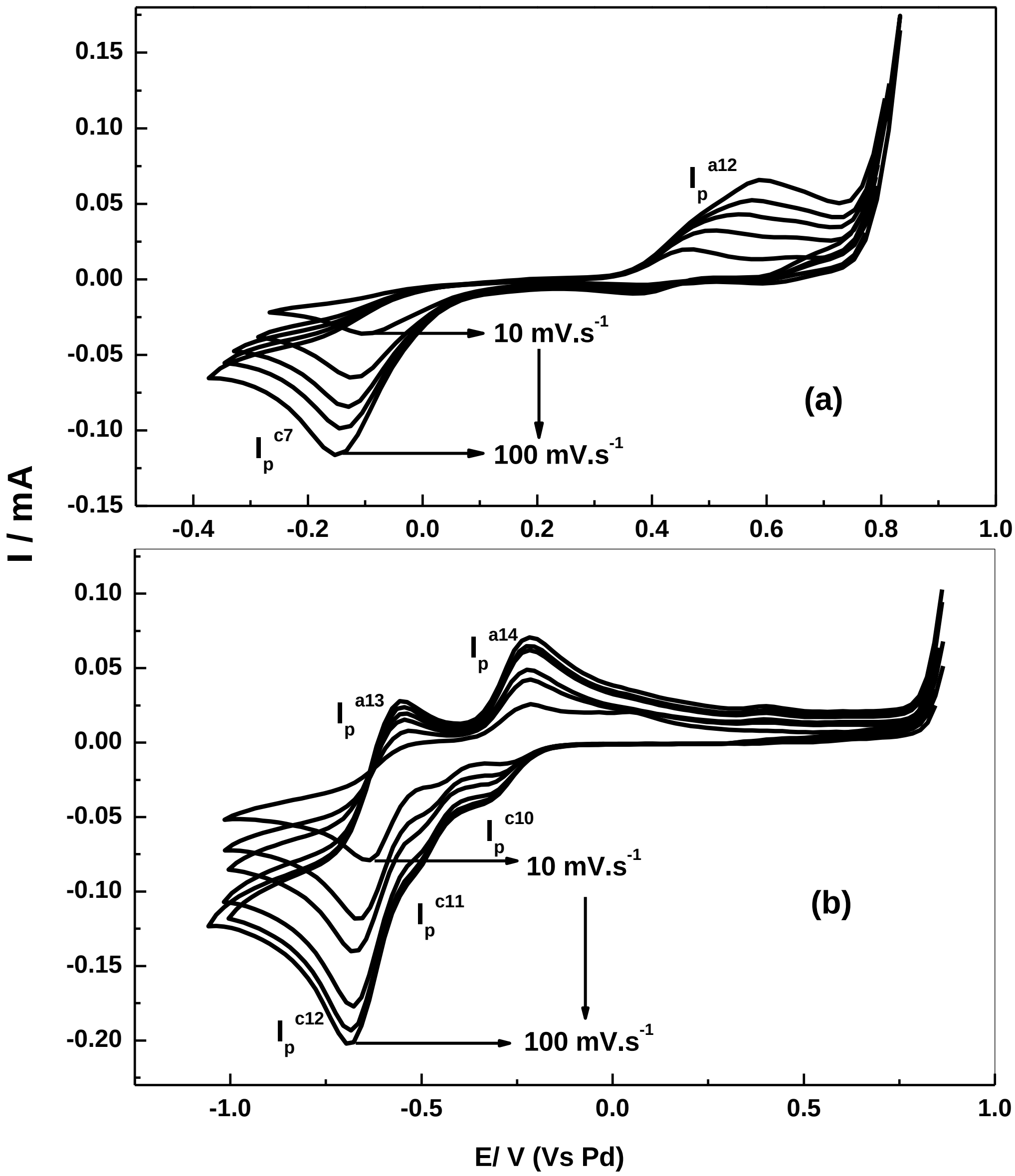

Figure 3.9. CV of (a) Ru^{3+} (50 mM) and (b) combined system (25 mM UO_2^{2+} + 25 mM Ru^{3+}) in C_4mimCl recorded at glassy carbon electrode at various scan rates. Temperature = 353 K.

The cyclic voltammogram of the solution containing 25 mM UO_2^{2+} + 25 mM Ru^{3+} in C_4mimCl was recorded as a function of scan rate at 353 K. The results are shown in figure 3.9. The figure also shows the cyclic voltammogram of 50 mM Ru^{3+} in C_4mimCl recorded at various scan rates at 353 K. It is difficult to derive the diffusion coefficients of UO_2^{2+} and Ru^{3+} from these voltammograms as the redox reactions and nature of voltammograms are very complex.

Table 3.1. Diffusion coefficients of UO_2^{2+}, Pd^{2+}, Eu^{3+}, Ru^{3+} in C_4mimCl and UO_2^{2+} in the combined solution containing (UO_2^{2+} + Pd^{2+}) or (UO_2^{2+} + Eu^{3+}) in C_4mimCl determined by cyclic voltammetry. T = 353 K

Metal ion in C_4mimCl	**Diffusion coefficient x 10^8/ $cm^2.s^{-1}$**	**k_s x 10^4/cm.s^{-1}**
UO_2^{2+}	6.2	2.01
Pd^{2+}	5.4	0.04
Eu^{3+}	3.2	0.25
Ru^{3+}	4.5	
(UO_2^{2+} + Pd^{2+})	4.8	
UO_2^{2+} in (UO_2^{2+} + Eu^{3+})	0.2	

The uncertainty in the measurement of diffusion coefficients is less than 5%

3.1.1.6. Cathodic peak potentials in combined system.

Table 3.2 compares the cathodic peak potential of UO_2^{2+} to UO_2 reduction in C_4mimCl with those observed in the mixed solutions. It could be seen that the reduction of UO_2^{2+} to UO_2 in C_4mimCl occurs at -0.67 to -0.68 V. In the presence of Pd^{2+}, Eu^{3+} and Ru^{3+}, the cathodic peak potential pertaining to the reduction of UO_2^{2+} to UO_2 is shifted anodically by a margin of ~10 mV in many cases, indicting the underpotential deposition of uranium oxide in the presence of these metal ions.

Table 3.2. Cathodic peak potentials of UO_2^{2+} in C_4mimCl separately and in presence of Pd^{2+}, Eu^{3+} and Ru^{3+} at 353 K.

Scan rate / $mV.s^{-1}$	Cathodic peak potential (in V (Vs Pd)) of			
	UO_2^{2+}/ C_4mimCl	UO_2^{2+} in (UO_2^{2+} + Pd^{2+}) / C_4mimCl	UO_2^{2+} in (UO_2^{2+} + Eu^{3+}) / C_4mimCl	UO_2^{2+} in (UO_2^{2+} + Ru^{3+}) / C_4mimCl
10	-0.672	-0.624	-0.649	-0.644
30	-0.677	-0.646	-0.650	-0.665
50	-0.679	-0.669	-0.652	-0.675
70	-0.682	-0.684	-0.658	-0.678
90	-0.686	-0.697	-0.666	-0.684
100	-0.688	-0.699	-0.673	-0.687

3.1.1.7. Quasi-reversibility

A marginal shift in the cathodic peak potential with an increase in the scan rate, shown in figure 3.4 and 3.6 indicates that the reduction of UO_2^{2+} or Pd^{2+} or Eu^{3+} at the glassy carbon electrode could be quasi-reversible. This indicates that the reduction of these metal ions is not only controlled by their diffusion to at the working electrode, but also by the rate of the charge transfer between the electrode electrolyte interface [17, 18]. The charge transfer rate constant, k_s (cm/s), in such cases could be determined by using equations (3.3) to (3.5) [17, 18].

$$k_s = 2.18\,[D_{U(VI)}\,(\alpha n_\alpha)\,\upsilon F/RT]^{1/2} \exp[\alpha^2 nF/RT(E_p^{c1}-E_p^{a1})] \qquad (3.3)$$

$$k_s = 2.18\ [D_{Pd(II)}\ (\alpha n_\alpha)\ \upsilon F/RT]^{1/2} \exp\ [\alpha^2 nF/RT(E_p^{c2}-E_p^{a3})] \qquad (3.4)$$

$$k_s = 2.18\ [D_{Eu(III)}\ (\alpha n_\alpha)\ \upsilon F/RT]^{1/2} \exp\ [\alpha^2 nF/RT(E_p^{c4}-E_p^{a8})] \qquad (3.5)$$

where D pertains to the diffusion coefficient of the ion, R is the universal gas constant, T is the temperature and the other factors have the same meaning as explained before.

From the values of k_s, these electrode reactions could be classified [25] into reversible when $k_s \geq 0.3\ \upsilon^{1/2}$, quasi-reversible when $0.3\ \upsilon^{1/2} \geq k_s \geq 2\times10^{-5}\ \upsilon^{1/2}$ and irreversible when $k_s \leq 2 \times 10^{-5}\ \upsilon^{1/2}$. Inserting the diffusion coefficient of UO_2^{2+}, Pd^{2+} and Eu^{3+} into equations (3.3), (3.4) and (3.5) respectively, the magnitude of these rate constants were determined at 353 K and the values are tabulated in table 3.1. It can be seen that the magnitude of k_s lies in the range of $0.3\ \upsilon^{1/2} \geq k_s \geq 2 \text{ x } 10^{-5}\ \upsilon^{1/2}$, confirming that the reduction of UO_2^{2+} or Pd^{2+} or Eu^{3+} at the glassy carbon electrode is quasi-reversible [17, 18]. For Ru^{3+} (individually) as well as in the mixtures, this equation could not be used as the anodic and cathodic peak potentials could not be delineated well. Therefore, table 3.1 shows the k_s values peartining to UO_2^{2+}, Pd^{2+} and Eu^{3+} reductions in C_4mimCl medium.

3.1.2. Conclusions

The electrochemical behaviour of UO_2^{2+} in C_4mimCl was studied in the presence of Pd^{2+}, Eu^{3+} and Ru^{3+}. The cathodic wave pertaining to the reduction of UO_2^{2+} to UO_2 was shifted anodically in the presence of these metal ions. Both Pd^{2+} and UO_2^{2+} underwent reduction at cathodic potentials quite close to that of their mixture whereas the cathodic potentials needed for the reduction of Eu^{3+} and Ru^{3+} were quite different than that pertaining to the reduction of UO_2^{2+} to UO_2. The apparent diffusion coefficients of UO_2^{2+}, Pd^{2+}, Eu^{3+}, Ru^{3+} in C_4mimCl and UO_2^{2+} in the presence of other metal ions were of the order 10^{-8} cm^2/s. However, the presence of Pd^{2+} and Eu^{3+} was found to deminish the diffusion coefficient of UO_2^{2+} in a mixture. The diffusion coefficient of metal ions in their individual solution increased in the following order: $Eu^{3+} < Ru^{3+} < Pd^{2+} < UO_2^{2+}$. The close proximity of these reduction potentials indicates that the presence of Pd^{2+}, Eu^{3+}, Ru^{3+} could reduce the current efficiency during the electrodeposition of uranium oxide from UO_2^{2+} in an IL.

3.2. Dissolution of U_3O_8 in 1-butyl-3-methylimidazolium chloride and Spectroscopic and the electrochemical behavior of U(VI) in the resultant solution

Most studies reported in the literature pertaining to the dissolution of uranium compounds indicate that the freely soluble uranium salt ($[UO_2Cl_4]^{2-}$, $[UO_2(NO_3)_3]^{3-}$ etc.,) was taken for the dissolution of uranium in IL [5, 19]. However, the spent nuclear fuel contains uranium oxide, that is poorly soluble in the IL. Therefore, the dissolution of uranium oxide in an IL calls for the development of a suitable procedure. In this context, Biju joseph *et al*. [6] studied the dissolution behaviour of UO_2 and UO_3 in C_4mimCl medium by passing Cl_2 gas. Eventhough this procedure was tedious, it was reported that with the help of this method, UO_2 completely dissolved in C_4mimCl. Nevertheless, from practical application point of view, it is desirable to develop an easy and technically viable method for the dissolution of uranium oxide. Moreover, further methods need to be derived through electrochemical studies for the subsequent recovery of uranium from the resultant solution. Billard *et al*. [19] studied the dissolution behaviour of uranium oxide in 1-butyl-3-methylimidazolium bis(trifluoromethanesulfonyl) imide (C_4mimNTf$_2$) in the presence of small amounts of HNO_3 and characterized the uranyl species in IL. However, the electrochemical behaviour of UO_2^{2+} in the resultant solution was not reported.

In this chapter, we report the oxidative dissolution of uranium oxide (U_3O_8) in C_4mimCl IL in the presence of small quantities of nitric acid, marginally higher than the stoichiometric amount, needed for the dissolution of U_3O_8 and investigations on the electrochemical behaviour of UO_2^{2+} present in the resultant solution by cyclic voltammetry and chronopotentiometry. The speciation of uranium in C_4mimCl solution containing nitric acid, was investigated by UV-Visible, ATR-FTIR and Raman spectroscopy. C_4mimCl was chosen in the present study, since the Cl^- ions present in this IL could facilitate the easy dissolution of UO_2^{2+}, that was obtained after the oxidation of

U_3O_8 by nitric acid. It is well-known fact that UO_2^{2+} present in traditional high temperature molten salts, composed of alkali-alkaline earth chlorides, complexes with Cl^- ions present in molten salt medium [20]. Therefore, it can be expected that the Cl^- ion of C_4mimCl also form stable complex with UO_2^{2+} and facilitate oxidative dissolution of U_3O_8 in C_4mimCl.

Experimental procedure for the present study has been discussed in the section 2.4.2 and synthesis of IL (C_4mimCl) has been detailed in the section 2.5.1.

3.2.1. Results and discussions

3.2.1.1. Dissolution of U_3O_8

Table 3.3. Dissolution behavior of U_3O_8 in C_4mimCl in the presence of nitric acid.

Uranium taken as U_3O_8 / mmoles	Weight of C_4mimCl / g	HNO_3 added / mmoles	HNO_3/U mole ratio	Time taken for complete dissolution / hours
0.75	10	0	0 : 1	No dissolution
0.75	10	3	4 : 1	58
0.75	10	4.5	6 : 1	52
0.75	10	6	8 : 1	45

The first step in the oxide-electrowinning method for the non-aqueous reprocessing of spent nuclear fuel involves the dissolution of the spent fuel oxide in a molten salt medium [21]. Table 3.3 shows the results on the dissolution of U_3O_8 in C_4mimCl in the presence and absence of nitric acid. The uranium to HNO_3 mole ratio needed for the stoichiometric oxidation of U_3O_8 is 1 : 2.3 [22]. In the absence of nitric acid the solubility of U_3O_8 in C_4mimCl was very poor, even after contacting U_3O_8 with C_4mimCl for more than 100 h. However, addition of a small quantity of HNO_3 facilitates the dissolution of U_3O_8. When the U : HNO_3 mole ratio was matianed at 1 : 4, complete dissolution of U_3O_8 was achieved in about 58 h. Further increase in nitric acid concentration reduced the time required for the complete dissolution of U_3O_8. After dissolution, the U(VI) present in the resultant solution could co-ordinate either with the nitrate or chloride ions present in the IL. Therefore, it is useful to understand and speciate the uranyl complex present in the resultant solution. For this purpose, a detailed characterization of the uranium complex present in the C_4mimCl was carried out by using UV-Vis, FT-IR and Raman spectroscopy.

3.2.1.2. UV-Visible absorption spectroscopy

In order to character the uranyl species by UV-Visible absorption spectroscopy, a reference U(VI) spectrum is needed. For this purpose, the UV-Visible absorption spectrum of uranyl nitrate dissolved in a different IL, 1-butyl-3-methylimidazolium bis(trifluoromethanesulfonyl)imide (C_4mimNTf$_2$) was recorded in the presence and absence of different quantities of C_4mimCl. The purpose of choosing C_4mimNTf$_2$ was that NTf$_2^-$ is a non-complexing anion [23, 24] and C_4mim$^+$ is a common cation present both in C_4mimNTf$_2$ and C_4mimCl. The UV-Visible absorption spectrum pertaining to uranyl nitrate in C_4mimNTf$_2$ is shown in figure 3.10. The absorption spectrum is characterized by many bands at 428 nm, 440 nm, and 466 nm. The intensity of the other bands is less. The UV-Visible absorption spectrum of UO_2^{2+} obtained in C_4mimNTf$_2$ was found to match well [19, 25] with the absorption spectrum reported for the solution of uranyl nitrate in 14 M nitric acid. At 14 M nitric acid, Billard *et al*. [19] computed the composition of various uranyl species viz., ~ 2% UO_2^{2+}, ~ 65 % $UO_2(NO_3)^+$ and 33 % of $UO_2(NO_3)_2$ at 14 M HNO_3. Since the absorption spectrum of uranyl nitrate in C_4mimNTf$_2$ matches well with the absorption spectrum of uranyl nitrate in 14 M nitric acid medium, it is reasonable to presume that majority of uranyl species present in C_4mimNTf$_2$ is $UO_2(NO_3)_2$. Moreover, the NTf$_2^-$ anion present in the IL is poorly co-ordinating [19, 23, 24] as compared to NO_3^- ions. Therefore, it was concluded that the uranyl ions present in C_4mimNTf$_2$ co-ordinates predominantly with NO_3^- ions and exist as $UO_2(NO_3)_2$ in C_4mimNTf$_2$ [25, 26], as well.

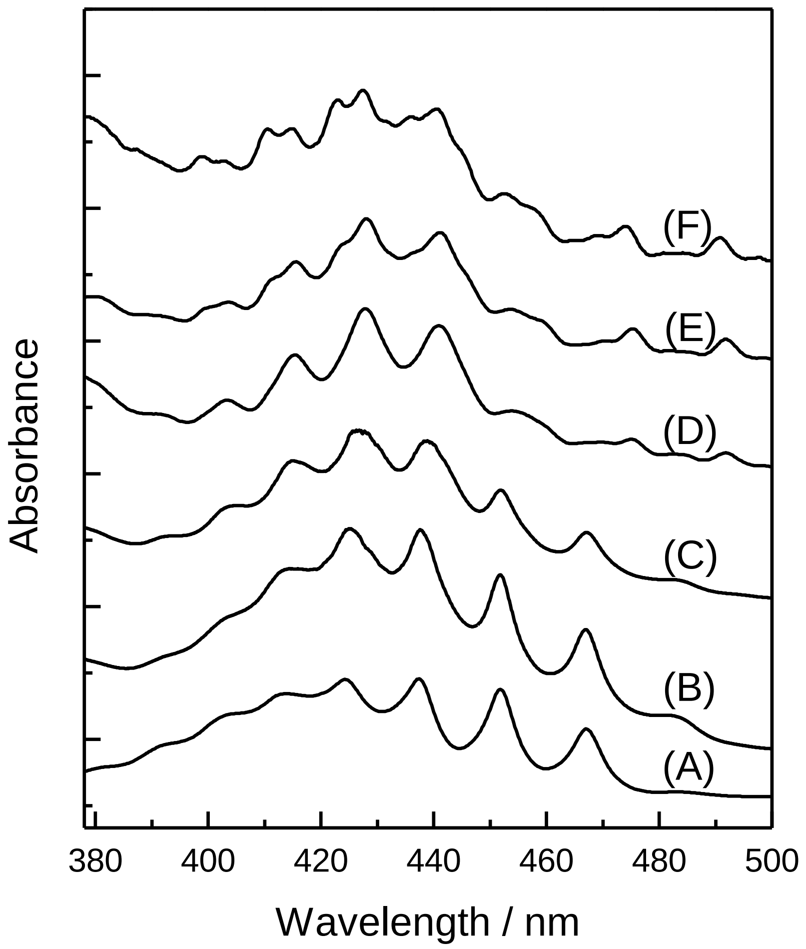

Figure 3.10. UV-Visible absorption spectrum pertaining to uranyl nitrate in C_4mimNTf$_2$, in the presence and absence of C_4mimCl. The mole ratio of Cl : U is 0 : 1 in (A), 1 : 1 in (B), 2 : 1 in (C), 4 : 1 in D and 6 : 1 in (E). The spectrum F represents the UV-Visible absorption spectrum of UO_2^{2+} obtained after the dissolution of U_3O_8 in HNO_3 (HNO_3 : U mole ratio = 4 : 1) present in C_4mimCl IL.

Figure 3.10 also shows the absorption spectrum peartaining to uranyl nitrate in C_4mimNTf$_2$ in the presence of varying quantities of C_4mimCl. It is interesting to note that the intensity of the bands at 451 nm, 466 nm, and 482 nm decreases and that of 403 nm, 415 nm and 428 nm increases with in the quantity of C_4mimCl present in the solution.

When the mole ratio of Cl^- : UO_2^{2+} is lower than 4 : 1, the intensity of bands at 428 nm and 440 nm are comparable. At higher Cl^- : UO_2^{2+} ratios (more than 4 : 1), the intensity of the bands at 428 nm is more than that of the other bands. A similar result was also reported by Gillard *et al.* [27] for the UV-Visible absorption spectrum of UO_2^{2+} in $C_4mimNTf_2$ in the presence of varying quantities of tetrabutylammonium chloride. In addition, these authors also speciated the uranyl ion in this IL solution with the help of EXAFS. It was reported that when the mole ratio of NO_3^- : Cl^- : UO_2^{2+} was 2 : 4 : 1, the UO_2^{2+} in the solution exists in the form of $[UO_2Cl_3(NO_3)]^{2-}$. At higher Cl^- concentrations, the uranyl ion is completely converted into $[UO_2Cl_4]^{2-}$. In view of this, as well as due to the similarity of the UV-Visible absorption spectrum obtained in the present study with that reported by Gaillard *et al.* [27] the uranyl ion in $C_4mimNTf_2$, in the presence of Cl^- ion at 4 : 1 (Cl^- : UO_2^{2+}) mole ratio, is likely to exist as $[UO_2Cl_3(NO_3)]^{2-}$.

At higher mole ratios of Cl^- : UO_2^{2+} more than 4 : 1, the bands are further split into doublets as shown in figure 3.10. When U_3O_8 in C_4mimCl was dissolved in the presence of nitric acid, the UV-Visible absorption spectrum of the resultant solution also shows the splitting of the bands into doublets. A similar observation was reported by Gaillard *et al.* [27]. These authors attributed the splitting of the absorption bands to the presence of $[UO_2Cl_4]^{2-}$. Therefore, it is reasonable to conclud that at higher Cl^- : UO_2^{2+} mole ratios than 4 : 1, the uranyl ion present in this IL gets converted entirely into $[UO_2Cl_4]^{2-}$ [27, 28].

3.2.1.3. ATR-FTIR spectroscopy

The formation of $[UO_2Cl_4]^{2-}$ species in C_4mimCl medium could be supported further by FTIR spectroscopy investigations. The FTIR spectroscopic studies on uranyl compounds reported in the literature indicate that the asymmetric stretching bands of

UO_2^{2+} occur at 900-950 cm^{-1} [29]. This transmittance band is strongly influenced by the nature of ligands co-ordinated to the uranyl ion. When UO_2^{2+} is co-ordinated with the nitrate ions, the UO_2^{2+} asymmetric stretching bands occur at ~940 cm^{-1}. However, co-ordination of a strong field ligand like Cl^- with UO_2^{2+}, results in the weakening of U=O bonds and shifts the UO_2^{2+} asymmetric stretching bands to a lower wave number (~920 cm^{-1}). Figure 3.11 shows the ATR-FTIR spectrum of $C_4mimNTf_2$ and uranyl nitrate dissolved in $C_4mimNTf_2$. The ATR-FTIR spectrum (spectrum A) shows the transmittance bands at ~940 cm^{-1}, which could be attributed to the asymmetric stretching of UO_2^{2+}. It should be noted that $C_4mimNTf_2$ also gives a weak transmittance band at 940 cm^{-1} (spectrum F). However, the intensity of this band increases significantly (spectrum A) with the addition of $UO_2(NO_3)_2$. The presence of the UO_2^{2+} asymmetric stretching bands at 940 cm^{-1} confirms the existence of uranyl nitrate specie, $UO_2(NO_3)_2$, in $C_4mimNTf_2$ medium. It would be interesting to notice the changes in the FTIR spectrum brought about by the addition of C_4mimCl to asolution of uranyl nitrate solution in $C_4mimNTf_2$.

Figure 3.11 also shows the ATR-FTIR spectrum (spectrum B to E) of a solution of uranyl nitrate in $C_4mimNTf_2$ at different mole ratios of Cl^- : UO_2^{2+}. The Cl^- : UO_2^{2+} ratio was varied from 1 : 1 to 6 : 1. In the absence of Cl^-, the UO_2^{2+} asymmetric stretching bands occur at 940 cm^{-1}, as indicated above (spectrum A). It is interesting to note that the intensity of the band at 940 cm^{-1} decreases with an increase in the Cl^- : UO_2^{2+} mole ratio. When the ratio of Cl^- : UO_2^{2+} is 4 : 1, the intensity of the band at 940 cm^{-1} due to UO_2^{2+} stretching completely disappears and merges with the bands of $C_4mimNTf_2$. Further addition of Cl^- ion to this solution (more than 4 : 1 ratio) does not change the nature of these bands at 940 cm^{-1}. All these observations indicate that that uranyl ion in $C_4mimNTf_2$ exists as uranyl nitrate species, $[UO_2(NO_3)_2]$. However, the addition of Cl^- ion to this solution decreases the abundance of uranyl nitrate species. When the ratio of

Cl^- : UO_2^{2+} is 4 : 1 or more, the nitrate ion in uranyl nitrate seems to completely get replaced with Cl^- ions leading to the formation of $[UO_2Cl_4]^{2-}$. These results are nearly in good agreement with those obtained from UV-Visible absorption spectra of UO_2^{2+} in $C_4mimNTf_2$ at different concentrations of C_4mimCl.

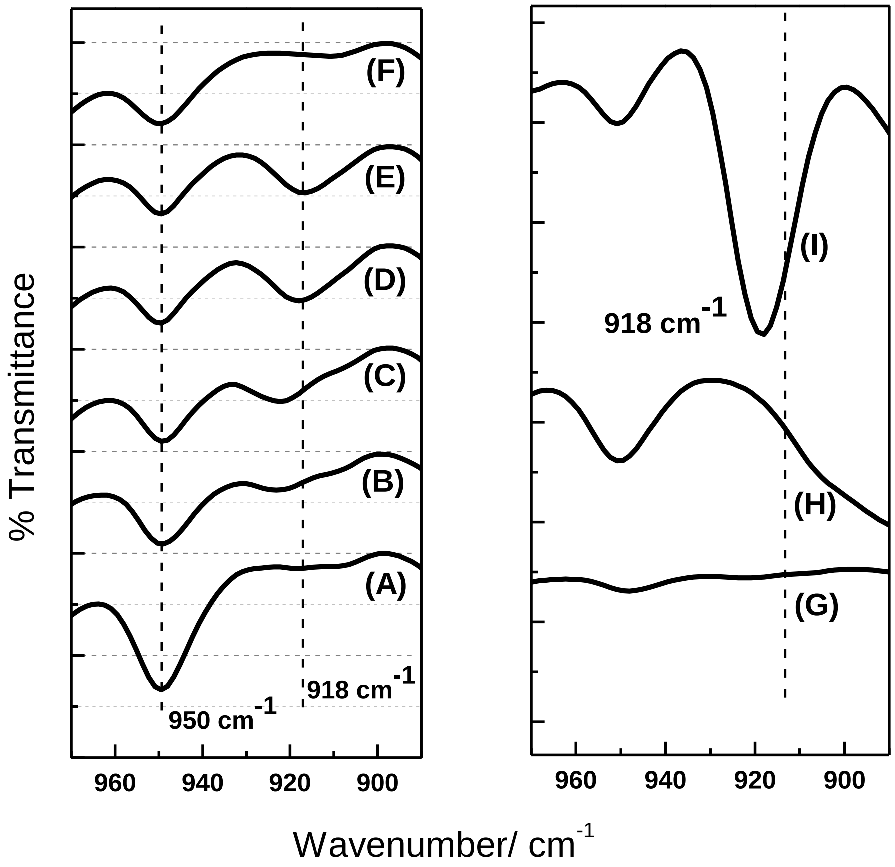

Figure 3.11. ATR-FTIR spectrum of uranyl nitrate in $C_4mimNTf_2$, in the presence and absence of C_4mimCl. The mole ratio of Cl^- : U is (A) 0 : 1, (B) 1 : 1, (C) 2 : 1, (D) 4 : 1, (E) 6 : 1 and (F) $C_4mimNTf_2$ alone, (I) represents the FTIR spectrum of UO_2^{2+} obtained after dissolving U_3O_8 in HNO_3 (HNO_3 : U mole ratio = 4 : 1) present in the C_4mimCl. G and H are the FTIR spectra of neat C_4mimCl and C_4mimCl + HNO_3. The dotted line represents the initial (950 cm^{-1}) and final (918 cm^{-1}) position of UO_2^{2+} asymmetric bands.

The formation of $[UO_2Cl_4]^{2-}$ with the addition of C_4mimCl is evident from the enhancement of the intensities of the bands pertaining to $[UO_2Cl_4]^{2-}$ at ~920 cm^{-1}. It is that an increase in the mole ratio of Cl^- : UO_2^{2+} from 1 : 1 to 4 : 1 results in the shift of the bands at 940 cm^{-1} to 930 cm^{-1} at the mole ratio 2 : 1, and to 920 cm^{-1} at the mole ratio 4 : 1. Increase in the Cl^- : UO_2^{2+} ratio does not result in any further shift of the UO_2^{2+} asymmetric bands beyond 920 cm^{-1}. These observations indicate that the specei $[UO_2Cl_4]^{2-}$ is formed at mole ratios above 4 : 1. Therefore, it could be concluded that the observation of the bands in between 940 cm^{-1} and 920 cm^{-1} pertain to the formation of mixed complexes viz., $[UO_2Cl_x(NO_3)_{4-x}]$. The extent of shift to a lower wavenumber region depends upon the degree of substitution of nitrate ion by chloride ion. When U_3O_8 in C_4mimCl was dissolved in the presence of nitric acid, the ATR-FTIR spectrum of the resultant solution (spectrum I) also showed a transmittance band at 920 cm^{-1}, confirming the formation of $[UO_2Cl_4]^{2-}$ species in that solution. In the figure 3.11 the ATR-FTIR spectrum of C_4mimCl (spectrum G) is also shown for comparison.

3.2.1.4. Raman spectroscopy

Figure 3.12 shows the Raman spectrum U_3O_8 dissolved in C_4mimCl in the presence of HNO_3. This spectrum was compared with the Raman spectrum obtained in the absence of uranyl ion. The sectrum of pure C_4mimCl liquid was also recorded for comparison. The Raman spectrum obtained in the present study for C_4mimCl compares well with the Raman bands of C_4mimCl reported in the literature [30, 31]. Addition of nitric acid to C_4mimCl results in the appearance of a new band at 1030 cm^{-1}, due to nitrate ion, and there is no change in the position of other bands. Literature reports on the Raman spectrum of uranyl compounds indicates that uranyl nitrate exhibits absorption bands at 860 cm^{-1} and the chlorocomplex of uranyl ion, $[UO_2Cl_4]^{2-}$ shows absorption bands at 830 cm^{-1} [26]. It is evident from figure 3.12 that there is a band at 830 cm^{-1} in C_4mimCl itself. The Raman spectrum of the uranyl solution in C_4mimCl, shows an increase in the intensity of the bands at 830 cm^{-1}as well as 1030 cm^{-1}. There is no change in the nature of bands at 860 cm^{-1}. This indicates that the uranyl ion in C_4mimCl solution exists as a chloro complex, $[UO_2Cl_4]^{2-}$. Therefore, all these spectroscopic studies on U(VI) in C_4mimCl solution, that were obtained after the dissolution of U_3O_8 in C_4mimCl in the presence of nitric acid, unambiguously confirm the presence of $[UO_2Cl_4]^{2-}$ species in IL medium.

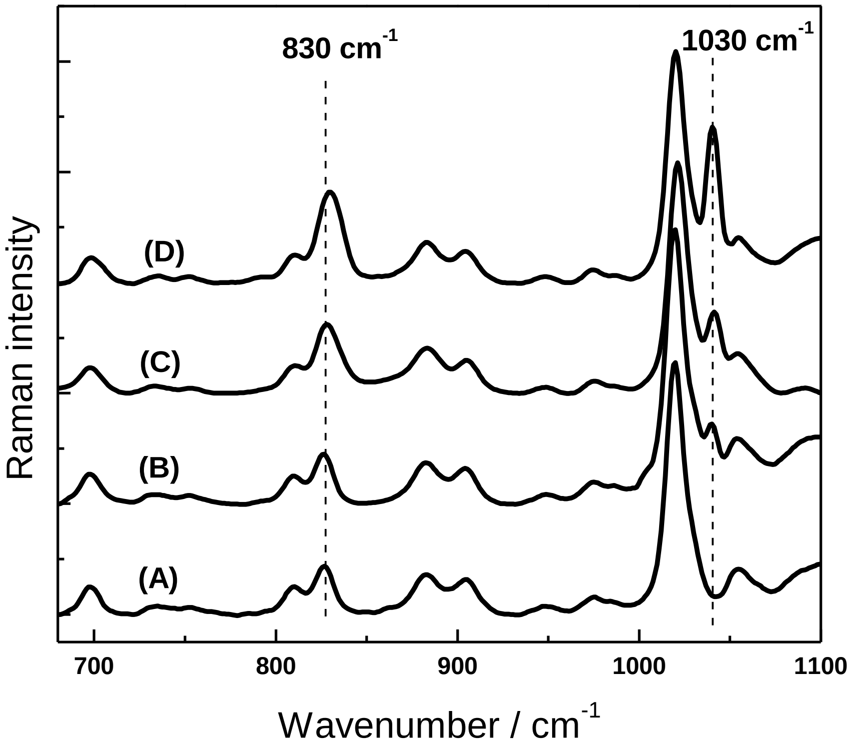

Figure 3.12. Raman spectrum of the solution obtained after the dissolution of U_3O_8 in C_4mimCl in the presence of nitric acid at HNO_3 : U mole ratio 6 : 1. The spectrum shows (A) C_4mimCl, (B) C_4mimCl + HNO_3, (C) 75 mM UO_2^{2+} in C_4mimCl + HNO_3, (D) 150 mM UO_2^{2+} in C_4mimCl + HNO_3.

3.2.1.5. Cyclic voltammetry

The cyclic voltammogram of C_4mimCl recorded at a glassy carbon electrode at a scan rate of 10 mV/s is shown in figure 3.13. Figure 3.13 also shows the cyclic voltammogram of UO_2^{2+} in C_4mimCl in the presence of a small quantity of nitric acid. This solution was obtained by the dissolution of U_3O_8 in C_4mimCl in the presence of nitric acid. This solution was subjected to voltammetric measurements without any pretreatment (i.e. without drying). The voltammogram (figure 3.13B) shows a weak cathodic wave (E_p^{c1}) at -0.4 V (Vs Pd) followed by a prominent cathodic wave at the peak potential (E_p^{c2}) of -0.85 V (Vs Pd). When the sweeping potential was reversed at -1.1 V, the cyclic voltammogram shows a weak anodic wave at the potential (E_p^{a1}) of -0.6 V (Vs Pd). In addition, a couple of oxidation waves, E_p^{a2} and E_p^{a3}, are observed at the peak potential of -0.03 V and 0.2 V (Vs Pd) respectively.

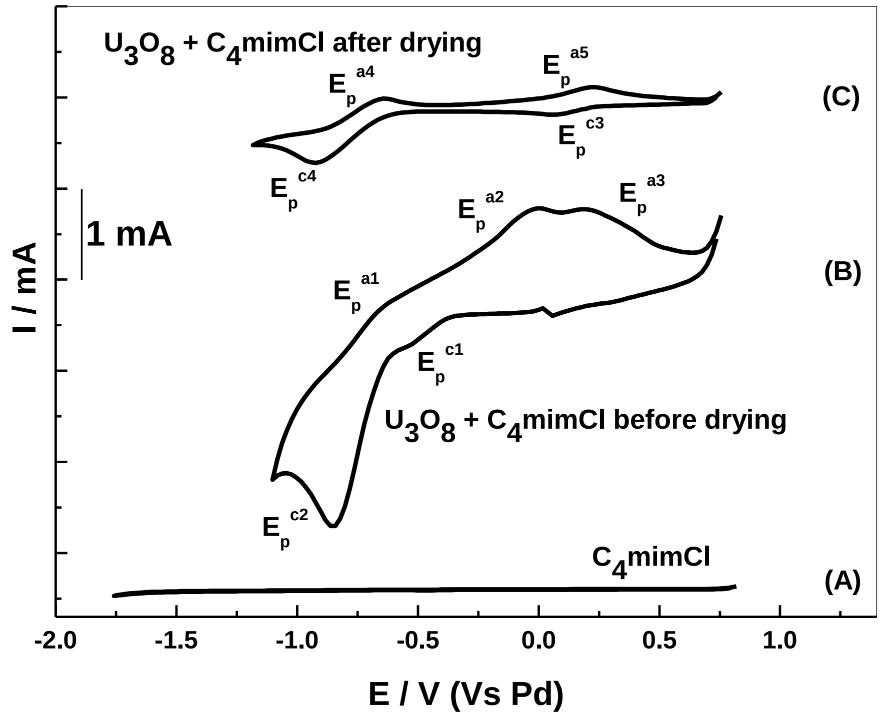

Figure 3.13. CV of (A) C_4mimCl and its solutions containing 150 mM UO_2^{2+} (U_3O_8 dissolved in the presence of nitric acid) (B) before drying and (C) after drying recorded at glassy carbon working electrode at the scan rate of 100 mV.s^{-1} at 373 K.

The CV pertaining to the dried solution (353 K, vaccum, 24 h) was recorded at a glassy carbon electrode at a scan rate of 100 mV/s at 373 K is shown in figure 3.13. The voltammogram (figure 3.13C) shows cathodic waves occurring at the peak potential

(E_p^{c3}) of 0.1 V, due to the reduction of nitric acid, and another wave at the peak potential (E_p^{c4}) of -0.9 V (Vs Pd), perataining to the reduction of UO_2^{2+} to UO_2. The oxidation waves observed at E_p^{a4} is due to the oxidation of UO_2. Therefore, the couple, $E_p^{c3}$and E_p^{a5}, could be the redox reactions occurring due to the presence of nitric acid in C_4mimCl.

In order to confirm that E_p^{c3} and E_p^{a5} are occurring due to the presence of nitric acid in C_4mimCl, the uranyl chloride hexahydrate ($UO_2Cl_2(H_2O)_6$) was dissolved in C_4mimCl and the resultant solution was dried at 353 K under vacuum for 24 hours. The cyclic voltammogram was recorded at a glassy carbon working electrode at a scan rate of 100 mV/s at 373 K. This CV displayed in figure 3.14, shows a cathodic wave occurring at the peak potential (E_p^{c5}) of -0.8 V (Vs Pd) which colud be assaigned to the reduction of UO_2^{2+} to UO_2 and its corresponding oxidation wave is observed at the peak potential of -0.6 V (Vs Pd) [5, 10]. This CV (figure 3.14C) is compared with that obtained after the dissolution of U_3O_8 in C_4mimCl in the presence of nitric acid after drying (figure 3.14D). Comparison of these two CVs clearly indicates that the couple occurring at E_p^{c3} and E_p^{a5} is only due to the presence of nitric acid. This inference is further confirmed by recording a CV after adding nitric acid to C_4mimCl and drying the solution (at 353 K for 24 hours under vacuum). The CV pertaining to C_4mimCl in the presence of nitric acid is shown in figure 3.14. This CV (figure 3.14B) shows a redox couple occuring at the peak potential of E_p^{c6} and E_p^{a7}. These peaks are absent in the CV pertaining to C_4mimCl (figure 3.14A) recorded in the absence of nitric acid under identical conditions. Moreover, the potential span pertaining to the redox reactions of nitric acid E_p^{c6} and E_p^{a7}, in the CV 3.14D is similar to the span between E_p^{c3} and E_p^{a5}. This observation confirms that E_p^{c3} and E_p^{a5} are due to the redox reaction involving nitric acid dissolved in C_4mimCl.

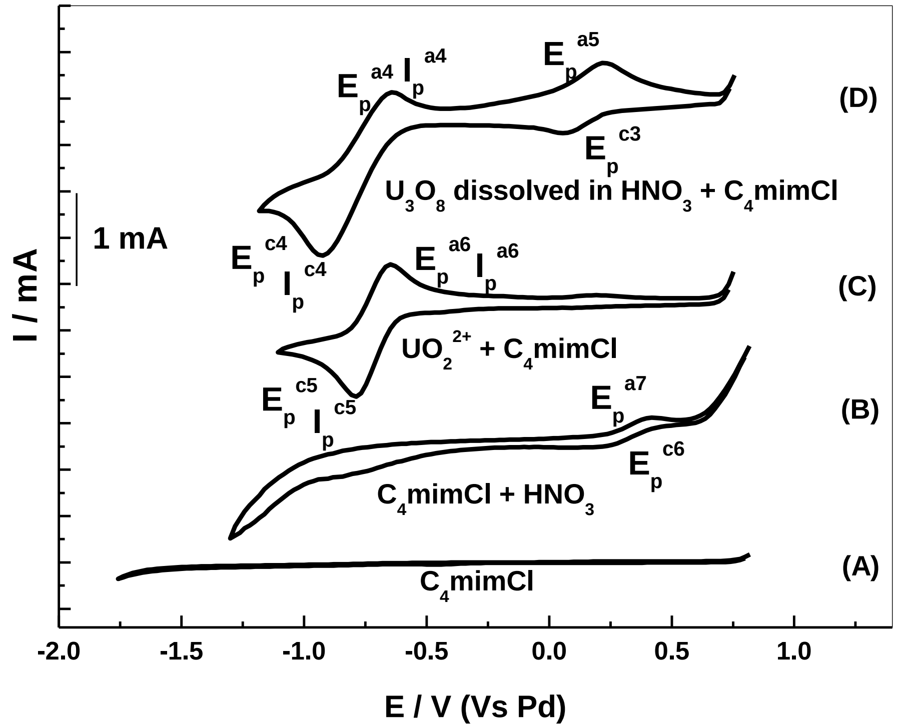

Figure 3.14. CV of (A) C_4mimCl and its solutions containing (B) 0.6 M HNO_3 or (C) 50 mM UO_2^{2+} (UO_2Cl_2 dissolved) or (D) 150 mM UO_2^{2+} (U_3O_8 dissolved in presence of nitric acid) recorded at a glassy carbon working electrode at a scan rate of 100 mV.s^{-1} at 373 K.

The electrochemical reactions occurring at E_p^{c4} and E_p^{a4} are due to the redox reactions of UO_2^{2+} to UO_2. Controlled potential electrolysis of a solution of U(VI) in C_4mimCl obtained after the dissolution of U_3O_8 in C_4mimCl in the presence of nitric acid at -1.0 V (Vs Pd) results in the deposition of UO_2 on the surface of the glassy carbon electrode. A similar behavior was reported by other authors [5-6, 10]. It is evident from figure 3.14D that the magnitude of the anodic current I_p^{a4} is lesser than that of I_p^{c4}. This could be due to the oxidation of uranium oxide deposit by nitric acid present in C_4mimCl. The oxidation results in lowering of the available concentration of uranium oxide at the working electrode. Therefore the anodic current I_p^{a4} observed in the CV (figure 3.14D) is lower than I_p^{c4}. However, it is to be noted that in the absence of nitric acid (figure 3.14C) the reduction current I_p^{c5} and oxidation current I_p^{a6} are quite comparable.

3.2.1.6. Diffusion coefficients

The CVs of UO_2^{2+} in C_4mimCl recorded at a glassy carbon working electrode at 373 K at different scan rates are shown in figure 3.15. The open circuit potential was fixed at 0.2 V (Vs Pd). The cathodic and anodic switching potentials were fixed at -1.2 V (Vs Pd) and 0.8 V respectively. It is evident from figure 3.15 that the cathodic peak potential (E_p^{c4}) gets shifted cathodically and the anodic peak potential (E_p^{a4}) gets shifted anodically with an increase in scan rate. The cathodic and anodic peak current also increases with an increase in scan rate. These observations are characteristic of an irreversible or quasi-reversible reduction (of UO_2^{2+} to UO_2). This indicates that the reduction of UO_2^{2+} is governed not only by the diffusion of UO_2^{2+} at the working electrode, but also by the kinetics of the electron transfer occurring across the electrode-electrolyte interface. Moreover, the nature of the electron transfer across the electrode-electrolyte interface could be determined by measuring the quantity $|E_p^{c4} - E_{p/2}^{c4}|$, where $E_{p/2}^{c4}$ is the half peak potential. If this value is more than 33 mV for the two electron transfer reaction at 373 K, then the electrode reaction occurring at the electrode-electrolyte interface could be regarded as irreversible or quasi-reversible. The value of $|E_p^{c4} - E_{p/2}^{c4}|$ was found to span from 80 mV to 128 mV at different scan rates of 10 mV/s to 100 mV/s. This observation confirms that the reduction of UO_2^{2+} to UO_2 at the working electrode is not only governed by diffusion of UO_2^{2+} but also by heterogeneous charge transfer kinetics occurring across the electrode-electrolyte interface [13, 14].

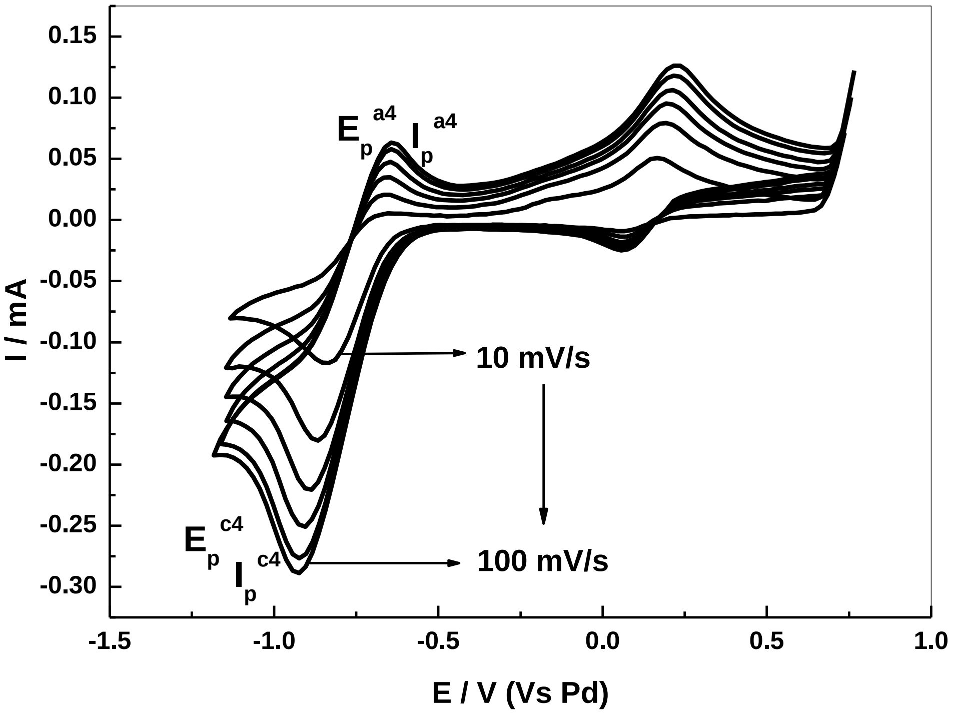

Figure 3.15. CV of 150 mM UO_2^{2+} (U_3O_8 dissolved in C_4mimCl in presence of nitric acid) recorded at a glassy carbon electrode at different scan rates, at 353 K.

The heterogeneous charge transfer coefficient (α) is a measure of the symmetry of the barrier in a non-reversible electron transfer reaction and it can have the values ranging from 0.1 to 0.9. The charge transfer coefficient for the reduction of UO_2^{2+} to UO_2 could be determined by using equation (3.6) [14].

$$|E_p^{c4} - E_{p/2}^{c4}| = 1.857RT/\alpha n_\alpha F \quad (3.6)$$

where E_p^{c4} and $E_{p/2}^{c4}$ are peak and half-peak potentials responsible for the reduction of UO_2^{2+} to UO_2. By substituting the values of $|E_p^{c4} - E_{p/2}^{c4}|$ determined from the CV, shown in figure 3.13, the value of αn_α was determined. It was found to vary from 0.42 to 0.49 with an increase in scan rate from 10 mV/s to 100 mV/s at 373 K. Since these variations in the magnitude of charge transfer coefficient are rather less, a value of 0.45

was taken as the value for αn_α, for determining diffusion coefficients over the entire scan rate.

The Berzin-Delahey relation for the irreversible or quasi-reversible reduction of soluble-insoluble (UO_2^{2+} to UO_2) couple is shown in equation A.5 (Annexure). The concentration of U(VI) present in C_4mimCl is 150 mM, and n is the number of electron transferred (=2). The plot of I_p^{c4} against square root of scan rate ($\upsilon^{1/2}$) at 373 K is shown in figure 3.17. It could be seen that this plot is linear and has a zero intercept. This indicates the validity of Berzin-Delahay equation for the reduction of UO_2^{2+} to UO_2 and enables the determination of the diffusion coefficient from the slope of the fitted straight line. The value of αn_α was taken to be 0.45, which was applicable over the entire scan rate (10 mV/s to 100 mV/s), for determining the diffusion coefficient. The apparent diffusion coefficient thus determined at 373 K is shown in table 3.3. A value of 3.1 X 10^{-12} m^2/s was obtained for the diffusion of UO_2^{2+} at the working electrode. This value compares well with the value of UO_2^{2+} diffusion coefficients determined by others [6, 11, 32].

3.2.1.7. Effect of temperature

Figure 3.16 shows the cyclic voltammogram of UO_2^{2+} in C_4mimCl recorded at a glassy carbon working electrode at a scan rate of 100 mV/s at four different temperatures. A solution containing uranyl ions was obtained by the dissolution of U_3O_8 in C_4mimCl in presence of nitric acid. Subsequently this solution was dried at 353 K under vacuum for 24 h. The CVs show that the peak current I_p^{c4} increases with temperature. In addition, the cathodic peak potential E_p^{c4} gets shifted anodically and the anodic peak potential gets shifted cathodically with an increase in temperature. Thus it is transfer reaction pertaining to the reduction of UO_2^{2+} to UO_2 is facilitated with an increase in temperature.

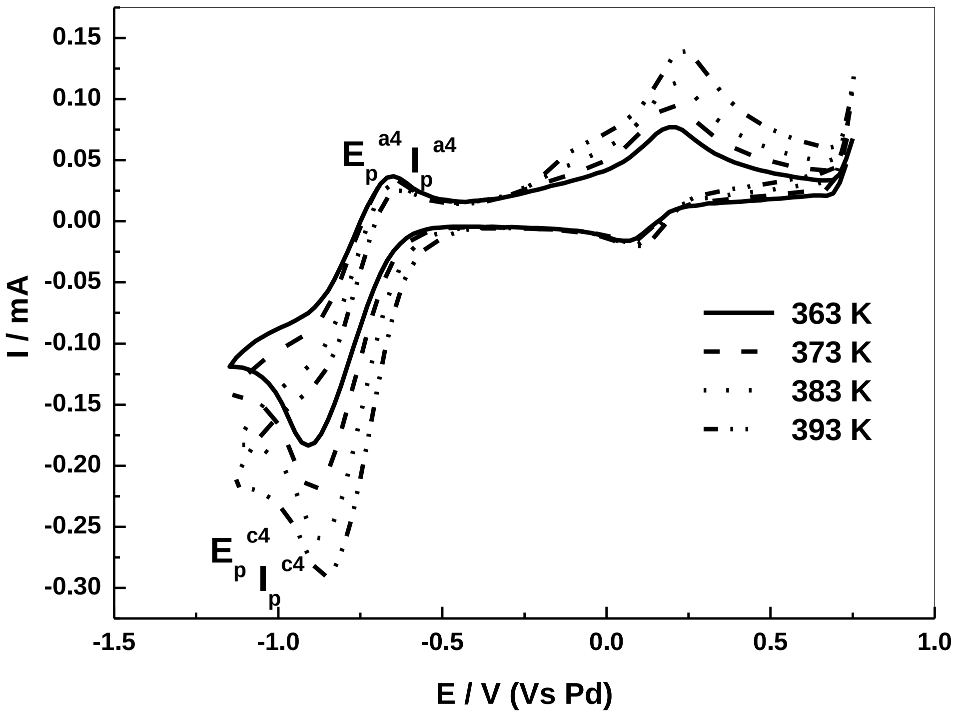

Figure 3.16. CV of 150 mM UO_2^{2+} (U_3O_8 dissolved in C_4mimCl in presence of nitric acid) recorded at a glassy carbon electrode at different temperatures at the scan rate = 100 mV.s^{-1}.

The CV pertaining to UO_2^{2+} in C_4mimCl was recorded as a function of scan rate at different temperatures. From those voltammograms and using equation 3.6, the magnitude of αn_α was determined at there temperatures. The average value of αn_α at a particular temperature is shown in table 3.4. It is evident that the magnitude of αn_α decreases with temperature, indicating a heterogeneous charge transfer symmetry barrier decreases with an increase in temperature. From the CV obtained at different scan rates and temperatures, the cathodic peak current was plotted as a function of square root of the scan rate. These results are shown in figure 3.17.

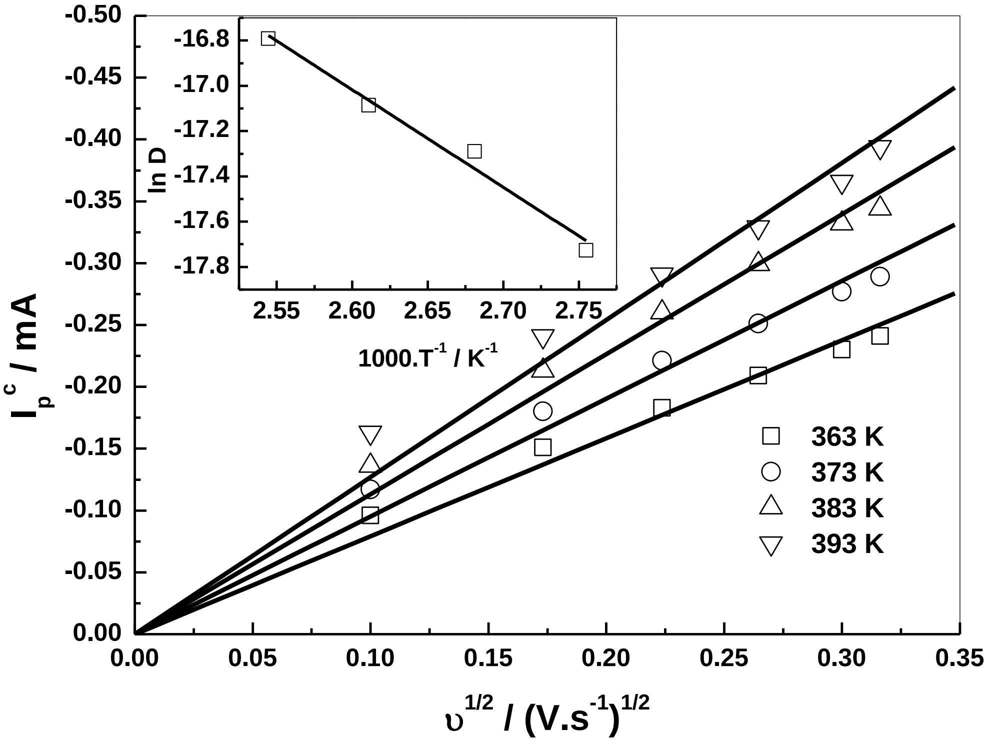

Figure 3.17. Plot of cathodic peak current against the square root of scan rate ($\upsilon^{1/2}$) pertaining to the reduction of 150 mM UO_2^{2+} (U_3O_8 dissolved in C_4mimCl in presence of nitric acid) at different temperatures. (Insert: Plot of ln D against reciprocal temperature)

It is evident that the peak current (I_p^{c4}) increases with increase of temperature. Using the value of αn_α determined at different temperatures and from the slope of the straight line shown in figure 3.17, the diffusion coefficient was determined at each of these temperatures using equation A.5 (Annexure). These D values are tabulated in table 3.4. It is obvious that the diffusion coefficient increases from 2.0 x 10^{-12} m^2/s to 5.1 x 10^{-12} m^2/s when the temperature is raised from 363 K to 393 K. The temperature dependence of the diffusion coefficient is given by the Arrhenius relation shown in equation 3.8

$$\ln D = \ln A - E_a/RT \qquad (3.8)$$

where A is the pre-exponential factor and E_a is the energy of activation. The plot of ln D against 1/T is shown as an insert in figure 3.17. From the slope of this fitted straight line, the value of E_a was determined to be 36 kJ/mol.

Table 3.4. Diffusion coefficient of U(VI) determined by cyclic voltammetry and chronopotentiometry.

Temperature / K	**αn_α**	**Diffusion coefficient X 10^{12} by cyclic voltammetry /$m^2.s^{-1}$**	**Diffusion coefficient X 10^{12} by chronopotentiometry /$m^2.s^{-1}$**
363	0.49	2.0	3.0
373	0.45	3.1	3.6
383	0.43	3.8	4.1
393	0.42	5.1	4.8

3.2.1.8. Chronopotentiometry

The electrochemical behavior of UO_2^{2+} in C_4mimCl containing nitric acid was further studied by chronopotentiometry. The solution was obtained by the dissolution of U_3O_8 in C_4mimCl medium in the presence of nitric acid and the solution was dried at 353 K under vacuum for 24 hours. Figure 3.18 shows the chronopotentiogram of UO_2^{2+} in C_4mimCl recorded at a glassy carbon working electrode at different applied currents, varying from -0.25 mA to -0.35 mA. The chronopotentiogram shows a sudden surge in the cathodic potential of the working electrode to a potential value corresponding to the reduction of UO_2^{2+} to UO_2. These after the potential of the electrode remain constant over a period of time depending upon the applied potential. Subsequently, the cathodic potential increases again with increase of time. As indicated in figure 3.18, the transition time (τ) is the duration at which the potential of the working electrode remains constant. The relation between the applied current and the transition time is given by the Sand relation shown in equation A.7 (Annexure)

The plot of i against $\tau^{-1/2}$ is shown in insert in figure 3.18. Linear regression of the experimental data results in a straight line with a zero intercept. This indicates the validity of Sand equation and enables the determination of diffusion coefficient from the slope of the fitted linear relation and using equation 2.7.

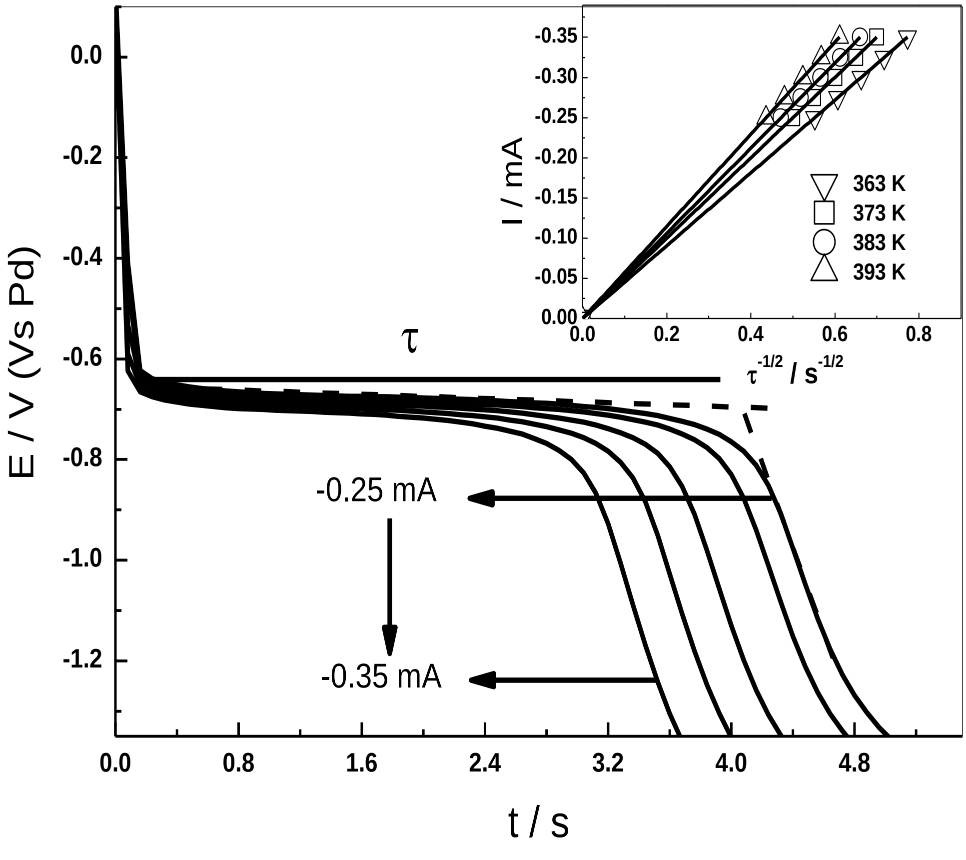

Figure 3.18. Comparison of cathodic chronopotential transients for 150mM UO_2^{2+} (U_3O_8 dissolved in C_4mimCl in presence of nitric acid) at different applied currents, at 373 K. (Insert: Plot of applied current against inverse of square root of transient time)

Figure 3.19 shows the chronopotentiogram of UO_2^{2+} in C_4mimCl recorded at different temperatures. It is evident that the transition time (τ) increases with increase of temperature. This is plaussibly due to the increase in the diffusion of UO_2^{2+} from bulk leading to an increase in the abundance of UO_2^{2+} ions at the working electrode at higher temperatures. Therefore, the potential of the working electrode remains constant for longer duration. Similar to the procedure indicated above, the diffusion coefficients of UO_2^{2+} was determined at different temperatures, from the slope obtained from the plot shown in figure 3.19. The diffusion coefficients are listed in table 3.4. It is seen from this tabulation that the D values increases with temperature and the values obtained in the chronopotentiometry runs are comparable with those obtained in cyclic voltammetry.

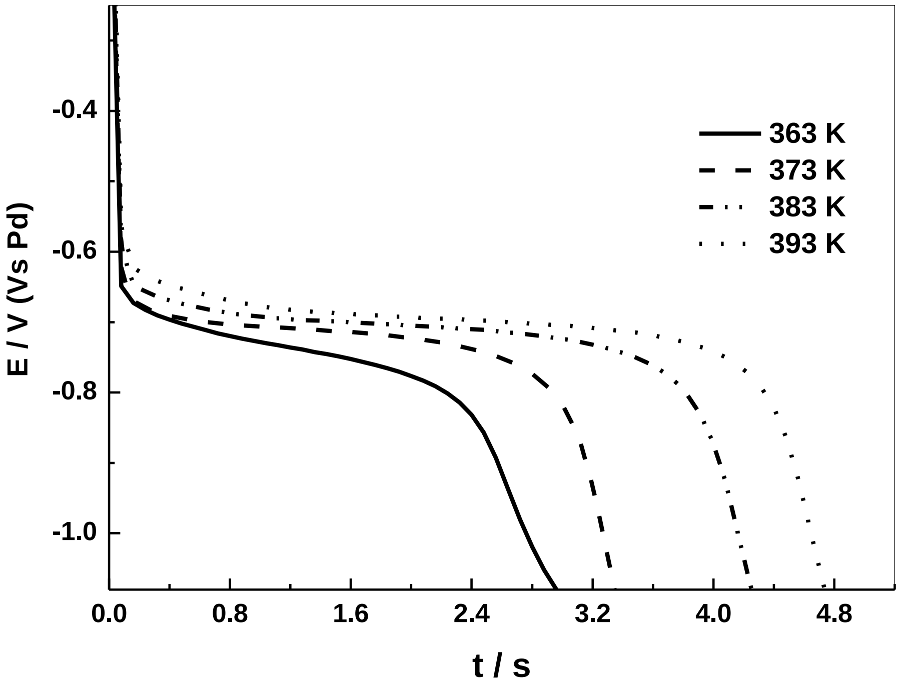

Figure 3.19. Comparison of the cathodic chronopotential transients for 150mM UO_2^{2+} (U_3O_8 dissolved in C_4mimCl in presence of nitric acid) at various temperatures at an applied potential of -0.35 mA.

3.2.2. Conclusions

U_3O_8 could be dissolved in C_4mimCl only in the presence of a small amount of nitric acid. The UO_2^{2+} ion present in the resultant solution forms a variety of complexes with both nitrate as well as chloride ions present in the medium. UV- Visible absorption spectra indicate that U(VI) could exist in the form of mixed complexes, $[UO_2Cl_x(NO_3)_{4-x}]^{2-}$, in the IL when the ratio of Cl : UO_2^{2+} is 4 : 1 or less. Beyond 4 : 1 mole ratio, the specie $[UO_2Cl_4]^{2-}$ dominates, as evidented by the splitting of the bands in the UV-Visible spectrum. The ATR-FTIR spectroscopic studies also indicate that the addition of Cl^- ion to uranyl nitrate sequentially leads to the substitution of nitrate ions by Cl^- ions. At a mole ratio of Cl^- : UO_2^{2+} is 4 : 1 or above, the transmittance bands get shifted to 920 cm^{-1} indicating the formation of $[UO_2Cl_4]^{2-}$. All the spectroscopic studies including Raman spectroscopy clearly established the formation of $[UO_2Cl_4]^{2-}$ in the C_4mimCl solution.

The electrochemical behavior of $[UO_2Cl_4]^{2-}$ in the IL, C_4mimCl was investigated by CV and CP. The reduction of UO_2^{2+} to UO_2 occurred at a potential of -0.8 V (Vs Pd) and the redox reaction of the residual nitric acid present in the IL occurred at 0.1 V (Vs Pd). The diffusion coefficient of UO_2^{2+} in the dissolver solution was determined to be of the order of 10^{-8} cm^2/s and increased with temperature. This study showed that $[UO_2Cl_4]^{2-}$ underwent a two electron transfer electrochemical reduction yeilding UO_2 at the working electrode.

References

1. Spent Fuel Reprocessing Options, IAEA-TECDOC-1587, 2008.
2. Y. Sakamura, T. Omori, Electrolytic reduction and electrorefining of uranium to develop pyrochemical reprocessing of oxide fuels, Nucl. Technol. 171 (2010) 266–275.
3. K. Kosugi, M. Fukushima, M. Myochin, K. Mizuguchi, T. Oomori, Deposition behaviour of UO_2 and noble-metal elements in oxide-electrowinning reprocessing, J. Phys. Chem. Solids 66 (2005) 629–633.
4. Y. Ikeda, N. Asanuma, Y. Ohashi, Electrochemical studies on uranyl(VI) species in 1-butyl-3-methylimidazolium based ionic liquids and their application to pyro-reprocessing and treatment of wastes contaminated with uranium, in: A. Kokorin (Ed.), Ionic Liquids: Applications and Perspectives, InTech 2011, pp. 659–674.
5. N. Asanuma, M. Harada, Y. Yasuike, M. Nogami, K. Suzuki, Y. Ikeda, Electrochemical properties of uranyl ion in ionic liquids as media for pyrochemical reprocessing, J. Nucl. Sci. Technol. 44 (2007) 368–372.
6. B. Joseph, K. A. Venkatesan, K. Nagarajan, P. R. Vasudeva Rao, Electrowinning of UO_2 from ionic liquid medium, Sep. Sci. Technol. 48 (2013) 2506–2511.
7. W.J. Pemberton, J.E. Droessler, J.M. Kinyanjui, K.R. Czerwinski, D.W. Hatchett, Electrochemistry of soluble UO_2^{2+} from the direct dissolution of UO_2CO_3 in acidic ionic liquid containing water, Electrochim. Acta 93 (2013) 264–271.
8. J.W. Freiderich, E. Wanigasekara, X.G. Sun, R.A. Meisner, H.M. Meyer, H. Luo, L.H. Delmau, S. Dai, B.A. Moyer, Direct Electrodeposition of UO_2 from Uranyl bis(trifluoromethanesulfonyl)imide dissolved in 1-Ethyl-3-methylimidazolium Bis(trifluoromethanesulfonyl)imide room temperature ionic liquid system, Electrochim. Acta 115 (2014) 630–638.

9. V.A. Volkovich, A.I. Bhatt, I. May, T.R. Griffiths, R.C. Thied, A spectroscopic study of uranium species formed in chloride melts, J. Nucl. Sci. Technol. 39 (2002) 595–598.
10. N.N. Greenwood, A. Earnshaw, Chemistry of Elements, second edition Butterworth-Heinemann, 1997.
11. P. Giridhar, K.A. Venkatesan, T.G. Srinivasan, P.V. Rao, Electrochemical behavior of uranium (VI) in 1-butyl-3-methylimidazolium chloride and thermal characterization of uranium oxide deposit, Electrochim. Acta 52 (2007) 3006–3012.
12. R.H. Wopschall, I. Shain, Effects of adsorption of electroactive species in stationary electrode polarography, Anal. Chem. 39 (1967) 1514–1527.
13. A.J. Bard, L.R. Faulkner, Electrochemical Methods-Fundamentals and Applications, Wiley, New York, 1980.
14. K. Aoki, K. Tokuda, H. Matsuda, Theory of linear sweep voltammetry with finite diffusion space, J. Electroanal. Chem. Interfacial Electrochem. 146 (1983) 417–424.
15. M. Jayakumar, K.A. Venkatesan, T.G. Srinivasan, Electrochemical behavior of fission palladium in 1-butyl-3-methylimidazolium chloride, Electrochim. Acta 52 (2007) 7121–7127.
16. C.J. Rao, K.A. Venkatesan, K. Nagarajan, T.G. Srinivasan, P.V. Rao, Electrochemical and thermodynamic properties of europium (III), samarium (III) and cerium (III) in 1-butyl-3-methylimidazolium chloride ionic liquid, J. Nucl. Mater. 399 (2010) 81–86.
17. R.J. Klingler, J.K. Kochi, Electron-transfer kinetics from cyclic voltammetry. Quantitative description of electrochemical reversibility, J. Phys. Chem. 85 (1981) 1731–1741.

18. A.S.A. Khan, R. Ahmed, M.L. Mirza, Kinetics and electrochemical studies of uranium in acetate and formate media by cyclic voltammetry, Radiochim. Acta 95 (2007) 693-699.

19. I. Billard, C. Gaillard, C. Hennig, Dissolution of UO_2, UO_3 and of some lanthanide oxides in BumimTf$_2$N: Effect of acid and water and formation of $UO_2(NO_3)_3^-$, Dalton Trans. 37 (2007) 4214.

20. R.W. Stromatt, Studies on the electroreduction of uranyl (VI) in molten equimolar KCl-NaCl by chronopotentiometric and electrode impedance measurements, J. Electrochem. Soc. 110 (1963) 1277.

21. K. Kosugi, M. Fukushima, M. Myochin, K. Mizuguchi, T. Oomori, Deposition behavior of UO_2 and noble-metal elements in oxide-electrowinning reprocessing, J. Phy. Chem. Solids 66 (2005) 629.

22. J.J. Katz, E. Rabinowitch, The Chemistry of Uranium, McGraw Hill (Ed), New York, (1961) p. 327.

23. C. Gaillard, I. Billard, A. Chaumont, S. Mekki, A. Ouadi, M.A. Denecke, G. Moutiers, G. Wipff, Europium(III) and its halides in anhydrous room-temperature imidazolium-based ionic liquids: a combined TRES, EXAFS, and molecular dynamics study, Inorg. Chem. 44 (2005) 8355.

24. C. Gaillard, A. El Azzi, I. Billard, H. Bolvin, C. Hennig, Uranyl complexation in fluorinated acids (HF, HBF_4, HPF_6, HTf$_2$N): a combined experimental and theoretical study, Inorg. Chem. 44 (2005) 852.

25. C. Gaillard, A. Chaumont, I. Billard, C. Hennig, A. Ouadi, G. Wipff, Uranyl coordination in ionic liquids: The competition between ionic liquid anions, uranyl counterions, and Cl- anions investigated by extended X-ray absorption fine

structure and UV−Visible spectroscopies and molecular dynamics simulations, Inorg. Chem. 46 (2007) 4815.

26. S. Georg, I. Billard, A. Ouadi, C. Gaillard, L. Petitjean, M. Picquet, V. Solov'ev, Determination of successive complexation constants in an ionic liquid: complexation of UO_2^{2+} with NO_3^- in C_4mimTf_2N studied by UV−Vis spectroscopy, J. Phys. Chem. B 114 (2010) 4276.
27. C. Gaillard, A. Chaumont, I. Billard, C. Hennig, A. Ouadi, S. Georg, G. Wipff, Competitive complexation of nitrates and chlorides to uranyl in a room temperature ionic liquid, Inorg. Chem. 49 (2010) 6484.
28. P. Nockemann, K. Servaes, R. Van Deun, K. Van Hecke, L. Van Meervelt, K. Binnemans, C. Görller-Walrand, Speciation of uranyl complexes in ionic liquids by optical spectroscopy, Inorg. Chem. 46 (2007) 11335.
29. M. Gal, P.L. Goggin, J. Mink, Vibrational spectroscopic studies of uranyl complexes in aqueous and non-aqueous solutions, Spectrochim. Acta A 48 (1992) 121.
30. S. Hayashi, R. Ozawa, H. Hamaguchi, Raman spectra, crystal polymorphism, and structure of a prototype ionic-liquid [bmim]Cl, Chem. Lett. 32 (2003) 498.
31. M.B. Alves, V.C. Soares, P.A. Suarez, J.C. Rubim, Raman spectroscopy of ionic liquids derived from 1-n-butyl-3-methylimidazolium chloride and niobium chloride or zinc chloride mixtures, J. Raman Spectrosc. 39 (2008) 1388.
32. X.F. Tan, L.Y. Yuan, C.M. Nie, K. Lui, Z.F. Chai, W.Q. Shi, Electrochemical behaviour of uranyl in ionic liquid 1-butyl-3-methylimidazolium chloride mixture with water, J. Radioanal. Nucl. Chem. 302 (2014) 281.

Chapter 4. Electrochemical behavior of uranium and spectroscopic investigation of uranyl species in ionic liquid medium.

Introduction

In the previous couple of decades, researchers have exploited the desirable and environmentally benign properties of ILs for developing many advanced technological applications in different domains [1-6]. In nuclear fuel cycle, the ILs have been extensively investigated as electrolytic medium for applications related to non-aqueous reprocessing of spent nuclear fuels [1-5]. For advanced electrochemical applications such as electrowinning and electrorefining of nuclear fuels, it is essential for the IL to have a reasonable solubility of actinides in IL medium, high electrochemical stability and also displays low viscosity [5, 7, 8].

4.1. Electrochemical behavior and spectroscopic investigation of U(VI) in $C_4mimNTf_2$ in presence of tri-n-butyl phosphate, nitrate and chloride

ILs have been used in the process of EXtraction-ELectrodeposition (EX-EL) [9-11]. In this method, the hydrophobicity of the IL is taken advantage of for its deployment as a diluent to extarct the metal ion from aqueous wastes by solvent extraction. Coupled with this, the wide electrochemical stability of ILs has been ingeneously used to recover the extracted metal in a convenient solid form, by electrodeposition from the IL phase. Such a process helps produce the desired solid end product and avoids many intermediate steps.

In this context, Hussey *et al.* [12] investigated the feasibility of the electrodeposition of cesium and strontium containing calixerenes and crown ether ligands ionophores from IL. In addition, they also investigated the electrochemical behaviour of a solution containing some trivalent lanthanide ions, the neutral tridentate ligand, N,N,N′,N′-tetra(n-octyl)diglycolamide (TODGA) and choride ion in IL [13]. Matsumiya *et al*. [11] investigated the extraction and electrodeposition behaviour of some lanthanides (Pr, Nd and Dy) in a solution composed of tri-*n*-butyl phosphate (TBP) and IL. The extraction behaviour of rare earth elements in TODGA-IL system was investigated by Murakami *et al*. [14].

In the extracted phase, the electrochemical behavior and electrodepositon of the metal ion is governed by the nature of diffusing species at the working electrode and therefore, on the size of the complex and strength of the ligand coordinated to the metal ion. It has been reported that the diffusion of electroactive species at the working electrode is lowered in the presence of ligands and reduction potential of the electroactive species is shifted to more cathodic potentials [10, 12]. In such cases, the electrode process at the working electrode is very complex and irreversible in the presence of ligands. One way of minimising/eliminating this kind of complication is to add a new ligand preferably a monoatomic anion, whose coordinating ability with the metal ion is higher than the organic ligand. The addition of such a strong field ligand to the electrolytic medium displaces the big neutral organic ligand from the metal co-odination sphere, and the product formed after decomplexation is expected to undergo faster diffusion at the working electrode. In addition, the required ligand can be selected in such a way that it undergoes easy oxidation at the counter electrode during the reduction of metal species at the working electrode. One such monoatomic ligand could be a halide anion [13, 15, 16].

The electrochemical behaviour of UO_2^{2+} in IL solution containing TBP was reported by Giridhar *et al*. [10]. The electrochemical reduction of UO_2^{2+} in IL was very complex and the cathodic current was invariably very low, owing to the presence of TBP in the IL solution [10]. In order to tame the electrochemical behaviour of UO_2^{2+} in the presence of TBP, the voltammetric behaviour of UO_2^{2+} in presence of Cl^- ions, added in the form of 1-butyl-3-methylimidazolium chloride (C_4mimCl) was investigated. In this chapter, the effect of varying the chloride ion content in IL phase on the decomplexation behaviour UO_2^{2+} from TBP coordination, and the possibility of underpoential deposition of uranium oxide in $C_4mimNTf_2$ was investigated. The electrochemical and spectroscopic studies were carried out with mole ratio of U : NO_3 : TBP : Cl in IL solution was varied from of 1 : 2 : 2 : 0 to 1 : 2 : 2 : 6. The nature of uranyl species formed at various mole ratios was characterized by UV–Visible, ATR-FTIR and Raman spectroscopy. The diffusion behavior of UO_2^{2+} species was investigated at various chloride ion concentrations to calculate the diffusion coefficients with the nature of uranyl species.

Experimental parts of the present study have been discussed in 2.4.3 and synthesis of IL mentioned in 2.5.2 of chapter 2.

4.1.1. Results and discussion

4.1.1.1. Cyclic voltammetry of U(IV) in ionic liquid medium

The CV of $C_4mimNTf_2$ is shown in figure 4.1. It can be seen that $C_4mimNTf_2$ offers an electrochemical window of 5 V. The CV pertaining to $UO_2(NO_3)_2$ (U = 80 mM) present in a solution of TBP (160 mM) in $C_4mimNTf_2$, recorded at a glassy carbon working electrode at the scan rate of 100 mV/s is also shown in figure 4.1. The uranyl nitrate in TBP/$C_4mimNTf_2$ shows the onset of reduction occurring at the potential of -0.5 V (Vs Pd) resulting in a weak peak, at the potential (E_p^{c1}) of -0.9 V (Vs Pd), which could be attributed to the reduction of UO_2^{2+} to UO_2 [10]. The corresponding oxidation wave occurs at the peak potential (E_p^{a1}) of -0.1 V (Vs Pd). When the scan was reversed at -2 V, the voltammogram showed a continuous surge of cathodic current beyond the peak current (I_p^{c1}). It should be noted that the magnitude of peak current density is quite low and the peak potential is more negative than the peak potential reported for the reduction of UO_2^{2+} to UO_2 in other ILs [7, 14-16]. For instance, the cyclic voltammogram of 80 mM UO_2Cl_2 in C_4mimCl, under identical conditions is shown in the same for comparison. The the poor cathodic current density and overpotential observed for the reduction of UO_2^{2+} to UO_2 in TBP/$C_4mimNTf_2$ could be attributed to the formation of bulky electroactive species $[UO_2(NO_3)_2(TBP)_2]$ in the $C_4mimNTf_2$ phase. It is well-recognised that uranyl nitrate forms 1 : 2 (U : TBP) complex with TBP in ILs as well as other molecular diluent media [17, 18]. The anion NTf_2^- does not co-ordinate with uranyl ion, since NTf_2^- is a weak field ligand as compared to NO_3^- [15, 16, 19, 20].

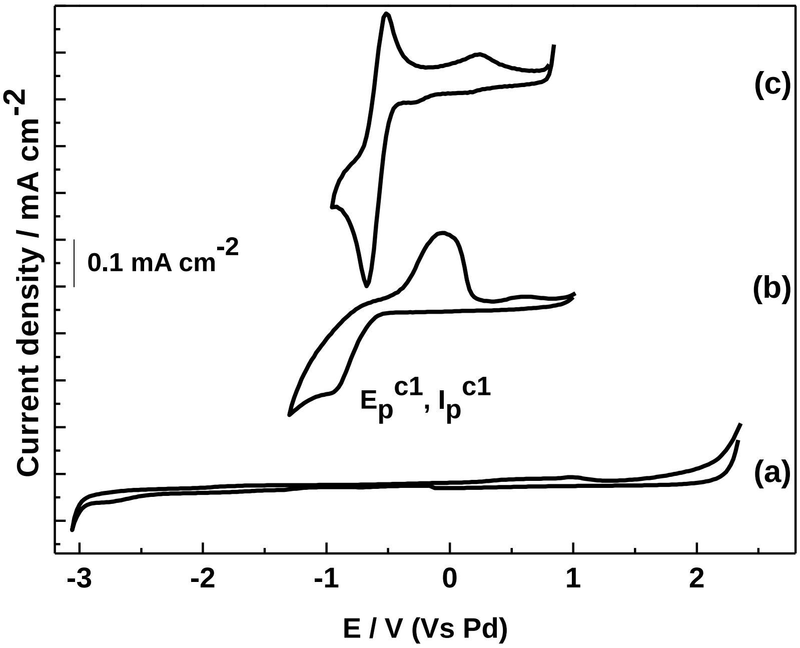

Figure 4.1. CV of (a) $C_4mimNTf_2$, (b) 80 mM $UO_2(NO_3)_2$ dissolved in $C_4mimNTf_2$ containing TBP (160 mM) and (c) 80 mM UO_2Cl_2 dissolved in C_4mimCl recorded at a glassy carbon working electrode at the scan rate of 100 mV.s^{-1} at 373 K.

4.1.1.2. Cyclic voltammetry of U(VI) in the presence of C_4mimCl

The CV pertaining to uranyl ion in $C_4mimNTf_2$, recorded at a glassy carbon working electrode at a scan rate of 100 mV/s, at 373 K showed in figure 4.2. The mole ratio, U : NO_3 : Cl was varied from 1 : 2 : 0 to 1 : 2 : 6. The TBP was also present in the solution at the U : TBP mole ratio of 1 : 2. It is evident that the current density of UO_2^{2+} reduction increases in all cases with the Cl^- content. The cathodic peak potential observed for the reduction of UO_2^{2+} increases in the following order; $E_p^{c1} < E_p^{c3} < E_p^{c4} < E_p^{c5}$, that corresponds to an increasing order of Cl^- ion content in the IL. However, at the mole ratio 1 : 1 of U : Cl, a weak cathodic peak is observed at E_p^{c2}, whose potential is higher than E_p^{c5} i.e. $E_p^{c5} < E_p^{c2}$. All these observations indicate that the addition of Cl^- to the IL is likely to convert the $UO_2(NO_3)_2(TBP)_2$ specie into various anionic chloro complexes of uranium, as discussed above. Since TBP does not co-ordinate with these anionic uranyl chloro complexes, it gets displaced from the uranyl coordination sphere. The decomplexed uranyl specie (from TBP), thus produced, seems to undergo faster diffusion and favourable reduction at the working electrode. However, it is necessary to confirm the nature of the electroactive specie reduced at different potentials (E_p^{c2}, E_p^{c3}, E_p^{c4}, E_p^{c5}) in order to understand its electrochemical behavior. In this context, the speciation of uranyl ion in the presence of nitrate, Cl and TBP was investigated by UV-Visible, ATR-FTIR and Raman spectroscopy and the results are discussed below.

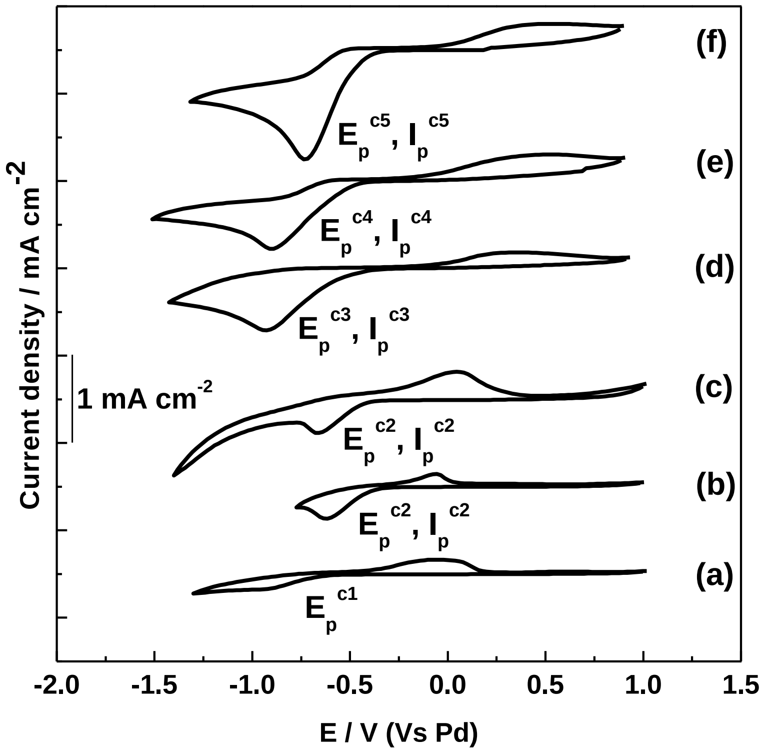

Figure 4.2. CV pertaining to 80 mM $UO_2(NO_3)_2$ in $C_4mimNTf_2$ containing TBP (160 mM) recorded at a glassy carbon electrode at a scan rate of 100 mV.s^{-1} at 373 K, in the presence and absence of C_4mimCl. The mole ratio of U : NO_3 : TBP : Cl is (a) 1 : 2 : 2 : 0, (b) 1 : 2 : 2 : 1, (c) 1 : 2 : 2 : 1 but reversed at -1.45 V, (d) 1 : 2 : 2 : 2, (e) 1 : 2 : 2 : 4 and (f) 1 : 2 : 2 : 6.

4.1.1.3. Speciation of Uranyl Ion in ionic liquid medium

In order to increase the current density and reduce the overpotential needed for the reduction of UO_2^{2+} to UO_2, C_4mimCl was added to the uranyl nitrate - TBP solution. The added chloride ion could form a series of complexes with uranyl ion depending upon the mole ratio of U : NO_3 : Cl. The following reactions could be proposed for the complexation of neutral uranyl nitrate with chloride ion.

$$UO_2(NO_3)_2 + Cl^- \rightleftharpoons [UO_2(NO_3)_2Cl]^- \tag{4.1}$$

$$UO_2(NO_3)_2 + 2Cl^- \rightleftharpoons [UO_2(NO_3)_2Cl_2]^{2-} \tag{4.2}$$

$$UO_2(NO_3)_2 + 2Cl^- \rightleftharpoons [UO_2(NO_3)Cl_2]^- + NO_3^- \tag{4.3}$$

$$UO_2(NO_3)_2 + 3Cl^- \rightleftharpoons [UO_2(NO_3)Cl_3]^{2-} + NO_3^- \tag{4.4}$$

$$UO_2(NO_3)_2 + 4Cl^- \rightleftharpoons [UO_2Cl_4]^{2-} + 2NO_3^- \tag{4.5}$$

It should be noted that the abundance of the different uranyl species in C_4mimNTf$_2$ medium depends upon relative mole ratio of U : NO_3 : Cl, as well as on the relative stability of the resultant complex in the IL. In this context, Gaillard *et al.* [12] studied the competitive complexation of nitrates and chlorides with uranyl ion in C_4mimNTf$_2$ and reported the coordination behaviour uranyl ion in that solution. When the mole ratio of U : NO_3 : Cl was 1 : 2 : 1, the most dominant specie was $[UO_2(NO_3)_2Cl]^-$, and at higher Cl : U ratio (4 or higher), the uranyl ion forms mixture of complexes such as $[UO_2Cl_3(NO_3)]^{2-}$ and $[UO_2Cl_4]^{2-}$. However, it is important to note that TBP was not present in the IL medium, investigated by Gaillard *et al.* [15].

Nevertheless, literature indicates that TBP and NO_3^- were not "strong field" ligands as compared to Cl^- ions, and they could be easily substituted from uranyl coordination sphere by a near stoichiometric or slightly excess quantity of Cl^- ions [15, 16, 19-21]. Moreover, it should be noted that TBP being a neutral ligand, could form a complex essentially with neutral uranyl species like $[UO_2X_2]$, where X = Cl^- or NO_3^-. Therefore, the addition of C_4mimCl to $[UO_2(NO_3)_2(TBP)_2]$ in C_4mimNTf$_2$ could result in the displacement of TBP from uranyl co-ordination sphere and facilitate the formation of anionic chloro complexes of uranyl ion as indicated in equations (4.1) to (4.5). Since the co-ordination of TBP was responsible for the low cathodic current and overpotential reduction of UO_2^{2+} to UO_2, the decomplexation of TBP from uranyl coordination sphere is expected to facilitate the reduction of UO_2^{2+} to UO_2 at lower negative potentials and increase the current density.

4.1.1.4. Visible Absorption Spectroscopy of uranyl ion in ionic liquid medium

The co-ordination environment of uranyl ion can be ascertained to some extent by comparing the visible absorption spectrum of the uranyl species obtained at various mole ratios of Cl^- ion with those reported in the literature [15, 16]. It should be noted that in all visible absorption spectrum investigations, the ratio U : NO_3 : TBP was kept at 1 : 2 : 2 and C_4mimCl was added to this solution to increase the Cl^- ion concentration, such that the U : NO_3 : TBP : Cl could be varied from 1 : 2 : 2 : 0 to 1 : 2 : 2 : 6. This visible absorption spectrum of uranyl nitrate in C_4mimNTf$_2$ at U : NO_3 : TBP mole ratio of 1 : 2 : 2 is shown in figure 4.3. This spectrum of uranyl nitrate in TBP/C_4mimNTf$_2$ is characterised by the presence of bands at 428 nm, 440 nm, 451 nm and 465 nm. The intensity of other bands is less. The absorption spectrum of uranyl nitrate in 14 M nitric acid, shown in the same figure 4.3 matches well with the visible absorption spectrum of uranyl nitrate in TBP/C_4mimNTf$_2$. Literature indicates that a major fraction of the of uranyl ion exists as neutral $UO_2(NO_3)_2$ in 14 M nitric acid [22]. The similarity in the absorption bands of uranyl nitrate in TBP/C_4mimNTf$_2$ with those observed for uranyl nitrate in 14 M nitric acid, indicates that the overall structure of uranyl nitrate specie in the IL is not affected to a great extent by the addition of TBP. Therefore, it is quite likely that uranyl nitrate is essentially solvated by TBP and exists as $UO_2(NO_3)_2(TBP)_2$ in C_4mimNTf$_2$ [21, 22]. Moreover, it should be noted that the anonic component NTf_2^- of this IL is relatively bulky and is a weak field ligand [15, 16, 19-21] as compared to nitrate. Therefore, NTf_2^- does not participate in the coordination with UO_2^{2+} ion in the presence of nitrate.

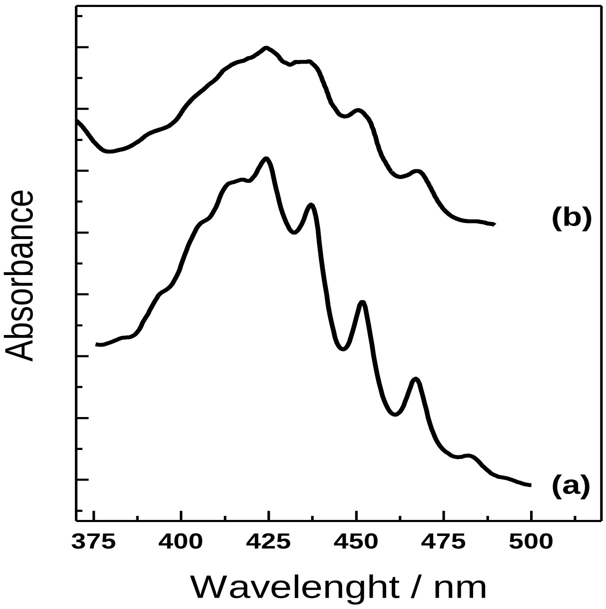

Figure 4.3. UV-Visible absorption spectrum of (a) 80 mM $UO_2(NO_3)_2$ dissolved in C_4mimNTf$_2$ containing TBP (160 mM) and (b) 80mM $UO_2(NO_3)_2$ dissolved in 14 M HNO_3.

It would be be interesting to understand the variation in the visible-absorption bands of uranyl species in the presence of Cl^- ions. Figure 4.4 shows the visible-absorption spectrum of uranyl species at different mole ratios of U : NO_3 : TBP : Cl. In all these cases the ratio U : NO_3 : TBP was maintained constant at 1 : 2 : 2. It could be seen that the addition of Cl^- ions decreases the intensity of the absorption bands at 451 nm, 467 nm and 482 nm and increases the intensity of those at 403 nm, 415 nm and 423 nm. When the mole ratio of U : NO_3 : TBP : Cl is 1 : 2 : 2 : 4, a couple of new bands emerge at 457 nm and 475 nm and become prominent when the mole ratio of U : NO_3 : TBP : Cl reaches 1 : 2 : 2 : 6. In addition, these bands are further broadened at 1 : 2 : 2 : 6 (U : NO_3 : TBP : Cl) mole ratio.

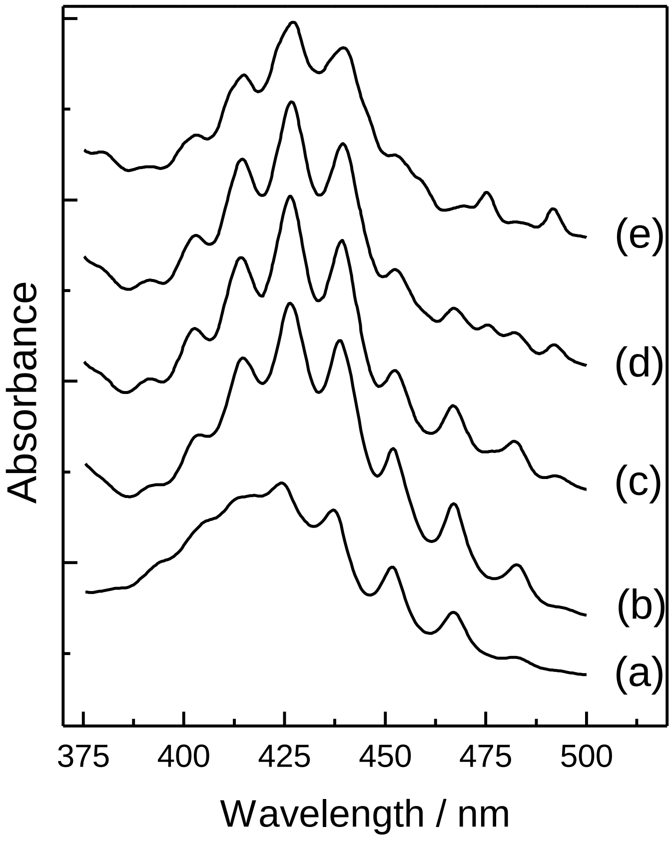

Figure 4.4. UV-Visible absorption spectra of 80 mM $UO_2(NO_3)_2$ dissolved in C_4mimNTf$_2$ containing TBP (160 mM), in the presence and absence of C_4mimCl. The mole ratio of U : NO_3 : TBP : Cl is (a) 1 : 2 : 2 : 0, (b) 1 : 2 : 2 : 1, (c) 1 : 2 : 2 : 2, (d) 1 : 2 : 2 : 4 and (e) 1 : 2 : 2 : 6.

Gaillard *et al.* [15] reported a similar behaviour in the UV-Visible absorption spectrum of uranyl nitrate in C_4mimNTf$_2$. These authors added tetrabutylammonium chloride to vary the U : NO_3 : Cl content in this IL. Gaillard *et al.* [15] also studied the speciation of uranyl ion by EXAFS in the presence of Cl^- ions. But TBP was not present in the solution. When the mole ratio of U : NO_3 : Cl was 1 : 2 : 2, majority of the uranyl species was reported to exist in the form of $[UO_2Cl(NO_3)_2]^-$. At 1 : 2 : 6 mole ratio, the dominant species reported was a mixture of $[UO_2Cl_4]^{2-}$ and $[UO_2Cl_3(NO_3)]^{2-}$. Thus, the visible absorption spectra of uranyl ion in the presence of Cl^- and TBP with those reported by Gaillard *et al.* [15] are quite similar. Thus it is reasonable to conclude that the uranyl ion in the presence of TBP exists in the form of anionic complexes viz., $[UO_2Cl(NO_3)_2]^-$ or $[UO_2Cl_3(NO_3)]^{2-}$ or $[UO_2Cl_4]^{2-}$, depending upon the mole ratio of U : NO_3 : TBP : Cl. Since TBP is a neutral and a weak ligand as compared to NO_3^- and Cl^-, it is not likely to be involved in co-ordination with these anionic uranyl species.

4.1.1.5. Raman Spectroscopy of "Free" Nitrate

The equations (4.1) to (4.5) indicate that the addition of Cl^- ions to $UO_2(NO_3)_2$ present in C_4mimNTf$_2$ leads to the substitution of nitrate ion by Cl^- ions. The nitrate ion released from uranyl coordination sphere could be easily monitored by the NO_3^- symmetric stretching bands in Raman spectra at 1042 cm^{-1} [23]. For instance, when the U : NO_3 : Cl mole ratio is 1 : 2 : 1 the following reactions could take place.

$$UO_2(NO_3)_2 + Cl^- \rightleftharpoons [UO_2(NO_3)_2Cl]^- \qquad (4.6)$$

$$UO_2(NO_3)_2 + 2Cl^- \rightleftharpoons [UO_2(NO_3)Cl_2]^- + NO_3^- \qquad (4.7)$$

The added Cl^- reacts with the uranyl nitrate leading to the formation of $[UO_2(NO_3)_2Cl]^-$ or the uranyl nitrate present in the solution is partially converted to $[UO_2(NO_3)Cl_2]^-$. During the partial conversion, the unreacted $UO_2(NO_3)_2$ remains in the

IL. Among these two reactions, the reaction (4.7) results in the release of nitrate ion from uranyl coordination sphere. Monitoring the liberated "free" or "unco-ordinated" nitrate ion in Raman spectrum at 1042 cm^{-1} would provide more insights into the possibility of the above reactions and the relative abundance of uranyl species. It should be noted that the absorption bands of nitrate ion "co-ordinated" to uranyl ion occurs at 1010 to 1030 cm^{-1}. Since these bands are completely masked by the absorption bands pertaining to the IL at 1020 cm^{-1}, the co-ordinated nitrate bands could not be observed in the Raman spectra.

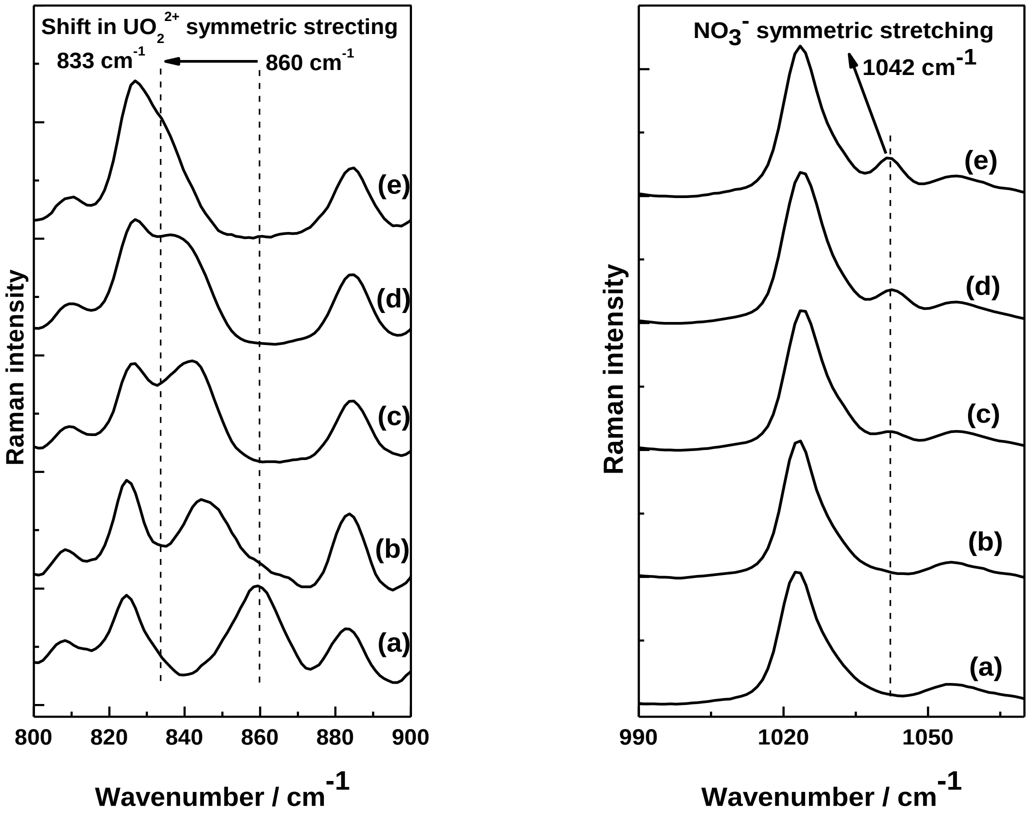

Figure 4.5. Raman spectrum of 80 mM $UO_2(NO_3)_2$ dissolved in $C_4mimNTf_2$ containing TBP (160 mM), in the presence and absence of C_4mimCl. The mole ratio of U : NO_3 : TBP : Cl is (a) 1 : 2 : 2 : 0, (b) 1 : 2 : 2 : 1, (c) 1 : 2 : 2 : 2, (d) 1 : 2 : 2 : 4, (e) 1 : 2 : 2 : 6.

Figure 4.5 shows the Raman spectra pertaining to uranyl ion at U : NO_3 : TBP : Cl mole ratio ranging from 1 : 2 : 2 : 0 to 1 : 2 : 2 : 6. It is evident that the bands pertaining to the unbound (free) nitrate at 1042 cm^{-1} are not present, in the absence of Cl^- ion i.e., at 1 : 2 : 2 : 0 mole ratio as well as at 1 : 2 : 2 : 1 mole ratio. This indicates that NO_3^- ion is not "free" in both these cases. The absence of "free" nitrate ion peaks in the Raman spectra indicates that the dominant uranyl specie is $[UO_2(NO_3)_2Cl]^-$ at 1 : 2 : 2 : 1 mole ratio. At 1 : 2 : 2 : 2 mole ratio of U : NO_3 : TBP : Cl, the reactions shown in (4.2) and (4.3) are possible. The Raman spectrum of the IL solution at 1 : 2 : 2 : 2 mole ratio, shows the presence of a new band at 1042 cm^{-1} indicating the presence of "free" nitrate ion in IL medium. This nitrate ion is possibly liberated from the uranyl ion co-ordination sphere by the reactions shown in equation (4.3). This indicates that the dominant uranyl specie at 1 : 2 : 2 : 2 mole ratio is likely to be $[UO_2(NO_3)Cl_2]^-$. It is also noted that increasing the concentration of Cl^- ions increases the intensity of 1042 cm^{-1} band. This indicates the sequential substitution of NO_3^- ions present in the uranyl co-ordination sphere by Cl^- ions upon the reactions shown in equations (4.4) and (4.5). All these observations confirm that $[UO_2(NO_3)_2(TBP)_2]$ present in IL is gradually converted to different anionic species by the addition of C_4mimCl, and the abundance of these uranyl species increases as we proceed from reaction (4.1) to (4.5) i.e. with an increase in the mole ratio of Cl^- ion in the solution. At higher mole ratio of U : NO_3 : TBP : Cl, i.e., at 1 : 2 : 2 : 6, the dominant specie likely to be present in the solution is $[UO_2Cl_4]^{2-}$.

The gradual substitution of NO_3^- ions present in the uranyl ion coordination sphere by Cl^- ions could also be monitored by recording the position of U=O stretching bands in the Raman spectrum. Literature reports on the Raman spectrum of uranyl compound indicate that uranyl nitrate can be easily identified by the presence of an absorption band at 860 cm^{-1} and that of chlorocomplex, $[UO_2Cl_4]^{2-}$ by the absorption bands at 830 cm^{-1}

[24]. Figure 4.5 shows the Raman spectrum of uranyl species at various mole ratios of U : NO_3 : TBP : Cl varied from 1 : 2 : 2 : 0 to 1 : 2 : 2 : 6. These Raman spectra show the presence of an absorption band at 860 cm^{-1}, which is characteristic to uranyl nitrate as expected at 1 : 2 : 2 : 0 mole ratio. The absorption band at 830 cm^{-1} could be attributed to the IL, $C_4mimNTf_2$. It is noted that the relative intensity of 860 cm^{-1} and 830 cm^{-1} are comparable at 1 : 2 : 2 : 0 mole ratio. The addition of Cl^- ion to $UO_2(NO_3)_2(TBP)_2$ solution results in the gradual shift of 860 cm^{-1} to lower frequencies. At the mole ratio U : NO_3 : TBP : Cl of 1 : 2 : 2 : 1, the 860 cm^{-1} absorption band is partially shifted to 850 cm^{-1} and the original band at 860 cm^{-1} appears as a shoulder to the 850 cm^{-1} band. The presence of a weak shoulder at 860 cm^{-1} indicates that $UO_2(NO_3)_2(TBP)_2$ is still present in the solution, possibly with low abundance. However, the dominant specie seems to be $[UO_2(NO_3)_2Cl]^-$ at 1 : 2 : 2 : 1 mole ratio. Further, addition of Cl^- ion, shifts the position of U=O stretching bands to 830 cm^{-1}, with negligible intensity at 860 cm^{-1}. This indicates that the abundance of $UO_2(NO_3)_2(TBP)_2$ species is negligible at U : NO_3 : TBP : Cl mole ratio of 1 : 2 : 2 : 2. The intensity of 830 cm^{-1} (due to IL) and 850 cm^{-1} (due to U=O stretching) at 1 : 2 : 2 : 2 mole ratio are equal in this case. At 1 : 2 : 2 : 4 mole ratio of U : NO_3 : TBP : Cl, the U=O stretching band is shifted further from 850 cm^{-1} to 840 cm^{-1} and appear as a shoulder to the 830 cm^{-1} band. At 1 : 2 : 2 : 6 mole ratio, the U=O band completely merges with the IL band at 830 cm^{-1}. Further addition of Cl^- did not shift the position of 830 cm^{-1} band further. Therefore, this study indicates that uranyl nitrate-TBP complex is gradually converted to various chloro complexes with the addition of C_4mimCl. At 1 : 2 : 2 : 1 mole ratio of U : NO_3 : TBP : Cl, majority of the uranium species exists as $[UO_2(NO_3)_2Cl]^-$ with residual $[UO_2(NO_3)_2(TBP)_2]$ and at 1 : 2 : 2 : 6 mole ratio and above, the dominant uranium specie is $[UO_2Cl_4]^{2-}$.

4.1.1.6. ATR-FTIR Spectroscopy of U=O and P=O Stretching

The formation of chloro complexes of uranium in $C_4mimNTf_2$ could be further evidenced by probing the transmittance bands of U=O stretching frequencies by FTIR spectroscopy. The FTIR spectroscopic studies on uranium complexes reported in literature indicate that O=U=O asymmetric stretching bands occur at 900 to 950 cm^{-1}. The position of this asymmetric stretching band in FTIR spectrum depends upon the nature of ligands co-ordinated to uranyl ion. When UO_2^{2+} was co-ordinated by two molecules of nitrate ion, the O=U=O stretching band occurs at 940 cm^{-1}. The $[UO_2(NO_3)_2(TBP)_2]$ complex has also reported to show the O=U=O asymmetric bands at 940 cm^{-1} [24]. However, the co-ordination of strong field ligands like Cl^- ion as compared to TBP and NO_3^- ion, results in weakening of U=O bonds and shift the O=U=O asymmetric stretching bands from 940 cm^{-1} to a lower wavenumber. $[UO_2Cl_4]^{2-}$ complex was reported to show a band pertaining O=U=O transmittance band 918 cm^{-1} [25].

When the position and shift of U=O and P=O (of TBP) stretching bands with the addition of Cl^- ions was probed by ATR-FTIR spectroscopy, it was found that the region from 1500 to 800 cm^{-1} was completely masked by the strong transmittance bands of the IL, $C_4mimNTf_2$. In view of this, it was necessary to correct the spectrum of the sample with respect to the $C_4mimNTf_2$ background and present as the differential ATR-FTIR spectrum of the sample. Several authors have reported such differential spectra when the FTIR spectrum of the sample was masked by the solvent [26-28]. Figure 4.6 shows the differential ATR-FTIR spectrum of $UO_2(NO_3)_2$ in $C_4mimNTf_2$. The uranyl nitrate spectrum was corrected with respect to the spectrum of $C_4mimNTf_2$ and presented as differential spectrum in figure 4.6. The corrected spectrum shows the presence of transmittance bands at 950 cm^{-1}. This indicates that UO_2^{2+} is co-ordinated to nitrate ions in the form of $UO_2(NO_3)_2$ in IL. The addition of TBP to $UO_2(NO_3)_2/C_4mimNTf_2$, at U :

NO_3 : TBP mole ratio of 1 : 2 : 2, results in the shift of O=U=O asymmetric stretching bands from 950 cm^{-1} to 942 cm^{-1}. This can be attributed to the co-ordination of uranyl nitrate complex by TBP resulting in the weakening of U=O bands.

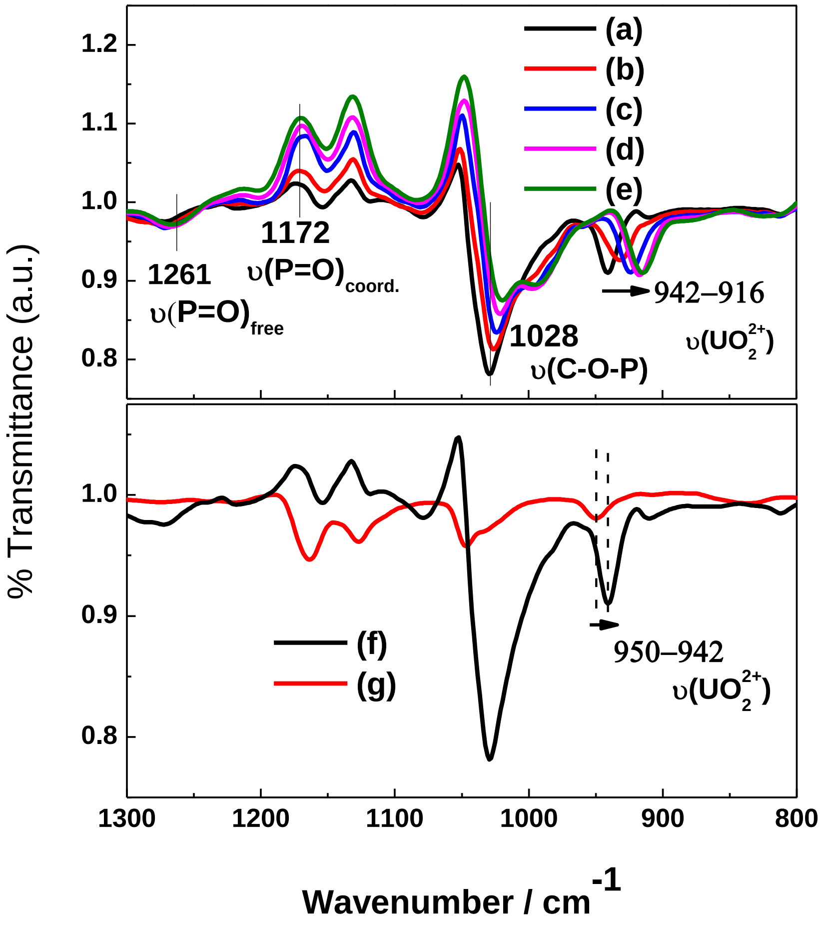

Figure 4.6. ATR-FTIR spectrum of 80 mM $UO_2(NO_3)_2$ dissolved in C_4mimNTf$_2$ containing TBP (160 mM), in the presence and absence of C_4mimCl. The mole ratio of U : NO_3 : TBP : Cl is (a) 1 : 2 : 2 : 0, (b) 1 : 2 : 2 : 1, (c) 1 : 2 : 2 : 2, (d) 1 : 2 : 2 : 4, (e) 1 : 2 : 2 : 6, (f) 1 : 2 : 2 : 0 and (g) 10 mM $UO_2(NO_3)_2$ dissolved in C_4mimNTf$_2$ without TBP.

Figure 4.6 also shows the differential ATR-FTIR spectrum of uranyl nitrate solution in C_4mimNTf$_2$, at various mole ratios of U : NO_3 : TBP : Cl, varied from 1 : 2 : 2 : 0 to 1 : 2 : 2 : 6. The differential spectrum shows the gradual shift of O=U=O asymmetric stretching bands from 942 cm^{-1} to 916 cm^{-1} when the mole ratio of U : NO_3 :

TBP : Cl was increased from 1 : 2 : 2 : 0 to 1 : 2 : 2 : 4. Further addition of Cl^- ions does not shift the position of transmittance bands from 916 cm^{-1}. All these observations indicate that uranyl nitrate in TBP/C_4mimNTf$_2$ exists in the form of $UO_2(NO_3)_2(TBP)_2$; however the addition of Cl^- ions to the solution gradually substitutes the nitrate ion present in the uranium coordination sphere by Cl^- ions. When the mole ratio of U : NO_3 : TBP : Cl is 1 : 2 : 2 : 4 or above (i.e., Cl^- is more) a major fraction of the uranyl ion exists in the form of $[UO_2Cl_4]^{2-}$ in IL. These results are in good agreement with the visible absorption and Raman spectrum of uranyl species discussed above.

The ligand TBP exhibits a strong P=O stretching transmittance bands at ~1280 cm^{-1} [26]. Literature shows that co-ordination of uranyl nitrate with TBP results in the shift of P=O stretching bands from 1280 cm^{-1} (uncoordinated P=O) to 1170 cm^{-1} (coordinated P=O). However, the IR region spanning from 1240 cm^{-1} to 1320 cm^{-1} is completely masked by the transmittance bands of the IL. Therefore, it was difficult to arrive at any meaningful conclusion on the co-ordination behaviour of TBP with uranyl ion by FTIR spectroscopy. Nevertheless, the differential ATR-FTIR spectrum shows that the transmittance bands at 1172 cm^{-1}, which is due to the stretching bands of co-ordinated P=O groups with uranyl ion. It is interesting to note that the intensity of the differential spectrum at 1172 cm^{-1} increases above the value of unity when the mole ratio of U : NO_3 : TBP : Cl increases from 1 : 2 : 2 : 0 to 1 : 2 : 2 : 6. The increase in the transmittance value above unity in the differential spectrum could be taken as indicative of lowering of the abundance of co-ordinated P=O groups upon increasing the Cl^- ion content. This is possible only when TBP is decomplexed from the uranyl co-ordination sphere upon Cl^- addition. A similar explanation was also provided by other researchers [16, 19, 20]. Nevertheless, the ATR-FTIR spectrum both co-ordinated and unco-ordinated of P=O bonds show that it is difficult to arrive at any significant conclusion on co-ordination and decomplexation behaviour of TBP upon Cl^- addition, due to masking of P=O stretching bands by $C_4mimNTf_2$.

Based on the spectroscopic studies discussed above, the following conclusions can be drawn. Table 4.1 summarises the dominant uranyl species as a function of Cl^- ions at various U : NO_3 : TBP : Cl mole ratios. Since Cl^- is a strong field ligand as compared to the neutral TBP and nitrate ions, the addition of Cl^- ions gradually displaces the TBP and substitutes the nitrate ions present in the uranyl co-ordination sphere. Addition of C_4mimCl changes the nature of uranyl species from $UO_2(NO_3)_2(TBP)_2$ to $[UO_2Cl_4]^{2-}$ with the change in mole ratio of U : NO_3 : TBP : Cl from 1 : 2 : 2 : 0 to 1 : 2 : 2 : 6.

Table 4.1. Uranyl species proposed to be existing at various mole ratios of U : NO_3 : TBP : Cl and the cathodic peak potential obtained from the CV (figure 4.2).

Mole ratio of U : NO_3 : TBP : Cl	Predicted predominant uranyl species	Peak potential
1 : 2 : 2 : 0	$UO_2(NO_3)_2(TBP)_2$	-1
1 : 2 : 2 : 1	$[UO_2(NO_3)_2Cl]^-$, $UO_2(NO_3)_2(TBP)_2$*	-0.62
1 : 2 : 2 : 2	$[UO_2(NO_3)Cl_2]^-$, $[UO_2(NO_3)_2Cl_2]^{2-}$*	-0.93
1 : 2 : 2 : 4	$[UO_2(NO_3)Cl_3]^{2-}$, $[UO_2Cl_4]^{2-}$*	-0.89
1 : 2 : 2 : 6	$[UO_2Cl_4]^{2-}$, $[UO_2(NO_3)Cl_3]^{2-}$*	-0.73

* indicates that the abundance of this species is far less as compared to the co-existing predominant species.

4.1.1.7. Correlation between CV of U(VI) and Spectroscopic Features

Based on the spectroscopic studies discussed above, the CV behaviour of uranyl ion shown in figure 4.2, could be correlated to the nature of uranyl specie present in the IL medium. In figure 4.2, the mole ratio of U : NO_3 : TBP : Cl was varied from 1 : 2 : 2 : 0 to 1 : 2 : 2 : 6. At the mole ratio 1 : 2 : 2 : 1, the CV shows a cathodic wave (E_p^{c2}) at a peak potential of -0.7 V (Vs Pd). This is probably due to the reduction of $[UO_2(NO_3)_2Cl]^-$ specie, that is predominant in the IL. The reduction at E_p^{c2} in the voltammogram is followed by continuous increase in the cathodic current possibly attributed to the reduction of $[UO_2(NO_3)_2(TBP)_2]$ specie that is also present in the solution in significant concentration at this mole ratio. Since reduction of $[UO_2(NO_3)_2Cl]^-$ seems to be favourable (discussed below), the cathodic peak current, I_p^{c2}, is more than that observed at I_p^{c1} in figure 4.2. It is evident from figure 4.2 that the current density pertaining to the reduction of UO_2^{2+} increases with the Cl^- ion content in the IL, in the following order: $I_p^{c1} < I_p^{c2} < I_p^{c3} < I_p^{c4} < I_p^{c5}$. This could be attributed to the conversion of uranyl nitrate-TBP complex into different chloro complexes as represented in the equations (4.1) to (4.5). At 1 : 2 : 2 : 6 mole ratio, the cathodic peak current (I_p^{c5}) is significantly high due to the formation of $[UO_2Cl_4]^{2-}$ species. The redox reaction of $[UO_2Cl_4]^{2-}$ could be represented by the reduction UO_2^{2+} at the working electrode and oxidation of Cl^- to Cl_2 at the counter electrode (4.8)

$$[UO_2Cl_4]^{2-} \rightarrow UO_2 \text{ (at the working electrode)} + 2Cl^- + Cl_2 \text{ (at the counter electrode)} \quad (4.8)$$

Similarly the reduction of uranyl nitrate at the working electrode requires the oxidation of nitrate at the counter electrode.

$UO_2(NO_3)_2 \rightarrow UO_2$ + oxidation products of NO_3^- (4.9)

The oxidation of Cl^- to Cl_2 at the counter electrode appears to be favoured more than the oxidation of nitrate. In view of this, the cathodic peak potential observed for the reduction of UO_2^{2+} at various mole ratios of U : Cl increases in the order: $E_p^{c1} < E_p^{c3} < E_p^{c4} < E_p^{c5}$, which is the increasing order of Cl^- ion content in IL. However, it is not clear from the present study why the cathodic peak E_p^{c2} was higher than E_p^{c5} i.e. $E_p^{c5} < E_p^{c2}$ and more studies are needed in this direction to understand the nature of specie undergoing reduction at the peak potential, E_p^{c2}.

4.1.1.8. Diffusion coefficients

The CV pertaining to UO_2^{2+} in $C_4mimNTf_2$ recorded at a glassy carbon working electrode at a mole ratio of U : NO_3 : TBP : Cl varying from 1 : 2 : 2 : 1 to 1 : 2 : 2 : 6. The scan rate at 373 K was varied from 20 mV/s to 100 mV/s. These results are shown in figure 4.7. It is evident from this figure that the cathodic peak potential in all these cases gets shifted cathodically while the anodic peak potential is shifted anodically with an increase in scan rate. The cathodic and anodic peak currents are also increases with the scan rate. This observation is characteristic to the irreversible or quasi-reversible reduction of UO_2^{2+} to UO_2. This indicates that the reduction of UO_2^{2+} is governed not only by the diffusion of UO_2^{2+} at the working electrode, but also by the kinetics of the electron transfer occurring across the electrode-electrolyte interface. The nature of electron transfer occurring across the electrode-electrolyte interface could be determined by measuring the quantity $|E_p^c – E_{p/2}^c|$, where $E_{p/2}^c$ is half peak potential. If this value is more than 33 mV for the two electron transfer taking place at 373 K, the electrode reaction occurring at the electrode-electrolyte interphase can be regarded as irreversible or quasi-reversible. The value of $|E_p^c – E_{p/2}^c|$ was determined to be more than 60 mV in all cases. This observation confirms that the reduction of UO_2^{2+} to UO_2 at the working electrode is not only governed by the diffusion of UO_2^{2+} but also by the heterogeneous charge transfer kinetics occurring across the electrode-electrolyte interface [29, 30].

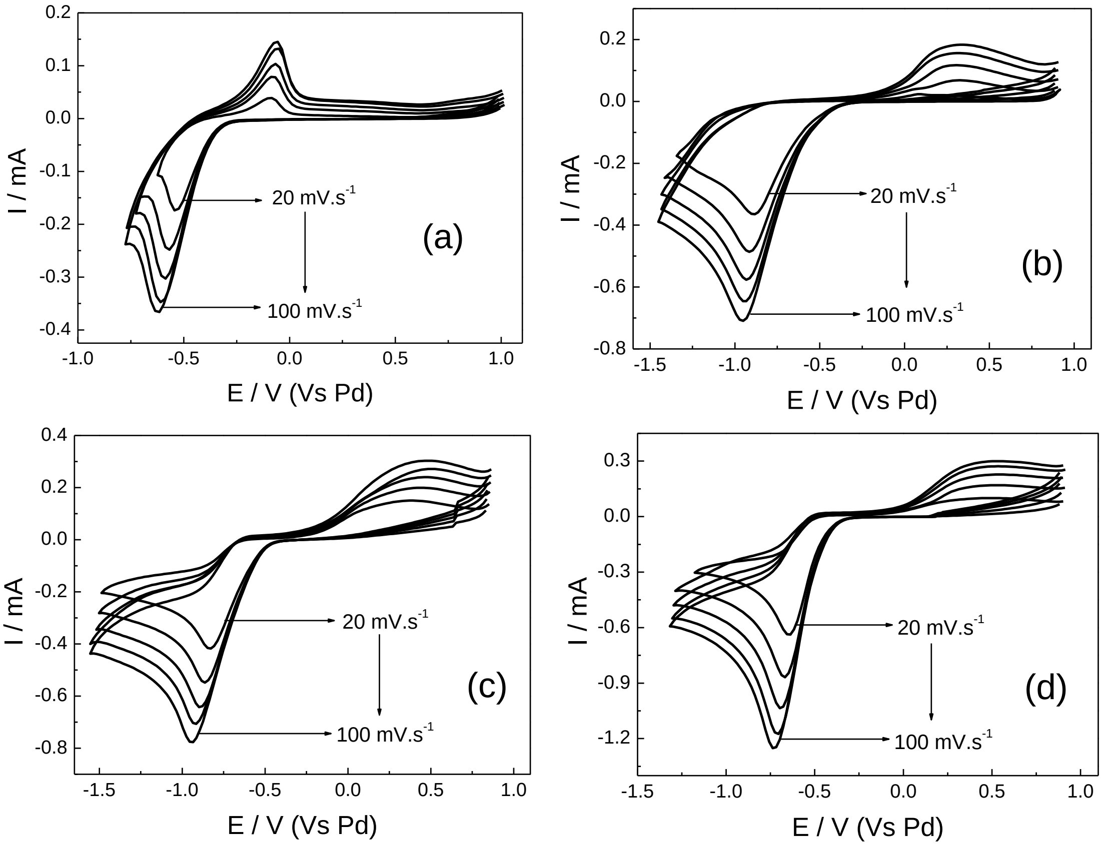

Figure 4.7. CV pertaining to 80 mM $UO_2(NO_3)_2$ in $C_4mimNTf_2$ containing TBP (160 mM) recorded at a glassy carbon electrode at different scan rates at 373 K, in the presence of C_4mimCl. The mole ratios; U : NO_3 : TBP : Cl are (a) 1 : 2 : 2 : 1, (b) 1 : 2 : 2 : 2, (c) 1 : 2 : 2 : 4 and (d) 1 : 2 : 2 : 6.

The heterogeneous charge transfer coefficient (α) is a measure of the symmetry barrier in a non-reversible electron transfer reaction and it could have values ranging from 0.1 to 0.9. The charge transfer coefficient for the reduction of UO_2^{2+} to UO_2 could be determined by using equation A.4 (Annexure) [30]. where E_p^c and $E_{p/2}^c$ are peak and half-peak potentials responsible for the reduction of UO_2^{2+} to UO_2. By substituting the values of $|E_p^c–E_{p/2}^c|$ determined from the cyclic voltammogram, shown in figure 4.7, the value of αn_α was determined. This value was found to vary from 0.3 to 0.6.

The Berzin-Delahey relation for an irreversible or quasi-reversible reduction of soluble-insoluble (UO_2^{2+} to UO_2) couple is shown in equation A.5 (Annexure), where the surface area of the glassy carbon electrode is 0.16 cm^2, the concentration of U(VI) present in $C_4mimNTf_2$ is 80 mM and the number of electron transferred is 2.

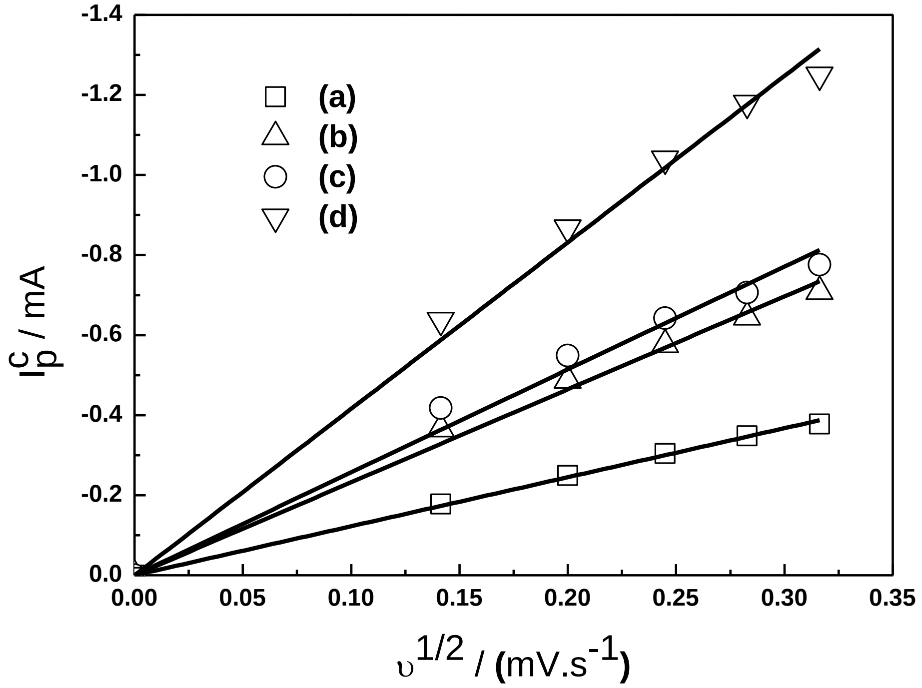

Figure 4.8. Plot of the cathodic peak current against the square root of scan rate ($\upsilon^{1/2}$) pertaining to the reduction of 80 mM $UO_2(NO_3)_2$ in $C_4mimNTf_2$ containing TBP (160 mM) recorded at a glassy carbon electrode at 373 K, in the presence of C_4mimCl. The mole ratio of U : NO_3 : TBP : Cl is (a) 1 : 2 : 2 : 1, (b) 1 : 2 : 2 : 2, (c) 1 : 2 : 2 : 4 and (d) 1 : 2 : 2 : 6.

A plot of I_p^c against the square root of scan rate ($\upsilon^{1/2}$) at 373 K is shown in figure 4.8. It is evident from this figure that this dependence is linear with a zero intercept. This indicates that the Berzin-Delahay equation holds good for the reduction of UO_2^{2+} to UO_2 and thus enables the determination of the diffusion coefficient from the slope of the straight line. The values of the apparent diffusion coefficient thus determined at 373 K are shown in table 4.2. These values increase from 6.8 X 10^{-8} to 1.0 X 10^{-6} cm^2/s with an increase in the mole ratio, U : NO_3 : TBP : Cl varied from 1 : 2 : 2 : 1 to 1 : 2 : 2 : 6. Since the addition of Cl^- ion converts the bulky and neutral $[UO_2(NO_3)_2(TBP)_2]$ complex into a smaller anionic complex viz., $[UO_2(NO_3)_2Cl]^-$, $[UO_2Cl_4]^{2-}$ etc., the diffusion coefficient increases with the increase in the concentration of Cl^- in the IL. This observation is in good agreement with the spectroscopic evidences discussed in the foregoing reactions.

Table 4.2. Diffusion coefficients of uranyl specie in $C_4mimNTf_2$ at different mole ratios of U : NO_3 : TBP : Cl.

Mole ratio of U : NO_3 : TBP : Cl	Diffusion coefficient / $cm^2.s^{-1}$
1 : 2 : 2 : 1	6.9 X 10^{-8}
1 : 2 : 2 : 2	4.5 X 10^{-7}
1 : 2 : 2 : 4	5.6 X 10^{-7}
1 : 2 : 2 : 6	1.0 X 10^{-6}

4.1.2. Conclusions

The voltammetric behaviour of $UO_2(NO_3)_2$ in a solution of TBP/C_4mimNTf$_2$ was quite complicated owing to the coordination of TBP with uranyl nitrate viz., $[UO_2(NO_3)_2(TBP)_2]$ in C_4mimNTf$_2$. The cathodic peak current density pertaining to the reduction of UO_2^{2+} to UO_2 in the presence of TBP was found to be quite low. In order to increase the current density and favour an underpotential reduction of UO_2^{2+}, C_4mimCl was added to the uranyl nitrate - TBP solution. The U : NO_3 : TBP : Cl mole ratio was varied from 1 : 2 : 2 : 1 to 1 : 2 : 2 : 6 in the IL. Addition of C_4mimCl to this IL increased the cathodic current density and favoured underpotential reduction of UO_2^{2+} to UO_2. The diffusion coefficient of UO_2^{2+} increased from 6.8×10^{-8} to 1.0×10^{-6} cm^2/s with the increase in mole ratio of U : NO_3 : TBP : Cl from 1 : 2 : 2 : 1 to 1 : 2 : 2 : 6, due to the conversion of the bulky and neutral $[UO_2(NO_3)_2(TBP)_2]$ complex into a smaller anionic complex like $[UO_2(NO_3)_2Cl]^-$, $[UO_2Cl_4]^{2-}$ etc..

In order to understand the electrochemical behavior of the uranyl ion observed in the presence of neutral and anionic ligands, the speciation of uranyl ion containing moities in the presence of NO_3^-, Cl and TBP was investigated by UV-Visible, ATR-FTIR and Raman spectroscopy. The visible absorption spectrum of uranyl nitrate in the presence of TBP showed that complexes containing the uranyl ion like $UO_2(NO_3)_2(TBP)_2$ existed in C_4mimNTf$_2$ in the absence of C_4mimCl. However, in the presence Cl^- ions, the uranyl nitrate gets transformed into different anionic complexes viz., $[UO_2Cl(NO_3)_2]^-$ or $[UO_2Cl_3(NO_3)]^{2-}$ or $[UO_2Cl_4]^{2-}$, depending upon the mole ratio of U : NO_3 : Cl. Since TBP is a neutral as well as weak ligand, it did not participate in the complexation with the anionic uranyl species. The ATR-FTIR spectroscopic studies also indicated that the addition of Cl^- ions to $UO_2(NO_3)_2(TBP)_2$ gradually lead to the substitution of nitrate ions by Cl^- and displaces TBP from the coordination sphere of uranyl ions. When the mole ratio U : NO_3 : TBP : Cl was 1 : 2 : 2 : 4 or above (i.e., Cl^- is more), a major fraction of the uranyl ions existed in the form of $[UO_2Cl_4]^{2-}$ in the IL. Raman spectroscopic studies showed that majority of uranyl species existed as $[UO_2(NO_3)_2Cl]^-$ with residual $[UO_2(NO_3)_2(TBP)_2]$ at 1 : 2 : 2 : 1 mole ratio, whereas at 1 : 2 : 2 : 6 mole ratio the dominant uranium specie is $[UO_2Cl_4]^{2-}$. This study thus confirmed that the addition of Cl^- ion converted the bulky $[UO_2(NO_3)_2(TBP)_2]$ complex into a smaller $[UO_2Cl_4]^{2-}$ complex. Since the reduction of this chlorocomplex resulted in the liberation of Cl_2 at the counter electrode, the reduction of UO_2^{2+} at the working electrode was favorable than the reduction of uranyl nitrate-TBP complex.

4.2. Coordination and electrochemical behavior of U(VI) in dicyanamide ionic liquid

Introduction

The literature survey revealed that the solubility of metal salts in IL media is governed by the solvation of metal salt in the IL, which in turn primarily depends upon the columbic forces [1, 5, 31]. The interactions between oppositely charged ions are not always adequate for complete dissolution of a given actinide salt in significant quantities in the IL [1, 5, 31, 32]. For instance, the solubility of uranyl nitrate in $C_4mimNTf_2$ or C_4mimPF_6 is very poor [15]. Hence, it is necessary to develop advanced ILs that can dissolve actinide salts through other mechanisms in addition to the coloumbic intearation, that enhance the dissolution of actinides ions in IL. This should be accomplished, without compromising the wide electrochemical window and low viscosity that are necessary for electrochemical applications. The solubility of a given actinide salt in an IL could be increased by exploiting the co-ordinate bond forming tendency of inner 7f-orbitals. This requires the appropriate choice of the IL containing a desirable anion that would efficiently complex with the actinide ion, and thus enhance the dissolution of the actinide salt. In the mean while this anion should also be hard to reduce, should interact poorly with the counter cation such that it exhibits a wide electrochemical window and low viscosity [1, 5, 8, 31-33].

In the recent past, the ILs with cyano anions have been used in many electrochemical applications [31-37]. These cyano anions, include thiocyanate $[SCN]^-$, dicyanamide $[N(CN)_2]^-$ (DCA), tricyanomethamide $[C(CN)_3]^-$, and tetracyanoborate $[B(CN)_4]^-$ as electrolytes. Among these the imidazoium dicyanamide possesses a very low viscosity of ~25cP, and it is suited for electrochemical applications. The structure of the dicyanamide anion is shown in figure 4.9. In addition, the DCA^- anion exhibits linkage isomerism for it contains three conjugated nitrogen atoms among which the negative charge could be delocalized, as shown in figure 4.9. As a result, DCA^- could act both as a monodentate or bidentate ligand, and coordinates with actinide ions through nitrogen atom of nitrile or imide. Earliar work on the coordination behaviour of DCA^- with some of the transition metal ions show that DCA^- could act either as monodentate or bidentate or bridging ligand. In view of this, the dicyanamide $[N(CN)_2]^-$ based ILs are likely to dissolve significant amounts of actinide salts in IL. However, the dissolution of uranyl salt, like uranyl nitrate ($[UO_2(NO_3)_2]$) could result in the formation of many species like $[UO_2(DCA)_2]$ or $[UO_2(DCA)_4]^{2-}$ and mixed complexes. However, the coordination behaviour of DCA^- with uranyl ion and the speciation of uranyl ion in the presence of nitrate and DCA^- are not known.

The present chapter deals with the synthesis of a couple of ILs containing dicyanamide anion, namely 1-butyl-3-methylimidazolium dicyanamide (C_4mImDCA) and N-butyl-N-methylpyrrolidinium dicyanamide (C_4mPyDCA) and the electrochemical behaviour of uranyl ion (UO_2^{2+}) in these ILs. The chemical structures of these IL is shown in figure 4.9. The interaction between DCA^- and uranyl ion was characterised by Raman and FTIR spectroscopy to unravel the coordination behaviour of uranyl ion with DCA^-. The electrochemical behaviour of UO_2^{2+} in C_4mImDCA and C_4mPyDCA was studied at a glassy carbon working electrode at different temperatures by CV. These results are reported in this chapter.

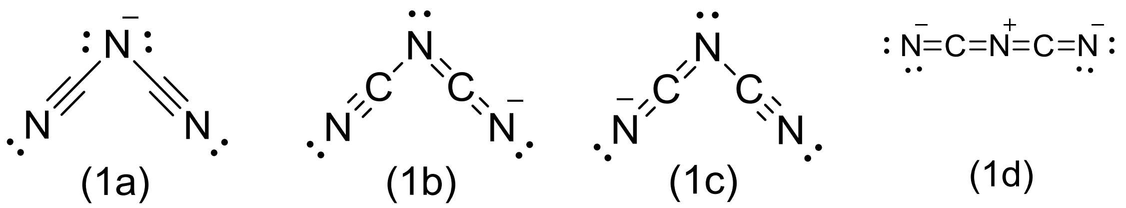

Resonance structures of dicyanamide anion

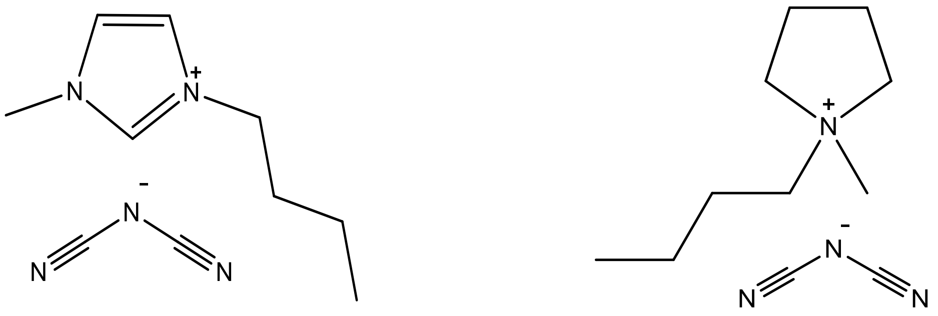

1-Butyl-3-methylimdazolium dicyanamide

N-Butyl-N-methylpyrrolidinium dicyanmide

Figure 4.9. Resonance structures of dicyanamide anion and structures of the ILs used in the present work.

Experimental parts of the present study have been discussed in the section 2.4.4 and the synthesis of ILs has been detailed in the sections 2.5.5 & 2.5.6 of chapter 2.

4.2.1. Results and Discussion

4.2.1.1. Raman spectroscopy of uranyl nitrate in dicyanamide ionic liquids

The ILs containing dicyanamide group exhibit low viscosity (29 cP) and good solubility of uranium salts (~0.5 M). These properties are indeed desirable for studying the electrochemistry of actinides and for evaluating the feasibility of using dicyanamide ILs for non-aqueous reprocessing applications. The Raman spectrum of C_4mImDCA and C_4mPyDCA are shown in figure 4.10. The characteristic bands observed in the Raman spectrum could be assigned to different vibrational stretching frequencies of this IL and the same are tabulated in table 4.3. Figure 4.10 compares the Raman spectra of uranyl nitrate (0.3 M) dissolved in C_4mImDCA and that of the pure IL [21, 24, 37-39]. It is evident that there is a new Raman band occurring at 852 cm^{-1} after dissolving uranyl nitrate in C_4mImDCA, which could be attributed to the O=U=O symmetric stretching frequency. It should be noted that the position of O=U=O stretching band can occur in the wavenumber range 820 to 860 cm^{-1}, depending upon the nature of the ligand co-ordinated to the UO_2^{2+} ion. Weak field ligands such as nitrate ion and tri-n-butyl phosphate when coordinated to UO_2^{2+} exhibit a Raman band at 860 cm^{-1} [25, 40]. Co-ordination with a strong filed ligand such as Cl^-, weakens the U=O bond, and shifts the U=O stretching frequencies to a lower wavenumber (830 cm^{-1}). Previously, we studied the spectroscopic behaviour of uranyl nitrate dissolved in ILs viz., C_4mIm bis(trifluoromethanesulfonyl)imide (C_4mImNTf$_2$), wherein the NTf_2^- anion is a big, poorly co-ordinating ligand [21, 40]. In these cases, the O=U=O stretching frequency of uranyl nitrate (860 cm^{-1}) was not affected upon the dissolution of uranyl nitrate in C_4mImNTf$_2$, indicating that the NTf_2^- anion was not involved in the coordination with UO_2^{2+} ion. However, the appearance of the O=U=O symmetric stretching band at 852 cm^-

[1]; in the present case, indicates that DCA^- could be co-ordinating to uranyl ion in IL and thus shifts the O=U=O stretching frequency of uranyl nitrte from 860cm^{-1} to 852 cm^{-1}.

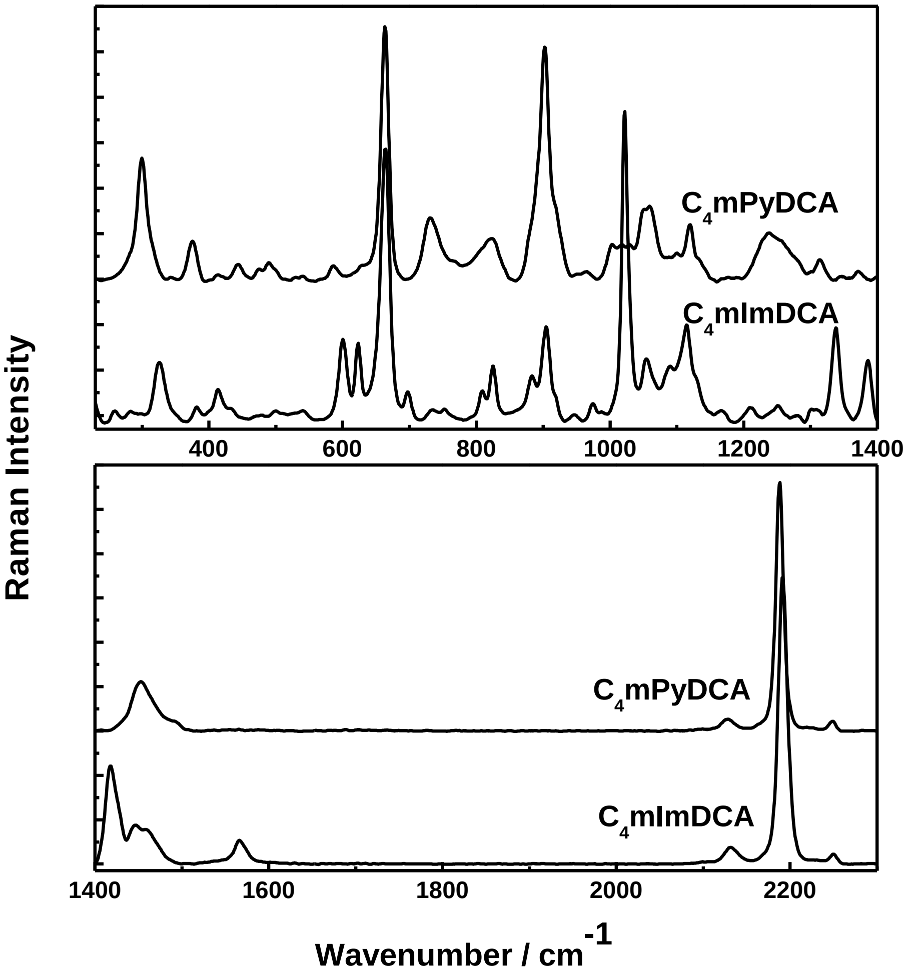

Figure 4.10. Raman spectra of C_4mImDCA and C_4mPyDCA ILs.

Co-ordination of DCA^- with uranyl ion in C_4mImDCA medium should result in the liberation of nitrate ion from the co-ordination sphere of uranyl ion [40]. This could cause changes in the stretching frequencies of both nitrate and –C≡N. The –C≡N stretching pertaining to C_4mImDCA occurs at 2190 cm^{-1} in the Raman spectrum, as shown in figure 4.11. Addition of uranyl nitrate to C_4mImDCA results in the appearance of a new band at 2220 cm^{-1}. This could be due to –C≡N stretching of the DCA^- co-ordinated with the uranyl ion [38, 39]. The formation of a coordinate bond between UO_2^{2+} and DCA^- results in a reduction of negative charge density on the nitrogen atom. Consequently, bond strength and the stretching frequencies of –C≡N bond increases leading to the appearance of a band at 2220 cm^{-1}, as shown in figure 4.11. This is evidently due to the coordination of uranyl ion with the DCA^- ion.

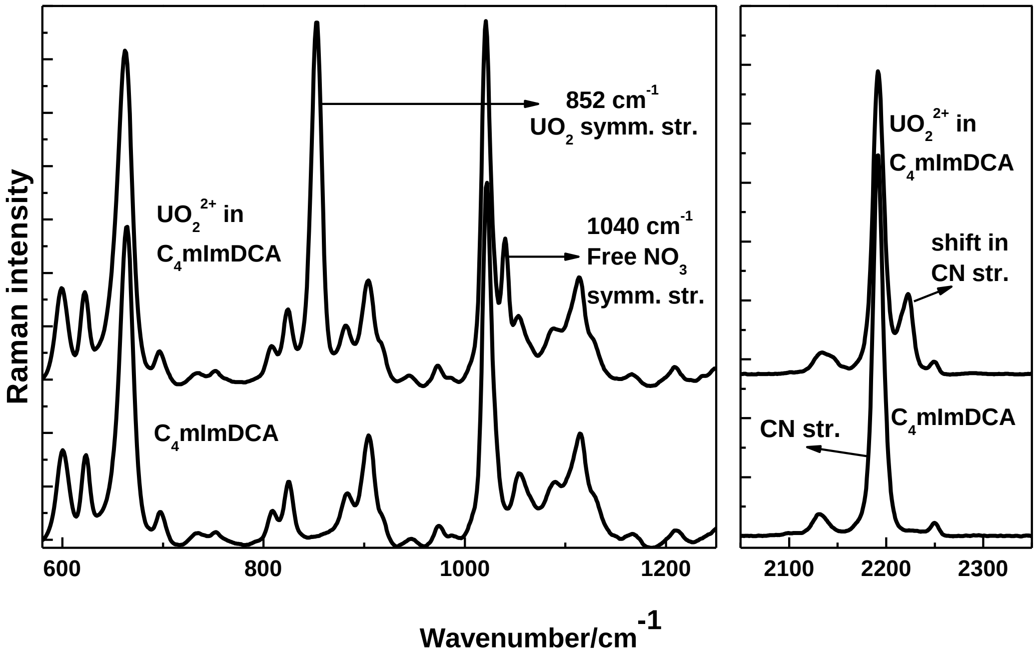

Figure 4.11. Raman spectrum of C_4mImDCA (below) and 0.3 M $UO_2(NO_3)_2$ dissolved in C_4mImDCA (above).

Table 4.3. Assignment of Raman and IR bands to the vibrational stretching frequencies of C$_4$mImDCA and C$_4$mPyDCA with and without uranyl nitrate.

Ionic Liquid	Raman band / cm^{-1}		IR band / cm^{-1}		Assignment
	Without	With	Without	With	
	$UO_2(NO_3)_2$		$UO_2(NO_3)_2$		
C$_4$mImDCA	2191	2222			Symmetric CN stretching
	2131	2133			Asymmetric CN stretching
			1302	1345	Asymmetric CNC stretching
			2125	2155	Asymmetric CN stretching
			2225	2280	Fermi asym. + Symmetric CNC stretching
			2191	2196	Symmetric CN stretching
	-	852			Symmetric stretching of O=U=O
			-	935	Asymmetric stretching of O=U=O
	-	1040			Symmetric stretching of Free nitrate
C$_4$mPyDCA	2188	2222			Symmetric stretching
	2128	2130			Asymmetric CN stretching
			1304	1355sh	Asymmetric CNC stretching
			2125	2155	Asymmetric CN stretching
			2227	2283	Fermi asym. + Symmetric CNC stretching
			2190	2192	Symmetric CN stretching
	-	852			Symmetric stretching of O=U=O
			-	931	Asymmetric stretching of O=U=O
	-	1040			Symmetric stretching of Free nitrate

Substitution of nitrate by DCA$^-$ ion in the co-ordination sphere of UO_2^{2+} should result in the liberation of nitrate ions into IL. This could be easily verified by the appearance of a Raman band at 1040 cm^{-1}, that could be attributed to the symmetric stretching frequency of the "free" nitrate ion (un-coordinated) [40]. The symmetric stretching frequency of nitrate ion coordinated with UO_2^{2+} occurs at 1030 cm^{-1}. Figure 4.11 also shows the comparison in the Raman spectrum of C_4mImDCA and its solution with uranyl nitrate. The appearance of a band at 1040 cm^{-1} is due to the presence of "free" nitrate ions in the IL. This observation confirms that a fraction of nitrate ions gets partially liberated from uranyl co-ordination sphere, when uranyl nitrate is added to C_4mImDCA. A similar behaviour has also been observed when uranyl nitrate was added to C_4mPyDCA as shown in figure 4.12.

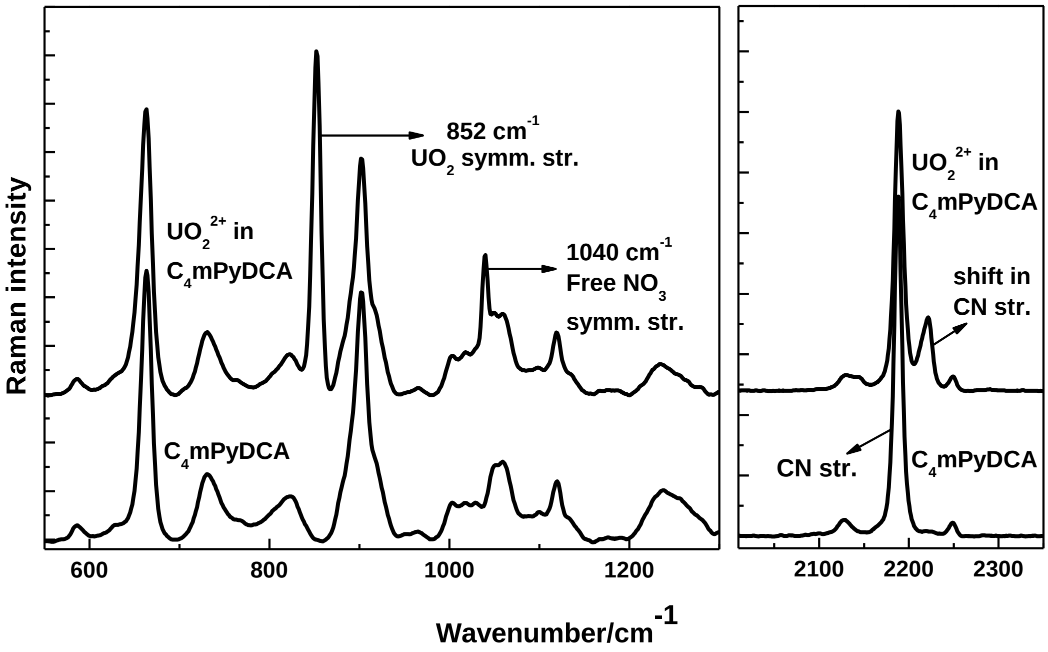

Figure 4.12. Raman spectra of C_4mPyDCA (below) and 0.3 M $UO_2(NO_3)_2$ dissolved in C_4mPyDCA (above).

4.2.1.2. FTIR spectroscopy of uranyl nitrate in dicyanamide ionic liquids

Figure 4.13 compares the ATR-FTIR spectrum of C_4mImDCA and C_4mPyDCA, and their solution with uranyl nitrate. The transmittance bands observed in the FTIR spectra have been assigned different stretching frequencies and their assignments have been tabulated in table 4.3. The ATR-FTIR spectra of both C_4mImDCA and C_4mPyDCA show the presence of bands at 1260 cm^{-1} pertaining to C-N-C asymmetric stretching, 2122 cm^{-1} due to Fermi asymmetric + symmetric C-N-C stretching. These stretching bands are shifted partially to higher wavenumbers at 1302 cm^{-1}, 2125 cm^{-1} and 2225 cm^{-1} from their original position upon adding uranyl nitrate to the IL [38, 39]. This is possible only if the DCA^- ion is co-ordinated to the uranyl ion and the nitrate ion present in the co-ordination sphere of uranyl ion is substituted by a DCA^- ion. Since DCA^- is a strong filed ligand as compared to nitrate, co-ordination of DCA^- with uranyl ion weakens the U=O stretching frequency. The O=U=O asymmetric stretching bands occurs at 942 cm^{-1}, when nitrate ion is co-ordinated to the uranyl ion [21, 25, 40]. The appearance of O=U=O asymmetric stretching bands at 931 cm^{-1} in the spectrum of the solution containing uranyl nitrate in the IL, indicates that DCA^- present in C_4mImDCA and C_4mPyDCA is co-ordinated to uranyl ion. This observation confirms that the addition of uranyl nitrate in the IL results in the formation of a uranyl DCA complex.

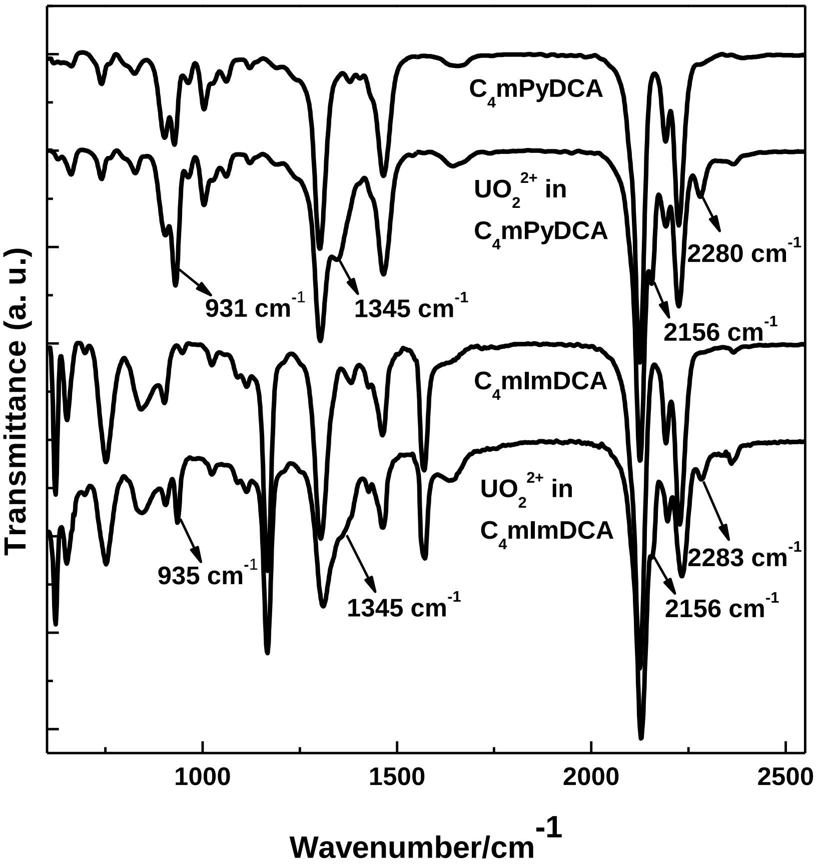

Figure 4.13. ATR-FTIR spectra of C_4mImDCA, C_4mPyDCA and 0.3 M $UO_2(NO_3)_2$ dissolved in both these ILs.

4.2.1.3. Raman spectroscopy of uranyl nitrate in ionic liquid at different DCA$^-$ to uranium mole ratios

Substitution of nitrate ion in uranyl nitrate [$UO_2(NO_3)_2$] by the DCA$^-$ anion results in the formation of either [$UO_2(DCA)_2$] or [$UO_2(DCA)_4$]$^{2-}$. In addition, the DCA$^-$ anion could exhibit linkage isomerism, for it contains three conjugated nitrogen atoms facilitating the delocalization of the negative charge as shown in figure 4.9 [41]. As a result, the DCA$^-$ acts as a monodentate or bidentate ligand depending upon the stability of uranyl DCA complex. Among the different resonance structures, the hybrid (1d) is a linear structure having positive charge on the imide nitrogen and a partial negative charge on both the nitrile groups. Coordination of such charge dispersed linear hybrid structure (1d) to the uranyl ion is quite unfavourable owing to the low negative charge on the nitrogen atom and earlier studies also indicates that there are no coordinate complexes involving the linear DCA^- molecule with a metal atom. In contrast, a few reports are available in the literature on the possible coordination of DCA^- molecule with a transition metal ion through a monodentate or bidentate or bridging ligand [40-42]. However, the coordination and linkage behaviour of DCA^- with the uranyl ion has not been reported in literature so far. In view of the above, the coordination behaviour of DCA^- complexes with the uranyl ion was further investigated by both FTIR and Raman spectroscopy and the results are presented and discussed below.

Probing the substitution reaction of uranyl nitrate by DCA^- requires an IL that reasonably solubilizes uranyl nitrate yet possesses an anion that does not coordinate with the uranyl ion. Such ILs are rather limited. In this context, the 1-butyl-3-methylimidazolium tetrafluoroborate (C_4mImBF_4) IL has been chosen in the present investigation, for studying the uranyl-DCA complex by Raman and FTIR spectroscopy at different mole ratios of uranium to DCA^-, and to understand the coordination behaviour of DCA^- with the uranyl ion. Since the BF_4^- anion is a polyatomic singly charged anion it does not coordinate efficiently with the uranyl ion as compared to a bidentate nitrate or DCA^- ion. However, the solubility of uranyl nitrate in C_4mimBF_4 is rather low, viz., ~10 mM.

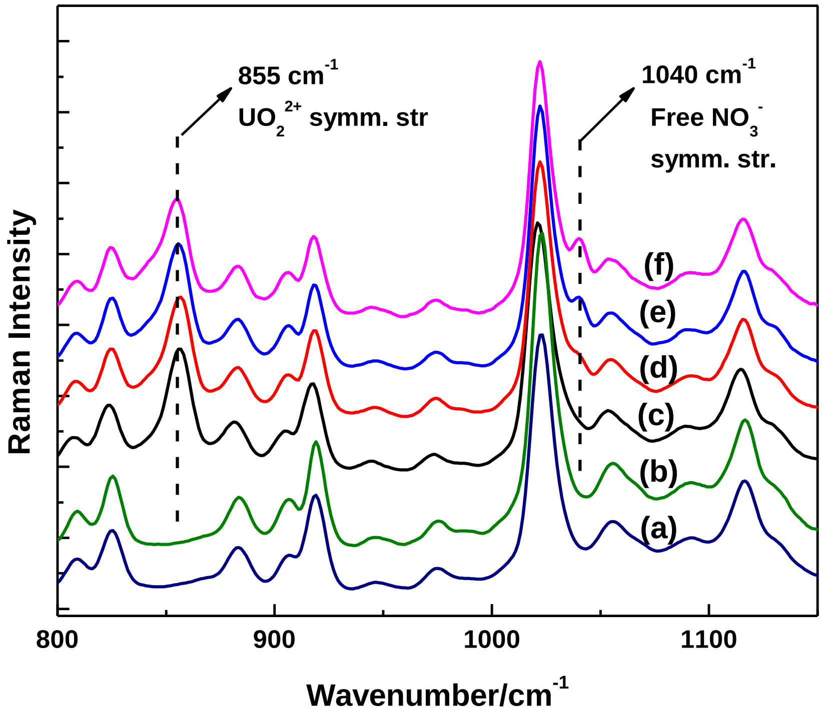

Figure 4.14. Raman spectra of (a) neat C_4mimBF_4, (b) C_4mimBF_4 containing 0.5 M $C_4mimDCA$; and 100 mM $UO_2(NO_3)_2$ dissolved in C_4mimBF_4, in the presence of $C_4mimDCA$,with a mole ratio U : NO_3 : DCA (c) 1 : 2 : 2, (d) 1 : 2 : 3, (e) 1 : 2 : 4 and (f) 1 : 2 : 5.

The Raman spectra of $UO_2(NO_3)_2$ in C_4mImBF_4 at different mole ratios of uranium to DCA^- is shown in the figures 4.14(c) to 4.14(f). These spectra are compared with those obtained in the absence of uranyl nitrate (figure 4.14(b)) as well as DCA^- (figure 4.14(a)). It is evident that that the addition of uranyl nitrate to the IL results in the appearance of a Raman band at 852 cm^{-1} due to the O=U=O symmetric stretching. The Raman spectrum of uranyl nitrate in IL, shown in figure 4.14c, did not reveal any difference in features when the mole ratio of DCA^- to uranium was less than 2 : 1. Hence, they have not included in figure 4.14.

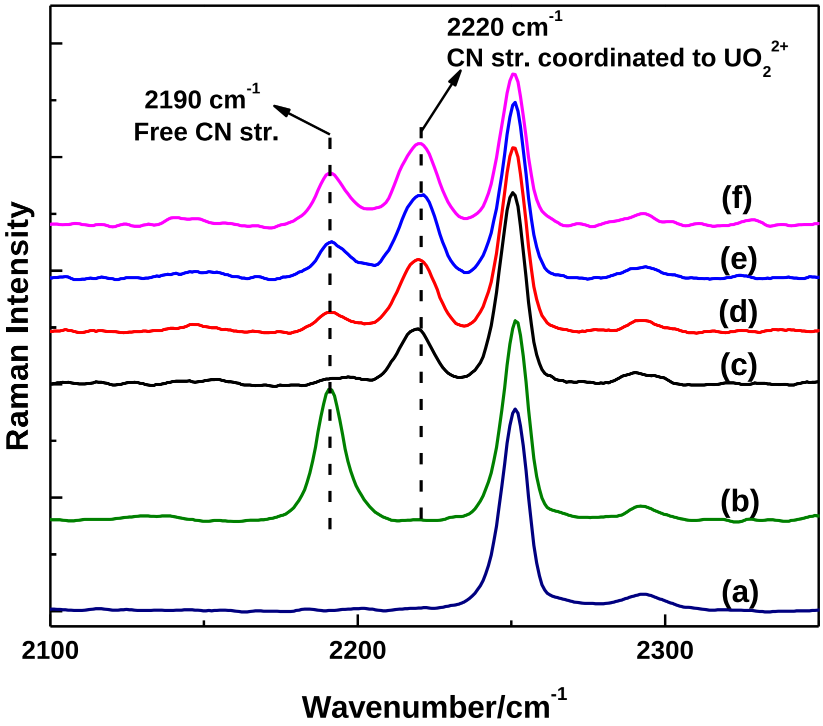

Figure 4.15. Raman spectra of (a) neat C_4mimBF_4, (b) C_4mimBF_4 containing 0.5 M $C_4mimDCA$; and 100 mM $UO_2(NO_3)_2$ dissolved in C_4mimBF_4, in the presence of $C_4mimDCA$,with a mole ratio U : NO_3 : DCA (c) 1 : 2 : 2, (d) 1 : 2 : 3, (e) 1 : 2 : 4 and (f) 1 : 2 : 5.

Depending on the mole ratio of DCA^- to uranium, DCA^- could coordinate with uranyl ion plausibly through the reactions represented by equations (4.10) and (4.15), where the subscripts “m” and “b” refer to the monodentate and bidentate coordination of DCA^-, respectively.

$$UO_2(NO_3)_2 + DCA^- \rightarrow UO_2(NO_{3b})(DCA_b) + NO_3^- \qquad (4.10)$$

$$UO_2(NO_3)_2 + DCA^- \rightarrow [UO_2(NO_{3b}) (NO_{3m}) (DCA_m)]^- \qquad (4.11)$$

$$UO_2(NO_3)_2 + 2\,DCA^- \rightarrow UO_2 (DCA_b)_2 + 2\,NO_3^- \qquad (4.12)$$

$$UO_2(NO_3)_2 + 2\,DCA^- \rightarrow UO_2(NO_{3b}) (DCA_b) + NO_3^- \qquad (4.13)$$

$UO_2(NO_3)_2 + 2\ DCA^- \rightarrow [UO_2(NO_{3b})\ (NO_{3m})\ (DCA)]^- + DCA^-$ (4.14)

$UO_2(NO_3)_2 + 2\ DCA^- \rightarrow [UO_2\ (NO_{3m})_2\ (DCA)_2]^{2-}$ (4.15)

In the equations (4.10), (4.12) and (4.13), DCA^- has been assumed to act as a bidentate ligand, DCA_b. In such an instance, the reaction of DCA^- with the uranyl nitrate should result in the liberation of a nitrate ion (free nitrate). This "free nitrate" ion gives rise to a peak at 1040 cm^{-1} in the Raman spectrum perataining to its symmetric stretching [40]. The absence of such a peak in the Raman spectrum in the mixtures with a DCA^- to uranium mole ratio lower than 2 : 1 reveals that DCA^- does not function as a bidentate ligand. Moreover, the bidentate coordination of DCA^- is not favoured possibly due to conformational and steric factors also (vide figure 4.9 resonance structures). Hence, bidentate coordination of DCA^- is not considered further and the results discussed below also reaffirm that DCA^- does not function as a bidentate ligand.

The absence of "free nitrate" ion peak at 1040 cm^{-1} in the Raman spectrum at a DCA^- to uranium mole ratios lower than 1 : 2, also confirms that the nitrate ion is not librated from the uranyl coordination sphere with the addition of DCA^-. This is possible only when the reactions represented by the equations (4.11), (4.14) and (4.15) occur upon the addition of one or two molecules of DCA^- per uranyl ion. The equation 4.16 shows that all the added DCA^- need not react with the uranyl nitrate quantitatively, but could leave a small quantity of unreacted DCA^- behind (to be discussed below) in the IL. Increasing the mole ratio of DCA^- to uranium above 2 : 1 results in the appearance of a peak at 1040 cm^{-1} (figure 4.13), pertaining to "free nitrate" stretching, affirming the liberation of the nitrate ion. The intensity of the "free nitrate" peak increases further with the mole ratio of DCA^- to uranium. At a mole ratio above 5 : 1, it is observed in the Raman spectrum that there is no further significant increase in the intensity pertaining to the free nitrate peak at 1040 cm^{-1}. The results shown in figure 4.15 could be explained by the reactions shown in equations (4.16) to (4.22). From these results, it appears that the uranyl predominantly exists as $[UO_2\ (DCA)_4]^{2-}$ at DCA^- in the IL solutions at and above the ratio of $DCA^- : UO_2^{2+}$ of 4 : 1.

$$UO_2(NO_3)_2 + \ 3\ DCA^- \rightarrow [UO_2(NO_{3b})\ (DCA)_2]^- + DCA^- + NO_3^- \qquad (4.16)$$

$$UO_2(NO_3)_2 + \ 3\ DCA^- \rightarrow [UO_2\ (NO_{3m})\ (DCA)_3]^{2-} + NO_3^- \qquad (4.17)$$

$$UO_2(NO_3)_2 + \ 4\ DCA^- \rightarrow [UO_2\ (NO_{3m})\ (DCA)_3]^{2-} + DCA^- + NO_3^- \qquad (4.18)$$

$$UO_2(NO_3)_2 + 4\ DCA^- \rightarrow [\ UO_2\ (DCA)_4]^{2-} + 2\ NO_3^- \qquad (4.19)$$

$$UO_2(NO_3)_2 + 5\ DCA^- \rightarrow [UO_2\ (DCA)_4]^{2-} + DCA^- + 2\ NO_3^- \qquad (4.20)$$

The results discussed above indicate that the addition of DCA^- results in the liberation of nitrate ion from the uranyl ion coordination sphere. However, these do not provide any conclusive evidence for the coordination behavior of DCA^- with the uranyl ion. Moreover, it is not clear if the uranyl nitrate is quantitatively converted into a uranyl DCA complex upon the addition of DCA^-. In order to understand its coordination behavior, the Raman spectrum of DCA^- was recorded at different mole ratios of DCA^- to uranyl and these results are shown in figure 4.15. It is evident from this figure that the un-coordinated or "free nitrile" (-C≡N) stretching band occurs at 2190 cm^{-1} as shown in figure 4.15b [39]. Addition of uranyl nitrate to the IL medium (DCA^- to uranium mole ratio of 2 : 1), results in the shift of the nitrile stretching bands from 2190 cm^{-1} to 2220 cm^{-1} [39, 43]. However, it is also evident that a weak band at the original position (2190 cm^{-1}) is present in the Raman spectrum indicating that a small amount of the unreacted DCA^- is remaining in the IL. These results indicate that uranyl in IL predominantly exists in the form $[UO_2\ (NO_{3m})_2\ (DCA)_2]^{2-}$, without libration of the nitrate ion observed at a

DCA to uranium mole ratio 2 : 1. These results also show that a small amount of $[UO_2(NO_{3b})(NO_{3m})(DCA)]^-$ could be present in the IL at this mole ratio. Increasing the mole ratio of DCA^- to uranium, increases the intensity of both the peaks (co-ordinated and uncoordinated) and this feature continues up to the mole ratio of 4 : 1. This shows that DCA^- is not entirely coordinated to the uranyl ion, and a small fraction of unreacted DCA^- remains in the IL. Further increase in the DCA^- to uranium mole ratio above 4 : 1 does not increase the intensity of the band at 2220 cm^{-1} significantly. However, the intensity of the band at 2190 cm^{-1} is increased significantly. This shows that the uranyl in IL is possibly completely converted into the form $[UO_2 (DCA)_4]^{2-}$ at DCA^- to uranium mole ratios above 4 : 1.

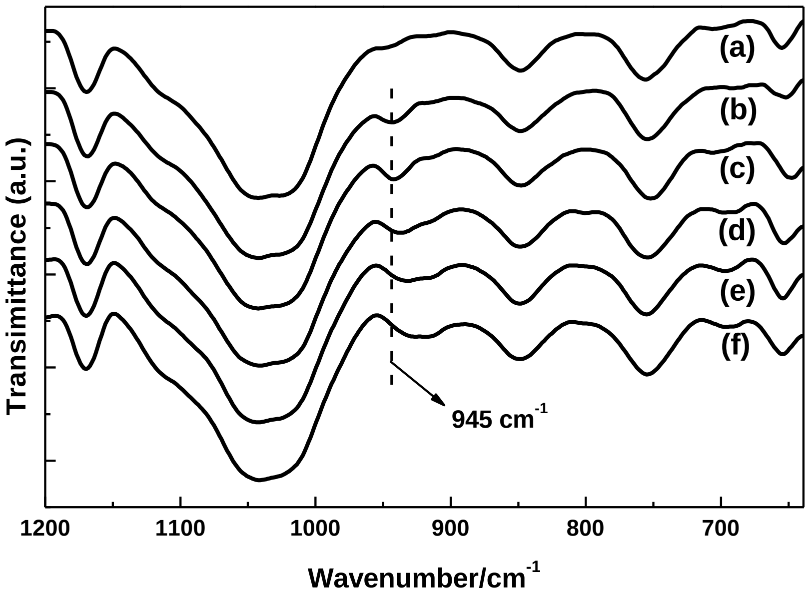

Figure 4.16. Infrared spectra of (a) neat C_4mImBF_4, (b) 10 mM $UO_2(NO_3)_2$ in C_4mImBF_4; and 100 mM $UO_2(NO_3)_2$ dissolved in C_4mImBF_4, in the presence of $C_4mImDCA$ with the mole ratio of U : NO_3 : DCA is (c) 1 : 2 : 2, (d) 1 : 2 : 3, (e) 1 : 2 : 4, (f) 1 : 2 : 5.

A similar behavior could be inferred from the variation in the (O=U=O) asymmetric stretching frequencies the FTIR spectrum upon the addition of DCA^- to the IL. The asymmetric stretching of uranyl ion in the uranyl nitrate is seen at 950 cm^{-1} in the IR spectrum [43]. Depending upon the ligand field strength, the position of the O=U=O asymmetric stretching bands occurs in the range from 950 cm^{-1} to 920 cm^{-1} for the coordination of a weak field ligand such as nitrate and TBP, and a strong field ligands like chloride respectively. Addition of small amounts of DCA^- to uranyl nitrate in C_4mimBF_4 results in the broadening of the band at 940 cm^{-1}, as shown in figure 4.16. Later it gets shifted to 930 cm^{-1} and merges with the IL peak at 930 cm^{-1} upon increasing the mole ratio of DCA^- to uranium to 4 : 1. Further increase in the mole ratio above 4 : 1 does not shift the O=U=O stretching frequency to a significant extent. This shows that a major fraction of the uranyl ion exists in the form $[UO_2\ (DCA)_4]^{2-}$ at DCA to uranium mole ratios above 4 : 1.

4.2.1.4. CV of UO_2^{2+} in ionic liquid medium

The abundances of various uranium species at different mole ratios of DCA^- to uranium are provided based on the spectroscopic investigations discussed above in table 4.4. When the DCA^- to uranium mole ratios is above 4 : 1, the uranyl ion predominantly exists in the form $[UO_2\ (DCA)_4]^{2-}$. Since the solution taken for the electrochemical investigation contained 60 mM of uranyl nitrate in $C_4mImDCA$ or $C_4mPyDCA$, it is expected that the uranyl ion in these solutions would exclusively exist in the form of $[UO_2\ (DCA)_4]^{2-}$.

Table 4.4. Proposed uranyl species existing at various mole ratios of DCA : U : NO_3.

Mole ratio of DCA : U : NO_3	Uranium species
1 : 1 : 2	$[UO_2(NO_{3b})(NO_{3m})(DCA)]^-$
2 : 1 : 2	$[UO_2(NO_{3m})_2(DCA)_2]^{2-} > [UO_2(NO_{3b})(NO_{3m})(DCA)]^-$
3 : 1 : 2	$[UO_2(NO_{3m})(DCA)_3]^{2-} > [UO_2(NO_{3m})_2(DCA)_2]^{2-} \sim$ $[UO_2(NO_{3b})(DCA)_2]^-$
4 : 1 : 2	$[UO_2(DCA)_4]^{2-} > [UO_2(NO_{3m})(DCA)_3]^{2-}$
Above 4 : 1 : 2	$[UO_2(DCA)_4]^{2-}$

The electrochemical behaviour of the uranyl ion (UO_2^{2+}) present in C_4mImDCA was studied at a glassy carbon working electrode and the results are discussed below. Since the viscosity (29 cP) and melting point (-6 °C) of DCA based ILs are quite low, it was possible to investigate the electrochemical behaviour of UO_2^{2+} at near ambient conditions [34, 35]. Figure 4.17 shows the CV pertaining to C_4mImDCA and C_4mPyDCA recorded at a glassy carbon working electrode at a scan rate of 100 mV/s at 303 K. The voltammogram shows that these ILs are stable upto 1.3 V (Vs Pd) in the anodic side and upto -2.5 V (Vs Pd) in the cathodic side. The electrochemical window provided by these ILs would be sufficient for studying the electrochemical behaviour of UO_2^{2+} in C_4mImDCA and C_4mPyDCA. The CV pertaining to UO_2^{2+} in C_4mImDCA shows a surge in the cathodic current at -0.75 V, resulting in a cathodic wave (E_p^{c1}) at -1.0 V. This is followed by another cathodic wave (E_p^{c2}) at -2.2 V. A similar behaviour is also observed in the case of UO_2^{2+} in C_4mPyDCA (figure 4.17(e) and 4.17(f)). The cathodic wave (E_p^{c1}) occurring at -1.0 V can be attributed to the reduction of UO_2^{2+} to UO_2^+ and the cathodic wave occurring at E_p^{c2} could be attributed to the reduction of UO_2^+ to UO_2. The cathodic wave E_p^{c1} was accompanied by an anodic wave E_p^{a1} at -0.1 V (Vs Pd) when the cathodic scan was reversed at -1.7 V. However, when the cathodic scan was reversed at -2.3 V, a couple of anodic peaks, viz., a prominent (E_p^{a2}) and a weak (E_p^{a3}) were observed at 0.1 V and 0.5 V respectively.

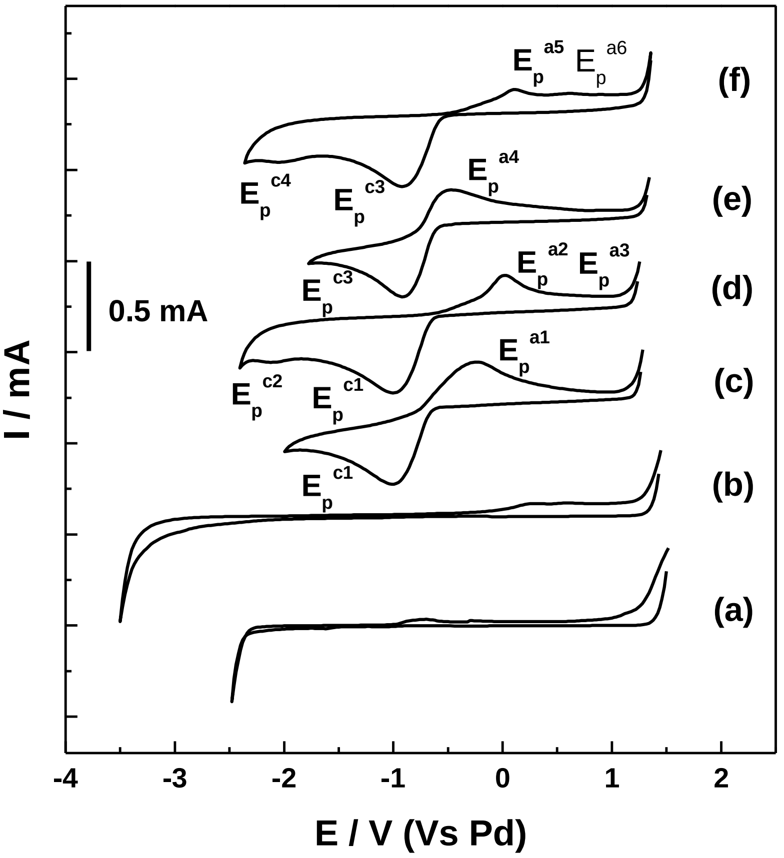

Figure 4.17. Cyclic volatmmogram of (a) neat C_4mImDCA, (b) C_4mPyDCA, 62 mM UO_2^{2+} in C_4mImDCA, (c) scan reversed at -2 V and (d) scan reversed at -2.5 V, 62 mM UO_2^{2+} in C_4mPyDCA, (e) scan reversed at -2 V and (f) scan reversed at -2.5 V recorded on glassy carbon working electrode at 100 mVps at 303 K.

4.2.1.5. Determination of diffusion coefficients

The effect of scan rate on the one-electron reduction of UO_2^{2+} to UO_2^{+} in C_4mImDCA (or C_4mPyDCA) at 303 K is shown in figure 4.18. It is seen that the cathodic peak current (I_p^{c1}) obtained in case of C_4mImDCA gets shifted cathodically and the anodic peak (I_p^{a1}) gets shifted anodically with an increase in scan rate. This shows that the reduction of UO_2^{2+} to UO_2^{+} occurring at the glassy carbon working electrode is not reversible.

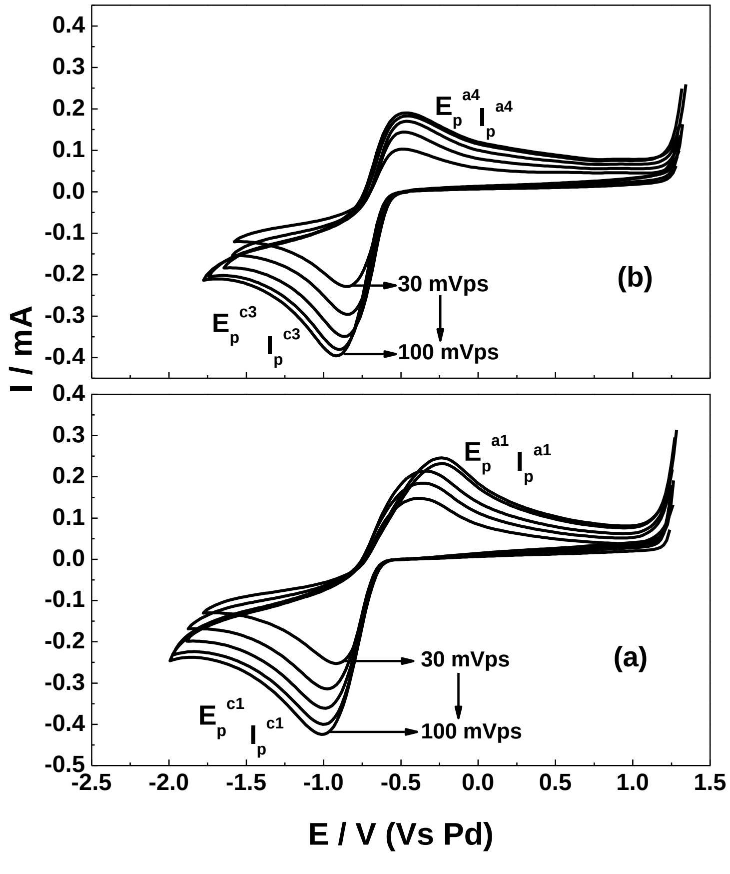

Figure 4.18. CV pertaining to 62 mM UO_2^{2+} in (a) C_4mImDCA and (b) C_4mPyDCA recorded at a glassy carbon electrode at different scan rates at 303 K.

The relation between the cathodic peak and the scan rate in such instance is given by equation (A.5) (Annexure) [29, 30]. where the electrode area (A) is 0.3 cm^2, the UO_2^{2+} concentration (C) is 62 mol cm $^{-3}$ and the number of electrons (n) exchanged is 1. Therefore, a plot of I_p^{c1} against the square root of the scan rate should result in a straight line passing through the origin. The results presented in figure 4.19. This result confirms the validity of equation (4.23) and facilitates the determination of diffusion coefficient of UO_2^{2+} in C_4mImDCA as well as C_4mPyDCA.

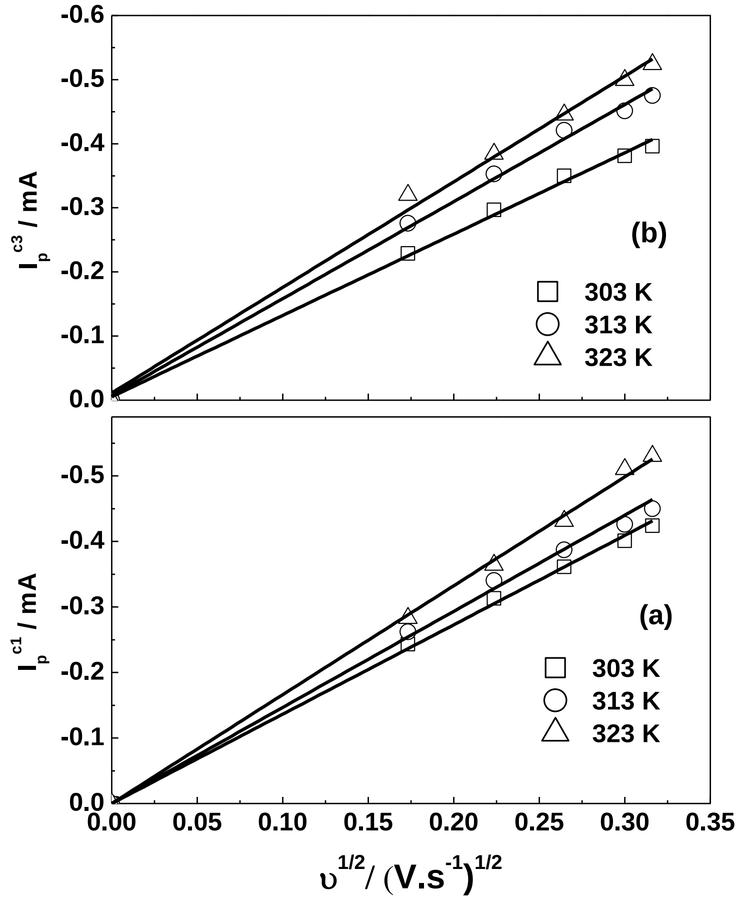

Figure 4.19. Dependence of the peak current on the square root of scan rate ($\upsilon^{1/2}$) perataining to the reduction of 62 mM UO_2^{2+} in (a) C_4mImDCA and (b) C_4mPyDCA recorded at a glassy carbon electrode at different temperatures.

The value of αn_α required for the determination of diffusion coefficient can be obtained from the CV shown in figure 4.18 by using equation (A.5) (Annexure) [29, 30]. where $E_{p/2}^{c1}$ or $E_{p/2}^{c3}$ are the half-peak potentials responsible for the reduction of UO_2^{2+} to UO_2^{+} in C_4mImDCA and C_4mPyDCA respectively. The value of αn_α obtained at 303 K was then substituted into equation (4.24) and the diffusion coefficients thus obtained are listed in table 4.5. The diffusion coefficient obtained in the present study at 303 K is nearly on order higher than the diffusion coefficient reported for UO_2^{2+} in other ILs under similar conditions (see table 4.5). This could be attributed to the low viscosity exhibited by dicyanamide ILs (29 cP) that make the diffusion of UO_2^{2+} relatively fast as compared to that in other ILs.

Table 4.5. Diffusion coefficients of uranyl ion in C_4mImDCA and C_4mPyDCA at different temperatures obtained in the present study and those reported in the literature.

Ionic liquid	Diffusion coefficient x 10^7 /$cm^2.s^{-1}$	Temperature/K
C_4mImDCA	1.73	303
	2.19	313
	2.47	323
C_4mPyDCA	1.42	303
	1.91	313
	2.26	323
C_4mImCl	0.17	373 [44]
	0.48	353 [45]
$HbetNTf_2$	0.63	373 [46]
C_2mImCl + C_2mImBF_4	0.37	298 [47]
$C_4mimNTf_2$	5.8	353 [48]

4.1.2.6. Effect of temperature

The voltammogram pertaining to UO_2^{2+} present in C_4mImDCA and C_4mPyDCA recorded at different temperatures at a scan rate of 100 mV/s is shown in figure 4.20. It is seen that the cathodic peak potentials (E_p^{c1} and E_p^{c3}) gets shifted anodically and the peak currents (I_p^{c1} and I_p^{c3}) increase with temperature in both these ILs. This indicates that the diffusion of UO_2^{2+} is facilitated with an increase in temperature.

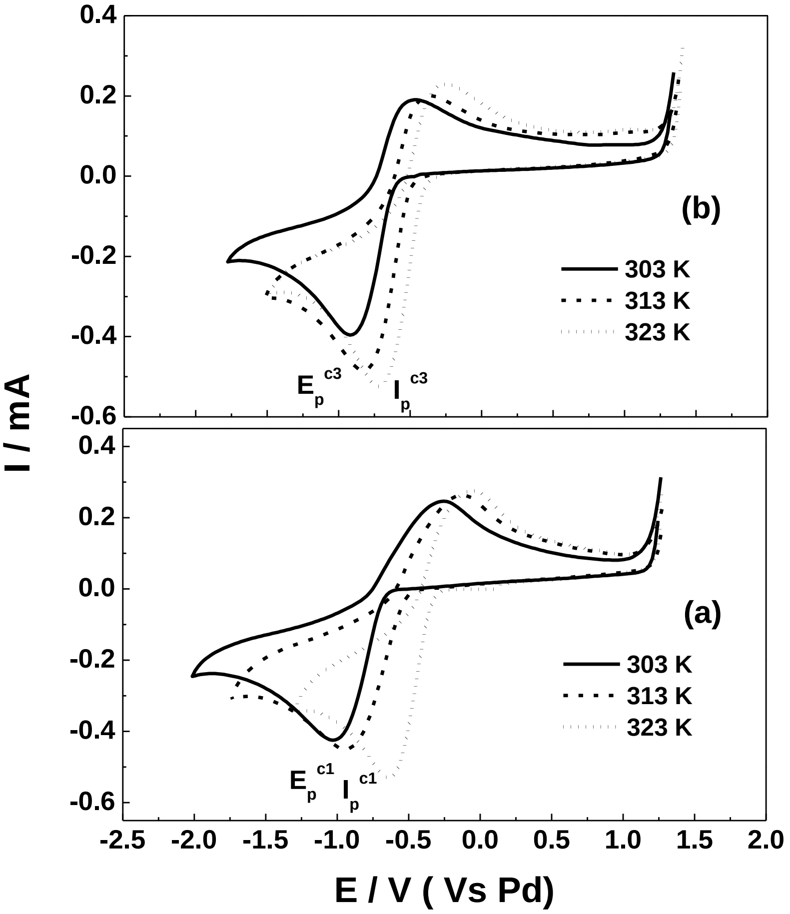

Figure 4.20. CV pertaining to 62 mM UO_2^{2+} in (a) C_4mImDCA and (b) C_4mPyDCA recorded at a glassy carbon electrode at different temperatures at 100 mVps.

The CV peartaining to the reduction of UO_2^{2+} to UO_2^{+} as a function of scan rate was recorded at different temperatures and the plot of I_p^{c1} and I_p^{c3} against square root of scan rate is shown in figure 4.19. It is seen that the cathodic currents (I_p^{c1} and I_p^{c3}) obtained at a particular scan rate increase with an increase in temperature. This could be due to the increase in the diffusion coefficient of UO_2^{2+} in the IL with temperature. The linear dependency of I_p^{c1} on the square root of the scan rate at different temperatures permits the determination of the diffusion coefficient of UO_2^{2+} by using equations (4.23) and (4.24), as discussed above. The values of diffusion coefficients thus obtained are tabulated in table 4.5.

4.2.2. Conclusions

The imidazolium and pyrrolidinium ILs containing dicyanamide anion, C_4mImDCA and C_4mPyDCA, displayed low viscosity (29 cP) and good solubility for uranium nitrate (~0.5 M). The coordination behaviour of dicyanamide anion with uranyl ion was characterized by Raman and FTIR spectroscopy. A Raman band observed at 852 cm^{-1} and an IR band at 931 cm^{-1} in the case of uranyl nitrate present in C_4mImDCA and C_4mPyDCA was attributed to the U=O stretching frequency and the position of the band at 852 cm^{-1} in the Raman and 931 cm^{-1} in FTIR spectra showed that the DCA^- anion was coordinated to the uranyl ion. Coordination of DCA^-, liberated the nitrate ions from the coordination sphere of uranyl ion, as confirmed by the appearance of a Raman band at 1040 cm^{-1} that could be attributed to “free” nitrate ion.

The sequential substitution and linkage behaviour of DCA^- in a solution of the latter with uranyl nitrate was investigated in C_4mImBF_4 IL at various mole ratios of uranium to DCA^-. The absence of the bands pertaining to symmetrical stretch of the “free nitrate” in the Raman spectrum in a mixture with DCA^- to uranium mole ratio lower than 2 : 1 confirmed that DCA^- was not acting as a bidentate ligand. Increasing the mole ratio of DCA^- to uranium above 2 : 1 resulted in the substitution of nitrate ion by DCA^- ion. The sequential substitution reaction by DCA^- resulted in a change in the coordination of the nitrate ion from bidentate to monodentate, followed by the liberation of the latter into the IL. This sequence of reactions continued with an increase in the mole ratio of DCA^- to uranium up to 4 : 1. At mole ratios above 4 : 1, a major fraction of uranyl ion in the IL seems to have been converted into the form $[UO_2(DCA)_4]^{2-}$. Therefore, the spectroscopic investigations revealed that UO_2^{2+} in C_4mImDCA and C_4mPyDCA existed as $[UO_2(DCA)_4]^{2-}$.

The electrochemical behaviour of UO_2^{2+} present in C_4mImDCA and C_4mPyDCA was studied at a glassy carbon working electrode. The CV of uranyl ion displayed a couple of cathodic and anodic waves in both these ILs. The cathodic peaks were attributed to a two step-one electron transfer reduction of UO_2^{2+} to UO_2^+ and then to UO_2. The diffusion coefficient of UO_2^{2+} was found to be in the order 10^{-7} cm^2/s, which is about an orderof magnitude higher than those observed in other ILs, plausibly due to the low viscosity offered by C_4mImDCA and C_4mPyDCA.

References

1. F. Liu, Y. Deng, X. Han, W. Hu, C. Zhong, Electrodeposition of metals and alloys from ionic liquids, J. Alloys Compd. 654 (2016) 163–170.
2. M. Galiński, A. Lewandowski, I. Stępniak, Ionic liquids as electrolytes, Electrochim. Acta 51 (2006) 5567–5580.
3. M. Armand, F. Endres, D.R. MacFarlane, H. Ohno, B. Scrosati, Ionic-liquid materials for the electrochemical challenges of the future, Nat. Mater. 8 (2009) 621–629.
4. D.D. Patel, J.M. Lee, Applications of ionic liquids, Chem. Rec. 12 (2012) 329–355.

5. P.R.V. Rao, K.A. Venkatesan, A. Rout, T.G. Srinivasan, K. Nagarajan, Potential applications of room temperature ionic liquids for fission products and actinide separation, Sep. Sci. Technol. 47 (2012) 204–222.

6. F. Javed, F. Ullah, M.R. Zakaria, H.M. Akil, An approach to classification and hitech applications of room-temperature ionic liquids (RTILs): a review, J. Mol. Liq. 271 (2018) 403–420.

7. K.A. Venkatesan, T.G. Srinivasan, P.R. Vasudeva Rao, A review on the electrochemical applications of room temperature ionic liquids in nuclear fuel cycle, J. Nucl. Radiochem. Sci. 10 (2009) R1–R6.

8. A.P. Abbott, K.J. McKenzie, Application of ionic liquids to the electrodeposition of metals, Phys. Chem. Chem. Phys. 8 (2006) 4265–4279.

9. P. Giridhar, K. A. Venkatesan, T. G. Srinivasan, P. V. Rao, Extraction of fission palladium by Aliquat 336 and electrochemical studies on direct recovery from ionic liquid phase, Hydrometallurgy 81 (2006) 30–39.

10. P. Giridhar, K. A. Venkatesan, S. Subramaniam, T. G. Srinivasan, P. V. Rao, Extraction of uranium(VI) by 1.1 M tri-n-butylphosphate/ionic liquid and the feasibility of recovery by direct electrodeposition from organic phase, J. Alloys Compd. 448 (2008) 104–108.

11. M. Matsumiya, Y. Kikuchi, T. Yamada, S. Kawakami, Extraction of rare earth ions by tri-n-butylphosphate/phosphonium ionic liquids and the feasibility of recovery by direct electrodeposition, Sep. Purif. Technol. 130 (2014) 91–101.

12. P. Y. Chen, C. L. Hussey, Electrochemistry of ionophore-coordinated Cs and Sr ions in the tri-1-butylmethylammonium bis((trifluoromethyl)sulfonyl)imide ionic liquid, Electrochim. Acta 50 (2005) 2533–2540.

13. Y. Pan, C. L. Hussey, Electrochemical and spectroscopic Investigation of Ln^{3+} (Ln= Sm, Eu, and Yb) solvation in bis (trifluoromethylsulfonyl) imide-based ionic liquids and coordination by N, N, N′, N′-Tetraoctyl-3-oxa-pentane diamide (TODGA) and chloride, Inorg. Chem. 52 (2013) 3241–3252.
14. S. Murakami, M. Matsumiya, T. Yamada, K. Tsunashima, Extraction of Pr(III), Nd (III), and Dy(III) from HTFSA aqueous solution by TODGA/phosphonium-based ionic liquids, Solvent Extr. Ion Exc. 34 (2016) 172–187.
15. C. Gaillard, A. Chaumont, I. Billard, C. Hennig, A. Ouadi, S. Georg, G. Wipff, Competitive complexation of nitrates and chlorides to uranyl in a room temperature ionic liquid, Inorg. Chem. 49 (2010) 6484–6494.
16. P. Nockemann, K. Servaes, R. Van Deun, K. Van Hecke, L. Van Meervelt, K. Binnemans, C. Gçrller-Walrand, Speciation of uranyl complexes in ionic liquids by optical spectroscopy, Inorg. Chem. 46 (2007) 11335–11344.
17. R. Rama, A. Rout, K. A. Venkatesan, M. P. Antony, A. Suresh, Comparision in the solvent extraction behavior of uranium(VI) in some trialkyl phosphates in ionic liquid, Radiochim. Acta 104 (2016) 865–872.
18. K. Naito, T. Suzuki, The mechanism of the extraction of several uranyl salts by tri-n-butyl phosphate, J. Phys. Chem. 66 (1962) 989–995.
19. S. Georg, I. Billard, A. Ouadi, C. Gaillard, L. Petitjean, M. Picquet, V. Solov’ev, Determination of successive complexation constants in an ionic liquid: Complexation of UO_2^{2+} with NO_3^- in C_4mimTf_2N studied by UV− Vis spectroscopy, J. Phys. Chem. B 114 (2010) 4276–4282.
20. C. Gaillard, A. El Azzi, I. Billard, H. Bolvin, C. Hennig, Uranyl complexation in fluorinated acids (HF, HBF_4, HPF_6, HTf_2N): a combined experimental and theoretical study, Inorg. Chem. 44 (2005) 852–861.

21. G.M. Krishna, A.S. Suneesh, R. Kumaresan, K.A. Venkatesan, M.P. Antony, Dissolution of U_3O_8 in 1-butyl-3-methylimidazolium chloride and spectroscopic and electrochemical behavior of U(VI) in the resultant solution, J. Electroanal. Chem. 795 (2017) 51–58.
22. I. Billard, C. Gaillard, C. Hennig, Dissolution of UO_2, UO_3 and of some lanthanide oxides in $BumimTf_2N$: effect of acid and water and formation of $UO_2(NO_3)_3^-$. Dalton Trans. 37 (2007) 4214–4221.
23. M. H. Brooker, C. B. Huang, J. Sylwestrowicz, Raman spectroscopic studies of aqueous uranyl nitrate and perchlorate systems, J. Inorg. Nucl. Chem. 42 (1980) 1431–1440.
24. K. Ohwada, T. Ishihara, Infra-red spectrophotometry of uranyl nitrate/tri-n-butyl phosphate in organic solvents, J. Inorg. Nucl. Chem. 28 (1966) 2343–2345.
25. M. Gal, P.L. Goggin, J. Mink, Vibrational spectroscopic studies of uranyl complexes in aqueous and non-aqueous solutions, Spectrochim. Acta Part A: Mol. Spectrosc. 48 (1992) 121–132.
26. Y. Wang, Y. Liu, T. Chu, Spectroscopic studies on uranyl complexes with tri-n-butyl phosphate (TBP) in ionic liquids, J. Radioanal. Nucl. Chem. 308 (2016) 1071–1079.
27. D. L. Quach, C. M. Wai, S. P. Pasilis, Characterization of uranyl (VI) nitrate complexes in a room temperature ionic liquid using attenuated total reflection-Fourier transform infrared spectrometry, Inorg. Chem. 49 (2010) 8568–8572.
28. S. P. Pasilis, A. Blumenfeld, Effect of nitrate, perchlorate, and water on uranyl(VI) speciation in a room-temperature ionic liquid: a spectroscopic investigation, Inorg. Chem. 50 (2011) 8302–8307.

29. A.J. Bard, L.R. Faulkner, Electrochemical Methods-Fundamentals and Applications, Wiley, New York, 1980.

30. K. Aoki, K. Tokuda, H. Matsuda, Theory of linear sweep voltammetry with finite diffusion space, J. Electroanal. Chem. Interfacial Electrochem. 146 (1983) 417.

31. H.Y. Huang, P.Y. Chen, Voltammetric behavior of Pd(II) and Ni(II) ions and electrodeposition of PdNi bimetal in N-butyl-N-methylpyrrolidinium dicyanamide ionic liquid, Electrochim. Acta 56 (2011) 2336–2343.

32. M.J. Deng, P.Y. Chen, T.I. Leong, I.W. Sun, J.K. Chang, W.T. Tsai, Dicyanamide anion based ionic liquids for electrodeposition of metals, Electrochem. Commun. 10 (2008) 213–216.

33. D.R. MacFarlane, S.A. Forsyth, J. Golding, G.B. Deacon, Ionic liquids based on imidazolium, ammonium and pyrrolidinium salts of the dicyanamide anion, Green Chem. 4 (2002) 444–448.

34. W.L. Yuan, X. Yang, L. He, Y. Xue, S. Qin, G.H. Tao, Viscosity, conductivity, and electrochemical property of dicyanamide ionic liquids, Front. Chem. 6 (2018) 59.

35. Q.B. Zhang, C. Yang, Y.X. Hua, Y. Li, P. Dong, Electrochemical preparation of nanostructured lanthanum using lanthanum chloride as a precursor in 1-butyl-3-methylimidazolium dicyanamide ionic liquid, Phys. Chem. Chem. Phys. 17 (2015) 4701–4707.

36. S. Shrestha, E.J. Biddinger, Palladium electrodeposition in 1-butyl-1-methylpyrrolidinium dicyanamide ionic liquid, Electrochim. Acta 174 (2015) 254–263.

37. H. Roohi, S. Khyrkhah, Ion-pairs formed in $[Mim^+][N(CN)_2^-]$ ionic liquid: structures, binding energies, NMR SSCCs, volumetric, thermodynamic and topological properties, J. Mol. Liq. 177 (2013) 119–128.

38. T.C. Penna, L.F. Faria, M.C. Ribeiro, Raman band shape analysis of cyanate-anion ionic liquids, J. Mol. Liq. 209 (2015) 676–682.

39. J. Kiefer, K. Noack, T.C. Penna, M.C. Ribeiro, H. Weber, B. Kirchner, Vibrational signatures of anionic cyano groups in imidazolium ionic liquids, Vib. Spectrosc. 91 (2017) 141–146.

40. G.M. Krishna, A.S. Suneesh, R. Kumaresan, K.A. Venkatesan, M.P. Antony, Electrochemical behavior of U(VI) in imidazolium ionic liquid medium containing Tri-n-butyl phosphate and chloride ion and spectroscopic characterization of uranyl species, Chem. Select 2 (2017) 8706–8715.

41. S.R. Marshall, C.D. Incarvito, W.W. Shum, A.L. Rheingold, J.S. Miller, Novel coordination of dicyanamide,$[N(CN)_2]^-$: preferential binding of the amide nitrogen, Chem. Comm. 24 (2002) 3006–3007.

42. A.J. Perkins, Raman and infrared spectra of the dicyanamide ion, Dev. Appl. Spectrosc. 2 (1963) 43–51.

43. T.J. Simons, P.C. Howlett, A.A.J. Torriero, D.R. MacFarlane, M. Forsyth, Electrochemical, transport, and spectroscopic properties of 1-ethyl-3-methylimidazolium ionic liquid electrolytes containing zinc dicyanamide, J. Phys. Chem. C 117 (2013) 2662–2669.

44. P. Giridhar, K.A. Venkatesan, T.G. Srinivasan, P.V. Rao, Electrochemical behavior of uranium (VI) in 1-butyl-3-methylimidazolium chloride and thermal characterization of uranium oxide deposit, Electrochim. Acta 52 (2007) 3006–3012.

45. Y. Ikeda, K. Hiroe, N. Asanuma, A. Shirai, Electrochemical studies on uranyl (VI) chloride complexes in ionic liquid, 1-butyl-3-methylimidazolium chloride, J. Nucl. Sci. Technol. 46 (2009) 158–162.

46. C.J. Rao, K.A. Venkatesan, K. Nagarajan, T.G. Srinivasan, Dissolution of uranium oxides and electrochemical behavior of U (VI) in task specific ionic liquid, Radiochim. Acta 96 (2008) 403–409.

47. T. Ogura, K. Sasaki, K. Takao, T. Arai, Y. Ikeda, Electrochemical behavior of $[UO_2Cl_4]^{2-}$ in 1-ethyl-3-methylimidazolium based ionic liquids, Sci. China Chem. 55 (2012) 1699–1704.

48. R. Rama, A. Rout, K.A. Venkatesan, M.P. Antony, Effect of alkyl chain length of tri-*n*-alkyl phosphate extractants on the electrochemical behaviour of U(VI) in ionic liquid medium, J. Electroanal. Chem. 771 (2016) 87–93.

Chapter 5. Studies related to electrorefining of uranium and zirconium in ionic liquid medium

Introduction

Metallic fuel has been proposed for the rapid growth of Indian fast reactor program [1-2]. This is due to the favorable properties of the metallic fuel, viz., higher breeding ratio and its amenability towards pyrochemical reprocessing. It is proposed to use uranium-zirconium alloy as a candidate metallic fuel for fast research reactor, and uranium-plutonium-zirconium alloy for fast power reactor [1-5]. In these alloys, the maximum zirconium content is generally limited to the extent of 10 wt.%. It should be noted that zirconium is added to the metallic actinides to increase the solidus temperature of the ternary alloy [3]. In addition, the presence of zirconium increases the compatibility of the fuel with austenitic stainless-steel cladding material by suppressing the inter diffusion of the fuel and clad components [4-5].

Non-aqueous pyrochemical electrorefining method has been proposed for reprocessing of spent metallic fuels [6-8]. In this electrorefining method, the actinides present in the spent metallic fuel are anodically dissolved in of high-temperature eutectic mixture of molten LiCl–KCl and actinides are recovered by electrodeposition at the cathode [9, 10]. It should be noted that this process operates at temperatures at 773 K or above, depending up on the composition of the chosen electrolyte. The dissolution of metallic fuel elements in the molten salt medium is governed by the standard reduction potentials. The standard potential of Zr(IV)/Zr couple is reported to be more positive than that of U(III)/U and Pu(III)/Pu in LiCl–KCl melts [11,12]. This shows that zirconium should not dissolve in the molten salt medium during anodic dissolution of uranium and plutonium from the spent metallic fuel. However, practical considerations of the electrorefining method demand the operation of dissolution reaction at high current density for quantitative dissolution of the actinides, especially at the end of dissolution. Under such conditions, the anode is usually kept at much higher positive potentials, beyond the oxidation potentials of zirconium. Therefore, it indicates that a portion of zirconium also gets oxidized to Zr(IV) and dissolves in the molten salt medium. In addition, due to the low negative potential needed for electrodeposition of zirconium, it gets reduced to its metallic form along with actinides during the recovery. Therefore, the presence of zirconium in the molten salt is usually considered as an undesirable.

5.1. Electrochemical behaviour of zirconium(IV) in 1-butyl-3-methylimidazolium bis(trifluoromethylsulfonyl)imide ionic liquid

Many authors have investigated the co-ordination, spectroscopic and electrochemical behaviour of actinides in ammonium and imidazolium ILs. It is reported that these ILs offer a wide electrochemical window and it is indicated that it is feasible to reduce them into their metallic form [15, 16] in these ILs. Jagadeeswara Rao *et al.* [17] studied the suitability of using N-butyl-N-methylpyrrolidinium bis(trifluoromethylsulfonyl)imide ($BMPyNTf_2$) IL for the electrodeposition of europium. Extensive studies on the electrochemical behaviour and electrodeposition of different metals on different cathode materials have been investigated by Endres and co-workers. Giridhar *et al.* [18] studied the electrochemical behaviour of niobium in $BMPyNTf_2$ IL. These authors reported that niobium can be deposited in its metallic form from pyrrolidinium IL. However, this deposit also contained some oxides of niobium. Borisenko *et al.* [19] reported the electrodeposition of tantalum from IL medium containing TaF_5 and this deposition was monitored by Electrochemical Quartz Crystal Microbalance (EQCM). Similarly, the electrodeposition of Nb and Cu from 1-butyl-1-methylpyrrolidinium bis (trifluoromethylsulphonyl) imide was studied by Vacca *et al.* [20].

Many studies have been reported in the literature on the electrochemical behaviour of metal ions U(III) and Zr(IV) as well as the combined behaviour of U(III)-Zr(IV) in high temperature molten salts [21,22]. However, the reports on the electrochemical behaviour of these systems in RTILs are minimal. In the recent past, Rao *et al.* reported [23] the voltammetric behaviour of U(IV) in N-methyl-N-propylpiperidinium bis(trifluoromethylsulfonyl)imide ($MPPiNTf_2$) IL medium. The rate of dissolution of uranium oxide (UO_2) in $HNTf_2$ was studied at 353 K and the resultant

$U(NTf_2)_4$ was dissolved in $MPPiNTf_2$ for studying the electrochemical behaviour. As far as zirconium is concerned, only limitted information is available in the literature on the electrochemical behaviour of Zr(IV) in IL medium. Tsuda *et al.* [24] reported the electrochemistry of Zr(IV) in aluminium chloride-1-ethyl-3-methylimidazolium chloride IL. However, this kind of IL is sensitive to moisture and air. Fu *et al.* [25] reported the electrochemistry of zirconium tetrachloride in $BMPyNTf_2$. These authors reported the reduction of Zr(IV) to Zr(III) at a platinum electrode. Further reduction of Zr(III) to a lower valence state or to the metal was not observed. More recently Vacca *et al.* [26] reported the electrochemical behavior of Zr(IV) in1-butyl-1-methylpyrrolidinium-bis(trifuoromethylsulphonyl)imide IL, investigated by CV and chronopotentiometry. These authors observed that Zr(IV) undergoes a two-step, two-electron transfer reduction reaction to metallic zirconium on different substrates. However, the diffusion coefficients, electron transfer kinetics, nucleation phenomenon and chronoamperometry were not reported.

In view of the paucity of data on the electrochemical behaviour of Zr(IV) in ILs and in order to develop ILs suitable for metallic fuel reprocessing, the electrochemical behaviour of Zr(IV) present in 1-butyl-3-methylimidazolium bis(trifluoromethylsulfonyl)imide ($C_4mimNTf_2$) IL medium was studied. The apparent diffusion coefficients of Zr(IV) in ILs is key parameter that needs to be determined. Therefore, in this chapter, we report the “apparent diffusion coefficient” of Zr(IV) and its electron transfer kinetics involved in the electrodeposition.

Synthesis of IL, $C_4mimNTf_2$ has been discussed in section 2.5.2 and the experimental procedure for voltammetric, electrodeposition studies and characterisation have been described in the section 2.4.5.

5.1.1. RESULTS AND DISCUSSION

5.1.1.1. Cyclic voltammetry of Zr(IV) in $C_4mimNTf_2$

The cyclic voltammogram of $C_4mimNTf_2$ recorded at a glassy carbon working electrode at a scan rate 100 mV/s at 353 K is shown in figure 5.1. It is seen that the cation reduction occurs at -2.7 V (Vs Pd) and the anion gets oxidised at +2.0 V (Vs Pd), thus offering an electrochemical window of about 4.7 V. The cathodic stability offered by $C_4mimNTf_2$ is adequate for the reduction of Zr(IV) to metallic form. The cyclic voltammogram of Zr(IV) recorded at a glassy carbon working electrode at a scan rate of 100 mV/s at 353 K is also shown in figure 5.1. It is seen that the voltammogarm consists of a minute cathodic wave occurring at a peak potential of +0.2 V (Vs Pd), which could be due to the reduction of Zr(IV) to Zr(II), and a prominent cathodic wave occurring at -1.3 V (Vs Pd) due to the reduction of Zr(II) to Zr(0). The reduction at -1.3 V (Vs Pd), which is accompanied by a nucleation loop at -1.6 V during the scan reversal at -2.0 V. The voltammogram also shows oxidation waves at -0.6 V (Vs Pd) and at +0.5 V (Vs Pd) pertaining to the oxidation of Zr(0) to Zr(II) and Zr(II) to Zr(IV) respectively. The oxidation of Cl^- to Cl_2 occurs at +0.8 V (Vs Pd). The voltammogarm thus shows that Zr(IV) undergoes a two-step two-electron transfer reduction to zirconium metal in $C_4mimNTf_2$ at the working electrode. A similar behaviour was also reported by Chen *et al.* [27] for the reduction of Zr(IV) in a high temperature molten salt composed LiCl-KCl electrolytic medium. Fu *et al.* [25] studied the electrochemical behaviour of Zr(IV) in N-butyl –N-methyl pyrrolidinium bis(trifluoromethylsulfonyl)imide IL. It was reported that Zr(IV) undergoes reduction to Zr(III). However, further reduction to lower valent states of Zr was not observed in that IL. Tsuda *et al.* [24] reported the electrochemical behaviour of Zr(IV) to Zr(II) and the electrodeposition of Al-Zr alloy in the acidic $AlCl_3$-1-ethyl -3- methyl imidazolium chloride molten salt at 353 K. It was reported that Zr(IV) undergoes a two electron transfer reduction to Zr(II) prior to the formation of Al-Zr alloy. Therefore, the present study suggests that Zr(IV) in $C_4mimNTf_2$ probably undergoes a two-step, two-electron transfer (in each step) to produce zirconium metal, similar to the observations reported in the high-temperature molten salt and imidazolium IL, studies.

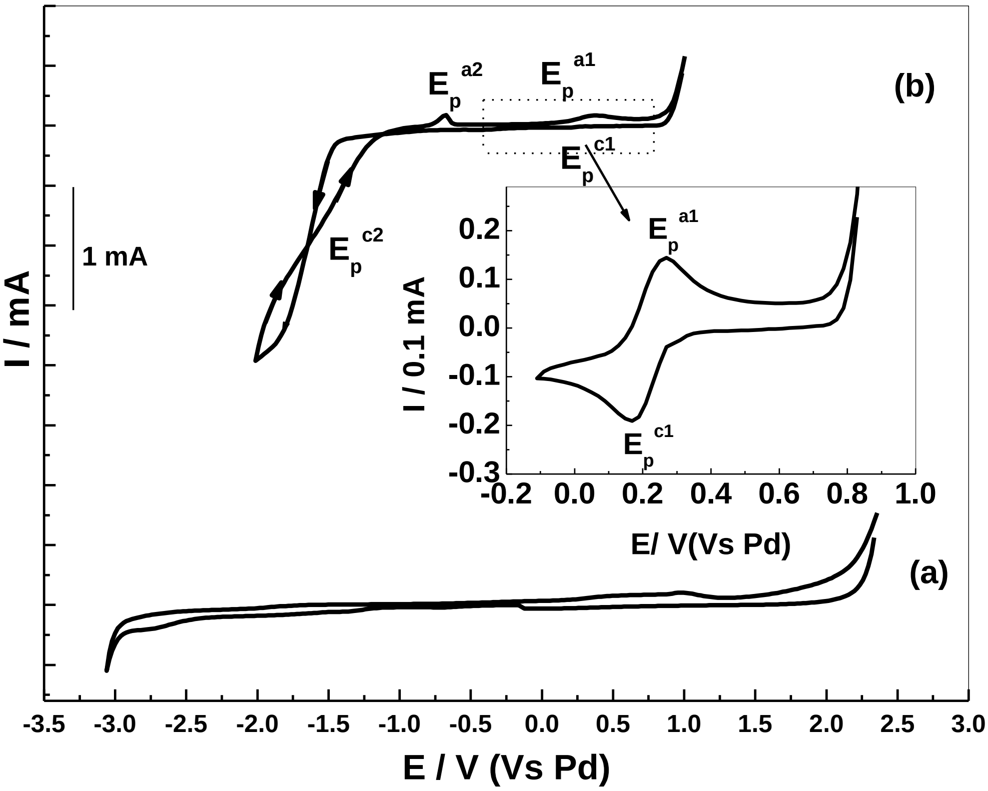

Figure 5.1. CV pertaining to (a) neat $C_4mimNTf_2$ (b) solution of Zr(IV) in $C_4mimNTf_2$ from -2.0 V to +0.8 V. Working electrode: glassy carbon (cylindrical SA= 0.16 cm^2), counter electrode: glassy carbon (cylindrical SA= 0.25 cm^2), quasi-reference electrode: palladium wire (SA, 0.10 cm^2), at 353 K; and scan rate: 100 mV/s.

5.1.1.2. Diffusion coefficient of Zr(IV)

The cyclic voltammogram of Zr(IV) in $C_4mimNTf_2$ as a function of scan rate at 353 K is shown in figure 5.2. The cathodic and anodic switching potentials were fixed at -0.1 V (Vs Pd) and 0.9 V (Vs Pd) respectively during this scan. It is seen that the cathodic peak potential (E_p^{c1}) gets shifted cathodically and the cathodic peak current (i_p^{c1}) increases with the scan rate, indicating that the reduction of Zr(IV) to Zr(II) is not reversible. It is well recognised that reversible process is diffusion controlled, and the irreversible (or quasi-reversible) process is both diffusion and charge transfer controlled [28, 29].

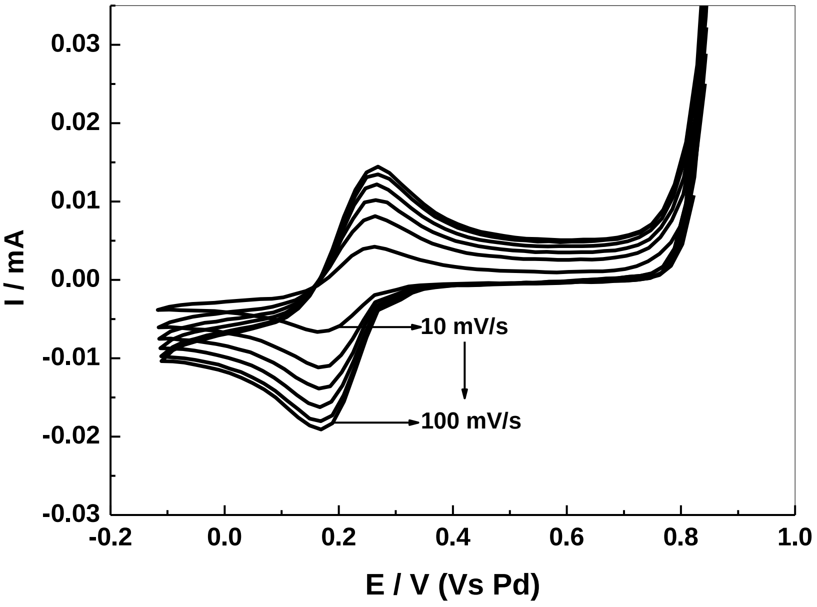

Figure 5.2. Comparison of CV of a solution of 30 mM Zr(IV) in $C_4mimNTf_2$ at different sweeping potentials at 353 K. Working electrode: glassy carbon (cylindrical SA= 0.16 cm^2), counter electrode: glassy carbon (cylindrical SA= 0.25 cm^2), quasi-reference electrode: palladium wire (SA, 0.10 cm^2), at 353 K.

The value of $|E_p^{c1} - E_{p/2}^{c1}|$ pertaining to the rduction of Zr(IV) to Zr(II) is higher (71 mV at 353 K) than the value needed for a reversible (33.5 mV at 353 K) two-electron transfer process [28, 29]. This shows that the reduction of Zr(IV) to Zr(II) is probably quasi-reversible. This also indicates that the reduction Zr(IV) to Zr(II) is not only controlled by the diffusion of Zr(IV) at the working electrode, but also by a heterogeneous charge transfer across the electrode-electrolyte interface. The charge transfer coefficient (α) is a measure of the symmetry barrier in a non-reversible (both quasi and irreversible process) electrode reaction and it could be determined from the magnitude of $|E_p^{c1}-E_{p/2}^{c1}|$ by using equation A.4 (Annexure) [28-30] with the help of equation 2.4, the value of αn_α was found to vary from 0.8 to 0.9 when the scan rate was increased from 10 mV/s to 100 mV/s at 353 K.

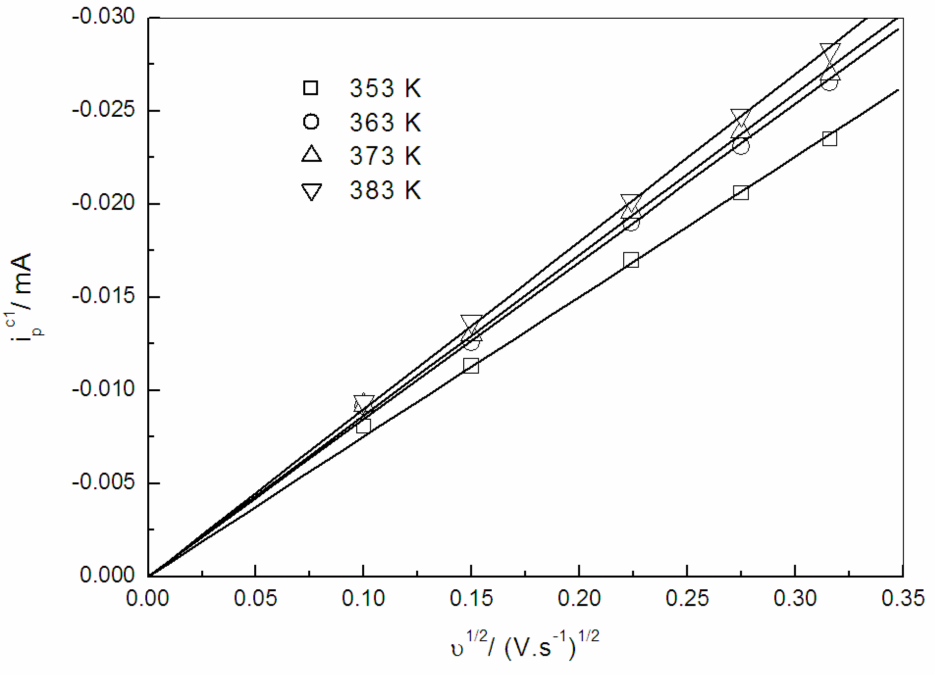

Figure 5.3: Dependence of cathodic peak currents (i_p^{c1}) on the square root of scan rate ($\upsilon^{1/2}$) pertaining to the reduction of Zr(IV) (30 mM) in C_4mImNTf$_2$ at different temperatures.

The relation between the cathodic peak current (i_p^{c1}) and the scan rate for an irreversible or quasi reversible reduction of soluble-soluble Zr(IV)-Zr(II) couple is given by Berzins-Delahay equation (A.5) (Annexure). A plot of i_p^{c1} against square root of scan rate ($\nu^{1/2}$) at 353 K for the reduction of Zr(IV) to Zr(II) in C_4mimNTf$_2$ is shown in figure 2.5. It is seen that the cathodic peak current increases with $\upsilon^{1/2}$. Linear dependence of the cathodic peak current with a zero-intercept indicates the validity of equation (2.5). Compliance to this equation suggests the involvement of the heterogeneous charge transfer coefficient, αn_α, pertaining to a heterogeneous charge transfer mechanism in the reduction of Zr(IV) to Zr(II) operative at the electrode-electrolyte interface. The apparent diffusion coefficient of Zr(IV) in this IL could be derived from the slope of the fitted least squares linear regression plot shown in figure 5.3. The apparent diffusion coefficient of Zr(IV) in C_4mImNTf$_2$ was determined to be 10^{-10} cm^2/s.

5.1.1.3. Effect of temperature

The CV pertaining to Zr(IV) in C_4mImNTf$_2$ recorded at a glassy carbon working electrode at a scan rate of 100 mV/s at different temperatures is shown in figure 5.4. It is seen that the cathodic peak potential (E_p^{c1}) is shifted anodically and the cathodic peak current (i_p^{c1}) increases with temperature. In addition, the CV pertaining to Zr(IV) in C_4mImNTf$_2$ as a function of scan rate was recorded at different temperatures. The plot of i_p^{c1} against the square root of scan rate ($\upsilon^{1/2}$) is shown in figure 5.3. A linear dependence of i_p^{c1} and $\upsilon^{1/2}$ indicates the validity of equation (5.2) over the entire temperature range of investigation employed in the present study. The diffusion coefficient of Zr(IV) at different temperatures was determined as described above. These values are tabulated in table 5.1. It is seen that the diffusion coefficient increases with temperature. The Arrhenius relation between the diffusion coefficient and temperature is shown in equation 5.1.

$$\ln D = \ln A - E_a/RT \qquad (5.1)$$

where A is the pre-exponential factor and E_a is the energy of activation. A plot of ln D against 1/T is shown in figure 5.5. From the slope of the fitted least squares linear regression, the energy of activation, E_a, for the diffusion of Zr(IV) in $C_4mImNTf_2$ was determined to be 16.5 kJ/mol.

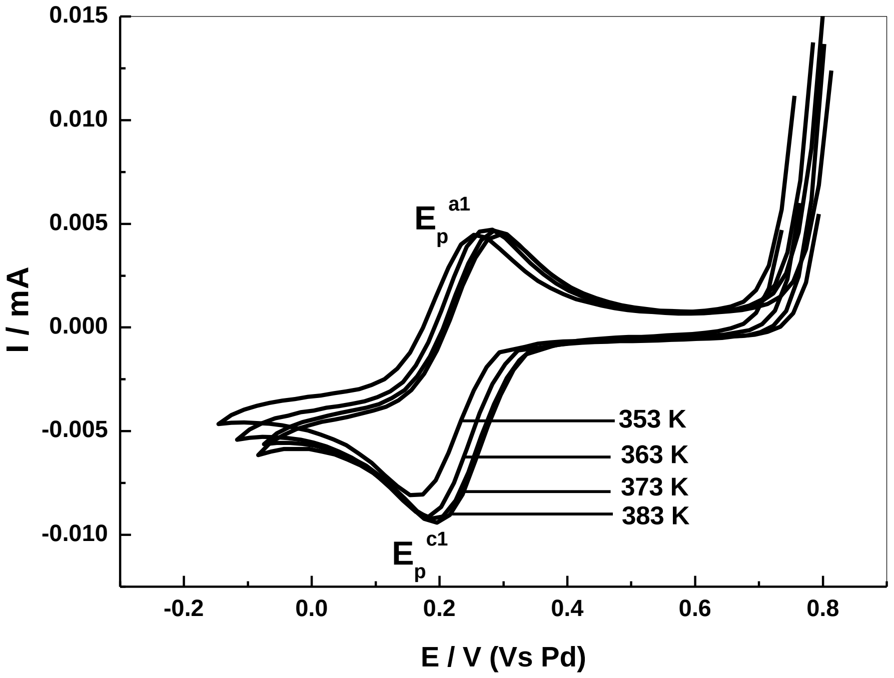

Figure 5.4: Comparison of CV of a solution of 30 mM Zr(IV) in $C_4mImNTf_2$ at different temperatures. Working electrode: Glassy carbon (Cylindrical SA= 0.16 cm^2), counter electrode: glassy carbon (cylindrical SA= 0.25 cm^2), Quasi-reference electrode: Palladium wire (SA, 0.10 cm^2). Scan rate = 10 mV/S.

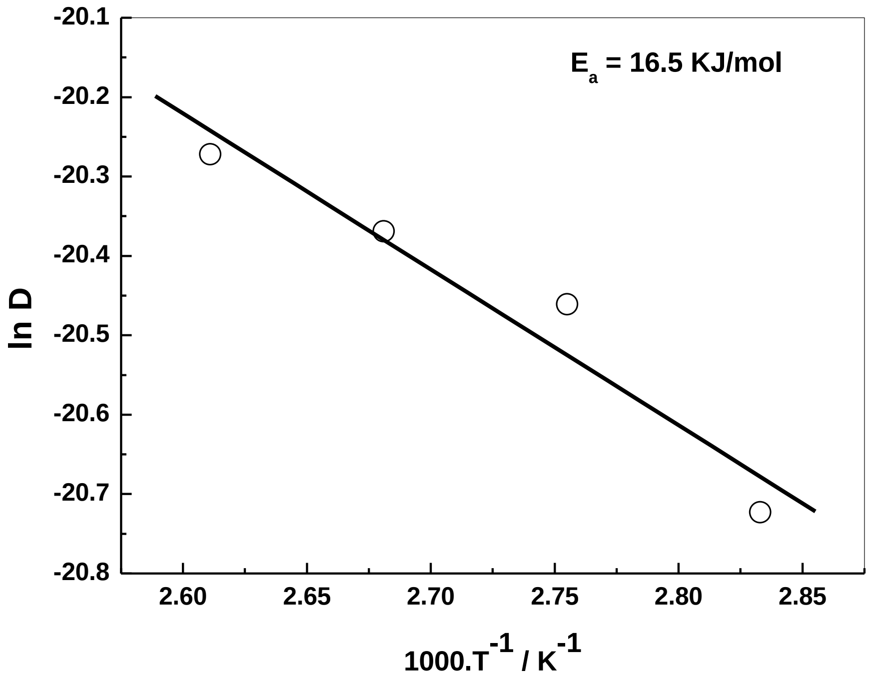

Figure 5.5: Temperature dependence of D pertaining to the reduction of 30 mM Zr(IV) in $C_4mimNTf_2$.

Table 5.1: Diffusion coefficient of Zr(IV) in $C_4mImNTf_2$ determined from cyclic voltammogram at different temperatures.

Temperature/ K	D x 10^{10}/ $cm^2.s^{-1}$
353	7.58
363	13.0
373	14.3
383	15.7

5.1.1.4. Chronoamperometry

Chronoamperometric measurements were performed to obtain the current transient curves for the electrochemical reduction of Zr(IV) to Zr(0). The nucleation phenomenon observed in the CV for the reduction of Zr(IV) to Zr(0) at a glassy carbon electrode was studied by chronoamperometry. To obtain this chronocurrent transient, the potential of the working electrode was varied from -1.6 V to -1.7 V. The chronoamperograms corresponding to the reduction of Zr(IV) to Zr are shown in figure 5.6. These are typical and represent nucleation and growth of a metal deposit on a heterogeneous surface [31-33]. The reduction of Zr(IV) to Zr(II) was not observed in the chronoamperogram probably due to the higher negative potential applied at the working electrode. The transient shows a initial decrease of the negative current, due to the charging of the double layer and the formation of the first nuclei on a glassy carbon working electrode. This is followed by an increase in the negative current leading to a maximum value (i_{max}) at time t_{max} (see figure 5.6). The increase in the negative current is due to the three-dimensional growth of zirconium metal deposit over the nuclei resulting in an increase of the surface area. Finally the negative current decays with time after reaching a maximum. The time corresponding to the i_{max} (t_{max}) depends upon the magnitude of the applied potential. Higher the negative potential lower would be the value of t_{max}.

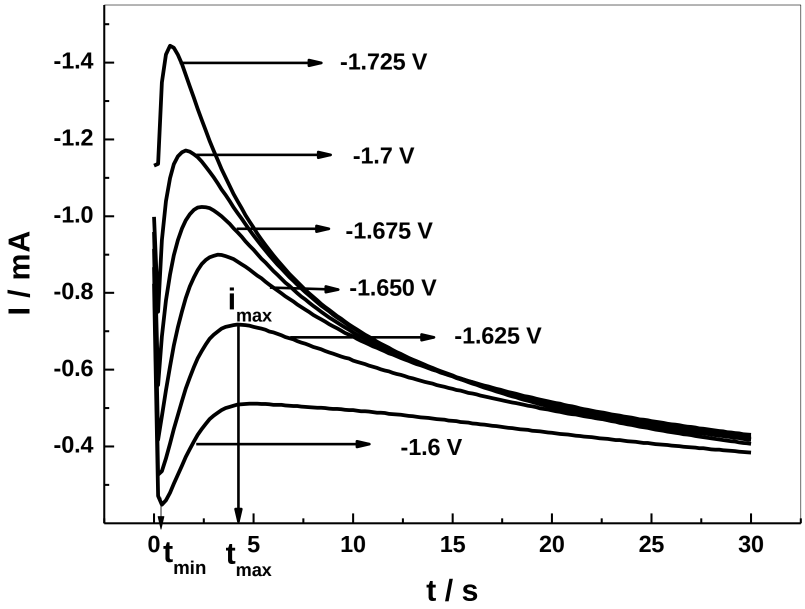

Figure 5.6: Comparison of chronoamperograms of a solution of 30 mM Zr (IV) in $C_4mimNTf_2$ at different applied potentials at 353 K. Working electrode: Glassy carbon (Cylindrical SA= 0.16 cm^2), counter electrode: glassy carbon (cylindrical SA= 0.25 cm^2), Quasi-reference electrode: Palladium wire (SA, 0.10 cm^2).

There are several models proposed for the nucleation and growth of metal deposits on heterogeneous surfaces [31-33]. Among these models, the most widely accepted models progressive and instantaneous nucleation models. Scharifker and Hills [34] have theoretically derived a mathematical function for describing the entire chronocurrent transient from the beginning of three-dimensional nucleation growth to the decay of current. This model assumes that the growth of nuclei occurs by hemi-spherically after the formation of first nuclei on the electrode. As these nuclei grow the surface area of the electrode increases resulting in an increase in the cathodic current until it attains a maximum value as shown in figure 5.6. The transient current for instantaneous and progressive nucleation models are represented in equations (5.2) and (5.3).

$$\left(\frac{i}{i_{max}}\right)^2 = 1.9542\frac{[1-\exp(-1.2564(t/t_{max}))]^2}{(t/t_{max})} \qquad (5.2)$$

$$\left(\frac{i}{i_{max}}\right)^2 = 1.2254\frac{[1-\exp(-2.3367(t/t_{max})^2)]^2}{(t/t_{max})} \qquad (5.3)$$

It is seen from figure 5.6, that there is an induction time, t_{min}, that correspond to the duration required for charging of the double layer and the formation of the first nuclei on the electrode. It is observed from figure 5.6 that this induction time is characteristic of the applied potential. Therefore, the actual time for the onset of the growth of the nuclei followed by decay of the current needs to be corrected with respect to the induction time, t_{min}. The corrected time is given by $t_{corr} = t - t_{min}$ and $t_{m(corr)} = t_{max} - t_{min}$. By substituting the corrected time in equations (5.2) and (5.3), equations (5.4) and (5.5) respectively are derived.

$$\left(\frac{i}{i_{max}}\right)^2 = 1.9542\frac{[1-\exp(-1.2564(t_{corr}/t_{m(corr)}))]^2}{(t_{corr}/t_{m(corr)})} \qquad (5.4)$$

$$\left(\frac{i}{i_{max}}\right)^2 = 1.2254\frac{[1-\exp(-2.3367(t_{corr}/t_{m(corr)})^2)]^2}{(t_{corr}/t_{m(corr)})} \qquad (5.5)$$

A plot of $(i/i_{max})^2$ against $t_{corr}/t_{m(corr)}$ is shown in figure 5.7. It is seen that for all the applied potentials, the nucleation growth (ascending part of the curve) is described well by the instantaneous nucleation model. The descending part of the chronocurrent transient could be fitted well only at certain applied potentials. For instance, when the applied potential is -1.65 V, the entire growth and decay of chronocurrent transient is described well. However, at higher negative potentials the descending part of the transient deviates, to some extent, from the instantaneous model. Nevertheless, it is reasonable to conclude that the electrodeposition of zirconium at a glassy carbon electrode follows instantaneous nucleation model, by and large.

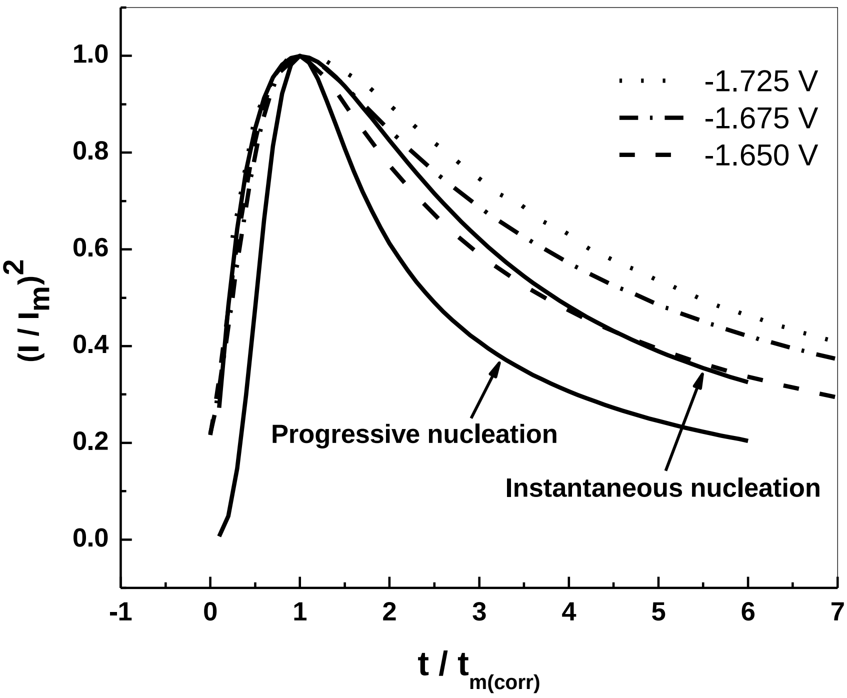

Figure 5.7: Comparison of experimental data obtained from chronocurrent transients with instantaneous and progressive nucleation models at an applied potential of -1.65 V.

The diffusion coefficient could also be calculated from the values of i_{max} and $t_{m(corr)}$ according [33] to equation (5.6). These values are shown in table 5.2.

$$i_{max}^2 t_{m(corr)} = 0.1629(nFAC)^2 D \tag{5.6}$$

A diffusion coefficient of 10^{-5} cm^2/s is obtained at 353 K in the present case. This magnitude is about five orders higher than the value determined by CV (table 5.1). The reason for the higher magnitude of this estimate of the diffusion coefficient derived from chronoamperometry could be attributed only to the nucleation phenomenon. Nucleation increases the surface area of the electrode. As the nuclei grow hemi-spherically over the surface of the electrode, the surface area of the electrode increases and facilitates further enhancement in diffusion. Moreover, it appears that the metallic zirconium nuclei formed over the substrate specifically interacts strongly with the zirconium(IV) in their vicinity and aid further deposition of zirconium metal. This would create a large concentration gradient at the electrode-electrolyte interface and facilitates the diffusion of Zr(IV) ion from the bulk. A substantial increase in cathodic current (i_p^{c2}) observed as a result of nucleation at E_p^{c2} as compared to cathodic current (i_p^{c1}) at E_p^{c1} in the CV, shown in figure 5.2, also supports the fact that nucleation phenomenon could enhance the diffusion of the metal ion to a significant extent.

To confirm the nucleation phenomenon, the SEM image of the deposit was recorded and displayed in figure 5.8. In order to obtain this deposit, electrolysis of Zr(IV) in C_4mimNTf$_2$ was carried out for about one hour at a glassy carbon working electrode at -1.7 V (Vs Pd). This deposit was washed with acetone and dried in air. The SEM-EDX pattern of the sample present on the glassy carbon substrate was recorded. The zirconium electrodeposit was removed and smeared on an aluminium sample holder for carrying out XRD measurements. The XRD pattern shown in figure 5.9 indicates the presence of metallic zirconium (JCPDS), while the EDAX recorded with the SEM-EDX analysis (figure 5.8) shows the presence of zirconium, oxygen and carbon on the surface of the working electrode. Carbon could be due to the remains of the electrode and oxygen could be due to the absorbed moisture. The SEM micrograph indicates features of the growing nuclei merging with other nuclei that are nearby.

Table 5.2: Diffusion coefficient of Zr(II) in $C_4mimNTf_2$ determined from chronoamperograms at different applied potentials at 353 K.

Applied Potential/ V	D X 10^5/ $cm^2.s^{-1}$
-1.60	0.87
-1.625	1.45
-1.650	1.81
-1.675	1.69
-1.700	1.52
-1.725	1.15

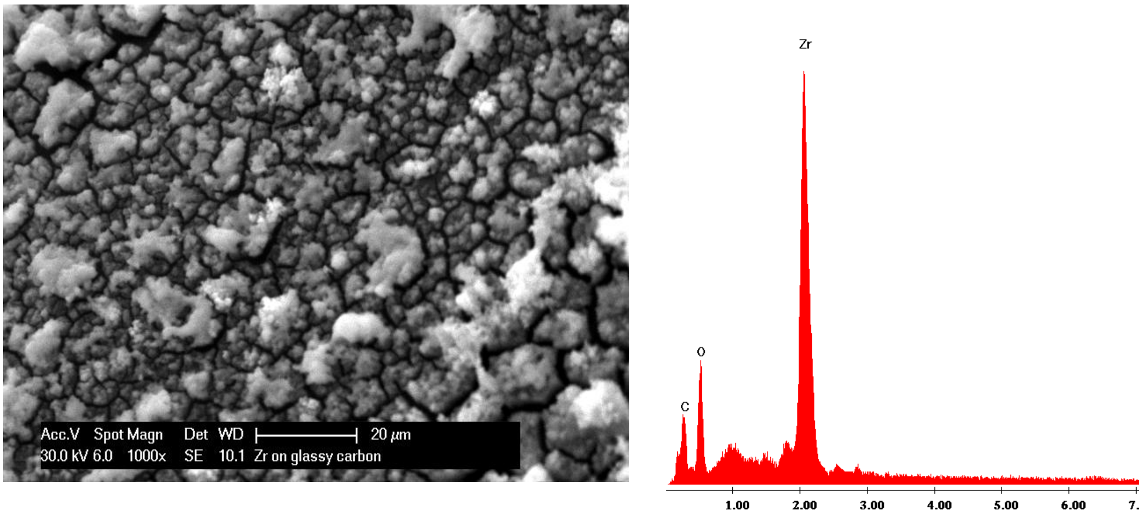

Figure 5.8: The SEM image and EDAX pattern of the zirconium deposit over the surface of glassy carbon working electrode.

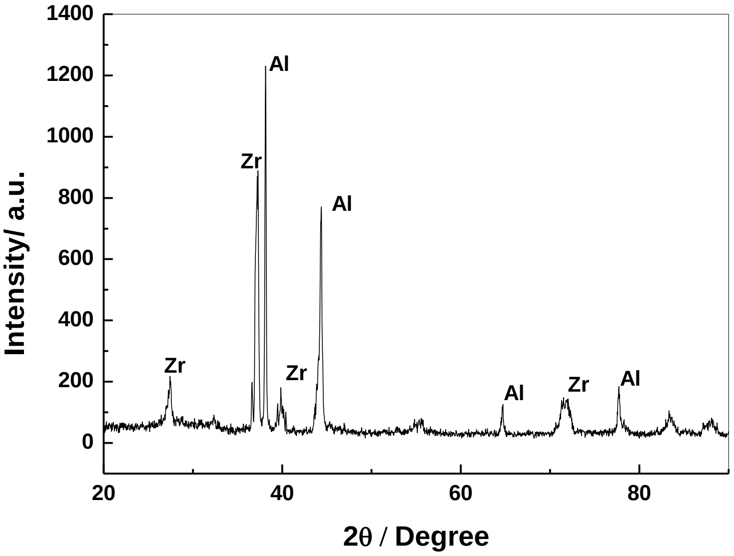

Figure 5.9: XRD pattern of the zirconium metal deposit.

5.1.1.5. Chronopotentiometry

Chronopotentiometry gives an idea about the transition state of the metal ion near to the working electrode. When a constant current is applied to the working electrode, concentration of the metal ions near the working electrode diminishes leading to a change in the potential of the working electrode. The duration over which the potential changes is known as the transition time (τ). Chronopotentiogram of zirconium (IV) chloride in $C_4mimNTf_2$ recorded at different applied currents are shown in figure 5.10. The chronopotential transient is characterized by a sudden drop from the rest potential followed by an increase in potential, at the start of chronopotentiogram. For instance, when the applied current is -0.825 mA the chronopotentiogram shows a drop from the rest potential to the value of -1.8 V (at t= 0.25 s) followed by an increase in the potential of the working electrode. The potential of the transient then remains constant for a few seconds, depending upon the initial applied current, followed by a decrease in potential. The occurrence of a minimum at $t \sim 0.2$ s followed by an increase in potential could be due attributed to the nucleation phenomenon. A similar feature was also reported [31] in the chronopoentiometry investigations on Pd(II) in C_4mimCl. A sudden drop from the rest potential to −1.8 V (at *t* = 0.2 s) could be attributed to the onset of the reduction of Zr(IV) to Zr(0) and the formation of the initial nuclei on the electrode. Once zirconium nuclei is formed over the surface of the working electrode, specific interaction between the zirconium metal and Zr(IV) ion in the IL occurs. Such a specific interaction results in an under potential deposition of zirconium over the nuclei. Therefore, the potential of the working electrode gets shifted to less negative values, as shown in the chronopotentiogram. Subsequently, the potential of the transient remains at a constant value over a few seconds, depending upon the magnitude of the applied current, as expected.

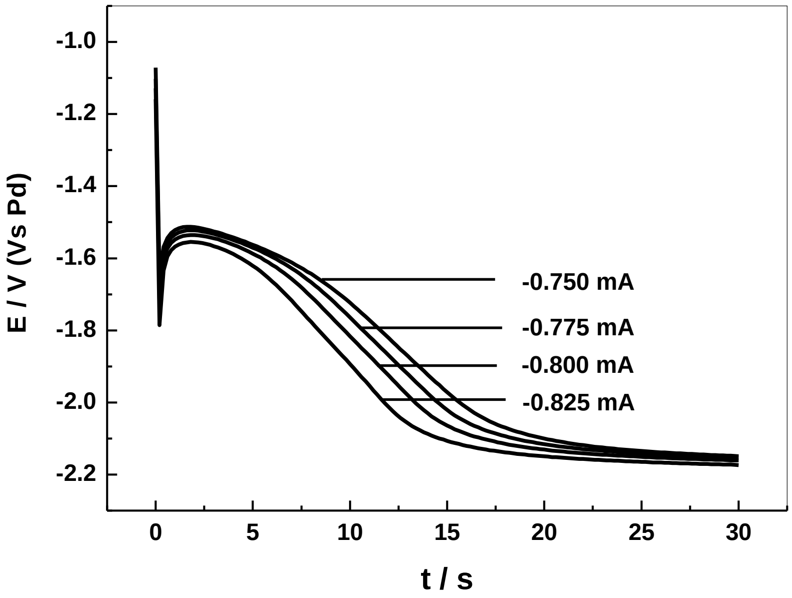

Figure 5.10: Comparison of cathodic chronopotential transients for 30mM Zr(IV) in C_4mimNTf$_2$ at different applied currents at 353 K. Working electrode: Glassy carbon (Cylindrical SA= 0.16 cm^2), counter electrode: glassy carbon (cylindrical SA= 0.25 cm^2), Quasi-reference electrode: Palladium wire (SA, 0.10 cm^2).

5.1.1.6. Measurement of open circuit potential

The open-circuit-potential (OCP) of Zr(IV) in $C_4mimNTf_2$ medium at a zirconium working electrode, against a Pd electrode was measured at different temperatures by immersing the former 30 mM Zr(IV) in $C_4mimNTf_2$. These potentials were measured in the temperature range 353 K to 383 K with an accuracy of ±0.001 V and are shown in figure 5.11. It is seen that the OCP values fall in the range -0.04 V to 0.07 V. It is also seen that the OCP decreases with an increase in temperature.

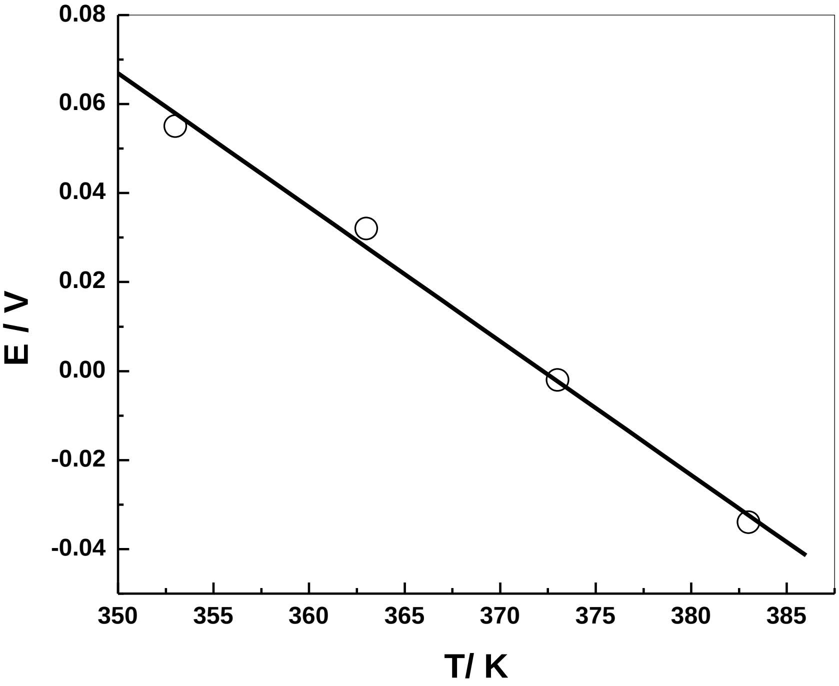

Figure 5.11: A plot of the open circuit potential against temperature. Working electrode: Zirconium rod (cylindrical)

5.1.2. Conclusions

The electrochemical behaviour of Zr(IV) in $C_4mimNTf_2$ was studied by CV, chronoamperometry and chronopotentiometry. The CV pertaining to Zr(IV) in $C_4mimNTf_2$ consisted of a couple of cathodic and anodic waves. A feable cathodic wave observed at the potential of +0.2 V (Vs Pd) was probably due to the reduction of Zr(IV) to Zr(II) and a prominent reduction wave observed at an onset potential of -1.3 V (Vs Pd) could be ascribed to the reduction of Zr(II) to Zr(0). The diffusion coefficient of Zr(IV) in $C_4mimNTf_2$ enumerated from the first cathodic wave was found to be 10^{-10} cm^2/s. However, a five order increase in the value of the diffusion coefficient (10^{-5} cm^2/s) was observed after the onset of nucleation at -1.6 V (Vs Pd). The nucleation loop observed at -1.6 V was studied in detail by chronoamperometry. Among the different models, the nucleation growth and decay of the chronocurrent transient could be best described with an instantaneous nucleation model. The nucleation phenomenon also influenced the nature of chronopotentiogram of Zr(IV) especially in the early part of the transient. This study revealed that Zr(IV) in $C_4mimNTf_2$ underwent a two-step two-electron transfer yeilding zirconium metal at the working electrode.

5.2. Anodic dissolution of uranium and zirconium metals and electrochemical behavior of U(IV) and Zr(IV) in ionic liquid medium for metallic fuel reprocessing

Literature pertaining to the reprocessing of metallic fuels by pyroelectrochemical methods salts indicate that extensive research have been carried out on the studies related to the electrochemical behavior of the metal ions viz., U(III), Pu(III) and Zr(IV) in KCl-LiCl medium [35-41]. In addition, some studies have been also reported on the combined electrochemical behavior of U(III)-Zr(IV) in high temperature molten salt medium [12, 42]. However, it is also borne out that only a few reports are available on the electrochemical behavior of both uranium(IV) as well as Zr(IV) in RTILs [26, 43, 44]. Earlier, Rao *et al.* [23] studied the voltammetric behavior of U(IV) in N-methyl-N-butylpiperidinium bis(trifluoromethanesulfonyl)imide ($MPPiNTf_2$). This method was in fact proposed for the treatment of oxide fuel (UO_2) followed by the recovery of uranium in its metallic form by electrodeposition. The rate of dissolution of UO_2 in $HNTf_2$ was studied and the resultant product $U(NTf_2)_4$ was dissolved in $MPPiNTf_2$ in order to study its voltammetric behavior. Similarly, the electrochemical behavior of Zr(IV) in 1-butyl-3-methylimdazolium bis(trifluoromethanesulfonyl)imide was studied and it has been reported that Zr(IV) underwent a two-step, two-electron transfer reaction at the GC working electrode [45]. However, no studies have so far been reported on the electrochemical behavior of U(IV) and Zr(IV) together in an IL.

In view of the above, in the present study the electrochemical behavior of U(IV) and Zr(IV) in N-butyl-N-mehylpyrrolidinium bis(trifluoromethanesulfonyl)imide ($C_4MPyNTf_2$) IL was investigated. U(IV) and Zr(IV) were introduced into $C_4MPyNTf_2$ IL by anodic dissolution, quite similar to their dissolution in high temperature molten salts in the electrorefining method. The electrochemical behavior of U(IV) and Zr(IV) in $C_4MPyNTf_2$ was then studied by CV and chronoamperometry. To understand the electrochemistry of U(IV) in $C_4MPyNTf_2$, C_4MPyCl was added to the electrolytic medium to convert the free U(IV) ions present in the $C_4MPyNTf_2$ into $[UCl_6]^{2-}$. The results obtained from these studies are discussed in this chapter.

Syntheses of ILs (C_4MPyCl & $C_4MPyNTf_2$) have been discussed in section 2.5.3 & 2.5.4 and the experimental procedure employed in voltammetric measurments, anodic dissolution and preparation of samples for spectroscopic characterisation have been mentioned in section 2.4.6.

5.2.1. Results and discussion

5.2.1.1. Voltammetric and spectroscopic studies

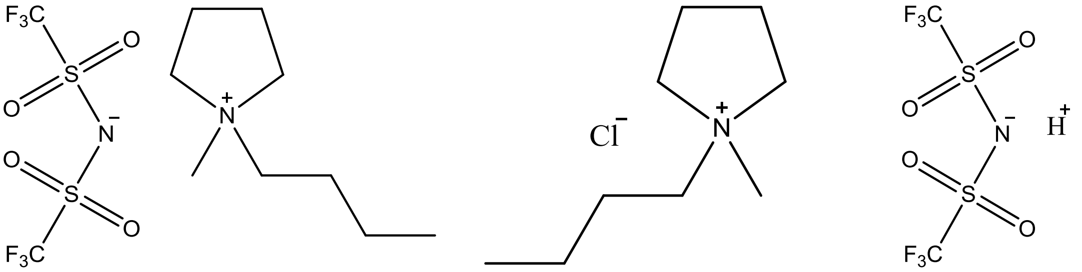

1-Butyl-1-methylpyrrolidinium bis(trifluoromethanesulfonyl)imide

1-Butyl-1-methyl pyrrolidinium chloride

Bis(trifluoromethanesulfonyl)imide acid

Figure 5.12: Structures of the ILs used in the present work.

Alkyl piperidinium and pyrrolidinium cations in combination with bis(trifluoromethylsulfonyl)imide anion were reported to have an electrochemical window more than 5 V with extended cathodic and anodic stability [17, 46, 47]. The CV pertaining to N-butyl-N-methylpyrrolidinium bis(trifluoromethylsulfonyl)imide ($C_4MPyNTf_2$), shown in figure 5.13, indicates that the latter offers an electrochemical window of 5.5 V with an extended cathodic and anodic stability upto -3.5 V and 2.7 V, respectively. This result indicates that it is quite possible to oxidise and dissolve the spent U-Pu-Zr alloys in $C_4MPyNTf_2$ and electrodeposit the actinides from that IL medium.

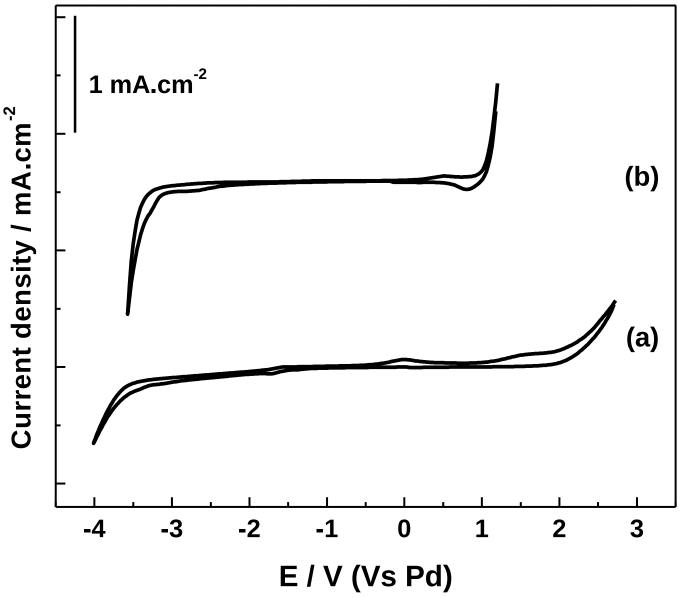

Figure 5.13: Cyclic voltammogram of (a) $C_4MPyNTf_2$ alone at 373 K and (b) C_4MPyCl in $C_4MPyNTf_2$ at 373 K at a glassy carbon working electrode at scan rate of 50 mV/s.

Since the first step in the high temperature electrorefining involves the anodic oxidation of spent nuclear fuel in LiCl-KCl eutectic, the oxidative dissolution behaviour of uranium and zirconium was studied in $C_4MPyNTf_2$. Metallic uranium or zirconium was used as the working electrode in those experiments, and the anodic linear sweep voltammogram was recorded from OCP to understand the oxidation behaviour of the working electrode. The voltammogram was recorded upto 2.5 V and 2.0 V when uranium and zirconium were used as the working electrodes, respectively. These results show that the anodic current obtained was negligible when the anodic potential was less than 1.5 V, indicating that the dissolution of uranium and zirconium in $C_4MPyNTf_2$ iss not favoured.

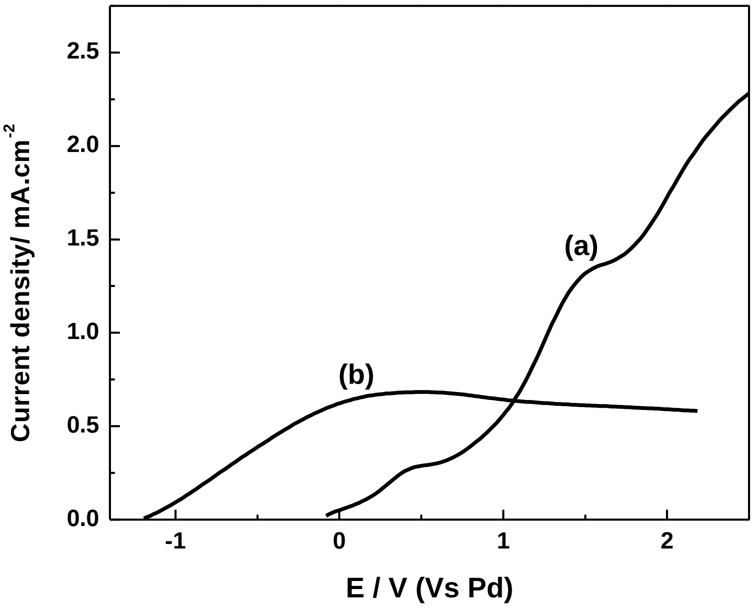

Figure 5.14: Linear sweep voltammogram pertaining to the anodic dissolution of (a) uranium and (b) zirconium, in the presence of 0.35 M of $HNTf_2$ recorded at a scan rate of 50 mV/s at 343 K. Electrolytic medium : $C_4MPyNTf_2$, Working electrode : U or Zr; Counter electrode : glassy carbon; Reference electrode : Pd.

In order to facilitate the dissolution of U and Zr in $C_4MPyNTf_2$, bis(trifluoromethylsulfonyl)imide acid ($HNTf_2$) was added to $C_4MPyNTf_2$ and the anodic linear sweep voltammogram was recorded from OCP. These results are shown in figure 5.14. It is seen that the anodic current increases with the anodic potential, in both the cases. The anodic peak observed at 1.5 V (Vs Pd) in the case of uranium and 0.5 V (Vs Pd) in the case of zirconium, corresponds to the oxidation of the respective metal working electrodes. The oxidation of these metallic electrodes subsequently leads to the dissolution of U and Zr in the IL. In order to dissolve a significant quantity of uranium in $C_4MPyNTf_2$ for carrying out the voltammetric studies, the anodic potential was kept at 1.5 V for about 2 h.

The uranium dissolved in $C_4MPyNTf_2$ was measured by determining its concentration in a known aliquot of $C_4MPyNTf_2$. This aliquot was initially treated with an excess of perchloric acid to destroy the organics, and the uranium concentration present in aqueous phase was then determined by ICP-AES. From the assay of uranium and the number of coulombs passed through the solution, the current efficiency of uranium dissolution in $C_4MPyNTf_2$ was determined to be 80 to 85%. Similarly, the current efficiency of zirconium dissolution at 0.5 V was determined to be 80 to 85%. The reduction in current efficiency to the tune of ~20% could be ascribed to the oxidation residual moisture present in the RTIL despite of the rigorous drying of the latter for more than 24 h in a rotary evaporator at 343 K. In addition, the impurities, if any, present in the IL also are susceptible to oxidation under the experimental condition, that would also consume current. The concentration of U(IV) and Zr(IV) in $C_4MPyNTf_2$ was determined to be ~ 80 mM.

The visible absorption spectrum of U(IV) in $C_4MPyNTf_2$ is shown in figure 5.15. The spectrum shows broad absorption bands at 425 nm, 475 nm and 540 nm. A strong absorption band and a shoulder are observed at 645 nm [48]. These absorption bands are characteristic of tetravalent uranium in $C_4MPyNTf_2$. The electronic transitions responsible for these absorption bands are shown in figure 5.15, as cited in earlier reports [49-52]. It should be noted that the spectrum (figure 5.15a) matches well with the absorption spectrum of U(IV) in perchlorate medium, reported elsewhere [48]. The latter is a weakly co-ordinating non-complexing anion. Since, NTf_2^- is also a weakly co-ordinating anion, similar to perchlorate [53-55], owing to the big size and delocalisation of negative charge over sulphonyl groups in the latter, it is quite likely that U(IV) in $C_4MPyNTf_2$ would also exists predominantly as free ion, similar to its existence in the perchlorate medium.

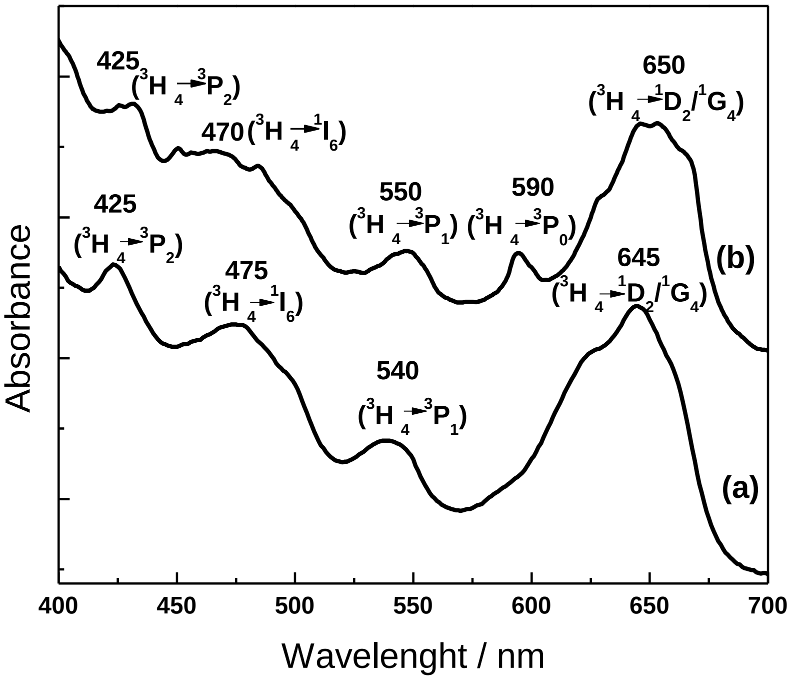

Figure 5.15: (a) Visible absorption spectrum of U(IV) (80 mM) obtained with a solution obtained by anodically dissolving U metal in $C_4MPyNTf_2$. This solution was dried at 353 K under vacuum in a rotary evaporator. (b) Visible absorption of spectrum solution of U(IV) in $C_4MPyNTf_2$ in the presence of C_4MPyCl at a U : Cl ratio of 1 : 6.

The cyclic voltammogram of U(IV) in $C_4MPyNTf_2$ recorded at a glassy carbon working electrode at a scan rate of 50 mV/s at 343 K is shown in figure 5.16(a). The voltammogram was recorded from an OCP of -0.05 V onwards and was switched at a cathodic potential of -3.7 V. The voltammogram was reversed again at the anodic potential of 2.3 V. The voltammogram recorded at 343 K shows a weak cathodic wave (E_p^{c1}) at -1.2 V. A surge in the cathodic current is observed at -2.2 V, resulting in a cathodic wave at -2.8 V (E_p^{c2}). This is followed by another wave at -3.3 V (E_p^{c3}). The corresponding anodic peaks are observed at -3.0 V (E_p^{a3}), -2.5 V (E_p^{a2}) and 0.7 V (E_p^{a1}) respectively for E_p^{c3}, E_p^{c2} and E_p^{c1}. In order to increase the cathodic and anodic currents and to obtain more clarity, the cyclic voltammogram recorded at 373 K and the same is also shown in the figure 5.16(b).

The current density pertaining to all the cathodic waves increased at 373 K, and interestingly the cathodic wave at E_p^{c1} is not observed in the voltammogram. Instead a couple of cathodic waves, E_p^{c4} and E_p^{c5} are observed at -0.5 V and -0.8 V. Since these cathodic waves are very close to each other and they are very weak, it is difficult to characterise the electrochemical reaction pertaining to E_p^{c4} and E_p^{c5}. The current density of other two cathodic waves (E_p^{c6} and E_p^{c7}) at -2.8 V and -3.2 V increased considerably at 373 K. The cathodic waves occurring at E_p^{c1}, E_p^{c2}, E_p^{c4}, E_p^{c5} and E_p^{c6} could be ascribed to the reduction of U(IV) to U(III) and the cathodic waves E_p^{c3} and E_p^{c7} could be due to the reduction of U(III) to U(0) [37, 23]. The details of these assignments are discussed below.

In order to understand the nature of U(IV) reduction happening at -3.0 V in $C_4MPyNTf_2$, C_4MPyCl was added to $C_4MPyNTf_2$ to facilitate the conversion of U(IV) free ion present in $C_4MPyNTf_2$ into the uranium chloro complexes of the form, $[UCl_6]^{2-}$. The redox behaviour of $[UCl_6]^{2-}$ in the IL as well as in high temperature molten salt medium have been well-documented [35-37]. Therefore, by comparing the U(IV) redox behaviour obtained in presence of C_4MPyCl in $C_4MPyNTf_2$ with those reported in the literature, it is possible to characterise the cathodic wave observed at -3.0 V. In view of this, C_4MPyCl was added to a solution of U(IV) in $C_4MPyNTf_2$ at a mole ratio of U(IV) to Cl as 1 : 6. The visible absorption spectrum of U(IV) solution obtained after the addition of C_4MPyCl is shown in figure 5.15. It is seen that the absorption spectrum obtained in the presence of C_4MPyCl is significantly different from the visible absorption spectrum of U(IV) in $C_4MPyNTf_2$. Moreover the absorption spectrum resembles the visible absorption spectrum of U(IV) reported in Cl^- medium such as those in high temperature LiCl-KCl molten salts [56, 57] and Cl^- based ILs [43].

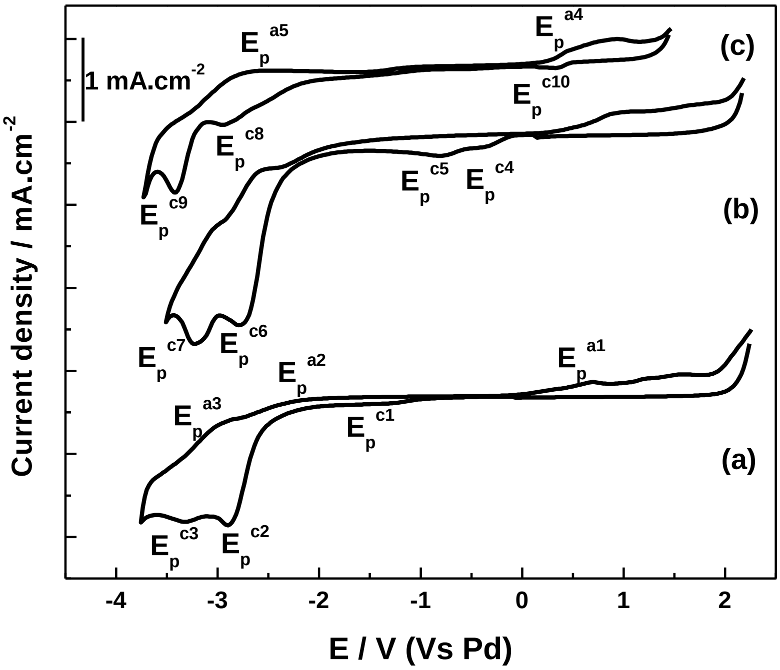

Figure 5.16: CV of 80 mM U(IV) recorded at glassy carbon in absence of C_4MPyCl at (a) 343 K, (b) 373 K. (c) The cyclic voltammogram of 80 mM U(IV) recorded in the presence of C_4MPyCl in the ratio of 1 : 6 at 373 K. The IL used in all these cases was $C_4MPyNTf_2$. Scan rate, 50mV/s.

Nikitenko *et al.* [43] studied the visible absorption spectra of U(IV) in Cl^- medium and reported that $[UCl_6]^{2-}$ exhibits a characteristic absorption band at 590 nm. In addition, these authors also observed the absorption bands at 425 nm, 470 nm, 550 nm and 650 nm with fine splitting structure for $[UCl_6]^{2-}$. It is seen from figure 5.15 that all these bands are present in the absorption spectrum of U(IV) obtained in the presence of C_4MPyCl in $C_4MPyNTf_2$. Therefore, it reasonable conclude that U(IV) in $C_4MPyNTf_2$ medium in the presence of C_4MPyCl exists predominantly in the form of $[UCl_6]^{2-}$. The electronic transitions responsible for these bands are indicated in the figure 5.15 [49-52].

The CV pertaining to U(IV) in $C_4MPyNTf_2$ recorded in the presence of C_4MPyCl (U : Cl = 1 : 6 mole ratio) at a glassy carbon electrode is shown in figure 5.16(c). The voltammogram was recorded from an OCP of -0.2 V. From the results is shown in figure 5.13, it is seen that the electrochemical window of neat $C_4MPyNTf_2$ in the presence of C_4MPyCl gets reduced on the anodic side owing to evolution of Cl_2 at 0.8 V. From figure 5.16(a), it is seen that the onset of a cathodic wave occurs at the potential of -1.0 V resulting in a cathodic peak (E_p^{c8}) at -3.0 V. This is followed by another cathodic peak at -3.4 V. After the scan reversal, a prominent anodic wave (E_p^{a4}) was observed at 1.0 V. When the scan was reversed again at the anodic potential of 1.5 V, a weak cathodic wave (E_p^{c10}) was observed at 0.5 V before reaching the OCP value. The redox couple (E_p^{a4} and E_p^{c10}) observed at 0.9 V could be due to the redox reaction involving U(IV) and U(V). The same redox couple (E_p^{a4} and E_p^{c10}) was also observed when the cyclic scan was done anodically from the OCP of -0.2 V. This confirms that U(IV) present in the IL is oxidised to U(V) at E_p^{a4}. A similar behaviour was also reported by Nikitenko *et al.* [43]. It is interesting to note that the cathodic current observed at E_p^{c6} in the absence of C_4MPyCl, is reduced to a small cathodic wave at E_p^{c8} in the presence of C_4MPyCl. Nikitenko *et al.* [43] proposed that the first cathodic wave in Cl^- medium was due to the reduction of U(IV) to U(III) and the second cathodic wave was due to U(III) to U reduction. Since the CV observed in the present study in the presence of Cl^- is similar to those reported by Nikitenko *et al.* [43], it is reasonable to assume that the cathodic wave observed at E_p^{c9} in the presence of Cl^- ion as well as E_p^{c7} observed in the absence of Cl^- ion could be due to the deposition of metallic uranium at the glassy carbon working electrode. In view of the above, the cathodic wave observed at E_p^{c6} could be assigned to the reduction of $U(IV)(NTf_2)_x$ to $U(III)(NTf_2)_x$ complex, and the other cathodic waves observed at E_p^{c1}, E_p^{c4} and E_p^{c5} could be assigned to the reduction reactions involving structural changes with respect to the NTf_2^- anion in the $U(IV)(NTf_2)_x$ complex, as discussed in reference [58].

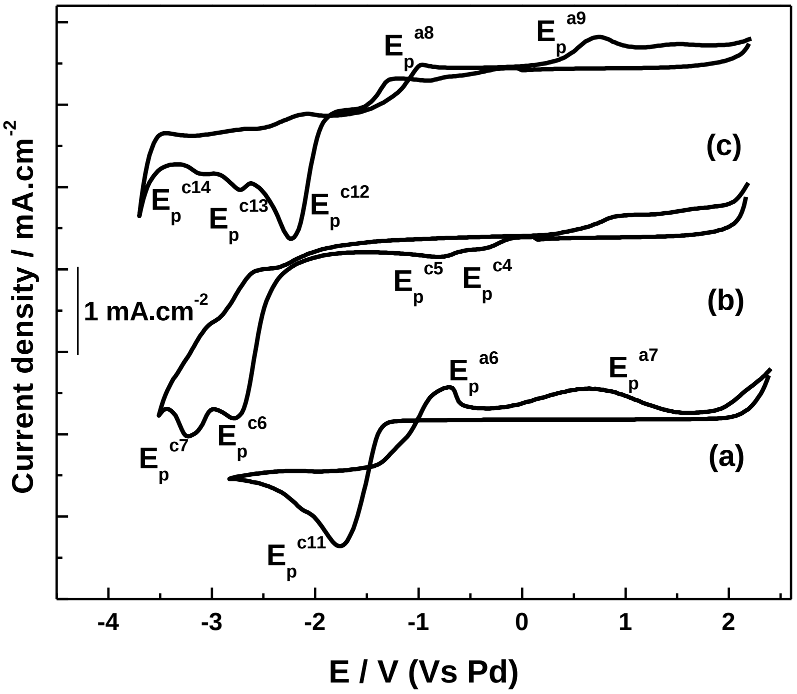

Figure 5.17: CV pertaining to (a) neat 50 mM Zr(IV), (b) 80 mM U(IV) recorded at glassy carbon electrode at 373 K. (c) The CV of a solution containing 40 mM U(IV)- 45 mM Zr(IV) recorded at a glassy carbon at 373 K. The IL used in all these cases was $C_4MPyNTf_2$. Scan rate, 50mV/s.

The metallic fuel is as an alloying addition zirconium [1-2]. During electrorefining it is quite likely that zirconium could also undergo partial dissolution in the IL, as evidented by the linear sweep voltammogram (figure 5.14). The cyclic voltammogram of zirconium(IV) in $C_4MPyNTf_2$ recorded at a scan rate of 50 mV/s at a glassy carbon electrode at 373 K is shown in figure 5.17. This voltammogram is compared with that pertaining to U(IV) obtained in the absence of Cl^- ion under identical conditions. The Zr(IV) voltammogram shows the onset of reduction current at -1.5 V culminating in a cathodic peak (E_p^{c11}) at -1.8 V. A nucleation loop is observed at -1.6 V upon scan reversal at -2.8 V. In addition, a couple of anodic waves E_p^{a6} and E_p^{a7} are observed at -0.7 V and 0.6 V respectively. The cathodic peak observed at E_p^{c11} is due to the direct reduction of

Zr(IV) to Zr. However, the oxidation of Zr from the working electrode seems to involve two steps, probably Zr to Zr(II) and Zr(II) to Zr(IV) at E_p^{a6} and E_p^{a7} respectively. A similar behaviour have also been reported for the reduction of Zr(IV) in other ILs [26]. Previously, we also studied [45] the electrochemical behaviour of Zr(IV) in 1-butyl-3-methyl imidazolium bis(trifluoromethylsulfonyl)imide ($C_4mimNTf_2$) IL. It was reported that the reduction of Zr(IV) involves a two-step reduction reaction in which Zr(IV) was reduced to Zr(II) which was then followed by the reduction of Zr(II) to Zr [45]. The direct reduction of Zr(IV) to Zr observed in the present IL, as compared to the two-step reduction observed in $C_4mimNTf_2$ [26, 45], shows that depending upon the nature of the cation associated with the IL the reduction behaviour of Zr could be different.

Comparing the voltammogram of Zr(IV) and U(IV) in $C_4MPyNTf_2$ medium shown in figure 5.17, it is evident that the deposition of uranium at the working electrode occurs at a more negative potential (by 1.5 V) as compared to that of zirconium deposition. This indicates that uranium could be deposited without the interference of zirconium, if zirconium is not present in the IL. However, in reality, it is quite likely that significant amounts of zirconium also get dissolved along with uranium during the anodic dissolution of uranium-zirconium alloy in the IL. Under such a condition it is necessary to study the electrochemical behaviour of both U(IV) and Zr(IV) present in $C_4MPyNTf_2$. The CV pertaing to a solution of U(IV) (40 mM) and Zr(IV) (45 mM) in $C_4MPyNTf_2$ recorded at a glassy carbon working electrode at a scan rate of 50 mV/s at 373 K is shown in figure 5.17. It is seen that the cathodic wave occurring at a potential (E_p^{c12}) of -2.2 V is due to the deposition of Zr and the cathodic wave at E_p^{c14} is due to uranium deposition (U(III) to U) and E_p^{c13} is due to the reduction U(IV) to U(III). The anodic waves E_p^{a8} and E_p^{a9} correspond to the two-step oxidation of zirconium to zirconium (IV) similar to E_p^{a6}

and E_p^{a7}. Nucleation is observed in this case as well. Therefore, this study shows that it is necessary to electrodeposit zirconium from IL, before recovering uranium.

5.2.2. Conclusions

The electrochemical behaviour of U(IV) and Zr(IV) was studied in $C_4MPyNTf_2$ to understand the feasibility of using $C_4MPyNTf_2$ for electrorefining application of spent metallic fuels. The anodic dissolution of metallic U and Zr was insignificant in $C_4MPyNTf_2$. However, the dissolution was facilitated by adding $HNTf_2$. Dissolution of U and Zr results in the formation of $U(NTf_2)_4$ and $Zr(NTf_2)_4$ complexes in $C_4MPyNTf_2$. Since NTf_2^- is a weakly co-ordinating anion, the electrochemical behaviour of U(IV) at a glassy carbon working electrode was a bit complex. However, the reduction of U(IV) to metallic form occurred at -3.2 V, possibly through the reduction of U(IV) to U(III) at still lower cathodic potentials. The reduction of zirconium occurs at -1.5 V, which was about 1.7 V more anodic as compared to the potential at which uranium could be deposited. This shows that zirconium needs to be removed from $C_4MPyNTf_2$ medium prior to the recovery of uranium and the same could be accomplished easily. Nevertheless, this study also showed that RTILs such as $C_4MPyNTf_2$ are promising candidates for the electrodeposition of uranium and electrorefining of metallic fuels. However, more studies, viz., investigations at higher concentrations of U(IV), studies in the presence of fission products, radiation stability etc., are necessary in order to evaluate the suitability of ILs for spent metallic fuel reprocessing applications.

References

1. B. Raj, Plutonium and the Indian atomic energy programme, J. Nucl. Mater. 385 (2009) 142-147.
2. J. Banerjee, E. R. Prakasan, T. R. G. Kutty, K. Bhanumurthy, Trends of publications and patents on metallic fuel development for fast reactors, Curr. Sci. 110 (2016) 36.
3. W. J. Carmack, D. L. Porter, Y. I. Chang, S. L. Hayes, M. K. Meyer, D. E. Burkes, C. B. Lee, T. Mizuno, F. Delage, J. Somers, Metallic fuels for advanced reactors, J. Nucl. Mater. 392 (2009) 139-150.
4. G. L. Hofman, L. C. Walters, T. H. Bauer, Metallic fast reactor fuels, Prog. Nucl. Energy 31 (1997) 83-110.
5. Y. I. Chang, Technical rationale for metal fuel in fast reactors, Nucl. Eng. Technol. 39 (2007) 161-170.
6. J.P. Ackerman, Chemical basis for pyrochemical reprocessing of nuclear fuel, Ind. Eng. Chem. Res. 30 (1991) 141–145.
7. T. Inoue, L. Koch, Development of pyroprocessing and its future direction, Nucl. Eng. Technol. 40 (2008) 183–195.
8. C.C. Mcpheeters, R.D. Pierce, T.P. Mulcahey, Application of the pyrochemical process to recycle of actinides from LWR spent fuel, Prog. Nucl. Energy 31 (1997) 175–186.
9. T. Koyama, K. Kensuke, T. Inoue, M. Ougier, R. Malmbeck, J.P. Glatz, L. Koch, Study of molten salt electrorefining of U–Pu–Zr alloy fuel, Proceedings of Actinide 2001: International Conference, November 4-9, 2001 (Hayama, Japan.).
10. I. Johnson, The thermodynamics of pyrochemical processes for liquid metal reactor fuel cycles, J. Nucl. Mater. 154 (1988) 169–180.

11. M.W. Chase Jr. (Ed.), NIST-JANAF Thermochemical Tables, third ed., Part 1, Am. Chem. Soc., New York, 1985.
12. T. Murakami, T. Kato, M. Kurata, H. Yamana, Electrochemical formation of uranium–zirconium alloy in LiCl–KCl melts, J. Nucl. Mater. 394 (2009) 131–135.
13. R.D. Rogers, K.R. Seddon, Ionic liquids: solvents of the future, Science 302 (2003) 792–793.
14. N.V. Plechkova, K.R. Seddon, Applications of ionic liquids in the chemical industry, Chem. Soc. Rev. 37 (2008) 123–150.
15. K.A. Venkatesan, M. Jayakumar, T.G. Srinivasan, P.R. VasudevaRao, Electrolysis: theory, types and applications, in: S. Kuai, JiMeng (Eds.), Novel Electrochemical Approaches for the Recovery of Fission Platinoids Using Room Temperature Ionic Liquids, Nova Science Publishers 2008, pp. 405–428.
16. M. Armand, F. Endres, D.R. MacFarlane, H. Ohno, B. Scrosati, Ionic-liquid materials for the electrochemical challenges of the future, Nat. Mater. 8 (2009) 621–629.
17. C.J. Rao, K.A. Venkatesan, K. Nagarajan, T.G. Srinivasan, P.R. Vasudeva Rao, Electrochemical behavior of europium(III) in N-butyl-N-methylpyrrolidinium bis(trifluoromethylsulfonyl)imide, Electrochim. Acta 54 (2009) 4718–4725.
18. P. Giridhar, S. Zein El Abedin, A. Bund, A. Ispas, F. Endres, Electrodeposition of niobium from 1-butyl-1-methylpyrrolidinium bis(trifluoromethylsulfonyl)amide ionic liquid, Electrochim. Acta 129 (2014) 312–317.
19. N. Borisenko, A. Ispas, E. Zschippang, Q. Liu, S.Z. El Abedin, A. Bund, F. Endres, In situ STM and EQCM studies of tantalum electrodeposition from TaF_5 in the air- and water-stable ionic liquid 1-butyl-1-methylpyrrolidinium bis(trifluoromethylsulfonyl) amide, Electrochim. Acta 54 (2009) 1519–1528.

20. M. Mascia, A. Vacca, L. Mais, S. Palmas, E. Musu, F. Delogu, Electrochemical deposition of Cu and Nb from pyrrolidinium based ionic liquid, Thin Solid Films 571 (2014) 325–331.

21. S.M. Jeong, H.S. Shin, S.S. Hong, J.M. Hur, J.B. Do, H.S. Lee, Electrochemical reduction behavior of U_3O_8 powder in a LiCl molten salt, Electrochim. Acta 55 (2010) 1749–1755.

22. R. Ahluwalia, T.Q. Hua, H.K. Geyer, Behavior of uranium and zirconium in direct transport tests with irradiated EBR-II fuel, Nucl. Technol. 126 (1999) 289–302.

23. C. JagadeeswaraRao, K.A. Venkatesan, K. Nagarajan, T.G. Srinivasan, P.R. Vasudevarao, Electrodeposition of metallic uranium at near ambient conditions from room temperature ionic liquid, J. Nucl. Mater. 408 (2011) 25–29.

24. T. Tsuda, C.L. Hussey, G.R. Stafford, O. Kongstein, Electrodeposition of Al–Zr alloys from Lewis acidic aluminum chloride-1-ethyl-3-methylimidazolium chloride melt, J. Electrochem. Soc. 151 (2004) C447–C454.

25. C. Fu, L. Aldous, N.S.A. Manan, R.G. Compton, Electrochemistry of zirconium tetrachloride in N-butyl-N-methyl pyrrolidium bis (trifluoromethylsulfonyl) imide : formation of Zr(III) and exploitation of $ZrCl_4$ as a facile ionic liquid drying agent, Electroanalysis 24 (2012) 210–213.

26. A. Vacca, M. Mascia, L. Mais, F. Delogu, S. Palmas, A. Pinna, Electrodeposition of zirconium from 1-butyl-1-methylpyrrolidinium bis(trifluoromethylsulfonyl)imide: electrochemical behavior and reduction pathway, Mater. Manuf. Process. 31 (2016) 74–80.

27. Z. Chen, Y.J. Li, S.J. Li, Electrochemical behavior of zirconium in the LiCl–KCl molten salt at Mo electrode, J. Alloys Compd. 509 (2011) 5958–5961.

28. A.J. Bard, L.R. Faulkner, Electrochemical Methods-Fundamentals and Applications, Wiley, New York, 1980.

29. P. Kissinger, W.R. Heineman (Eds.), Laboratory Techniques in Electroanalytical Chemistry, Revised and Expanded, CRC press, 1996.

30. K. Aoki, K. Tokuda, H. Matsuda, Theory of linear sweep voltammetry with finite diffusion space, J. Electroanal. Chem. Interfacial Electrochem. 146 (1983) 417–424.

31. M. Jayakumar, K.A. Venkatesan, T.G. Srinivasan, Electrochemical behavior of fission palladium in 1-butyl-3-methylimidazolium chloride, Electrochim. Acta 52 (2007) 7121–7127.

32. X. Luo, R. Li, L. Huang, T. Zhang, Nucleation and growth of nanoporous copper ligaments during electrochemical dealloying of Mg-based metallic glasses, Corros. Sci. 28 (2013) 100–108.

33. A. Mashreghi, H. Zare, Investigation of nucleation and growth mechanism during electrochemical deposition of nickel on fluorine doped tin oxide substrate, Curr. Appl. Phys. 16 (2016) 599–604.

34. B. Scharifker, G. Hills, Theoretical and experimental studies of multiple nucleations, Electrochim. Acta 28 (1983) 879–881.

35. S.A. Kuznetsov, M. Gaune-Escard, Electrochemical transient techniques for study of the electrochemistry and thermodynamics of nuclear materials in molten salts, J. Nucl. Mater. 389 (2009) 108-114.

36. Y. Sakamura, T. Hijikata, K. Kinoshita, T. Inoue, T.S. Storvick, C.L. Krueger, J.J. Roy, D.L. Grimmett, S.P. Fusselman, R.L. Gay, Measurement of standard potentials of actinides (U, Np, Pu, Am) in LiCl–KCl eutectic salt and separation of actinides from rare earths by electrorefining, J. Alloys Comp. 271 (1998) 592.

37. O. Shirai, T. Iwai, Y. Suzuki, Y. Sakamura, H. Tanaka, Electrochemical behavior of actinide ions in LiCl–KCl eutectic melts, J. Alloys comp. 271 (1998) 685-688.

38. J. Serp, R.J.M. Konings, R. Malmbeck, J. Rebizant, C. Scheppler, J.P. Glatz, Electrochemical behaviour of plutonium ion in LiCl–KCl eutectic melts, J. Electroanal. Chem. 561 (2004) 143.

39. H. Groult, A. Barhoun, H. El Ghallali, S. Borensztjan, F. Lantelme, Study of the electrochemical reduction of Zr^{4+} ions in molten alkali fluorides, J. Electrochem. Soc. 155 (2008) E19-E25.

40. T. Grechina, V. Barchuk, I. Sheiko, Cathodic polarization of molybdenum in the molten mixture of lithium-, potassium-, zirconium chlorides, Ukr. Khim. Zh. 39 (1973) 501-503.

41. M.V. Smirnov, A.N. Baraboshkin, V.E. Komarov, Cathodic processes in the deposition of zirconium from chloride melts, J. Chem. Phys. 37 (1963) 1669.

42. S. Ghosh, S. Vandarkuzhali, N. Gogoi, P. Venkatesh, G. Seenivasan, B. P. Reddy, K. Nagarajan, Anodic dissolution of U, Zr and U–Zr alloy and convolution voltammetry of $Zr^{4+}| Zr^{2+}$ couple in molten LiCl–KCl eutectic, Electrochim. Acta 56 (2011) 8204-8218.

43. S.I. Nikitenko, C. Cannes, C. Le Naour, P. Moisy, D. Trubert, Spectroscopic and Electrochemical Studies of U(IV)−Hexachloro Complexes in Hydrophobic Room-Temperature Ionic Liquids [BuMeIm][Tf_2N] and [$MeBu_3N$][Tf_2N], Inorg. Chem. 44 (2005) 9497-9505.

44. P.B. Hitchcock, T. J. Mohammed, K.R. Seddon, J.A. Zora, C.L. Hussey, E.H. Ward, Inorg. Chim. Acta 113 (1986) L25.

45. G.M. Krishna, A.S. Suneesh, K.A. Venkatesan, M.P. Antony, Electrochemical behavior of zirconium(IV) in 1-butyl-3-methylimidazolium

bis(trifluoromethylsulfonyl) imide ionic liquid, J. Electroanal. Chem. 776 (2016) 120-126.

46. G.B. Appetecchi, M. Montanino, D. Zane, M. Carewska, F. Alessandrini, S. Passerini, Effect of the alkyl group on the synthesis and the electrochemical properties of N-alkyl-N-methyl-pyrrolidinium bis(trifluoromethanesulfonyl) imide ionic liquids, Electrochim. Acta 54 (2009) 1325-1332.
47. Q. Zhou, W.A. Henderson, G.B. Appetecchi, M. Montanino, S. Passerini, Physical and electrochemical properties of N-alkyl-N-methylpyrrolidinium bis (fluorosulfonyl) imide ionic liquids: $PY_{1,3}FSI$ and $PY_{1,4}FSI$, J. Phys. Chem. B 112 (2008) 13577-13580.
48. A. Ikeda-Ohno, C. Hennig, S. Tsushima, A.C. Scheinost, G. Bernhard, T. Yaita, Speciation and structural study of U(IV) and (VI) in perchloric and nitric acid solutions, Inorg. Chem. 48 (2009) 7201-7210.
49. J.G. Conway, Absorption Spectrum of UF_4 and the Energy Levels of Uranium V, J. Chem. Phys. 31 (1959) 1002-1004.
50. D. Cohen, W.T. Carnall, Absorption spectra of uranium(III) and uranium(IV) in $DClO_4$ solution1, J. Phys. Chem. 64 (1960) 1933-1936.
51. W.T. Carnall, G.K. Liu, C.W. Williams, M.F. Reid, Analysis of the crystal-field spectra of the actinide tetrafluorides. I. UF_4, NpF_4, and PuF_4, J. Chem. Phys. 95 (1991) 7194-7203.
52. E. Hashem, A.N. Swinburne, C. Schulzke, R.C. Evans, J.A. Platts, A. Kerridge, L.S. Natrajan, R.J. Bake, Emission spectroscopy of uranium(IV) compounds: a combined synthetic, spectroscopic and computational study, RSC Adv. 3 (2013) 4350-4361.

53. C. Gaillard, A. Chaumont, I. Billard, C. Hennig, A. Ouadi, G. Wipff, Uranyl coordination in ionic liquids: the competition between ionic liquid anions, uranyl counterions, and Cl-anions investigated by extended X-ray absorption fine structure and UV−Visible spectroscopies and molecular dynamics simulations, Inorg. Chem. 46 (2007) 4815-4826.
54. M. Gal, P.L. Goggin, J. Mink, Vibrational spectroscopic studies of uranyl complexes in aqueous and non-aqueous solutions, Spectrochim. Acta A 48 (1992) 121-132.
55. P. Nockemann, K. Servaes, R. Van Deun, K. Van Hecke, L. Van Meervelt, K. Binnemans, C. Gorller-Walrand, Speciation of uranyl complexes in ionic liquids by optical spectroscopy, Inorg. Chem. 46 (2007) 11335-11344.
56. L. Heerman, R. De Waele, W. D’olieslager, Electrochemistry and spectroscopy of uranium in basic $AlCl_3$ + N-(n-butyl)pyridinium chloride room temperature molten salts, J. Electroanal. Chem. Interfacial Electrochem. 193 (1985) 289-294.
57. R. De Waele, L. Heerman, W. D’olieslager, Potentiometric and spectroscopic study of uranium(IV)-uranium(III) in acidic $AlCl_3$-N-(n-Butyl)pyridinium chloride melts, Journal of the Less Common Metals 122 (1986) 319-327.
58. A.I. Bhatt, H. Kinoshita, A.L. Koster, I. May, C.A. Sharrad, V.A. Volkovich, O.D. Fox, C.J. Jones, B.G. Lewin, J.M. Charnock, C. Hennig, Actinide, lanthanide, and fission product speciation and electrochemistry in ionic melts, ACS Symposium Series 933 (2006) 219-231.

Chapter 6 : Electrochemical behavior of lanthanides in ionic liquid medium in presence of organic ligand

Introduction

Lanthanides are one of the major fission products produced in a nuclear fission reaction. In general, the availability of lanthanides from sources (earth crust) is very less, so the recovery of these rare earth elements became more necessary for future use. A large number of reports are also available in the literature detailing the role of ILs in the recovery of actinides and lanthanides from the spent nuclear fuel reprocessing [1-5]. When ILs are used as diluents in the solvent extraction process employed for such a recovery, the extraction of the target metal ion proceeds through a unique mechanistic pathway, owing to the ionic enivironment present in the IL. Apart from solvent extraction applications, ILs are also being employed as electrolytes, in conjunction with various molecular extractants for studying the electrochemical behavior of the metal ions and the feasibility of direct deposition of metal ion from the loaded IL phase obtained through solvent extraction [6, 7].

Chapter 6

6.1. Electrochemical and Spectroscopic investigation of Eu(III) in T2EHDGA-[C_4mim][NTf_2] mixture

In the recent past, many reports have been published on the studies related to the electrochemical behavior of metal ions present in IL containing various extractants [6-12]. For instance, the electrochemical behavior of lanthanides such as Pr, Nd and Dy present in the IL ([P_{2225}][NTf_2]) containing tri-*n*-butylphosphate (TBP) as the ligating moiety reported by Matsumiya *et al*. [6]. Hussey *et al.* [7] investigated the coordination behavior of lanthanide ions (Ln = Sm, Eu, and Yb) with TODGA in $BuMe_3NTf_2N$ and $BuMePyrTf_2N$ by electrochemical and spectroscopic methods. Rama *et al.* [8, 9] studied the electrochemical behavior of Eu(III) and U(VI) containing *N,N*-dihexyloctanamide (DHOA), tri-*n*-butylphosphate (TBP) and trioctylphosphate (TOP) in the IL ([$C_n$mim][NTf_2]). Further, Rama *et al.* [10] studied the electrochemical behavior of Eu(III) in pyrrolidinium based IL ([C_4mpyr][NTf_2]) containing two different class of acidic extractans; viz., bis(ethylhexyl)phosphoric acid (D2EHPA) and bis(ethylhexyl)diglycolamic acid (HDGA) and correlated their study with the extraction behavior of Eu(III) in the same neat extractants without the IL. Gupta *et al.* [11] studied the luminescence and electrochemical behavior of Eu(III) in IL to elucidate the dynamics and co-ordination behavior of Eu(III) with dihexyl *N,N*-diethylcarbamoylmethylphosphonate (DHDECMP) extractant. Yuan *et al.* [12] reported the electrochemical behavior of Eu(III) in dicyanamide based ILs and calculated the diffusion coefficient, heterogeneous rate constant and the energy of activation for Eu(III)/Eu(II) couple. Since T2EHDGA is a well known diglycolamide ligand employed in the separation of trivalent metal ions from nitric acid medium [13-16], it is essential to investigate the electrochemical behavior of trivalents in T2EHDGA in IL in order to understand the feasibility of using an IL as an electrolyte medium for the electrodeposition. Since [C_4mim][NTf_2] possesses the desirable properties viz., high hydrophobicity, reasonable viscosity (~40 cP) and a good ability to solvate the extracted complex, it is advantageous to employ [C_4mim][NTf_2] in the electrochemical studies [8, 11, 17].

The electrochemical behavior of europium(III) in a solution of T2EHDGA in 1-butyl-3-methylimidazolium bis(trifluoromethanesulfonyl)imide ([C_4mim][NTf_2]) IL was studied and is being reported for the first time in the study. The electrochemical behavior of Eu(III) in an IL was studied by CV. The luminescence and aggregation behavior of the neat IL and that loaded with the metal was investigated in order to understand the salvation of Eu(III).

Synthesis of the IL (C_4mimNTf_2) has been discussed in section 2.5.2 and the experimental procedure used in the preparation of samples and voltammetric studies have been mentioned in section 2.4.7.

6.1.1. Results and Discussion

6.1.1.1. Cyclic voltammetry of Eu(III) in [C_4mim][NTf_2] and 0.02 M T2EHDGA/[C_4mim][NTf_2]

The CV pertaining to Eu(III) in [C_4mim][NTf_2] recorded at a glassy carbon electrode at a scan rate of 100 mV/s at 373 K is shown in Figure 6.1. It is seen that the onset of the reduction wave occurs at 0.04 V (Vs. Fc/Fc$^+$) and that the latter proceeds with a peak at the cathodic potential (E_p^c) of - 0.46 V (Vs. Fc/Fc$^+$) corresponding to the reduction of Eu(III) to Eu(II). The corresponding oxidation wave occurs at a peak potential of 0.3 V (Vs. Fc/Fc$^+$). The ILs, [C_4mim][NTf_2] and 0.02 M T2EHDGA/[C_4mim][NTf_2] possesses the electrochemical windows of 4.8 V and 3.6 V respectively. The cation reduction occurs at the potential of -2.8 V and -1.8 V (Vs. Fc/Fc$^+$) while the anion oxidation occurs at +2.0 V and +1.8 V (Vs. Fc/Fc$^+$) respectively in these media. Figure 6.1 displays the cyclic voltammogram of 0.02 M T2EHDGA/[C_4mim][NTf_2]. It is noticed that the electrochemical window decreases from 4.8 V to 3.6 V for Eu(III) in a solution of 0.02 M T2EHDGA in [C_4mim][NTf_2] under the same experimental conditions. It is seen that the cathodic wave occuring with an onset potential of 0.03 V (Vs. Fc/Fc$^+$), leads to a prominent cathodic wave at a peak potential of -0.53 V corresponding to the reduction of Eu(III) to Eu(II). The oxidation wave occurs at a peak potential of 0.14 V (Vs. Fc/Fc$^+$). A comparison of these peak potentials with those observed in the absence of T2EHDGA, shows that the presence of T2EHDGA in the IL shifts the reduction of Eu(III) to more negative potentials with a remarkable decrease in the current density, possibly due to the co-ordination of Eu(III) with T2EHDGA. Since the co-ordinated Eu(III) requires higher cathodic potentials for reduction, the peak potential is shifted cathodically for Eu(III) -T2EHDGA in the IL.

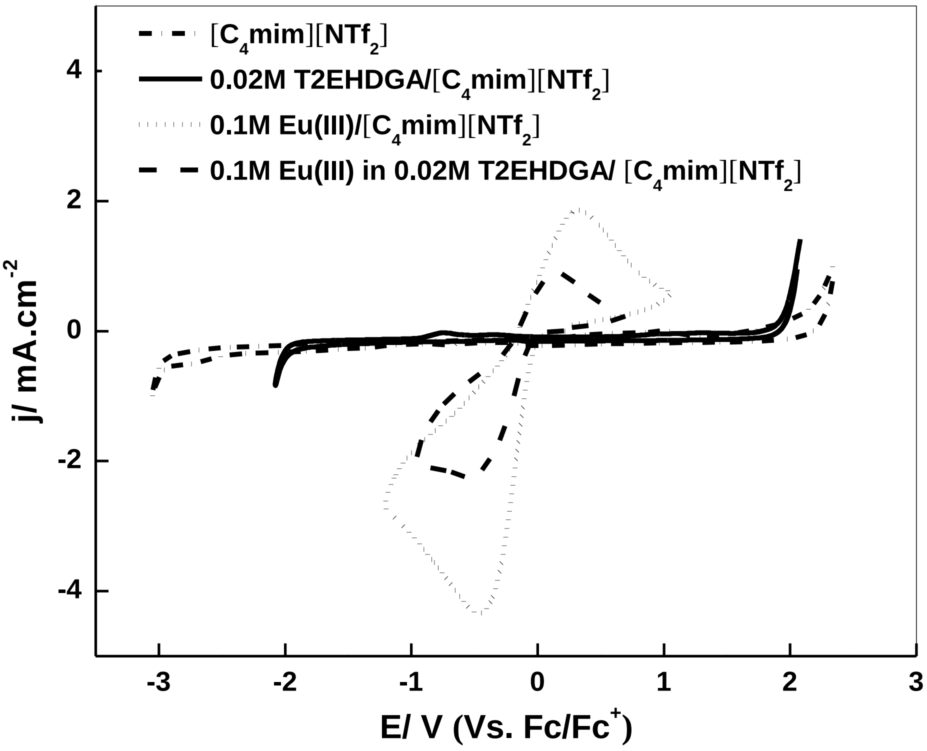

Figure 6.1. CV pertaining to [C_4mim][NTf_2], Eu(III) in [C_4mim][NTf_2] (or 0.02 M T2EHDGA/[C_4mim][NTf_2]) recorded at a glassy carbon electrode at 373 K, at a scan rate of 0.1 V/s. [Eu(III)] = 0.1 M.

The plausible electrochemical reaction occurring during the redox process is given by equation (6.1) and (6.2).

Eu^{3+} + 3 NTf_2^- ⇔ Eu^{2+} + Oxidised form of 3 NTf_2^- (6.1)

Eu^{3+} +T2EHDGA + 3 NTf_2^- ⇔ [Eu…T2EHGA]$^{2+}$ + Oxidised form of 3 NTf_2^- (6.2)

However, the electrochemical oxidation occurring at the counter electrode is not known. Perhaps NTf_2^- ion is oxidized at the counter electrode during the reduction of Eu(III). The CV pertaining to Eu(III) in [C_4mim][NTf_2] recorded at different sweep rates at a glassy carbon electrode at 373 K is shown in figure 6.2a. It is seen that the cathode current density (j_p^c) increases and the cathodic peak potential (E_p^c) is shifted cathodically with an increase in scan rate. Figure 6.2b also shows the variation of CV at different scan rates perataining to the reduction of Eu(III) in T2EHDGA/[C_4mim][NTf_2] at 373K. Similar to figure 6.2a, the cathodic peak current density increases and the cathodic peak potential (E_p^c) is shifted cathodically with increasing scan rate. These findings indicate that the reduction of Eu(III) to Eu(II) at a glassy carbon electrode is not reversible in both these cases. The values of $|E_p^c\text{-}E_{p/2}^c|$ obtained in these two experiments are quite significant (0.23 V for [C_4mim][NTf_2] and 0.25 V for 0.02 M T2EHDGA/[C_4mim][NTf_2] at 373 K) than the value needed for a reversible (0.07 mV at 373 K) one electron transfer process. This shows that the reduction of Eu(III) to Eu(II) could possibly be quasi-reversible and therefore it is reasonable to presume that this reduction is controlled not only by the diffusion of Eu(III) in [C_4mim][NTf_2] (or T2EHDGA/[C_4mim][NTf_2]) medium, but also by the a charge transfer reaction occurring at the electrode-electrolyte interface. The charge transfer coefficient (α, $0.1 \leq \alpha \leq 0.9$) for a non-reversible (both quasi and irreversible process) electrode reactions could be determined from the magnitude of $|E_p^c\text{-}E_{p/2}^c|$ by using equation (A.4) (Annexure).

By using equation (A.4) (Annexure) the value of αn_α was determined to be ~0.25 and ~0.23 for Eu(III) in [C_4mim][NTf_2] and Eu(III) in 0.02 M T2EHDGA/[C_4mim][NTf_2] at 373 K in a range of scan rates that varied from 0.02 V/s to 0.1 V/s. Rama *et al.* [8] reported a αn_α value of 0.34 for the charge transfer of Eu(III) to Eu(II) in [C_6mim][NTf_2] phase under similar conditions.

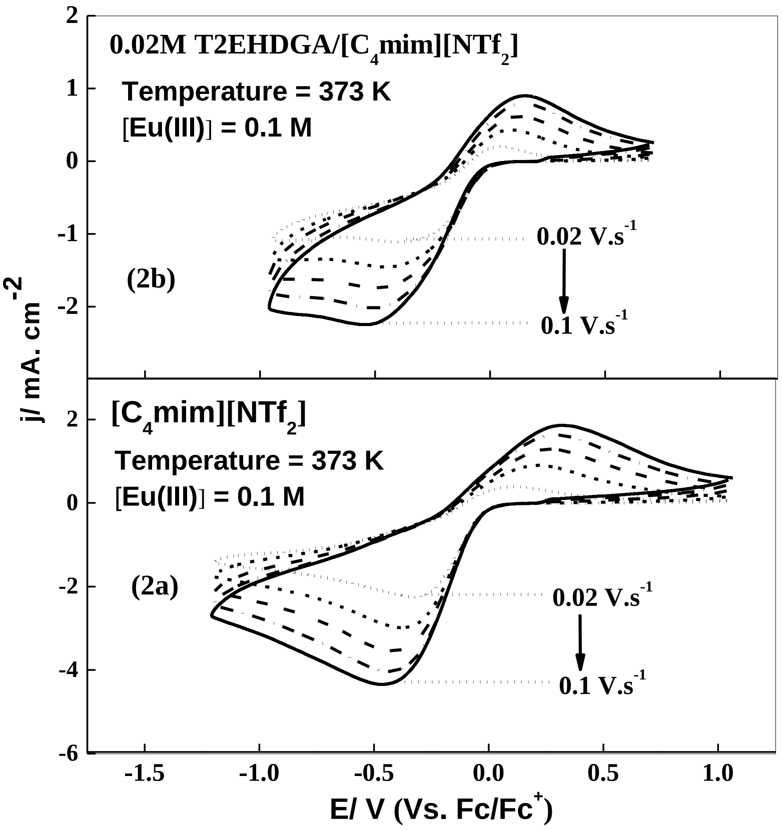

Figure 6.2. CV pertaining to (a) Eu(III) in [C_4mim][NTf_2] and (b) 0.02 M T2EHDGA/[C_4mim][NTf_2] recorded at glassy carbon electrode at different scan rates at 373 K. [Eu(III)] = 0.1 M.

6.1.1.2. Diffusion coefficient of Eu(III) in [C_4mim][NTf_2] and in T2EHDGA/[C_4mim][NTf_2]

The diffusion coefficient of Eu(III) could be determined from the CV by using equation (A.5) (Annexure) that relates the cathodic peak current (i_p^c) and the scan rate for an irreversible or quasi reversible reduction of soluble-soluble Eu(III)-Eu(II) couple. The electrode area was 0.3 cm^2 and Eu(III) concentration in IL was 1 x 10^{-4} mol cm^{-3}.

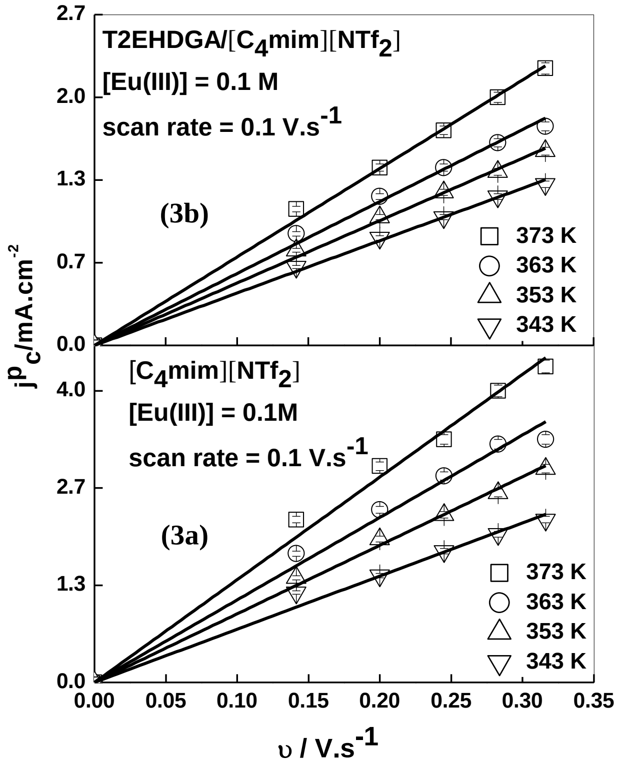

Figure 6.3. Dependence of i_p^c on the square root of scan rate ($\upsilon^{1/2}$) for the reduction of Eu(III) to Eu (II) in (a) [C_4mim][NTf_2] and (b) 0.02 M T2EHDGA/[C_4mim][NTf_2] at different temperatures (343 to 373 K). [Eu(III)] =0.1 M.

A plot of cathodic peak current (i_p^c) against the square root of the scan rate ($\upsilon^{1/2}$) at 373 K for the reduction of Eu(III) to Eu(II) in [C_4mim][NTf_2] is shown in figure 6.3a. It is seen that the cathodic peak current increases with $\upsilon^{1/2}$. A similar observation has been made in the reduction of Eu(III) to Eu(II) in 0.02 M T2EHDGA/[C_4mim][NTf_2]. The linear dependence of the cathodic peak current with a zero-intercept indicates the validity of equation (A.5) (Annexure). Therefore the diffusion coefficient of Eu(III) in [C_4mim][NTf_2] and 0.02 M T2EHDGA/[C_4mim][NTf_2] could be determined by using equation (2.5). From the slope of the straight line, the diffusion coefficients of Eu(III) in both the ILs were determined have been determined and these results are provided in table 6.1. The values of the diffusion coefficient of Eu(III) were found to be 9.2 x 10^{-8}

cm^2/s and 1.2 x 10^{-8} cm^2/s at 373 K in [C_4mim][NTf_2] and 0.02 M T2EHDGA/[C_4mim][NTf_2] respectively.

Table 6.1. The diffusion coefficients (D) of Eu enumerated from the reduction of Eu(III) to Eu(II) in [C_4mim][NTf_2] at a glassy carbon electrode at different temperatures; [Eu(III)] = 0.1 M and [T2EHDGA]= 0.02 M.

	D x 10^8/cm^2s^{-1}	
Temperature / K	**Eu(III) in [C_4mim][NTf_2]**	**Eu(III) in T2EHDGA /[C_4mim][NTf_2]**
343	2.1 ± 0.04	0.5 ± 0.01
353	4.2 ± 0.08	0.6 ± 0.012
363	6.1 ± 0.1	0.9 ± 0.018
373	9.2 ± 0.18	1.2 ± 0.02

6.1.1.3. Effect of temperature

The CV pertaining to Eu(III) in [C_4mim][NTf_2] and Eu(III) in 0.02 M T2EHDGA/[C_4mim][NTf_2]) recorded at a glassy carbon working electrode at different temperatures are shown in figure 6.4a and 6.4b respectively. It is seen that the peak potential (E_p^c) is shifted anodically and the cathodic peak current (i_p^c) increases with temperature in both these ILs. The CV pertaining to Eu(III) in [C_4mim][NTf_2] (or in 0.02 M T2EHDGA/[C_4mim][NTf_2]) phase at different scan rates were obtained at different temperatures and from the plot of i_p^c against the square root of the scan rate ($\upsilon^{1/2}$) the diffusion coefficient in both the ILs at these temperatures was determined. These values are tabulated in table 6.1. It is seen that the value of D increases from 2.1 x 10^{-8} cm^2/s to 9.2 cm^2/s and from 0.5 x 10^{-8} cm^2/s to 1.2 x 10^{-8} cm^2/s when the temperature is raised from from 343 K to 373 K (for Eu(III) in [C_4mim][NTf_2] and Eu(III) in 0.02 M T2EHDGA/[C_4mim][NTf_2] respectively). This could be due to the fact decrease in the viscosity with increase in temperature which enhances the rates of diffusion of Eu(III). The Arrhenius relation between the diffusion coefficient and temperature is shown in equation 6.3.

$$\ln D = \ln A - E_a/RT \qquad (6.3)$$

where A is the pre-exponential factor and E_a is the energy of activation.

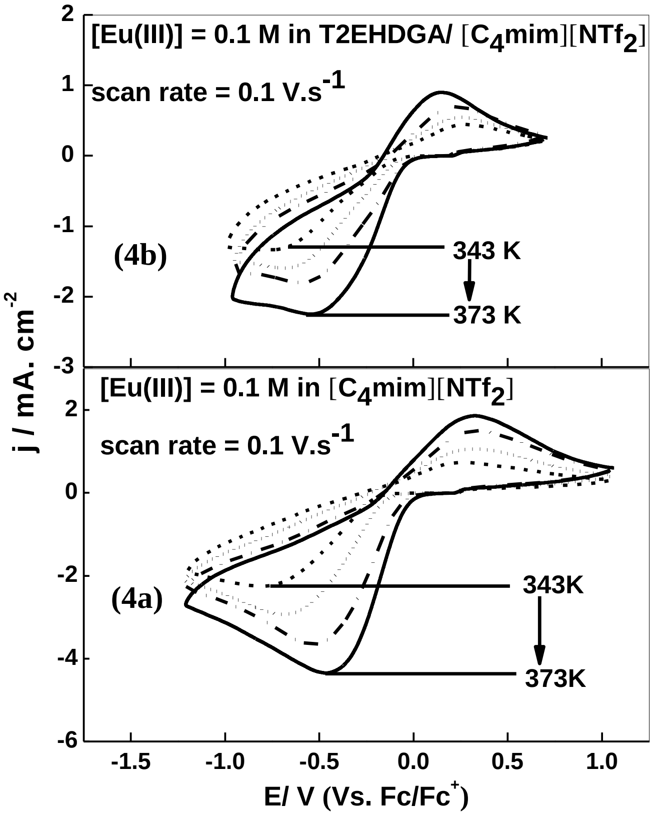

Figure 6.4. CV pertaining to Eu(III) in (a) $[C_4mim][NTf_2]$ and (b) 0.02 M T2EHDGA/$[C_4mim][NTf_2]$ recorded at a glassy carbon electrode at different temperatures in the range 343 to 373 K. [Eu(III)] = 0.1 M, scan rate =0.1 V/s.

Plots of ln D against 1/T pertaining to the diffusion of Eu(III) in the ILs both in the presence and absence of T2EHDGA are shown in figure 6.5. From the slopes of the linear fit, the energy of activation (E_a) for the diffusion of Eu(III) in $[C_4mim][NTf_2]$ and 0.02 M T2EHDGA/$[C_4mim][NTf_2]$) medium were determined to be 50 kJ/mol and 26 kJ/mol respectively. It is interesting to note that the Ea obtained for the diffusion of Eu(III) in [C_4mim][NTf_2] (50 kJ/mol) is more as compared to its corresponding value of Eu(III) in 0.02 M T2EHDGA/[C_4mim][NTf_2]. The diffusion coefficient has a stronger temperature dependence in [C_4mim][NTf_2]. Since Eu(III) is coordinated to T2EHDGA in the C_4mimNTf$_2$ medium, the effect of temperature on the diffusion coefficient has less effect in T2EHDGA/C_4mimNTf$_2$ medium. This explains the difference in the values of E_a mentioned above. Rama et al., [8] reported an energy of activation of 88 kJ/mol for the diffusion of Eu(III) in [C_6mim][NTf_2]. It is quite likely that [C_6mim][NTf_2] is more viscous than [C_4mim][NTf_2].

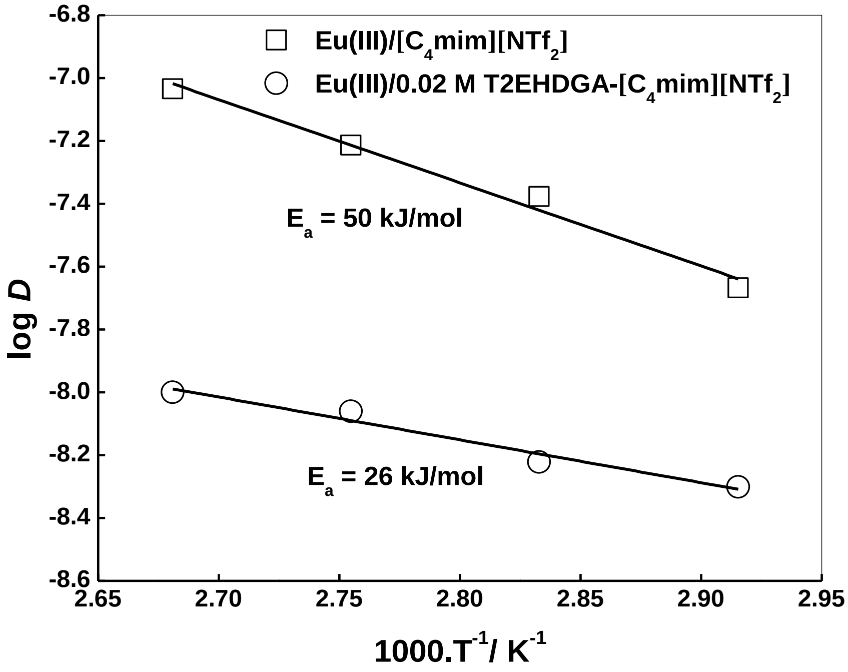

Figure 6.5. Dependence of ln D on 1/T for the reduction of Eu(III) to Eu (II) in [C_4mim][NTf_2] and 0.02M T2EHDGA/[C_4mim][NTf_2] in the temperature range 343 to 373 K.

6.1.1.4. Heterogeneous rate constant pertaining to the reduction of Eu(III) in [C_4mim][NTf_2] and in T2EHDGA/[C_4mim][NTf_2]

From the separation of the cathodic and anodic peaks in figure 6.2a and 6.2b, it could concluded that the reduction of Eu(III) to Eu(II) in [C_4mim][NTf_2] (or 0.02 M T2EHDGA/[C_4mim][NTf_2]) is quasi-reversible [19]. This in turn confirms that the reduction of Eu(III) to Eu(II) is not only controlled by diffusion of Eu(III) ion at the working electrode but also by the rate of charge transfer at the electrode electrolyte interface. In such cases, the charge transfer rate constant k_s (cm/s) could be determined by using equation (A.6) (Annexure) [8].

Substituting the value of diffusion coefficient of Eu(III) in equation (2.6), the rate constants were determined at each temperature and these values are tabulated in table 6.2. It is seen that the value of k_s increases with temperature both for [C_4mim][NTf_2] and 0.02 M T2EHDGA/[C_4mim][NTf_2] and the magnitude of k_s lies in the range of $0.3\ \upsilon^{1/2} \geq k_s \geq 2 \times 10^{-5}\ \upsilon^{1/2}$ cm/s, confirming that the reduction of Eu(III) at a glassy carbon electrode is quasi-reversible. The reason for such a behavior (increase in k_s with temperature) could be attributed to the decrease in the viscosity of the medium with an increase in temperature. This in turn leads to an increase in the relative abundance of the metal ions in the viscinity of the electrode thereby enhancing the electron transfer at electrode-electrolyte interface, and increases the value of k_s [10]. The lower values of k_s for 0.02 M T2EHDGA/[C_4mim][NTf_2] as compared to [C_4mim][NTf_2] could be attributed to the higher in viscosity of the latter.

Table 6.2. Temperature dependence of the heterogeneous rate constant (k_s) for the reduction of Eu(III) to Eu(II) in [C$_4$mim][NTf$_2$] and 0.02 M T2EHDGA/[C$_4$mim][NTf$_2$] at a glassy carbon electrode at different temperatures [Eu(III)] = 0.1 M.

	k_s x 10^4/cms^{-1}	
Temperature / K	**Eu(III) in [C$_4$mim][NTf$_2$]**	**Eu(III) in T2EHDGA /[C$_4$mim][NTf$_2$]**
343	0.54	0.075
353	0.98	0.18
363	1.18	0.4
373	1.26	0.6

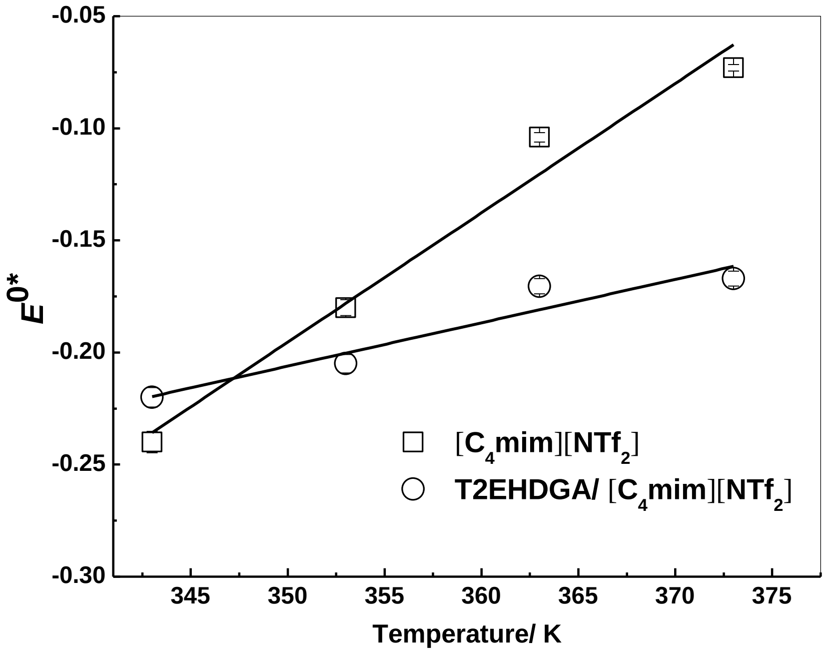

Figure 6.6. A plot of the temperature dependence of standard potential (E^{0*}).

6.1.1.5. An Inter-comparision of the electrolytic media

The electrochemical behavior of europium(III) in different IL media has already been reported in literature [8-10]. In this context, it would be prudent to compare the results obtained in this study on the reduction of Eu(III), especially the values of diffusion coefficient, charge transfer rate constant and energy of activation with those reported for the other ILs mixed with different extractants. Table 6.3 displays such a comaprision of D, k_s and E_a pertaining to Eu(III) reduction in [C$_4$mim][NTf$_2$] and 0.02 M T2EHDGA/[C$_4$mim][NTf$_2$] along with those pertaining to other ILs. It is seen that all these values obtained in this study are comparable with those reported for other systems earlier.

Table 6.3. A comparison of the diffusion coefficient, charge transfer rate constant and energy of activation pertaining to the reduction of Eu(III) obtained in different IL systems at 373 K.

Ionic liquid System	D x 10^8/cm^{2}s^{-1}	k_s x 10^4/ cms^{-1}	E_a/kJmol^{-1}
[C$_4$mim][NTf$_2$] *(present work)*	9.2	1.26	50
[C$_4$mpyr][NTf$_2$] *(Ref.10)*	3.8	0.15	60
[C$_4$mim][DCA] *(Ref. 12)*	67.9 #	6.09 #	27.3
[C$_6$mim][NTf$_2$] *(Ref.9)*	3.82	2.8.	88
0.02M T2EHDGA/[C$_4$mim][NTf$_2$] *(present work)*	1.2	0.6	37
0.02M HDGA/[C$_4$mpyr][NTf$_2$] (*Ref.10*)	1.1	0.09	38
0.02M DHOA/[C$_6$mim][NTf$_2$] (*Ref.9*)	2.9	2.7	94

at 333K

6.1.1.6. Spectroscopic investigation

In order to support the difference in the peak potentials pertaining to Eu(III)/Eu(II) couple both in presence and absence of T2EHDGA in [C$_4$mim][NTf$_2$] medium, luminescence spectra of the metal loaded IL phase was recorded and these results are presented in figure 6.7. The shape of the pattern and the relative intensities of $^5D_0 \rightarrow {}^7F_1$

(magnetic dipole transition) and $^5D_0\rightarrow{}^7F_2$ (electric dipole or hypersensitive transition) in Eu(III) in $[C_4mim][NTf_2]$ and Eu(III) in T2EHDGA/$[C_4mim][NTf_2]$ are entirely different. The peak at 615 nm is less intense than that obtained at 592 nm in case of $[C_4mim][NTf_2]$. This indicates that the Eu(III) coordination sphere is not distorted significantly by the IL anion (NTf_2^-) as the anion is same as that of the Eu(III) salt used in this study ($Eu(NTf_2)_3$) and there is no incorporation of a new ligating anion. In contrast to this, the peak at 615 nm ($^5D_0\rightarrow{}^7F_2$ transition) is much more intense than the peak at 592 nm ($^5D_0\rightarrow{}^7F_1$ transition) in the case of Eu(III) loaded T2EHDGA/$[C_4mim][NTf_2]$ system which confirms the strong coordination of Eu(III) with T2EHDGA, leading to a change in the local coordination sphere [19].

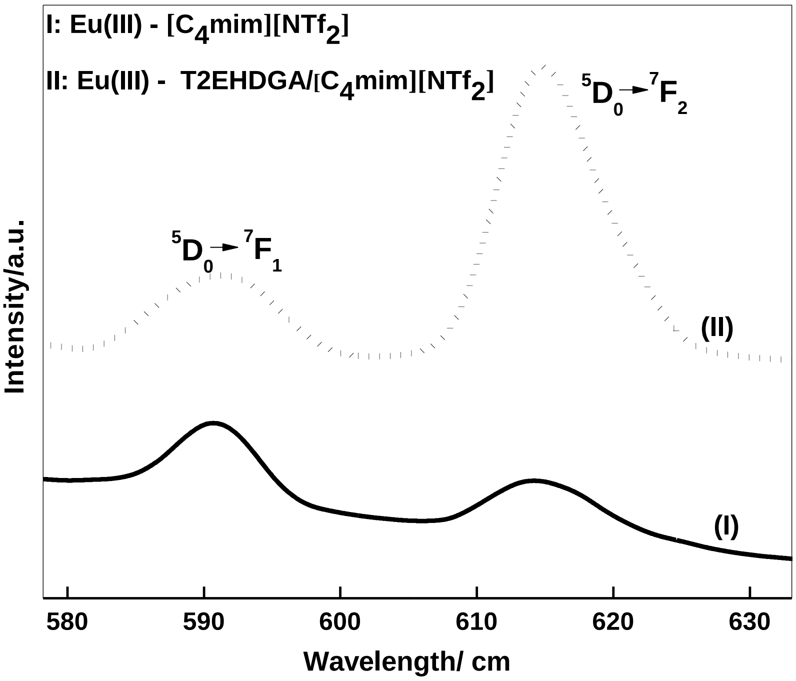

Figure 6.7. Emission spectra of Eu(III) in $[C_4mim][NTf_2]$ and 0.02 M T2EHDGA/$[C_4mim][NTf_2]$ medium. λex = 394 nm; temperature = 298 K.

The complexation of Eu(III) ion in ILs could be evaluated by monitoring the asymmetry factor (I_{615}/I_{592})) for Eu(III) in both [C_4mim][NTf_2] and 0.02 M T2EHDGA//[C_4mim][NTf_2]. From figure 6.7, the value of I_{615}/I_{592} was calculated to be 0.53 and 1.8 for [C_4mim][NTf_2] and 0.02 M T2EHDGA/[C_4mim][NTf_2] respectively. This indicates that the presence of T2EHDGA strongly distorts the local environment of Eu(III) upon complexation. In contrast to this, an asymmetry factor of 0.53 refers to a poor coordination of Eu(III) with the weakly ligating NTf_2^- ion in [C_4mim][NTf_2] phase alone.

Figure 6.8 shows the aggregate distribution measured for various IL phases namely, 0.02 M T2EHDGA/[C_4mim][NTf_2], Eu(III) (0.1 M) dissolved in [C_4mim][NTf_2] and Eu(III) (0.1 M) dissolved in 0.02 M T2EHDGA/[C_4mim][NTf_2]. The average aggregate size of 0.66 nm obtained for [C_4mim][NTf_2] appears as a single line with low FWHM. The average aggregate size of IL phase increases in the following order: [C_4mim][NTf_2] (0.66 nm) < 0.02 M T2EHDGA/[C_4mim][NTf_2] (10.4 nm) < Eu(III) loaded [C_4mim][NTf_2] (22 nm) << Eu(III) loaded 0.02 M T2EHDGA/[C_4mim][NTf_2] (53 nm). In addition, the distribution of aggregates in the IL also increases in the same order. This shows that the presence of Eu(III) in the IL phase facilitates the aggregation possibly due to the interactions between the Eu(III) and the anions of the ILs significant increase in the aggregate concentration size observed for Eu(III) in 0.02 M T2EHDGA/[C_4mim][NTf_2] could be due to the coordination of Eu(III) with T2EHDGA. The complexation of Eu(III) with T2EHDGA increases the polarity of Eu(III) – T2EHDGA complex. Because of the increase in the polarity of metal – solvate species, the interaction between the metal – solvate and IL increases. This results in an increase in the quantity of aggregate as well as the spread in their size. The lower values of the diffusion coefficient observed for Eu(III) in 0.02 M T2EHDGA/[C_4mim][NTf_2] as compared to that for Eu(III) in [C_4mim][NTf_2] alone (shown in table 6.1) compares well with the larger aggregate size observed in the case of Eu(III) in 0.02 M T2EHDGA/[C_4mim][NTf_2] (53 nm) as compared to Eu(III) in [C_4mim][NTf_2] (22 nm).

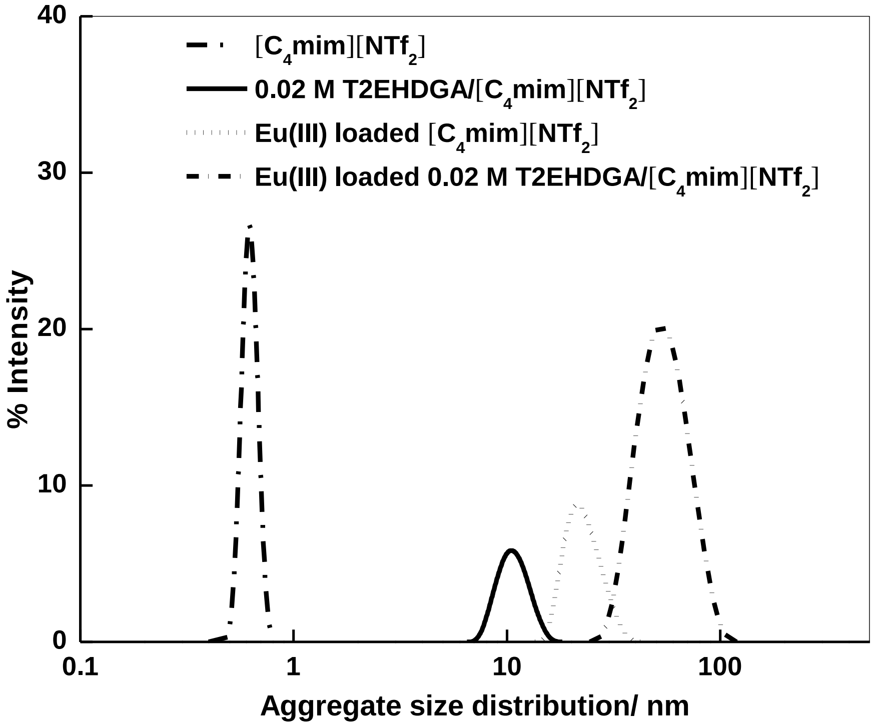

Figure 6.8. Aggregation behavior of the IL obtained by using DLS measurements. Organic phase: [C_4mim][NTf_2], 0.02 M T2EHDGA/[C_4mim][NTf_2] and their respective Eu(III) loaded phases at 298 K.

6.1.2. Conclusions

The electrochemical behavior of Eu(III) in [C_4mim][NTf_2] was studied at a glassy carbon working electrode both in the presence and absence T2EHDGA by using CV. The CV pertaining to Eu(III) exhibited a quasi-reversible redox couple in the potential range -1 V to +1 V. The addition of T2EHDGA to the Eu(III)/[C_4mim][NTf_2] solution lowered the cathodic peak current and shifted the cathodic peak potential cathodically due to the co-ordination of Eu(III) with T2EHDGA. A lower cathodic peak current observed in the presence of T2EHDGA was due to the aggregation of Eu(III)- T2EHDGA complex in the IL. The diffusion coefficient of Eu(III) was determined at different temperatures and was found to be in the order of ~10^{-8} cm^2/s. In the presence of a ligand, the diffusion coefficients decreased in the following order: Eu(III) - [C_4mim][NTf_2] > Eu(III) in T2EHDGA/[C_4mim][NTf_2]. Similarly, the charge transfer rate constant (k_s) was determined to have a value of about ~10^{-4} cm/s, and the presence of T2EHDGA in the IL decreased the k_s values as compared to the neat [C_4mim][NTf_2]. An increase in the temperature of the system enhanced the diffusion coefficient as well as the value of k_s. The activation energy was evaluated to be less in the case of Eu(III) in T2EHDGA/[C_4mim][NTf_2] (26 KJ/mol) as compared to that of Eu(III) in [C_4mim][NTf_2] (50 KJ/mol). Luminescence spectroscopy and DLS studies confirmed the fact that the complex environment gets modified and aggregation gets enhanced upon adding T2EHDGA.

6.2. Voltammetric investigation of some lanthanides in neutral ligand-ionic liquid

The ILs prepared from polynuclear organic ions invariably make them strongly hydrophobic and offer a wide electrochemical window, but provide only limited solubility of metal salts in them. As a result, the IL with a wide electrochemical window again becomes unsuitable for the electrodeposition. Nevertheless, a large number of studies have been reported in the literature with these ILs that offer large window but a poor solubility for metal salts [20, 21]. For instance, uranium or europium nitrate are sparingly soluble in $C_4mimNTf_2$, yet a number of studies have been reported in the literature on the electrochemical behavior of Eu(III) and U(IV) in these ILs [21-25].

There are a few methods available to increase the solubility of a given actinide or lanthanide salt in the IL with a wide electrochemical window. One way is to exploit the coordination behavior of the actinide to form a wide range of species with simple anions that are soluble in the IL. For instance the solubility of uranyl nitrate in $C_4mimNTf_2$ could be significantly improved by adding 1-butyl-3-methylimidazolium chloride (C_4mimCl). The addition of a stoichiometric amount of C_4mimCl results in the formation of anionic chlorocomplexes of uranium(IV). Since these chlorocomplexes easily dissolve in $C_4mimNTf_2$ the concentration of U(IV) in this IL could be increased to a level that is adequate enough for electrodeposition in $C_4mimNTf_2$ [24].

Another technique is to increase the solubility of metal salts in a hydrophobic IL by adding the ligands that can coordinate with the metal ion. In this case, the IL serves as the medium for electrodeposition and the coordinated ligand governs the solubility of the metals salt. It should be noted that the selected IL should undergo reduction only after the metal deposition. This kind of approach has been used in the extraction of metal salts from aqueous phase in to IL medium followed by the electrodeposition of the former directly from the IL phase. For instance, Matsumiya *et al.* [26] investigated the extraction and electrodeposition behaviour of some lanthanides in a solution composed of tri-n-butyl phosphate (TBP) in IL. Similarly, Murakami *et al.* [27] reported the extraction of rare earth elements in tetraoctylglycolamide (TODGA) present in $C_4mimNTf_2$ phase. The $[Nd(TODGA)_3]^{3+}$ complex thus extracted in the IL was reduced to Nd(0) at -3.0 V. In this system, these authors [27] reported that Nd(III) was extracted into the IL as $[Nd(TODGA)_3]^{3+}[(NTf_2)_3]^-$ ion pair, since NTf_2^- was a big non-coordinating anion.

If neodymium (III) can be extracted as $[Nd(TODGA)_3]^{3+}[(NTf_2)_3]^-$ ion pair in the organic phase, it could be employed for electrodeposition of metals. This is possible because the ligands coordinated to the metal are usually hard to reduce or oxidize. Such ion pairs are called as neutral ligand-ILs (NLILs), as suggested by Bagri *et al.*, [28]. It should be noted that these neutral ligand-ILs do not require any additional medium for the electrodepsoition of the metal associated with it, for the NLIL itself could serve as an electrolytic medium. Therefore, there is no need to search for an ionic liquid that offers wide electrochemical window for electrodeposition, if NLILs are prepared. Literature shows that it is possible to prepare the ion pair complex $Nd(NTf_2)_3$ with any suitable ligand existing in liquid form to obtain a neutral ligand IL with a typical formula $[Nd(ligand)_x]^{3+}[(NTf_2)_3]^-$. In this context, Bagri *et al.* [28] exploited that the advantages of these NLILs and prepared the NTf_2 salt of the rare earths with trimethyl phosphate ligand and demonstrated the electrodeposition of rare earths from the resultant NLIL. In the present chapter, the possibility of using CHON-based ligand namely dihexyloctanamide (DHOA) for the dissolution of $Ln(NTf_2)_3$ (Ln = Nd, Eu and Dy) salt and the electrochemical behavior of Ln(III) in the resultant NLIL namely, $[Ln(DHOA)_3]^{3+}$ $[(NTf_2)_3]^-$ was studied. The application of this method for the dissolution of rare earth oxides in NLIL medium followed by the electrodeposition of rare earths in their metallic form has also studied in the present work. This study can be applied to the electrochemical recovery of remaining lanthanides from their ionic salts or oxides.

Synthesis of the IL ($C_4mimNTf_2$) has been discussed in section 2.5.2 and experimental procedures pertaining to the preparation of NLIL, dissolution of the lanthanide oxidesin, in them and their voltammetric and electrodeposition studies have been described in section 2.4.5.

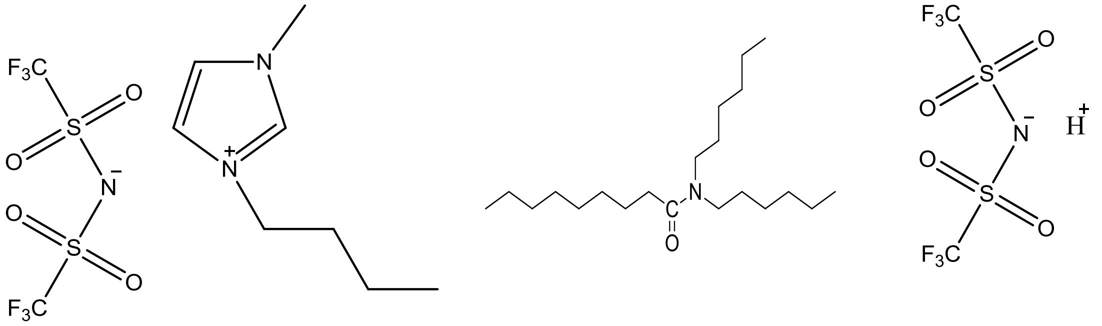

1-Butyl-3-methylimidazolium bis(trifluoromethanesulfonyl)imide

N,N-dihexyloctanamide (DHOA)

Bis(trifluoromethanesulfonyl)imide acid ($HNTf_2$)

Figure 6.9. Structures of the chemicals used in the present work.

6.2.1. Results and discussion

6.2.1.1. Spectroscopic and electrochemical studies

The NLIL was prepared by dissolving the required quantity of $Ln(NTf_2)_3$ (100 mM) (Ln = Nd, Eu and Dy) in DHOA. These lanthanide salts undergo facile dissolution in DHOA and the resultant solution was subjected to eletrcochemical and spectroscopic investigations. The FTIR spectrum of these NLILs recorded after the dissolution of $Nd(NTf_2)_3$ or $Eu(NTf_2)_3$ or $Dy(NTf_2)_3$ in DHOA are shown in figure 6.10. These spectra are compared with that pertaining to DHOA. It is seen that there is a strong transmittance band occurring at 1640 cm^{-1} due to the amidic C=O stretching frequency of DHOA. This transmittance band is partially shifted to 1585 cm^{-1} upon adding the $Ln(NTf_2)_3$. This indicates that DHOA is coordinated to Ln^{3+} ion through amidic carbonyl bonding.

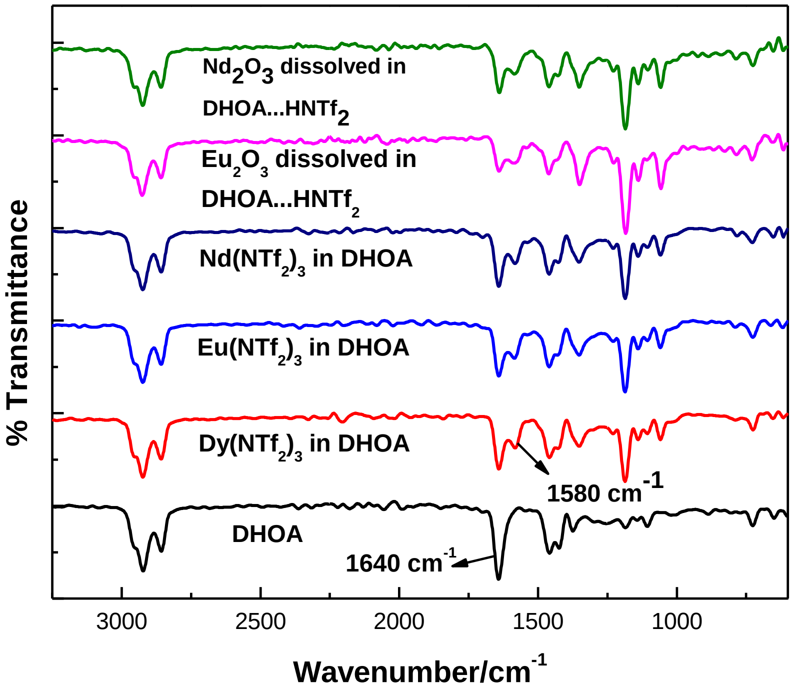

Figure 6.10. Fourier transform infrared spectra of NLILs containing $Ln(NTf_2)_3$ obtained through different routes.

In order to understand the stoichiometry of Ln^{3+}-DHOA complex existing in the NLIL, the CV pertaining to Eu^{3+} was recorded in the presence of DHOA at different Eu^{3+} : DHOA mole ratios. From the measurement of the cathodic current as function of Eu : DHOA mole ratio, it is quite possible to determine the approximate stoichiometry of the Eu to DHOA prevailing in the IL [8, 30]. For this purpose, it is necessary to obtain the reference CV pertaining to Eu^{3+} in the absence of DHOA. Figure 6.11 shows the CV of Eu^{3+} recorded at a glassy carbon electrode at a scan rate of 100 mV/s in the absence of DHOA in C_4mimNTf$_2$. This voltammogram shows a surge in cathodic current occuring at the potential of -0.5 V (Vs Pd), due to the reduction of Eu^{3+} to Eu^{2+}, which culminates in a peak (E_p^{c1}) at -1 V. The corresponding oxidation (E_p^{a1}) wave is observed at 0.1 V (Vs Pd). This voltammogram also shows a wave at 1.3 V (Vs Pd) pertaining to the oxidation of NTf_2^-, as discussed the reference [25]. This figure also compares the voltammogram of Eu^{3+} in the presence of DHOA at different Eu^{3+} : DHOA mole ratios in C_4mimNTf$_2$ medium. The Eu^{3+} to DHOA mole ratio was varied from 1 : 1 to 1 : 4. It is seen that the cathodic peak current (I_p^{c1}) dramatically decreases with the addition of DHOA. This could be ascribed to the co-ordination of DHOA with Eu^{3+} ion leading to the formation of a bulky $[Eu(DHOA)]^{3+}$ complex in the IL. Since the diffusion of such a bulky $[Eu(DHOA)]^{3+}$ would be slower than that of Eu^{3+} the cathodic peak current I_p^{c1} decreases with the addition of DHOA. Further addition of DHOA, results in the formation of still bigger $[Eu(DHOA)_2]^{3+}$ complex with an 1 : 2 stoichiometry. As a result the cathodic peak current is lowered further. The reduction in the cathodic current continues until the Eu^{3+} to DHOA mole ratio of 1 : 3 is reached. Thereafter, the addition of DHOA does not affect the cathodic current significantly. In view of this observation, it is quite likely that the stoichiometry of 1 : 3 for Eu : DHOA could be assured in a medium containing 100 mM

Eu^{3+} in DHOA. Therefore, it is reasonable to assume the Eu^{3+} exists in the form of $[Eu(DHOA)_3]^{3+}[(NTf_2)_3]^-$, in this NLIL.

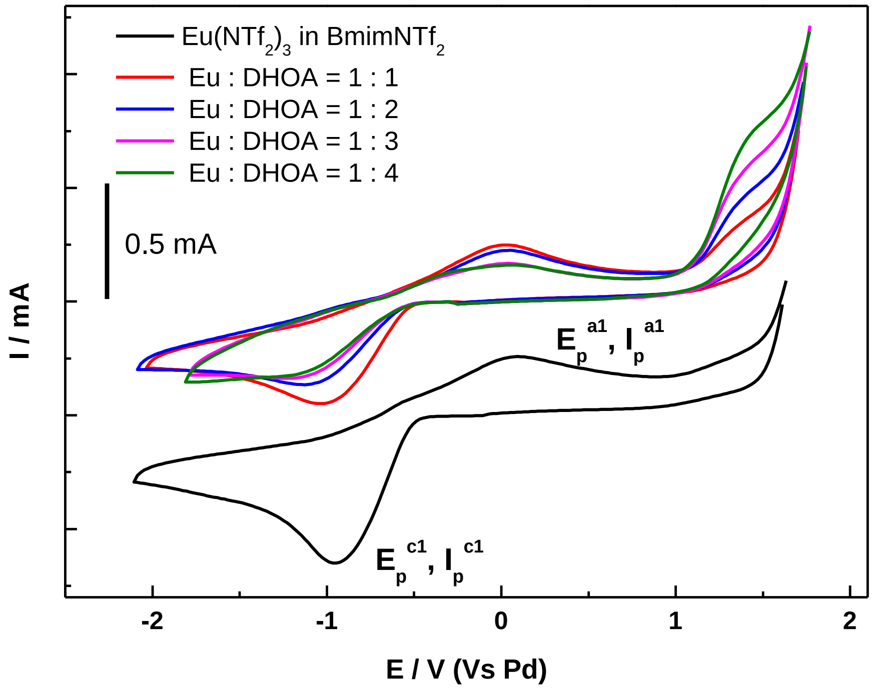

Figure 6.11. CV pertaining to Eu(III) in $C_4mimNTf_2$ at different Eu : DHOA mole ratios recorded at glassy carbon working electrode at the scan rate of 100 mVps at 323 K.

The CV pertaining to NLIL, $[Ln(DHOA)_3]^{3+}$ $[(NTf_2)_3]^-$ (Ln = Eu, Nd and Dy) recorded at a glassy carbon at a scan rate of 50 mV/s at 353 K is shown in figure 6.12. It is evident that the $Ln(NTf_2)_3$ concentration is 100 mM in DHOA. The voltammogram of Eu^{3+} shows a couple of cathodic waves (E_p^{c2}) at -2 V (Vs Pd) due to Eu^{3+} to Eu^{2+} reduction, and another at -3 V (Vs Pd) due to the reduction (E_p^{c3}) of Eu^{2+} to Eu^0. When the sweep is reversed at -2.5 V, an oxidation wave (E_p^{a2}) corresponding to Eu^{2+} to Eu^{3+} is observed at 0.9 V (Vs Pd). In contrast to the two step reduction observed for Eu^{3+}, the NLILs containing Nd^{3+} and Dy^{3+} undergoes a single step $3e^-$ transfer reduction at the glassy carbon electrode at a cathodic potential of -3 V. It is also noted that the oxidation waves (Nd^0 or Dy^0 to higher oxidation states) are not observed during scan reversal in these cases. The cathodic waves, E_p^{c3}, E_p^{c4} and E_p^{c5}, observed at -3 V could be attributed to the reduction of the NLIL cation to as shown in equation (6.4).

$$[Ln(DHOA)]^{3+} + 3e^- \Leftrightarrow Ln^0 + 3\ DHOA \qquad (6.4)$$

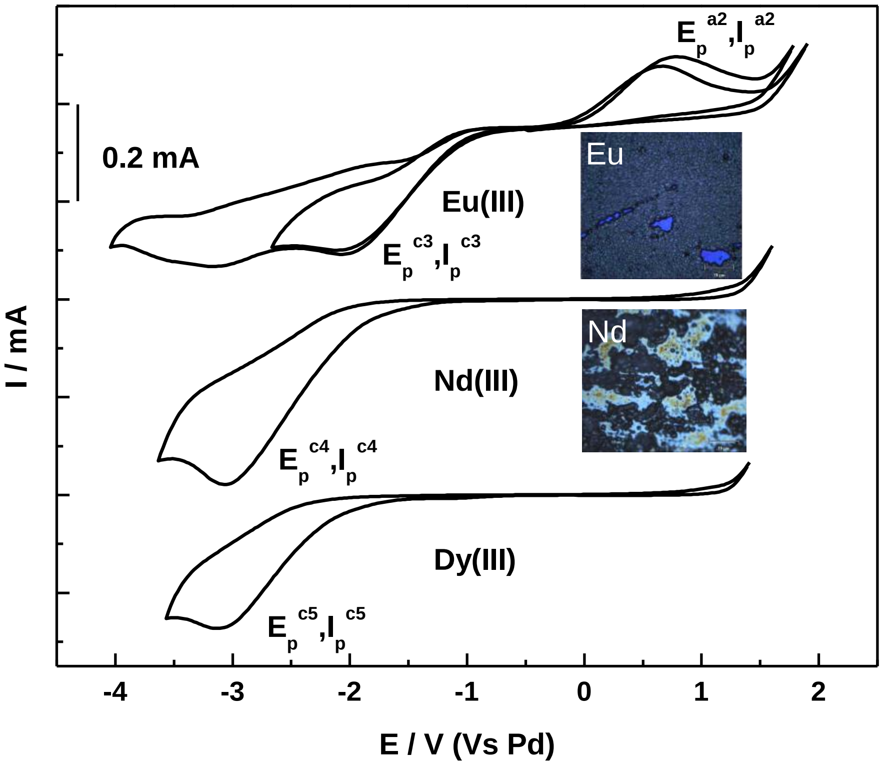

Figure 6.12. CV pertaining to 100 mM $Ln(NTf_2)_3$ in DHOA medium recorded at a glassy carbon working electrode at a scan rate of 50 mVps at 353 K. Insert shows the surface morphology of the electrodeposits obtained at the working electrode after electrolysis of 100 mM Ln^{3+} in NLIL at -3 V for about 2 hours.

It should be noted that trivalent lanthanides and actinides are known to undergo a single step reduction to the respective metals in different ILs. A similar mechanism was reported by Matsumiya [26] for the reduction of Ln^{3+} in phosphonium IL containing tri-n-butylphosphate as ligand. Bagri *et al.* [28] also proposed a similar mechanism for the reduction of rare earth metal ions co-ordinated to tri-methylphosphate based NLIL, in the absence of any supporting IL. The inset in figure 6.12 shows the photograph of the electrodeposit adhering onto the working electrode obtained after electrolysis of NLIL containing Eu^{2+} (100 mM) and Nd^{3+} (100 mM) at -3.0 V (Vs Pd) for about 2 h.

The diffusion coefficients of $[Ln(DHOA)_3]^{3+}$ could be determined by recording the CV pertaing to the NLIL containing Eu^{3+}, Nd^{3+} and Dy^{3+} and by using Berzin-Delahay equation for the soluble-soluble (for Eu^{3+}) and soluble-insoluble systems. Since Eu^{3+} present in the NLIL undergoes reduction to Eu^{2+}, which is also soluble in NLIL, the equation corresponding to soluble-soluble systems was employed. However, for Nd^{3+} and Dy^{3+} ions soluble-insoluble system was used in order to determine the diffusion coefficient. The relation between the cathodic peak current and diffusion coefficient for Eu^{3+} and for Nd^{3+} and Dy^{3+} are shown in equation (A.5) (Annexure) [18]. It should be noted that the cathodic peak current I_p^{c2} was utilised in equation 2.5 for Eu^{3+}, and I_p^{c4} and I_p^{c5} were employed for Nd^{3+} and Dy^{3+} respectively in equation (2.5). The surface area of the glassy carbon electrode was 0.16 cm^2 and the concentration of Ln(III) present in NLIL was ~ 100 mM.

Figure 6.13 shows the CV pertaining to of Eu^{3+}, Nd^{3+} and Dy^{3+} in NLIL systems recorded at different scan rates at a glassy carbon electrode at 353 K. It is seen that the in all these cases the cathodic peak current (I_p^c) increases with the scan rate and the cathodic peak potential (E_p^c) gets shifted cathodically. This shows that the reduction of Ln^{3+} in NLIL at a glassy carbon electrode is electrochemically irreversible, indicating that the reduction of Ln^{3+} is not only controlled by the diffusion of $[Ln(DHOA)_3]^{3+}$ at the working electrode but also by the rate of the electron transfer occurring across the electrode-electrolyte interface. The irreversibility factor (αn_α) is a measure of the symmetry barrier at the electrode-electrolyte interface for the electron transfer reaction. The magnitude of αn_α determined from equation (A.4) (Annexure) [31] was substituted in equation (2.5) in order to determine the diffusion coefficient of lanthanides.

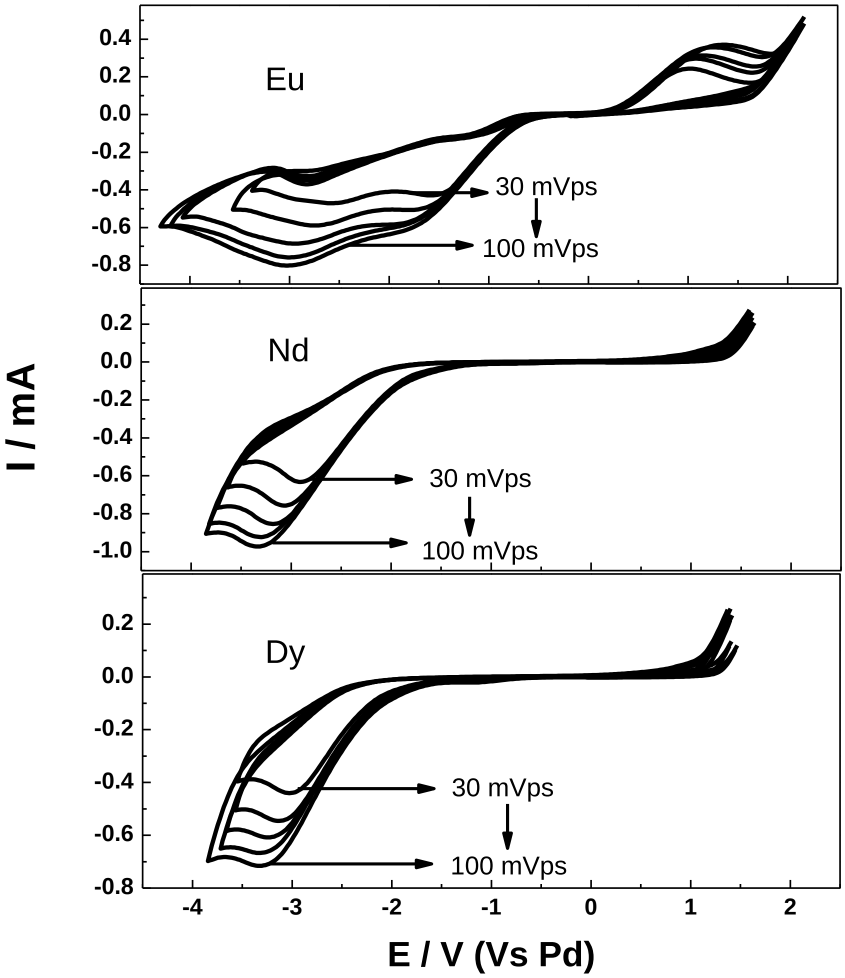

Figure 6.13. CV pertaining to 100 mM Ln$(NTf_2)_3$ in DHOA recorded as a function of scan rate at a glassy carbon working electrode at 353 K.

Figure 6.14 shows a plot of the cathodic peak current as a functionof the square root of the scan rate ($\upsilon^{1/2}$) for $[Ln(DHOA)_3]^{3+}$ at 353 K. It is seen that the dependence of the cathodic peak current on the square root of the scan rate is linear indicating the validity of equation (2.5), and from the slope of the straight line, the value of diffusion coefficient of $[Ln(DHOA)_3]^{3+}$ was determined. These diffusion coefficient of $[Ln(DHOA)_3]^{3+}$ containing Nd^{3+}, Dy^{3+} and Eu^{3+} determined at 353 K are tabulated in table 6.4. The values are in good agreement with the values reported in the literature for similar systems. A similar CV was recorded at different temperatures and the value of the diffusion coefficients obtained at different temperatures has also been tabulated in table 6.4. It is seen that the diffusion coefficient of $[Ln(DHOA)_3]^{3+}$ increases with the temperature of the system.

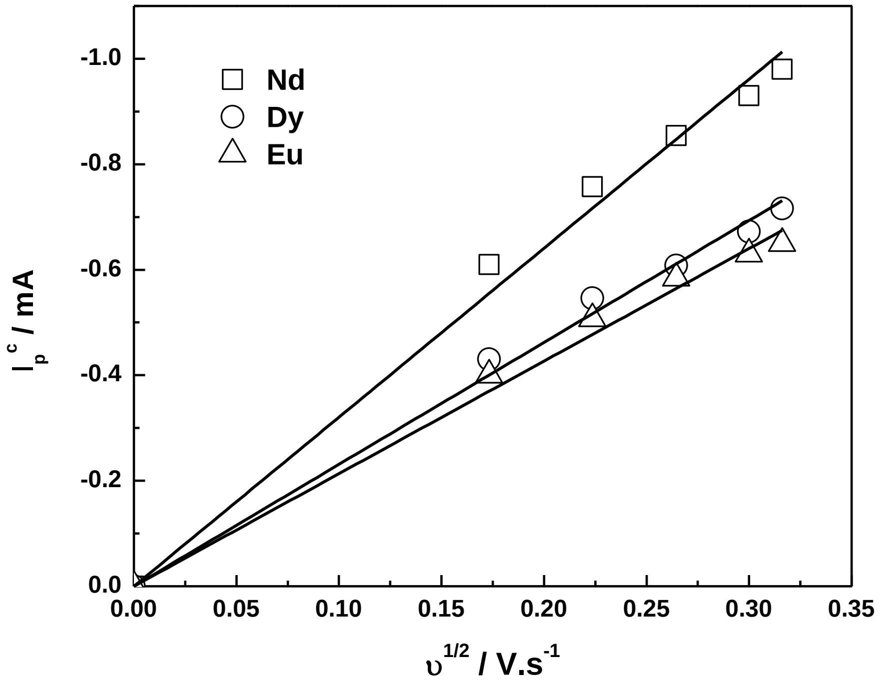

Figure 6.14. Dependence of the cathodic peak current (I_p^c) on the square root of scan rate ($\upsilon^{1/2}$) for the reduction of lanthanide ions from NLIL containing 100 mM $Ln(NTf_2)_3$ in DHOA at 353 K.

Table 6.4. Diffusion coefficients of $[Ln(DHOA)_3]^{3+}$ in NLIL at different temperatures.

Metal ion and concentration	Temperature / K	Diffusion coefficient (D x 10^8)/ $cm^2.s^{-1}$
Nd (0.105 M)	323	1.54
	333	1.93
	343	2.58
	353	3.76
Dy (0.094 M)	353	1.9
Eu (0.09 M)	353	2.3

6.2.1.2. Applications of NLILs

The NLIL seems to find a number of applications in reprocessing of spent nuclear fuels especially the spent metallic fuels. The presence of water in RTIL is the major issue in the electrodeposition of strongly electropositive metals such as lanthanides and actinides. Since the ligands employed in NLIL are strongly hydrophobic, the amount of water residue present in NLIL is significantly low as compared to that in the conventional RTILs used in the electrodeposition. Bagri *et al.* [28] reported that NLILs could be employed for electrorefining of metals. It was shown that Nd metal can be dissolved from the counter electrode (anode) in the NLIL containing trimethylphosphate (TMP) and $Nd(NTf_2)_3$ and the dissolved metal ion (Nd^{3+}) gets deposited as Nd matal at the working electrode (cathode). In addition to the eletrcorefining of metals, the oxides of rare earths could also be dissolved in DHOA…$HNTf_2$ adduct and the resultant NLIL could be employed for the electrodeposition of rare earths. For instance the dissolution of Nd_2O_3 in DHOA…$HNTf_2$ adduct, results in the formation of $[Nd(DHOA)_3]^{3+}[NTf_2]_3^-$. The NLIL formed was dried to remove water and excess $HNTf_2$ was removed by rotary evaporation and the product obtained was then subjected to spectroscopic and electrochemical studies. The FTIR spectrum of the dried NLIL is compared with the other FTIR spectra in figure

6.10. It is seen that the spectrum is quite similar to the FTIR spectrum of $[Nd(DHOA)_3]^{3+}$ $[(NTf_2)_3]^-$, which was prepared by dissolving $Nd(NTf_2)_3$ and DHOA. The 1640 cm^{-1} stretching band resulting from the amidic carbonyl stretching gets partially shifted to 1585 cm^{-1} upon dissolution of Nd_2O_3 in DHOA…$HNTf_2$ adduct.

The CV pertaining to the NLIL obtained after the dissolution of Eu_2O_3 and Nd_2O_3 in DHOA…$HNTf_2$ is shown in figure 6.15. This NLIL was dried at 343 K under vacuum in a rotary evaporator for more than 10 hours before recording the CV. The voltammogram of NLIL containing Eu^{3+} is characterized by a cathodic wave occurring at the potential of -1.2 V corresponding to the reduction of Eu^{3+} to Eu^{2+}, which is similar to that observed with $Eu(NTf_2)_3$ dissolved in DHOA (figure 6.12), followed by a continuous surge in the cathodic current beyond -3 V (Vs Pd), that is due to the reduction of Eu^{2+} to Eu. The CV pertaining to neat NLIL obtained after the dissolution of Nd_2O_3 also shows a continues surge in the cathodic current at -3 V (Vs Pd) due to the reduction of Nd^{3+} to Nd^0. Therefore, this study shows that NLIL containing rare earth metal ion could easily be prepared by dissolving Ln_2O_3 in DHOA…$HNTf_2$ adduct, and the rare earth metal ion could be reduced to the metal at -3 V (Vs Pd). In contrast to the wavy form of the cyclic voltammogram observed at -3 V for the NLIL prepared by reacting $Nd(NTf_2)_3$ in DHOA (figure 6.12), the wavy feature was not observed in the present case (figure 6.15). However, the reduction of lanthanide ions to the metal was found to occur at -3 V (Vs Pd) in both these cases.

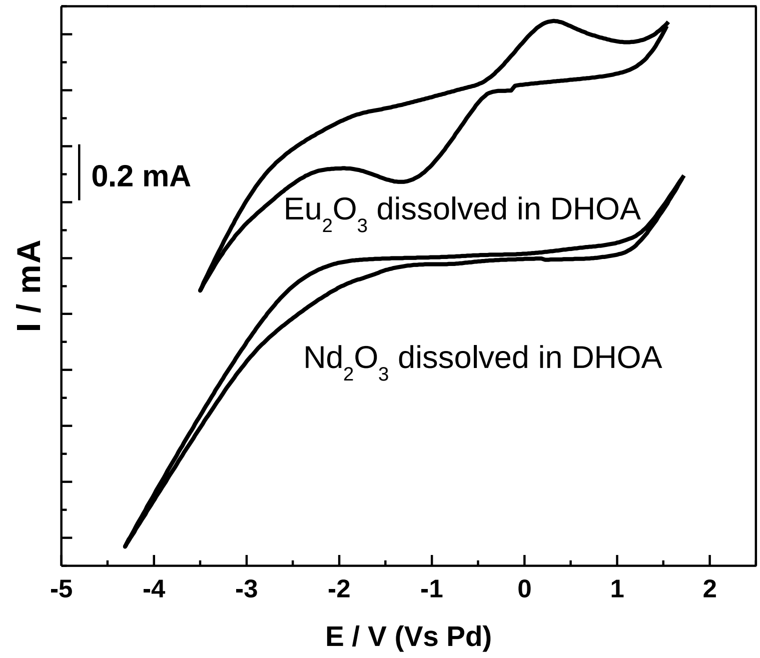

Figure 6.15. CV pertaining to Eu(III) and Nd(III) obtained after dissolution of Eu_2O_3 or Nd_2O_3 in DHOA…$HNTf_2$ recorded at a glassy carbon working electrode at a scan rate of 100 mVps at 323 K.

6.2.2. Conclusions

The NLILs containing rare earth ions were prepared by the dissolving of $Ln(NTf_2)_3$ (Ln = Eu, Nd, Dy) in DHOA. The added $Ln(NTf_2)_3$ was found to undergo facile dissolution in DHOA, resulting in the formation of the NLIL, $[Ln(DHOA)_3]^{3+}[(NTf_2)_3]^-$. The electrochemical behavior of Ln^{3+} present in this NLIL was investigated by CV. The CV pertaining to NLIL containing Eu^{3+} was characterized by a two step reduction to the metal with an Eu^{2+} intermediate. Whereas the NLILs containing Nd^{3+} and Dy^{3+} underwent a single step three electron transfer reduction to yield the metal. The stoichiometry of Ln(III) to DHOA in NLIL was determined to be 1 : 3, and the diffusion coefficient of the resultant complex $[Ln(DHOA)_3]^{3+}$ was found to be of the order 10^{-8} cm^2/s in the temperature range 323 to 353 K.

This study shows that NLILs could find many useful applications in the electrodeposition of lanthanides and actinides. Since the NLILs contain strongly hydrophobic ligands, they absorb minimal amount of water as compared to the conventional RTILs. Even though the ligands employed in these NLIL were strongly hydrophobic, still they dissolve significant quantity of metal salts as the solubility of the metal salts in the NLIL is governed by the ability of the ligand to coordinate. Since the NLILs containing metal salts themselves could act as an electrolyte, there is no need to look out for an IL for the electrodeposition of actinides and lanthanides. Apart from $Ln(NTf_2)_3$ salt, the oxides of lanthanides also easily dissolve in DHOA…$HNTf_2$ adduct, and the electrochemical investigation pertaining to the resultant NLIL showed the possibility of electrodepositing lanthanides as metals and demonstrated a new way for converting these oxides in to the corresponding metals.

References

1. X.Q. Sun, H.M. Luo, S. Dai, Ionic liquids-based extraction: a promising strategy for the advanced nuclear fuel cycle, Chem. Rev. 112 (2012) 2100-2128.
2. P.R. Vasudeva Rao, K.A. Venkatesan, A. Rout, T.G. Srinivasan, K. Nagarajan, Potential applications of room temperature ionic liquids for fission products and actinide separation, Sep. Sci. Technol. 47 (2012) 204-222.
3. P.K. Mohapatra, Actinide ion extraction using room temperature ionic liquids: opportunities and challenges for nuclear fuel cycle applications, Dalton Trans. 46 (2017) 1730-1747.
4. A. Rout, K.A. Venkatesan, T.G. Srinivasan, P.R. Vasudeva Rao, Tuning the extractive properties of purex solvent using room temperature ionic liquid, Sep. Sci. Technol. 48 (2013) 2576.
5. A. Rout, E.R. Souza, K. Binnemans, Solvent extraction of europium (III) to a fluorine-free ionic liquid phase with a diglycolamic acid extractant, RSC Adv. 4 (2014) 11899-11906.
6. M. Matsumiya, Y. Kikuchi, T. Yamada, S. Kawakami, Extraction of rare earth ions by tri-n-butylphosphate/phosphonium ionic liquids and the feasibility of recovery by direct electrodeposition, Sep. Purif. Technol. 130 (2014) 91-101.
7. Y. Pan, C.L. Hussey, Electrochemical and spectroscopic investigation of Ln^{3+} (Ln = Sm, Eu, and Yb) solvation in Bis(trifluoromethylsulfonyl)imide-based ionic liquids and coordination by TODGA and Chloride, Inorg. Chem. 52 (2013) 3241-3252.
8. R. Rama, A. Rout, K.A. Venkatesan, M.P. Antony, P.R. Vasudeva Rao, Electrochemical behavior of Eu(III) in imidazolium ionic liquid containing tri-*n*-butyl phosphate and N, N-dihexyloctanamide ligands, J. Electroanal. Chem. 757 (2015) 36-43.

9. R. Rama, A. Rout, K.A. Venkatesan, M.P. Antony, Effect of alkyl chain length of tri-n-alkyl phosphate extractants on the electrochemical behaviour of U(VI) in ionic liquid medium, J. Electroanal. Chem. 771 (2016) 87-93.

10. R. Rama, A. Rout, K.A. Venkatesan, M.P. Antony, Voltammetric studies on the complexing behaviour of Eu(III) with acidic extractants in 1-Butyl-1-methylpyrrolidinium Bis(trifluoromethanesulfonyl)imide, J. Electrochem. Soc. 163 (2016) 1113-1121.

11. R. Gupta, J. Gamare, K. Jayachandran, S.K. Gupta, K.V. Lohithakshan, J.V. Kamat, Electrochemical, thermodynamic and spectroscopic investigations of Ce(III) in a 1-Ethyl-3-methylimidazolium Ethyl Sulfate (EMIES) Ionic Liquid, Eur. J. Inorg. Chem. 26 (2015) 4396-4401.

12. W.L. Yuan, X. Yang, L. He, Y. Xue, S. Qin, G. H. Tao, Viscosity, conductivity and electrochemical properties of dicyanamide ionic liquids, Front. Chem. 6 (2018) 59.

13. S.A. Ansari, P.N. Pathak, P.K. Mohapatra, V.K. Manchanda, Chemistry of diglycolamides: promising extractants for actinide partitioning, Chem. Rev. 112 (2012) 1751-1772.

14. Y. Sasaki, Y. Sugo, S. Suzuki, S. Tachimori, Diglycolamide for the extraction of lanthanides and actinides in HNO_3-*n*-Dodecane system, Solvent Extr. Ion Exc. 19 (2001) 91-103.

15. Z. Zhu, Y. Sasaki, H. Suzuki, S. Suzuki, T. Kimura, Cumulative study on solvent extraction of elements by N,N,N′,N′-tetraoctyl-3-oxapentanediamide (TODGA) from nitric acid into n-dodecane, Anal. Chim. Acta 527 (2004) 163-168.

16. A. Rout, K.A. Venkatesan, M.P. Antony, P.R. Vasudeava Rao, Liquid–liquid extraction of americium (III) using a completely incenerable ionic liquid system, Sep. Purif. Technol. 158 (2016) 137-143.

17. P. Giridhar, K.A. Venkatesan, S. Subramaniam, T.G. Srinivasan, P.R. Vasudeva Rao, Extraction of uranium(VI) by 1.1 M tri-n-butylphosphate/ionic liquid and the feasibility of recovery by direct electrodeposition from organic phase, J. Alloys Compd. 448 (2008) 104-108.
18. A.J. Bard, L.R. Faulkner, Electrochemical Methods-Fundamentals and Applications, Wiley: New York, 1980.
19. K. Binnemans, Interpretation of europium(III) spectra, Coord. Chem. Rev. 295 (2015) 1–45.
20. J. G. Huddleston, A. E. Visser, W. M. Reichert, H. D. Willauer, G. A. Broker, R. D. Rogers, Characterization and comparison of hydrophilic and hydrophobic room temperature ionic liquids incorporating the imidazolium cation, Green Chem. 3 (2001) 156-164.
21. C. Gaillard, A. Chaumont, I. Billard, C. Hennig, A. Ouadi, S. Georg, G. Wipff, Competitive complexation of nitrates and chlorides to uranyl in a room temperature ionic liquid, Inorg. chem. 49 (2010) 6484-6494.
22. M. Yamagata, Y. Katayama, T. Miura, Electrochemical behavior of samarium, europium, and ytterbium in hydrophobic room-temperature molten salt systems, J. Electrochem. Soc. 153 (2006) E5-E9.
23. R. Nagaishi, M. Arisaka, T. Kimura, Y. Kitatsuji, Spectroscopic and electrochemical properties of europium (III) ion in hydrophobic ionic liquids under controlled condition of water content, J. alloys compd. 431 (2007) 221-225.
24. S. I. Nikitenko, C. Cannes, C. Le Naour, P. Moisy, D. Trubert, Spectroscopic and Electrochemical Studies of U(IV)−Hexachloro Complexes in Hydrophobic Room-Temperature Ionic Liquids [BuMeIm][Tf_2N] and [$MeBu_3N$][Tf_2N], Inorg. Chem. 44 (2005) 9497-9505.

25. C. J. Rao, K. A. Venkatesan, K. Nagarajan, T. G. Srinivasan, P. V. Rao, Electrodeposition of metallic uranium at near ambient conditions from room temperature ionic liquid, J. Nucl. Mater. 408 (2011) 25-29.

26. M. Matsumiya, Y. Kikuchi, T. Yamada, S. Kawakami, Extraction of rare earth ions by tri-n-butylphosphate/phosphonium ionic liquids and the feasibility of recovery by direct electrodeposition, Sep. Purif. Technol. 130 (2014) 91-101.

27. S. Murakami, M. Matsumiya, T. Yamada, K. Tsunashima, Extraction of Pr (III), Nd (III), and Dy (III) from HTFSA aqueous solution by TODGA/phosphonium-based ionic liquids, Solvent Extr. Ion Exc. 34 (2016) 172-187.

28. P. Bagri, H. Luo, I. Popovs, B. P. Thapaliya, J. Dehaudt, S. Dai, Trimethyl phosphate based neutral ligand room temperature ionic liquids for electrodeposition of rare earth elements, Electrochem. Commun. 96 (2018) 88-92.

29. A. I. Bhatt, I. May, V. A. Volkovich, D. Collison, M. Helliwell, I. B. Polovov, R. G. Lewin, Structural Characterization of a Lanthanum Bistriflimide Complex, La(N $(SO_2CF_3)_2)_3(H_2O)_3$, and an Investigation of La, Sm, and Eu Electrochemistry in a Room-Temperature Ionic Liquid, $[Me_3N^nBu][N(SO_2CF_3)_2]$, Inorg. chem. 44 (2005) 4934-4940.

30. Q. B. Zhang, C. Yang, Y .X. Hua, Y. Li, P. Dong, Electrochemical preparation of nanostructured lanthanum using lanthanum chloride as a precursor in 1-butyl-3-methylimidazolium dicyanamide ionic liquid, Phys. Chem. Chem. Phys. 17 (2015) 4701-4707.

31. K. Aoki, K. Tokuda, H. Matsuda, Theory of linear sweep voltammetry with finite diffusion space, J. Electroanal. Chem. Interfacial Electrochem. 146 (1983) 417-424.

Chapter 7: Summary, conclusions and scope of future work

In this chapter, the summary of the work discussed in the previous chapters and the scope of the future work are discussed.

7.1. Electrochemical reduction of UO_2^{2+} in ionic liquid medium

The oxide-electrowinning method involves the dissolution of spent oxide fuel in IL. During this process, the oxides of uranium, plutonium and fission products present in the spent nuclear fuel are converted to the corresponding oxychloride and chloride salts. Practical considerations of electrolysis demand the operation of cathodic reduction to be performed at high current density for quantitative recovery of uranium. Under such conditions, it is quite likely that the fission products present in the molten salt medium, albeit in low concentration, also undergo reduction or interfere in the electrochemical behaviour of UO_2^{2+}. In view of this, the electrochemical behaviour of UO_2^{2+} in 1-butyl-3-methylimidazolium chloride (C_4mimCl) IL in the presence of fission products such as palladium(II), ruthenium(III) and europium(III) was investigated by using cyclic voltammetry. These fission products were chosen for electrochemical interference studies since they are formed in significant concentration during fission reaction and their reduction potentials are very close to the reduction potential of UO_2^{2+} to UO_2. Since the dissolution of uranium oxide such as U_3O_8 was quite slow during chlorination, an attempt has been made to dissolve U_3O_8 in the IL, C_4mimCl, in the presence of a small quantity of nitric acid and the uranyl species present in the resultant solution was characterized by UV-Visible, ATR-FTIR and Raman spectroscopy. The electrochemical behaviour of UO_2^{2+} present in the resultant solution was studied at glassy carbon electrode by cyclic voltammetry and chronopotentiometry to understand the feasibility of using the resultant solution for the recovery of uranium oxide.

It was demonistrated that U_3O_8 could be dissolved in C_4mimCl only in the presence of a small amount of nitric acid (Table 3.3). The UO_2^{2+} ion present in the resultant solution forms a variety of complexes with both nitrate as well as chloride ions present in that medium. UV- Visible absorption spectra indicated that U(VI) could exist in the form of mixed complexes, $[UO_2Cl_x(NO_3)_{4-x}]^{2-}$, in the IL when the ratio of Cl : UO_2^{2+} is 4 : 1 or less. Beyond 4 : 1 mole ratio, the specie $[UO_2Cl_4]^{2-}$ dominates, as evidented by the splitting of the bands in the UV-Visible spectrum. The ATR-FTIR spectroscopic studies also indicated that the addition of Cl^- ion to uranyl nitrate sequentially leads to the substitution of nitrate ions by Cl^- ions. At a mole ratio of Cl^- : UO_2^{2+} 4 : 1 or above, the transmittance bands get shifted to 920 cm^{-1} indicating the formation of $[UO_2Cl_4]^{2-}$. All the spectroscopic studies including Raman spectroscopy clearly established the formation of $[UO_2Cl_4]^{2-}$ in the C_4mimCl solution.

The electrochemical behavior of $[UO_2Cl_4]^{2-}$ in the IL, C_4mimCl was investigated by CV and CP. The reduction of UO_2^{2+} to UO_2 occurred at a potential of -0.8 V (Vs Pd) and the redox reaction of the residual nitric acid present in the IL occurred at 0.1 V (Vs Pd). The diffusion coefficient of UO_2^{2+} in the dissolver solution was determined to be of the order of 10^{-8} cm^2/s and it was found to increase with temperature (Table 3.4). This study showed that $[UO_2Cl_4]^{2-}$ underwent a two electron transfer electrochemical reduction yeilding UO_2 at the working electrode.

The electrochemical behaviour of UO_2^{2+} in C_4mimCl was studied in the presence of Pd^{2+}, Eu^{3+} and Ru^{3+}. The cathodic wave pertaining to the reduction of UO_2^{2+} to UO_2 was shifted anodically in the presence of these metal ions (Table 3.2). Both Pd^{2+} and UO_2^{2+} underwent reduction at cathodic potentials quite close to that of their mixture whereas the cathodic potentials needed for the reduction of Eu^{3+} and Ru^{3+} were quite different than that pertaining to the reduction of UO_2^{2+} to UO_2. The apparent diffusion coefficients of UO_2^{2+}, Pd^{2+}, Eu^{3+}, Ru^{3+} in C_4mimCl and UO_2^{2+} in the presence of other metal ions were of the order 10^{-8} cm^2/s (Table 3.1). However, the presence of Pd^{2+} and Eu^{3+} was found to deminish the diffusion coefficient of UO_2^{2+} in a mixture. The diffusion coefficient of metal ions in their individual solutions increased in the following order: $Eu^{3+} < Ru^{3+} < Pd^{2+} < UO_2^{2+}$. The close proximity of these reduction potentials indicates that the presence of Pd^{2+}, Eu^{3+}, Ru^{3+} could reduce the current efficiency during the electrodeposition of uranium oxide from UO_2^{2+} in an IL.

7.2. Electrochemical behavior of uranium and spectroscopic investigation of uranyl species in IL

The electrochemical and spectroscopic studies on $UO_2(NO_3)_2$ in a hydrophobic IL, (C_4mimNTf$_2$) in the presence of tri-n-butyl phosphate, chloride and in dicyanamide based ILs (C_4mimDCA, C_4mPyDCA) have been investigated, for the first time.

The EXtraction-ELectrodeposition (EX-EL) approach has been proposed for the separation of the uranyl ion from nitric acid medium by a solvent phase containing tri-*n*-butyl phosphate (TBP) in IL, followed by electrodeposition of uranium oxide directly from the uranium(VI) extracted IL phase. However, the efficiency of electrodeposition was significantly low. To enhance the recovery or uranium oxide by electrodeposition, the electrochemical behaviour of $UO_2(NO_3)_2$ in a solution of TBP present in 1-butyl-3-methylimidazolium bis(trifluoromethylsulfonyl)imide (C_4mimNTf$_2$) IL was studied in the presence of chloride ion by adding C_4mimCl. It was expected that the presence of chloride ion in organic phase can decomplex uranyl ion (UO_2^{2+}) ion from TBP coordination, and favour underpotential reduction of UO_2^{2+}. The complexes formed in IL phase were characterized by UV-Visible, ATR-FTIR and Raman spectroscopy.

The voltammetric behaviour of $UO_2(NO_3)_2$ in a solution of TBP/C_4mimNTf$_2$ was quite complicated owing to the coordination of TBP with uranyl nitrate viz., $[UO_2(NO_3)_2(TBP)_2]$ in C_4mimNTf$_2$. The cathodic peak current density pertaining to the reduction of UO_2^{2+} to UO_2 in the presence of TBP was found to be quite low. In order to increase the current density and favour an underpotential reduction of UO_2^{2+}, C_4mimCl was added to the uranyl nitrate - TBP solution. The U : NO_3 : TBP : Cl mole ratio was varied from 1 : 2 : 2 : 1 to 1 : 2 : 2 : 6 in the IL. Addition of C_4mimCl to this IL increased the cathodic current density and favoured underpotential reduction of UO_2^{2+} to UO_2. The diffusion coefficient of UO_2^{2+} increased from 6.8 X 10^{-8} to 1.0 X 10^{-6} cm^2/s with the increase in mole ratio of U : NO_3 : TBP : Cl from 1 : 2 : 2 : 1 to 1 : 2 : 2 : 6 (Table 4.2), due to the conversion of the bulky and neutral $[UO_2(NO_3)_2(TBP)_2]$ complex into a smaller anionic complex like $[UO_2(NO_3)_2Cl]^-$, $[UO_2Cl_4]^{2-}$ etc..

In order to understand the electrochemical behavior of the uranyl ion observed in the presence of neutral and anionic ligands, the speciation of uranyl ion containing moities in the presence of NO_3^-, Cl and TBP was investigated by UV-Visible, ATR-FTIR and Raman spectroscopy. The visible absorption spectrum of uranyl nitrate in the presence of TBP showed that complexes containing the uranyl ion like $UO_2(NO_3)_2(TBP)_2$ existed in C_4mimNTf$_2$ in the absence of C_4mimCl. However, in the presence Cl^- ions, the uranyl nitrate gets transformed into different anionic complexes viz., $[UO_2Cl(NO_3)_2]^-$ or $[UO_2Cl_3(NO_3)]^{2-}$ or $[UO_2Cl_4]^{2-}$, depending upon the mole ratio of U : NO_3 : Cl. Since TBP is a neutral as well as weak ligand, it did not participate in the complexation with the anionic uranyl species. The ATR-FTIR spectroscopic studies also indicated that the addition of Cl^- ions to $UO_2(NO_3)_2(TBP)_2$ gradually lead to the substitustion of nitrate ions by Cl^- and displaces TBP from the coordination sphere of uranyl ions. When the mole ratio U : NO_3 : TBP : Cl was 1 : 2 : 2 : 4 or above (i.e., Cl^- is more), a major fraction of the uranyl ions existed in the form of $[UO_2Cl_4]^{2-}$ in the IL. Raman spectroscopic studies showed that majority of uranyl species existed as $[UO_2(NO_3)_2Cl]^-$ with residual $[UO_2(NO_3)_2(TBP)_2]$ at 1 : 2 : 2 : 1 mole ratio, whereas at 1 : 2 : 2 : 6 mole ratio the dominant uranium specie is $[UO_2Cl_4]^{2-}$. This study thus confirmed that the addition of Cl^- ion converted the bulky $[UO_2(NO_3)_2(TBP)_2]$ complex into a smaller $[UO_2Cl_4]^{2-}$ complex (Table 4.1). Since the reduction of this chlorocomplex resulted in the liberation of Cl_2 at the counter electrode, the reduction of UO_2^{2+} at the working electrode was more favored than the reduction of uranyl nitrate-TBP complex.

The solubility of uranyl nitrate in many ILs was invariably very low. For electrowinning applications, it was necessary to dissolve significant amount of uranium salt in IL that exhibits low viscosity also. In view of this, the dissolution of uranyl nitrate in IL containing dicyanamide anion was studied and the coordination and electrochemical behaviour of uranyl ion in IL was investigated by advanced spectroscopic and electrochemical techniques.

Similar to Cl^- ions, the dicyanamide ions were found to form efficient complex with uranyl ion. Moreover, the imidazolium and pyrrolidinium ILs containing dicyanamide anion, C_4mImDCA and C_4mPyDCA, displayed low viscosity (29 cP) and good solubility for uranium nitrate (~0.5 M). The coordination behaviour of dicyanamide anion with uranyl ion was characterized by Raman and FTIR spectroscopy (Table 4.3). A Raman band observed at 852 cm^{-1} and an IR band at 931 cm^{-1} in the case of uranyl nitrate present in C_4mImDCA and C_4mPyDCA was attributed to the U=O stretching frequency and the position of the band at 852 cm^{-1} in the Raman and 931 cm^{-1} in FTIR spectra showed that the DCA^- anion was coordinated to the uranyl ion. Coordination of DCA^-, liberated the nitrate ions from the coordination sphere of uranyl ion, as confirmed by the appearance of a Raman band at 1040 cm^{-1} that could be attributed to “free” nitrate ion.

The sequential substitution and linkage behaviour of DCA$^-$ in a solution of the latter with uranyl nitrate was investigated in C_4mImBF$_4$ IL at different mole ratios of uranium to DCA$^-$ (Table 4.4). The absence of the bands pertaining to symmetrical stretch of the “free nitrate” in the Raman spectrum in a mixture with DCA$^-$ to uranium mole ratio lower than 2 : 1 confirmed that DCA$^-$ was not acting as a bidentate ligand. Increasing the mole ratio of DCA$^-$ to uranium above 2 : 1 resulted in the substitution of nitrate ion by DCA$^-$ ion. The sequential substitution reaction by DCA$^-$ resulted in a change in the coordination of the nitrate ion from bidentate to monodentate, followed by the liberation of the latter into the IL. This sequence of reactions continued with an increase in the mole ratio of DCA$^-$ to uranium up to 4 : 1. At mole ratios above 4 : 1, a major fraction of uranyl ion in the IL seems to have been converted into the form $[UO_2(DCA)_4]^{2-}$. Therefore, the spectroscopic investigations revealed that UO_2^{2+} in C_4mImDCA and C_4mPyDCA existed as $[UO_2(DCA)_4]^{2-}$.

The electrochemical behaviour of UO_2^{2+} present in C_4mImDCA and C_4mPyDCA was studied at a glassy carbon working electrode. The CV of uranyl ion displayed a couple of cathodic and anodic waves in both these ILs. The cathodic peaks were attributed to a two step-one electron transfer reduction of UO_2^{2+} to UO_2^{+} and then to UO_2. The diffusion coefficient of UO_2^{2+} was found to be in the order 10^{-7} cm^2/s (Table 4.5), which is about an order of magnitude higher than those observed in other the ILs, plausibly due to the low viscosity offered by C_4mImDCA and C_4mPyDCA.

7.3. Studies related to electrorefining of uranium and zirconium in IL

The electrochemical behavior of Zr(IV) in C_4mImNTf$_2$ medium as well as the electrochemical behavior of U(IV) in the presence of Zr(IV) in C_4mPyNTf$_2$ were studied. These are relavent to the reprocessing of U-Pu-Zr ternary alloy fuels.

The metallic fuel in a nuclear reactor is composed of an alloy of uranium and zirconium (5-10 wt.%). Non-aqueous electrorefining method was employed for the reprocessing of spent nuclear fuel in molten salt medium. In electrorefining process, U-Zr alloy was anodically dissolved into electrolytic medium and the uranium was recovered as metal on the cathode material from zirconium and fission products. To understand the feasibility of using ILs for reprocessing of spent metallic fuels, the anodic dissolution of U and Zr metals and electrochemical behaviour of U(IV) and Zr(IV) was studied in the room temperature ILs such as $C_4mPyNTf_2$ and $C_4mimNTf_2$.

The electrochemical behaviour of Zr(IV) in $C_4mimNTf_2$ was studied by CV, chronoamperometry and chronopotentiometry. The CV pertaining to Zr(IV) in $C_4mimNTf_2$ consisted of a couple of cathodic and anodic waves. A feable cathodic wave observed at the potential of +0.2 V (Vs Pd) was probably due to the reduction of Zr(IV) to Zr(II) and a prominent reduction wave observed at an onset potential of -1.3 V (Vs Pd) could be ascribed to the reduction of Zr(II) to Zr(0). The diffusion coefficient of Zr(IV) in $C_4mimNTf_2$ enumerated from the first cathodic wave was found to be 10^{-10} cm^2/s (Table 5.1). However, a five order increase in the value of the diffusion coefficient (10^{-5} cm^2/s) was observed after the onset of nucleation at -1.6 V (Vs Pd) (Table 5.2). The nucleation loop observed at -1.6 V was studied in detail by chronoamperometry. Among the different models, the nucleation growth and decay of the chronocurrent transient could be best described with an instantaneous nucleation model. The nucleation phenomenon also influenced the nature of chronopotentiogram of Zr(IV) especially in the early part of the transient. This study revealed that Zr(IV) in $C_4mimNTf_2$ underwent a two-step two-electron transfer yeilding zirconium metal at the working electrode.

The electrochemical behaviour of U(IV) and Zr(IV) was studied in $C_4MPyNTf_2$ to understand the feasibility of using $C_4MPyNTf_2$ for electrorefining application of spent metallic fuels. The anodic dissolution of metallic U and Zr was insignificant in $C_4MPyNTf_2$. However, the dissolution was facilitated by adding $HNTf_2$. Dissolution of U and Zr results in the formation of $U(NTf_2)_4$ and $Zr(NTf_2)_4$ complexes in $C_4MPyNTf_2$. Since NTf_2^- is a weakly co-ordinating anion, the electrochemical behaviour of U(IV) at a glassy carbon working electrode was a bit complex. However, the reduction of U(IV) to metallic form occurred at -3.2 V, possibly through the reduction of U(IV) to U(III) at still lower cathodic potentials. The reduction of zirconium occurs at -1.5 V, which was about 1.7 V more anodic as compared to the potential at which uranium could be deposited. This shows that zirconium needs to be removed from $C_4MPyNTf_2$ medium prior to the recovery of uranium and the same could be accomplished easily. Nevertheless, this study also showed that RTILs such as $C_4MPyNTf_2$ are promising candidates for the electrodeposition of uranium and electrorefining of metallic fuels. However, more studies, viz., investigations at higher concentrations of U(IV), studies in the presence of fission products, radiation stability etc., are necessary in order to evaluate the suitability of ILs for spent metallic fuel reprocessing applications.

7.4. Electrochemical behavior of lanthanides in IL in presence of an organic ligand

The electrochemical behavior of Eu(III) in $C_4mimNTf_2$ in the presence and absence of T2EHDGA and in the neutral ligand-IL containing DHOA and $Ln(NTf_2)_3$ were investigated.

The solubility of lanthanide salts was very low in hydrophobic IL medium. It is necessary to enhance the solubility of rare earth metals, the IL containing lanthanide specific ligands and neutral ligand-ionic liquid were prepared and electrochemical and coordination behaviour of lanthanide salts present in those ILs was investigated by voltammetry and FTIR spectroscopy.

The electrochemical behavior of Eu(III) in [C_4mim][NTf_2] was studied at a glassy carbon working electrode both in the presence and absence T2EHDGA by using CV. The CV pertaining to Eu(III) exhibited a quasi-reversible redox couple in the potential range -1 V to +1 V. The addition of T2EHDGA to the Eu(III)/[C_4mim][NTf_2] solution lowered the cathodic peak current and shifted the cathodic peak potential cathodically due to the co-ordination of Eu(III) with T2EHDGA. A lower cathodic peak current observed in the presence of T2EHDGA was due to the aggregation of Eu(III)- T2EHDGA complex in the IL. The diffusion coefficient of Eu(III) was determined at different temperatures and was found to be in the order of ~10^{-8} cm^2/s (Table 6.1). In the presence of a ligand, the diffusion coefficients decreased in the following order: Eu(III) - [C_4mim][NTf_2] > Eu(III) in T2EHDGA/[C_4mim][NTf_2]. Similarly, the charge transfer rate constant (k_s) was determined to have a value of about ~10^{-4} cm/s (Table 6.2), and the presence of T2EHDGA in the IL decreased the k_s values as compared to the neat [C_4mim][NTf_2]. An increase in the temperature of the system enhanced the diffusion coefficient as well as the value of k_s. The activation energy was evaluated to be less in the case of Eu(III) in T2EHDGA/[C_4mim][NTf_2] (26 KJ/mol) as compared to that of Eu(III) in [C_4mim][NTf_2] (50 KJ/mol) (Table 6.3). Luminescence spectroscopy and DLS studies confirmed the fact that the complex environment gets modified and aggregation gets enhanced upon adding T2EHDGA.

The NLILs containing rare earth ions were prepared by the dissolving of $Ln(NTf_2)_3$ (Ln = Eu, Nd, Dy) in DHOA. The added $Ln(NTf_2)_3$ was found to undergo facile dissolution in DHOA, resulting in the formation of the NLIL, $[Ln(DHOA)_3]^{3+}[(NTf_2)_3]^{-}$. The electrochemical behavior of Ln^{3+} present in this NLIL was investigated by CV. The CV pertaining to NLIL containing Eu^{3+} was characterized by a two step reduction to the metal with an Eu^{2+} intermediate. Whereas the NLILs containing

Nd^{3+} and Dy^{3+} underwent a single step three electron transfer reduction to yield the metal. The stoichiometry of Ln(III) to DHOA in NLIL was determined to be 1 : 3, and the diffusion coefficient of the resultant complex $[Ln(DHOA)_3]^{3+}$ was found to be of the order 10^{-8} cm^2/s in the temperature range 323 to 353 K (Table 6.4).

This study shows that NLILs could find many useful applications in the electrodeposition of lanthanides and actinides. Since the NLILs contain strongly hydrophobic ligands, they absorb minimal amount of water as compared to the conventional RTILs. Even though the ligands employed in these NLIL were strongly hydrophobic, still they dissolve significant quantity of metal salts as the solubility of the metal salts in the NLIL is governed by the ability of the ligand to coordinate. Since the NLILs containing metal salts themselves could act as an electrolyte, there is not need to look out for an IL for the electrodeposition of actinides and lanthanides. Apart from $Ln(NTf_2)_3$ salt, the oxides of lanthanides also easily dissolve in DHOA…$HNTf_2$ adduct, and the electrochemical investigation pertaining to the resultant NLIL showed the possibility of electrodepositing lanthanides as metals and demonstrated a new way for converting these oxides in to the corresponding metals.

7.5. Scope of the future work

In this thesis, RTILs have been studied for electrochemical applications of RTILs as electrolytic medium and the results indicate that RTILs are promising candidates for the non-aqueous reprocessing of spent nuclear fuels. Though these new results hold great promise, some more studies need to be done in order to develop a robust technology based on RTIL medium. These include;

(i) The interference of fission products (other than those investigated in this study) dissolved during the chlorination reaction also needs to be investigated during the recovery of UO_2 by electrowinning.

(ii) It is necessary to investigate the electrochemical properties of other ligands such as DHOA and diglycolamides which were also used for reprocessing applications, to identify the suitable ligands to EX-EL process (The process of Extraction-Electrodeposition (EX-EL) has been applied for some metal ions only. The electrochemical behaviour of U(VI) was established with some anions and neutral ligand (TBP) in the present work).

(iii) The solubility of metal salts in mest or the hydrophobic ILs is invariably low. Even though DCA^- anion was found to enhance the solubility of uranyl ion to a significant extent, more studies has to be carried out to enhance the solubility of metal salts in the IL further, by using judicial combination of cation and anion and strongly coordinating neutral ligands.

(iv) The studies related to electrorefining have been introduced in the present work by dissolving uranium and zirconium metals and carrying out voltammetric investigation on the resultant solutions. Studies need to be carried out to dissolve higher amounts of uranium and electrochemical recovery of the uranium from zirconium and fission products using IL as an electrolytic medium is necessary in the actual applications.

(v) The electrochemical behaviour of Eu(III) was studied in the presence of T2EHDGA in the present work. It is better to study the dissolution and electrochemical behaviour of Eu(III) in the presence of other extractants in an IL for electrodeposition of Eu.

(vi) The suitability of NLIL containing La^{3+} and DHOA as an electrolytic medium has been investigated in this study. The solubility of lanthanide/actinide salts has to be checked in some other neutral ligands having good ligating ability and electrochemical stability. Moreover, electrochemical studies need to be carried out for electrodeposition of metals by using neutral ligands as electrolytic medium.

Annexure

A. Electroanalytical techniques

Electrochemical transient techniques are used to evaluate the momentary behavior of the analyte at the electrode-electrolyte interface after a small perturbation from its equilibrium position in an electrochemical system [1]. These include polarography, voltammetry (potentiostatic and galvanostatic) etc. The techniques used in this work have been described below.

A.1. Voltammetry

Voltammetric techniques are among the mostly used electrochemical transient techniques to study the behaviour of the analyte at an electrode-electrolyte interface. Mostly an electrochemical cell consisting of three electrodes (working electrode, counter electrode and reference electrode) is used in voltammetric techniques [2, 3]. The electrode at which the redox process of interest occurs is called as the working electrode. The working electrode provides the interface across which a charge can be transferred or its effects felt. Generally, the electrode may be made of metal or non-metal which conducts electrons. Commonly used working electrodes are glassy carbon rod, platinum, graphite rod, tungsten wires etc. The electrolyte could be a liquid containing ions or solid. The electrolyte is an ionic conductor and the electrodes are electronic conductors.

The potential and the current of the system are monitored across the working electrode and the current carrying electrode in the cell is the counter/auxiliary electrode at which the counter reaction (counter reaction to the reaction occurring at working electrode) takes place. The potential of the working electrode is monitored against the third electrode, called the reference electrode which carries no current. The reference electrode should pose a constant potential over a time and it should be reversible. In general, a standard hydrogen electrode, calomel electrode, Ag/Ag^+ and quasi-reference electrodes such as Ag or Pd wire are used as reference electrodes in both aqueous and non-aqueous electrolyte solutions. These voltammetric techniques are generally classified as potentiostatic and galvanostatic techniques [2, 3].

In potentiostatic technique, the potential of the system is controlled and the current response is measured, and in galvanostatic technique, the current of the system is controlled and the potential response is measured. Electroanalytical techniques are further categorized into sweep (potential) and step (for both and current) techniques according to the mode of imposition of potential/current. Sweep techniques involve continuous scanning of the potential applied at the working electrode from one potential to another. Voltammetric methods such as linear sweep voltammetry and cyclic voltammetry are sweep techniques. In step techniques, the potential or current is varied in a predetermined manner with time.

A.1.1. Cyclic voltammetry

Cyclic voltammetry (CV) is very often used technique because it offers insight into both the kinetic and thermodynamic details of many chemical systems [4]. It is the most versatile electroanalytical technique for the determining the electrochemical behaviour of electroactive species and mechanism involved in an electrochemical reaction [5]. In this technique, the potential of the working electrode with respect to the standard reference electrode is monitored by potentiostat and the current of the system is measured between working and counter electrodes. The potential of the working electrode is scanned from an initial point (where there is no faradaic process) to a specified final point and then switched back to other side of potential and then swept to the initial point. The potential of the working electrode is changed with time at some particular rate called the sweep rate or scan rate and denoted by υ. It has the units of volts per second, $V.s^{-1}$.

The response of the system is obtained in the form of a plot of current (Y-axis) versus applied potential (X-axis) called cyclic voltammogram (figure A.1). In the convention used in this thesis, cathodic currents are taken as negative and positive potentials are plotted to the right. In a typical CV experiment, the potential of the working electrode is continuously scanned from initial value to final value at a defined scan rate. The scan is started at a potential where no electrochemical reaction takes place (no current) and scanned to a region where electrochemical oxidation or reduction takes place.

It can be seen that from the figure A.1, no current flows at initial potential (E_i) where no faradaic electrochemical process occurs. If the potential is scanned in the cathodic direction (negative direction), reduction takes place at the electrode since according to the Nernst equation (equation A.1) product (R) formed towards negative potentials.

$$E = E^o + \left(\frac{RT}{nF}\right) ln \frac{C_O}{C_R} \qquad \text{(A.1)}$$

where C_R and C_O are concentrations of reduced and oxidized forms respectively. When the potential is scanned further, at E_{Onset}, the current starts increasing where the faradaic process (reduction) starts occurring and the ‘O’ (electroactive species) start to diffuse from bulk of the electrolyte to the electrode to compensate for the concentration drop at the electrode. Further scanning of the potential to more negative potentials leads to the maximum current, i_p (peak), where the concentration of ‘O’ species at electrode surface falls to zero and the current decays further as controlled by diffusion of ‘O’ from further layers. Similarly, if the potential is scanned in the anodic direction (positive direction) from the switching potential (E_λ), oxidation reaction occurs at the electrode.

The unique parameters associated with cyclic voltammogram

A typical cyclic voltammogram for a redox process is shown in figure A.1. The important characteristics of the voltammogram, which will be used in the analysis of the redox process, are given below [2, 3].

$\mathbf{E_p^c}$ = Cathodic peak potential (reduction); $\mathbf{E_p^a}$ = Anodic peak potential (oxidation)

$\mathbf{i_p^c}$ = Cathodic peak current; $\mathbf{i_p^c}$ = Anodic peak current

$\mathbf{E_{p/2}}$ = Half peak potential (the potential where the i_p is $i_{p/2}$)

$\mathbf{E_\lambda}$= Switching potential; $\mathbf{E_{1/2}}$ = half wave potential; $\mathbf{E_p} - \mathbf{E_{p/2}}$ is width of the peak

$\mathbf{E_{1/2}}$ = half wave potential = $\frac{E_p^{Red}+E_p^{Ox}}{2} = E^O$

Based on the comprehensive analysis of the cyclic voltammetry, the reversibility of the electrochemical processes can be judged as discussed below [2, 3, 6, 7].

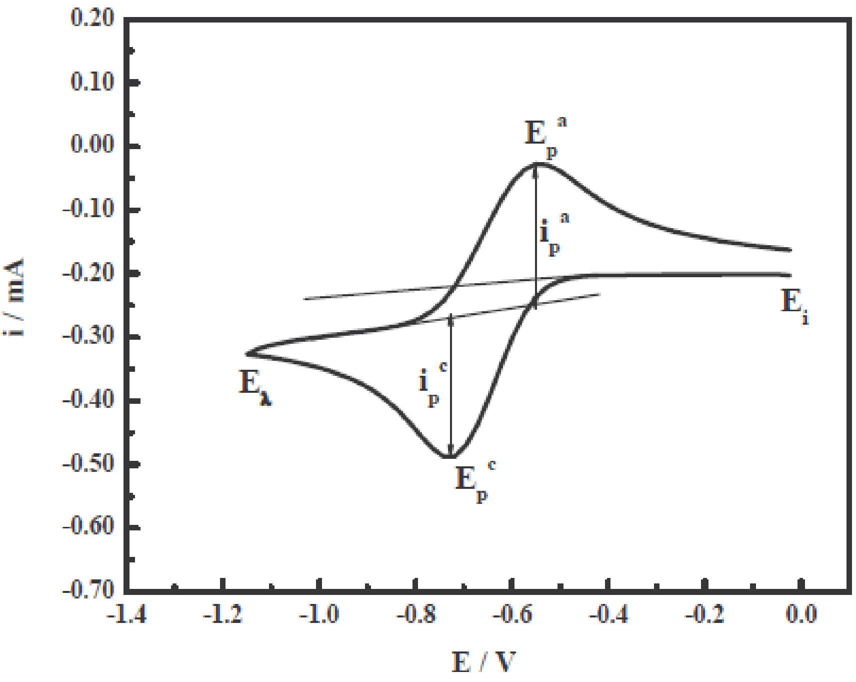

Fig. A.1. A typical cyclic voltammogram of redox couple

Reversible process

In reversible process, the rate of electrochemical reaction is controlled by diffusion (mass transfer) but not by charge transfer kinetics. In this process, the mass transfer is slow so it is the rate determining step and the charge transfer is rapid. The main criterion for a reversible charge transfer process is that peak potentials are independent of scan rate (υ) and the peak separation is given by equation A.2.

$$E_p^c - E_p^a = 2.29\frac{RT}{nF} \qquad \text{(A.2)}$$

The peak current is given by Randles-Sevcik [2].

$$i_\mathrm{p} = 0.4463\mathrm{nFC_OA}\upsilon^{\frac{1}{2}}\mathrm{D}_\mathrm{O}^{\frac{1}{2}}\left(\frac{\mathrm{nF}}{\mathrm{RT}}\right)^{\frac{1}{2}} \qquad \text{(A.3)}$$

where n is the number of electrons involved in the charge transfer reaction, F is the Faraday constant (96485.3 Coulombs/mol), C_O is the bulk concentration of electro-active substance (mol.cm^{-3}), A is area of the electrode (cm^2), R is the gas constant, T is the absolute temperature (K), υ is the scan rate (V.s^{-1}) and D_O is the diffusion coefficient (cm^2.s^{-1}) of ‘O’.

Irreversible process

In irreversible process, the rate of the redox process is mostly controlled by charge transfer kinetics and the important criterion of the irreversible charge transfer kinetics is the shift in the peak potential with scan rate. The peak separation (E_p^c - E_p^a) is very large and sometimes the reverse peak (oxidation peak) cannot be seen in the scan reversal of the cyclic voltammogram. The wave shape is determined by charge transfer coefficient (α), which is a measure of the symmetry of the energy barrier and is independent of scan rate. For the irreversible process the following equations can be used to deduce the important parameters using cyclic voltammetry.

$$\left|E_p^c - E_{P/2}^c\right| = \frac{1.857\,RT}{\alpha n_\alpha F} \qquad (\mathrm{A.4})$$

Charge transfer coefficient value is in the range of $0.1 \geq \alpha \geq 0.9$. Equation A.5 shows the current equation used in irreversible processes for soluble-soluble or soluble-insoluble redox process [2].

$$i_\mathrm{p} = 0.496\mathrm{nFC_OAD_O^{\frac{1}{2}}}\left(\frac{(\alpha \mathrm{n}_\alpha)\mathrm{F}\upsilon}{\mathrm{RT}}\right)^{\frac{1}{2}} \quad \text{or } i_p = 0.6105\mathrm{AC(nF)}^{\frac{3}{2}}\left(\frac{\mathrm{D}\upsilon}{\mathrm{RT}}\right)^{1/2} \qquad (\mathrm{A.5})$$

Quasi-reversible process

The process in which the rate of the electrochemical reaction is controlled by both diffusion and charge transfer kinetics is known as quasi-reversible process where the peak potential shifts with scan rate and the peak shape visually broadens as scan rate is increased. Similarly, the peak separation (ΔE_p) increases with scan rate and the average of the peak potentials ($(E_p^a + E_p^c) / 2$) is constant at different scan rates. Heterogeneous charge transfer coefficient, k_s, can be obtained by using the following equation which was proposed by Klingler and Kochi [3, 8].

$$k_s = 2.18\left[D_O(\alpha n_\alpha)\frac{\upsilon F}{RT}\right]^{1/2} \exp\left[\frac{\alpha^2 nF}{RT}\left(E_p^c - E_p^a\right)\right] \qquad (A.6)$$

Depending upon the value of k_s the electrode reaction can be categorized [2] as, reversible when $k_s \geq 0.3\ \upsilon^{1/2}$ cm.s^{-1}, quasi-reversible when $0.3\ \upsilon^{1/2} \geq k_s \geq 2 \times 10^{-5}\ \upsilon^{1/2}$ cm.s^{-1} and irreversible when $k_s \leq 2 \times 10^{-5}\ \upsilon^{1/2}$ cm.s^{-1}.

A.2. Chronopotentiometry (galvanostatic technique)

In this technique, the controlled current is applied between at the working electrode through counter electrode and the potential of the working electrode with respect to reference electrode is simultaneously monitored/measured as a function of time. The potential verses time will be plotted as response and the resulting plot is called as chronopotentiogram. When the controlled current is applied between the working and counter electrodes, the concentration of the analyte ion start decays and the potential of the working electrode changes. This process continues until the concentration of the analyte ion at the working electrode becomes zero. The time required for this potential change or the concentration change of the analyte ion is called as the transition time and is denoted by τ [9]. The relation between the applied current and transition time is derived by Sand [2, 3] and is shown in equation A.7.

$$i\tau^{1/2} = \frac{\mathrm{nFAD_O^{1/2}\pi^{1/2}C}}{2} \qquad (\mathrm{A.7})$$

The experimentally obtained value of τ at a particular i, can be used to calculate the diffusion coefficient (Do) using the above Sand's equation (equation A.7).

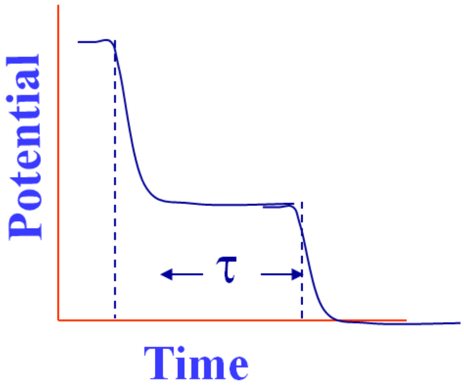

Fig. A.2. The measured response of potential verses t at constant applied current (chronopotentiogram).

A.3. Chronoamperometry (potentiostatic technique)

Chronoamperometry is the potential step technique in which constant potential step is applied to the working electrode and current is measured as a function of time [2, 10]. The instantaneous current obtained is given by the Cottrell equation (equation A.8) [2, 3]. The Cottrell plot of i Vs $t^{-1/2}$ is linear with zero intercept and it allows the conclusion of the simple diffusion controlled process and from the slope of the plot, diffusion coefficient, Do can be calculated.

$$i = \frac{\mathrm{nFAD_O^{1/2}C}}{(\pi \mathrm{t})^{1/2}} \qquad (\mathrm{A.8})$$

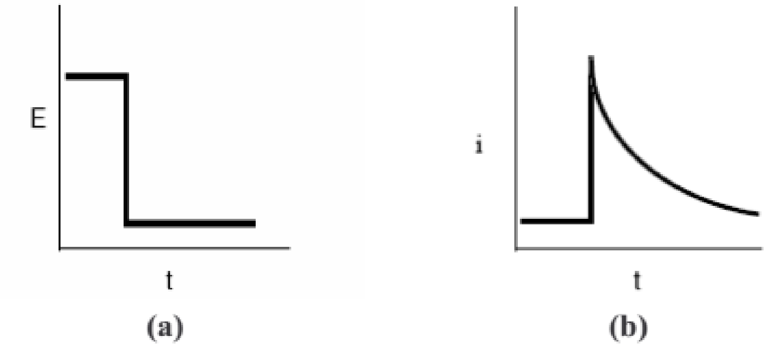

(a) (b)

Fig. A.3. (a) The constant potential step applied to system and (b) the measured response of i verses t (chronoamperogram)

References

1. M. Donald, Transient techniques in electrochemistry, Plenum Press, New York (1977).
2. A.J. Bard and L.R. Faulkner, Electrochemical Methods-Fundamentals and Applications, Wiley, New York, 1980.
3. E.R. Brown, J.R. Sandifer, Cyclic voltammetry AC polorography and Related Techniques, in: B.W. Rossiter, J.F. Hamilton (Eds.), Physical Methods of Chemistry-Volume II, Electrochemical Methods, Wiley, New York, 1986.
4. F. Scholz, Electroanalytical methods: Guide to Experiments and Applications, 1st Edition, Springer, Berlin, 2005.
5. P.T. Kissinger, W.R. Heineman, Cyclic voltammetry, J. Chem. Ed. 60 (1983) 702-706.
6. R.S. Nicholson, Semiempirical Procedure for Measuring with Stationary Electrode Polarography Rates of Chemical Reactions Involving the Product of Electron Transfer. Anal. Chem. 38 (1966) 1406-1406.
7. C.H. Bamford, C.F.H. Tipper, R.G. Compton (Eds.), Electrode Kinetics: Principles and Methodology (Vol. 26). Elsevier (1986).
8. R.J. Klingler, J.K. Kochi, Electron-transfer kinetics from cyclic voltammetry, Quantitative description of electrochemical reversibility, J. Phys. Chem. 85, no. 12 (1981) 1731-1741.
9. M. Paunovic, Chronopotentiometry, J. Electroanal. Chem. Interfacial Electrochem. 14 (1967) 447-447.
10. P. Delahay, New instrumental methods in electrochemistry: Theory, instrumentation and application to analytical and physical chemistry, Interscience, New York (1954).

Abbreviations

Abbreviations	**Full Name**
AHWR	Advance heavy water reactor
Aliquat 336	Tri-*n*-octylmethylammonium chloride
An	Actinide
ATR-FTIR	Attenuated total reflectance-Fourier transform infrared
BF$_4$	Tetrafluoroborate
BWR	Boiling Water Reactor
CMPO	*n*-Octyl(phenyl)-N,N-diisobutylcarbamoylmethyphosphine oxide
[C$_4$mim][NTf$_2$]	1-Butyl-3-methylimidazolium bis(trifluoromethanesulfonyl)imide
[C$_4$mim]Cl	1-Butyl-3-methylimidazolium chloride
[C$_4$mim] DCA	1-Butyl-3-methylimidazolium dicyanamide
[C$_4$mim][BF$_4$]	1-Butyl-3-methylimidazolium tetrafluoroborate
[C$_4$mpip][NTf$_2$]	1-Butyl-1-methylpiperidinium bis(trifluoromethanesulfonyl)imide
[C$_4$mpy][NTf$_2$]	1-Butyl-1-methylpyrrolidinium bis(trifluoromethanesulfonyl)imide
[C$_4$mpy]Cl	1-Butyl-1-methylpyrrolidinium chloride
[C$_4$mpy] DCA	1-Butyl-1-methylpyrrolidinium dicyanamide
CA	Chronoamperometry
CP	Chronopotentiometry
CV	Cyclic voltammetry
DCH18C6	Di-cyclohexano-18–crown 6
DCM	Dichloromethane
DGA	Diglycolamide
DLS	Dynamic light scattering
DHOA	*N*,*N*-Dihexyloctanamide
EDTA	Bis(ethylenediamine)tetraacetic acid
EX-EL	Extraction-Electrodeposition
FBTR	Fast breeder test reactor
FILs	Functionalized ionic liquids
FP	Fission product
HbetNTf$_2$	Betaine bis(trifluoromethylsulfonyl) imide
HDGA	Bis(2-ethylhexyl)diglycolamic acid
HDEHP	Di(2-ethylhexyl)phosphate
HLLW	High level liquid waste
HNTf$_2$	Bis(trifluoromethylsulfonyl)imide
IL	Ionic liquid
KAMINI	KAlpakkam MINI reactor
LiNTf$_2$	Lithium bis(trifluoromethansulfonyl)imide
Ln	Lanthanide

MA	Minor actinide
$MeBu_3NTf_2$	Tri-*n*-butylmethylammonium bis(trifluoromethansulfonyl)imide
n-DD	*n*-Dodecane
NFC	Nuclear fuel cycle
NLIL	Neutral ligand-ionic liquid
NTf_2	Bis(trifluoromethansulfonyl)imide
OA	Oxalic acid
Otf	Trifluoromethanesulfonate
PF_6	Hexafluorophosphate
PFBR	Prototype fast breeder reactor
PHWR	Pressurized heavy water reactor
PUREX	Plutonium Uranium Recovery by Extraction
PWR	Pressurized water reactor
RTIL	Room temperature ionic liquid
TBP	Tri-*n*-butylphosphate
TEA	Triethylamine
THF	Tetrahydrofuran
TODGA	*N,N,N’N’*-Tetraoctyldiglycolamide
TEHDGA	*N,N,N’,N′*-tetra-2-ethylhexyldiglycolamide
TOPO	Tri-*n*-octyl phosphinoxide
TSIL	Task specific ionic liquid
TRUEX	Transuranic extraction
VOCs	Volatile organic compounds